Semi-centralised Hydrogen Production

Techno-Economic Analysis of Offshore Wind-to-Hydrogen Configurations

MSc Thesis Sustainable Energy Technology

Jesse Blok

Delft University of Technology

TU Delft

Semi-centralised Hydrogen Production

Techno-Economic Analysis of Offshore Wind-to-Hydrogen Configurations

by

Jesse Blok

Student Name	Student Number
Jesse Blok	4599446

TU Delft Supervisor: Dr. ir. M. Zaayer (Committee)
Vattenfall Supervisors: S. Blok & Þ. Helgason (Committee)
Institution: Delft University of Technology
Faculty: Electrical Engineering, Mathematics and Computer Science, Delft

Cover: http://sheringhamshoal.co.uk/about/facts-and-figures.php

TU Delft

Acknowledgements

First off all, I want to extend my deepest gratitude to my exceptional supervisors - Michiel Zaayer from TU Delft, along with Sanne Blok and Þorkell Helgason from Vattenfall. Writing this thesis has been an enlightening challenge and it truly has had its ups and downs but I am extremely thankful for the limitless guidance you have provided.

Michiel, I am grateful for your exceptional guidance and feedback on my report and overall work. I truly appreciated your positive and immensely helpful mindset. Besides, your insightful comments enhanced my writing skills and the structure of the report. I am unsure if I fully succeeded in conveying the message in a more comprehensive manner, but your keen eye didn't miss a thing.

Sanne and Þorkell, it has been an absolute pleasure working with both of you week after week. Your guidance and support throughout the project have been invaluable. Sanne, your expertise in wind farm design, FEPM, business cases, and various other fields greatly contributed to structuring this exciting project and helped me navigate the world of wind farm design. Þorkell, your knowledge of hydrogen and modeling played a significant role in modeling the hydrogen infrastructure. I extend my sincere gratitude to both of you for providing extensive feedback on the report and always being available to discuss the topic and exchange ideas with me. I really enjoyed working with you!

The intended audience for this thesis includes researchers, academicians, and industry professionals interested in hydrogen production in offshore wind farms. Background in wind farm design and hydrogen technology could be beneficial for understanding. However, the report is written in a way that makes it accessible for readers from various disciplines with an interest in sustainable technologies.

Jesse Blok
Delft, September 2023

Abstract

The escalating demand for green hydrogen as a sustainable energy carrier has sparked significant interest in offshore wind-to-hydrogen systems, which hold the promise of expediting the transition towards renewable energy sources. The objective of this research is to provide insight in the techno-economic feasibility of semi-centralised electrolysis in an offshore wind farm. The semi-centralised offshore wind-to-hydrogen configuration will be compared with centralised and decentralised offshore wind-to-hydrogen to potentially reduce the levelised cost of hydrogen (LCOH) in future wind-to-hydrogen production designs.

This research was conducted in collaboration with Vattenfall, a leading player in offshore wind energy within Europe, who recognizes the potential of green hydrogen as a key driver in the ongoing energy transition. Vattenfall provided access to an in-house wind farm layout optimisation model to create optimised wind farm layouts as well as site specific data for the case study. This model and data allowed a narrowed focus on the hydrogen aspects of the wind-to-hydrogen configurations.

The technical examination explores crucial elements such as the conversion of wind energy into hydrogen through electrolysis, hydrogen transmission and variances in offshore substations and hydrogen wind turbines, to understand the technical differences between the different offshore wind-to-hydrogen configurations. Additionally, by analysing the hydrogen production process and comparing the scale of hydrogen production in offshore substations or hydrogen wind turbines, the study exhibits the technical feasibility of a wind-to-hydrogen farm with numerous semi-centralised monopile hydrogen substations in comparison with wind-to-hydrogen farms consisting of a single centralised jacket hydrogen substation or decentralised hydrogen wind turbines.

To enable a quantitative comparison of the different offshore wind-to-hydrogen setups in the economic analysis, the LCOH for each configuration was modelled. This process involved creating wind farm layouts and calculating the associated cost for a variety of offshore substations using Vattenfall's optimisation model. Moreover, aspects such as hydrogen production, the dimensions and cost of hydrogen pipelines, and the weight and expense of offshore hydrogen facilities were modelled to estimate the costs associated with hydrogen production and transmission for each configuration.

In the economic analysis, a detailed case study is conducted. The research investigates cost drivers, including wind farm expenses, hydrogen substation investments, and energy transmission infrastructure costs. The results reveal the economic viability of the semi-centralised configuration. The findings highlight the importance of considering monopile load capacity and substructure costs in determining the optimal number of hydrogen substations for semi-centralised configurations. However, the decentralised configuration exhibits a 5% lower LCOH compared to the centralised and semi-centralised configurations due to the lack of additional substructures and high voltage electrical equipment.

In conclusion, this research contributes comprehensive insights into the techno-economic feasibility of semi-centralised offshore wind-to-hydrogen configurations. The findings highlight the potential of semi-centralised configurations and call for further research and optimisations. Unlocking the potential of semi-centralised offshore wind-to-hydrogen configurations can drive the transition toward sustainable and renewable energy sources.

Contents

List of Figures

List of Tables

Nomenclature

Abbreviations

Abbreviation	Definition
AC	Alternating Current
AD	Annual Degradation
AE	Alkaline Electrolysis
AHP	Annual Hydrogen Production
BOP	Balance of Plant
CAPEX	Capital Expenditures
DC	Direct Current
DR	Discount Rate
ELEN	Electrical Energy
EPCm	Engineering, Procurement, Project and Construction Management
ES	Electrical System
FEPM	Front End Park Model
FLH	Full Load Hours
GBS	Gravity-Based Structures
HFR	Hydrogen Flow Rate
HHV	Higher Heating Value
HPU	Hydrogen production unit
HTV	Heavy Transport Vessel
HV	High Voltage
HVAC	High Voltage Alternating Current
HWT	Hydrogen Wind Turbine
IAC	Inter-array Cable
IF	Infield Flowlines
LT	Lifetime
LCOH	Levelised Cost of Hydrogen
LV	Low Voltage
LVAC	Low Voltage Alternating Current
LVDC	Low Voltage Direct Current
MV	Medium Voltage
OPEX	Operational Expenditures
OHF	Offshore Hydrogen Facility
OWHF	Offshore Wind-to-Hydrogen Farm
PEME	Proton Exchange Membrane Electrolysis
PSA	Pressure Swing Adsorption
PtH	Power-to-Hydrogen
RNA	Rotor Nacelle Assembly
SF	Scale Factor
SP	Steel Pipeline
SOE	Solid Oxide Electrolysis
SSCV	Semi-Submersible Crane Vessel
SWRO	Seawater Reverse Osmosis
TIC	Transport, Installation, and Commissioning
WP	Working Platform
WACC	Weighted Average Cost of Capital

Abbreviation	Definition
WTIV	Wind Turbine Installation Vessel

Symbols

Symbol	Definition	Unit
A	Area	[m^2]
c	Specific cost	[€ /unit]
C	Capital expenditures	[€]
C_{OPEX}	Operational expenditures	[€]
cf	Correction factor	[unit]
cf	Cost factor	[%]
c_v	Specific heat constant volume	[J/K·kg]
c_s	Specific heat constant pressure	[J/K·kg]
d_i	Differential wind speed	[m/s]
D	Diameter	[m]
f	Friction factor	[-]
f	Factor	[%]
f_{guess}	friction guess factor	[-]
f_{OPEX}	OPEX factor	[%]
g	Gravitational constant	[m/s^2]
G	Gas gravity of hydrogen	[-]
H	Head height	[m]
L	Length	[m]
M	Mass	[kg]
$\dot{m}$	Mass flow rate	[kg/s]
N	Number of segments	[-]
N_{repl}	Number of stack replacements	[-]
N_{ST}	Compressor stages	[-]
p	Specific power demand	[Watt/kg]
P	Power	[Watt]
p_i	Wind speed distribution	[%]
pd	Power distribution factor	[-]
Q	Volumetric flow rate	[l/s]
r_{stage}	Compressor ratio per stage	[-]
Re	Reynolds number	[-]
SF	Scale Factor	[-]
T	Thickness	[m]
T	Temperature	[K]
V	Velocity	[m/s]
z	Compressibility factor	[-]
ϵ	Absolute roughness	[m]
η	Efficiency	[%]
γ	Specific heat capacity	[J/K·kg]
μ	Dynamic viscosity	[-]
μ	Friction factor	[-]
ρ	Density	[kg/m^3]
Γ	Specific mass	[kg/unit]

1 Introduction

This chapter provides an introduction to the research topic. Section 1.1 presents a summary of the relevant background information, highlighting the recent surge of interest in offshore wind-to-hydrogen farms. Section 1.2 gives an overview of existing offshore wind-to-hydrogen farms, while Section 1.3 presents the problem analysis. In Section 1.4, the research objective and research questions are outlined. The methodology for addressing these research questions is detailed in Section 1.6. Lastly, Section 1.7 offers an overview of the report's layout and division.

1.1. Background

The surging demand for green hydrogen derives from its potential to facilitate the transition towards renewable energy sources [40]. When produced with renewable energy, hydrogen is a highly promising energy carrier, with the capacity to reduce carbon emissions in energy-intensive industries such as steel production, and to be used in energy storage and heavy transportation applications [33][75]. There are various methods for producing green hydrogen. Among these approaches, electrolysis of water is considered the most promising method [25]. In this method, electrolysers are employed to split water molecules into hydrogen and oxygen, using an electric current. If the electrical current is sourced from a renewable energy source, the resulting hydrogen is considered green hydrogen. At present, the production of green hydrogen is in its initial stages, with extensive research being conducted on large-scale green hydrogen projects [90][71][17].

The production of green hydrogen can be achieved using various renewable energy sources, including wind, solar, and hydro. European governments and industry are specifically focusing on offshore wind as a strategic choice for scaling up hydrogen production in Europe [20]. Several reasons contribute to this choice:

- The next generation of offshore wind projects is expected to encounter limited interconnection points and projected grid constraints. Consequently, these projects are well-suited for dedicated hydrogen production.
- Offshore wind farms are increasingly being located at far-offshore sites, making the utilization of a hydrogen pipeline infrastructure more feasible and cost-effective than deploying long-distance electrical infrastructure. This approach shows promise in reducing the expenses associated with transmitting energy over long distances [64].
- The interconnection of multiple offshore wind hydrogen projects presents the opportunity to establish offshore hydrogen production hubs with a capacity of several gigawatts. This interconnection also enables the utilization of a hydrogen backbone infrastructure, which optimises the transmission of energy over long distances. By establishing these hubs and implementing a robust hydrogen backbone infrastructure, the efficiency and effectiveness of long-distance energy transmission can be enhanced for offshore hydrogen production [32].
- Offshore wind shows a higher capacity factor compared to other renewable energy sources [20]. A high capacity factor specifically indicates a more efficient utilization of the installed capacity, resulting in a more consistent and sustained supply of electricity for electrolysis and hydrogen production.

- Many industries and facilities that can make use of hydrogen, such as refineries, the metal industry, marine transport, and export/import facilities, are predominantly located on the coast, in close proximity to offshore wind farm sites [20].

Offshore wind-to-hydrogen is the term used to describe the production of hydrogen through the utilization of offshore wind as a renewable energy source. In order to compete effectively with other green hydrogen production methods, it is imperative for offshore wind-to-hydrogen projects to prioritize the optimisation of production processes and achieve cost reductions in electricity generation and hydrogen production. The configuration of wind-to-hydrogen systems plays a critical role in achieving these objectives. Therefore, the primary aim of this research is to explore different offshore wind-to-hydrogen configurations for the generation of green hydrogen to significantly reduce production costs and enhance competitiveness with other green hydrogen projects by the year 2030.

This thesis was conducted in collaboration with Vattenfall, a leading player in offshore wind energy within Europe [85]. Vattenfall has a strong interest in future offshore wind-to-hydrogen farms, as they recognize the potential of green hydrogen as a key driver in the ongoing energy transition [84].

1.2. Offshore wind-to-hydrogen configurations

The production of green hydrogen using offshore wind energy can be accomplished through different wind-to-hydrogen configurations, which are determined by the placement of the electrolysers. These configurations can be categorized as either onshore or offshore, based on the location of the electrolysers. The distinction between onshore and offshore wind-to-hydrogen configurations has been studied and discussed in various sources [17], [71], [90], and [24].

In the onshore wind-to-hydrogen configuration, offshore wind energy is transmitted through electrical cables to the shore, where the electricity is utilized by an electrolyser to produce hydrogen onshore. In the offshore wind-to-hydrogen configuration, the electrolysers are placed within the wind farm and the hydrogen is produced offshore and transmitted via hydrogen pipelines to shore.

Prior research has demonstrated the potential advantages of offshore wind-to-hydrogen configurations in comparison to onshore wind-to-hydrogen configurations. This is primarily attributed to the absence of costly high voltage direct current transmission infrastructure required for onshore systems, particularly when the distance to shore increases [90]. As a result, this study will specifically concentrate on exploring offshore wind-to-hydrogen configurations as the preferred approach.

Current literature presents two distinct offshore wind-to-hydrogen configurations: centralised offshore wind-to-hydrogen, and decentralised offshore wind-to-hydrogen [17][71][90][24]. In the centralised offshore wind-to-hydrogen configuration, a large-scale centralised offshore electrolysis location, known as an offshore hydrogen substation, is established at a single location within the offshore wind farm. At this substation, hydrogen is produced where after transported via a hydrogen pipeline to the mainland. In the decentralised offshore wind-to-hydrogen configuration, each individual offshore wind turbine incorporates its own dedicated electrolysis system and related components, all situated on an additional wind turbine platform. This combined setup is commonly referred to as a hydrogen wind turbine. Subsequently, the produced hydrogen is transported to the shore through pipelines. The two offshore wind-to-hydrogen configurations currently reviewed in literature are depicted in Figure 1.1 and Figure 1.2. In this report, the term ”offshore hydrogen facility” (OHF) is used to collectively refer to the hydrogen substation and hydrogen wind turbine.

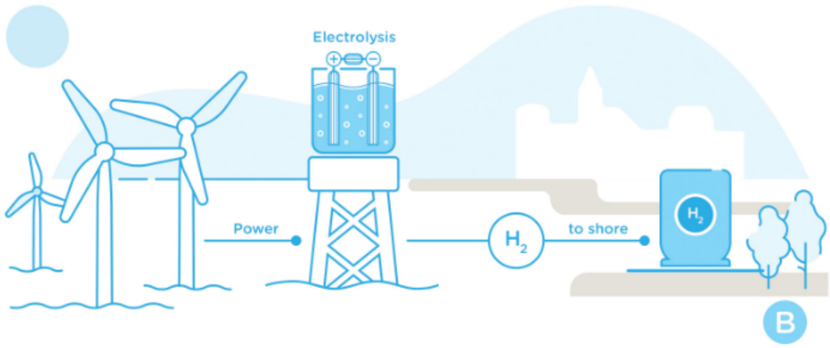

Figure 1.1: Schematic overview of centralised electrolysis in an offshore wind-to-hydrogen farm [58].

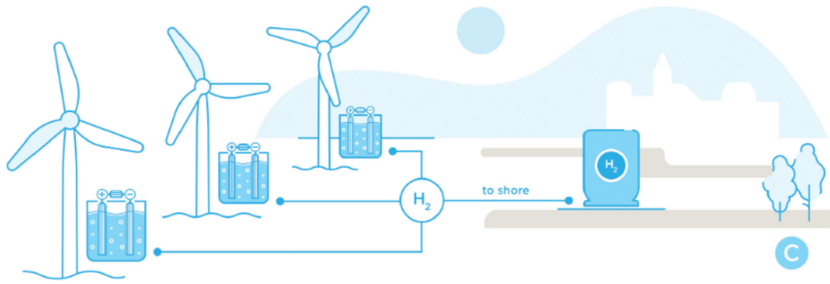

Figure 1.2: Schematic overview of decentralised electrolysis in an offshore wind-to-hydrogen farm [58].

Both offshore centralised and decentralised offshore wind-to-hydrogen have their advantages and disadvantages as stated in literature [71][39]. The main advantage of decentralised hydrogen production is the lack of both high voltage electrical equipment and an electrical inter-array cable infrastructure. The main advantage of centralised hydrogen production is economy of scale for the hydrogen production station compared to small scale electrolysis systems for every turbine in a wind farm.

To overcome the disadvantages and both advantages, semi-centralised electrolysis could be a solution. A high level overview of the semi-centralised configuration is shown in Figure 1.3. In an offshore wind farm, multiple electrolyser facilities called Semi-centralised offshore hydrogen substations, are connected to a cluster of wind turbines. This could possibly decrease the electrical cable length and still uses the economy of scale concerning the electrolysis similar to the centralised configuration. Furthermore, the expenses related to the transportation and installation of large-scale centralised hydrogen substations can be reduced by adopting a different approach. By constructing smaller hydrogen substations on the same foundation as the wind turbines, cost can reductions can be achieved. The synergistic utilization of the wind turbine substructure and the substructure of the substations, has the potential to reduce the expenses involved in offshore hydrogen substations.

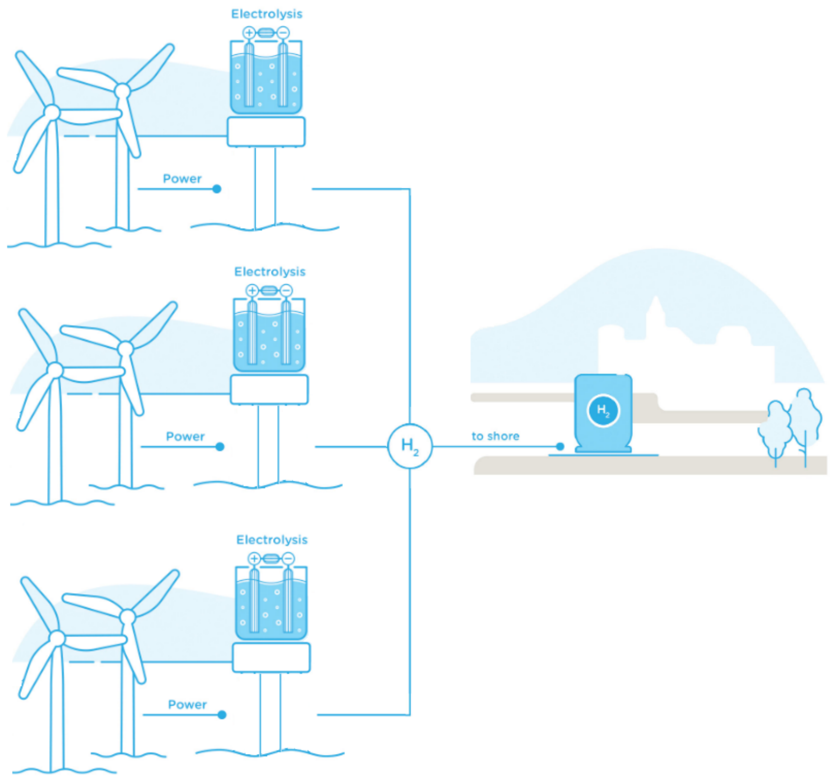

Figure 1.3: Schematic overview of semi-centralised electrolysis in an offshore wind-to-hydrogen farm [58].

In this study, an offshore wind-to-hydrogen configuration is defined as Semi-centralised when the number of hydrogen offshore substations ranges from two to half the total number of wind turbines within a wind farm. Conversely, the centralised offshore wind-to-hydrogen configuration encompasses a singular central hydrogen substation, whereas the decentralised wind-to-hydrogen configuration omits any hydrogen substations, given that the electrolysers are located at the wind turbines on the same platform. The quantity of hydrogen substations serves as a crucial factor in determining the techno-economic viability of offshore wind-to-hydrogen configurations. The hydrogen production unit capacity of decentralised, semi-centralised and centralised offshore hydrogen substations ranges roughly between 5-20MW, 30-600MW and 600+MW.

1.3. Problem analysis

The primary issue to be addressed concerns identifying the most viable offshore wind-to-hydrogen configuration for green hydrogen production from offshore wind energy, considering both technical and economic feasibility. Although existing literature provides both technical and economical insights into decentralised and centralised electrolysis [71] [39], a notable knowledge gap exists with respect to semi-centralised electrolysis configurations, as outlined in section 1.2. Consequently, the main challenges involve making configuration-specific assumptions regarding the costs and technical possibilities of offshore wind-to-hydrogen. Moreover, the limited information on offshore hydrogen transmission infrastructure poses an additional challenge. As a result, there is a scientific gap concerning the techno-economic analysis of the semi-centralised offshore wind-to-hydrogen configuration and its comparison with the centralised and decentralised offshore wind-to-hydrogen configurations.

1.4. Research objective

The objective of this research is to provide an insight in the techno-economic feasibility of semi-centralised electrolysis in an offshore wind farm. The semi-centralised offshore wind-to-hydrogen configuration will be compared with the centralised and decentralised offshore wind-to-hydrogen configurations to potentially reduce the levelised cost of hydrogen (LCOH) in future wind-to-hydrogen production designs. This research will address the techno-economic research gap regarding semi-centralised offshore wind-to-hydrogen electrolysis, as identified in section 1.3. Additionally, this study may contribute to the future design of offshore wind-to-hydrogen farm configurations. The main research question, formulated to achieve the research objective, is stated as follows:

What is the techno-economic feasibility of the semi-centralised offshore wind-to-hydrogen configuration compared with the centralised and decentralised offshore wind-to-hydrogen configurations?

To address the main research question, the following sub-questions have been formulated. These sub-questions will guide the research process and provide a structured approach to analyse the techno-economic feasibility of different offshore wind-to-hydrogen configurations.

1. What are the key technical differences between the centralised, decentralised, and semi-centralised offshore hydrogen production configurations?
2. How do the energy conversion efficiency, hydrogen transmission and electrical cable infrastructure differ among these configurations?
3. What are the primary cost and performance drivers for each configuration, considering capital expenditures (CAPEX) and total hydrogen production?
4. What determines the optimum number of semi-centralised offshore hydrogen substations in an offshore wind-to-hydrogen farm?
5. How do the levelised cost of hydrogen compare among these configurations?

1.5. Scope of research

This research aims to compare various offshore wind-to-hydrogen configurations by analysing optimised wind farm layouts with distinct numbers of hydrogen substations. The optimisation of wind farm layouts is within the scope of this research due to the availability of the in-house Vattenfall model.

The offshore wind-to-hydrogen configurations in this study are all hydrogen production systems. The electricity generated will be utilized exclusively for hydrogen production and will not be connected to the grid. Consequently, hydrogen is the only output of all wind-to-hydrogen configurations discussed in this research. All hydrogen production systems eliminate the need for electrical infrastructure and do not require additional grid capacity due to the absence of grid connection.

The offshore wind-to-hydrogen configuration boundary of this research is the hydrogen pipeline connection between an offshore hydrogen facility and an offshore hydrogen backbone pipeline from the hydrogen grid operator.

To limit the scope of this research, the findings will be based on a singular case study. For this case study, a representative wind farm site will be chosen in collaboration with Vattenfall, and the necessary specifications regarding site conditions will be supplied by Vattenfall.

With respect to wind turbine foundation structures, only monopiles will be considered. Monopiles are extensively employed in offshore wind turbine designs, particularly in the relatively shallow waters of the North Sea. Additionally, the monopile structure will serve as the foundation for the hydrogen substation design, resulting in increased synergy in the overall design.

1.6. Methodology

As described in Section 1.4, the primary objective of this project is to conduct a techno-economic analysis of semi-centralised electrolysis in an offshore wind farm, incorporating a comparison between centralised and decentralised offshore wind-to-hydrogen. In order to accomplish this objective, a comprehensive technical analysis encompassing centralised, semi-centralised, and decentralised offshore wind-to-hydrogen is carried out. This entails providing a detailed description of the technology and components involved in the offshore electrolysis, as well as a technical comparison of the offshore wind-to-hydrogen configurations.

For the economic analysis, financial metrics are outlined to assess the economic viability of the offshore wind-to-hydrogen configurations. In order to acquire the necessary variables for conducting the economic analysis and calculating financial metrics, a combination of existing in-house Vattenfall models and newly developed models is utilized. The optimised wind farm layouts and associated cost, are derived from an in-house Vattenfall model, which optimises substation placement, wind turbine placement, and cable routing to achieve the lowest possible levelized cost of electricity. The hydrogen production, hydrogen pipeline sizing, and associated costs are modeled and described. Lastly, a case study is conducted in which the existing and developed models are applied to a specific case. In addition, a sensitivity analysis is performed to assess the influence of the assumptions made on the results. This analysis allows for the identification of key assumptions that have a significant impact on the conclusions or recommendations derived from this research. An overview of the research activities is presented below.

Technical description

1. *System description*: Describe the working principles of offshore wind-to-hydrogen production. This includes an elaboration of the centralised, Semi-centralised and decentralised offshore wind-to-hydrogen configurations.
2. *System components*: Outline the technical aspects and type of the components selected for the offshore wind-to-hydrogen configurations.

Modeling

3. *Model overview description*: Describe the models necessary to compare the different offshore wind-to-hydrogen configurations.
4. *Hydrogen production modeling*: Model Hydrogen production, based on wind farm power curve, efficiencies and degradation's.
5. *Hydrogen pipeline sizing*: Model the hydrogen pipeline dimensions and cost.
6. *Hydrogen offshore substation modeling*: Mass and cost modeling of hydrogen substations.

Case study

7. *Case description*: Describe the selected case and elaborate why this case is representative for this project. This includes a selection of the capacity of different components of an offshore wind-to-hydrogen farm to meet the requirements of the case study.
8. *Wind farm layout creation*: Create the wind hydrogen layouts for the different offshore wind-to-hydrogen configurations. This relates to wind turbine placement, hydrogen substation placement and electrical cable and hydrogen pipeline infrastructure layout design.
9. *Preliminary optimisation*: Optimise a set of input parameters in the wind-to-hydrogen farm to achieve the lowest LCOH for each individual configuration.
10. *Semi-centralised configuration selection*: Select a semi-centralised configuration for the comparison with the centralised and decentralised wind-to-hydrogen configurations.
11. *Wind-to-hydrogen configuration comparison*: Compare the different wind-to-hydrogen configurations and evaluate the final results.
12. *Sensitivity analysis*: Assess the influence of different cost components on the techno-economical optimisation problem to identify the main factors and thus main cost and technical drivers of an offshore wind-to-hydrogen design.

1.7. Report layout

The purpose of this section is to present a comprehensive outline of the various segments within the report. Initially, the report offers a technical examination of offshore electrolysis driven by wind energy. This is achieved by delineating the distinct offshore wind-to-hydrogen configurations in Chapter 2. Subsequently, Chapter 3 elaborates on the hydrogen components of the offshore wind-to-hydrogen configurations.

Furthermore, the report encompasses an overview of the models utilized for the techno-economic assessment of the different offshore wind-to-hydrogen configurations. Chapter 4 provides an overview of the existing and new develop and elaborates on the workflow between the different models as well as an explanation of the financial metric employed to gauge the techno-economic performance of these configurations. Following this, Chapter 5 delves into the hydrogen production model, offering insights into the electrolysis process. Chapter 6 elucidates the pipeline sizing and cost model, while Chapter 7 expounds upon the mass and cost modeling pertaining to the offshore hydrogen facilities.

Hereafter, a case study is executed in Chapter 8, where the previously mentioned models are applied to analyse and compare the techno-economic viability of the various offshore wind-to-hydrogen configurations. Additionally, in the case study chapter, a sensitivity analysis is undertaken to investigate the influence of different assumptions made, aiming to identify the primary drivers concerning the techno-economic feasibility of the distinct offshore wind-to-hydrogen configurations. Furthermore, the case study chapter includes a discussion section to elaborate on the obtained results.

Finally, Chapter 9 provides the conclusion based on the key findings of this study, where after Chapter 10 offers recommendations for future work.

2
System configurations

The configuration type of an all-hydrogen offshore wind-hydrogen farm is determined by the placement of the electrolysers as stated in section 1.2. However, not only the electrolyser placement differs per configuration. Therefore, the goal of this chapter is to describe the working principle of the three system configurations and elaborate on the similarities and differences per configuration. This is done by first explaining the general working principle of offshore wind to hydrogen electrolysis. Hereafter, centralised offshore wind-to-hydrogen is discussed in section 2.2. This is followed by an elaboration of decentralised offshore wind-to-hydrogen in section 2.3 and semi-centralised offshore wind-to-hydrogen is discussed in section 2.4. Finally, Section 2.5 qualitatively compares the three offshore wind-to-hydrogen configurations.

2.1. Offshore wind-to-hydrogen system overview

To produce green hydrogen with electrolysis powered by offshore wind energy, several general steps need to be taken. These steps outline the general process of offshore electrolysis which enables the production of green hydrogen using offshore wind energy. The general steps involved in the process are elaborated as follows:

- *Electricity generation*: Offshore wind turbines convert the kinetic energy of wind into mechanical energy by utilizing rotating blades. This mechanical motion drives a generator, which generates alternating current (AC) electrical power as an output.
- *Power transformation*: When the power needs to be transmitted over longer distances, the electrical power generated by offshore wind turbines is transformed into high voltage AC power. This involves feeding the low-voltage AC power into power transformers, which step up the voltage to a higher level for efficient long-distance transmission. Additionally, when the high-voltage AC power reaches the offshore hydrogen substation, a step-down transformer is utilized to reduce the voltage to the required level for electrolysis.
- *Electricity Transmission*: The electricity generated by offshore wind turbines is transmitted to the offshore electrolysers using inter-array cables with a specific voltage and current depending on the distance and capacity of transmission.
- *Power Conversion*: The power generated by wind turbines is typically in the form of AC power. However, electrolysis processes require direct current (DC) power. As a result, a converter is required to transform the AC power into DC power for efficient operation. This converter facilitates the conversion of the electrical energy from the wind turbines, allowing it to be used effectively in the electrolysis process.
- *Water treatment*: For offshore electrolysis, desalinated and deionized water is required. Therefore, seawater undergoes a desalination and deionization process to remove impurities like salts and minerals, such as reverse osmosis to obtain purified water, ensuring the required quality for electrolysis. Deionization is applied to further purify the desalinated seawater.

- *Electrolysis*: The purified water obtained from desalination serves as the electrolyte in an electrolyser, consisting of an anode and a cathode separated by an electrolyte solution. Within this setup, electrolysis of water takes place.
- *Hydrogen purification*: The mixture of hydrogen and oxygen gases produced during electrolysis requires separation and purification. Various techniques, including pressure swing adsorption, catalytic purification, or membrane purification, are employed based on the specific purity requirements for the intended hydrogen application. The purification of hydrogen occurs subsequent to the electrolyser stacks.
- *Hydrogen Compression*: In instances where hydrogen needs to be transported to shore, compression is employed after the purification process. Compression becomes necessary when longer distances of hydrogen transmission are involved, requiring the overcoming of higher pressure drops. By compressing the hydrogen, its density increases and its storage volume decreases, facilitating more efficient and economical transportation to the desired onshore locations.
- *Hydrogen Transmission*: Offshore hydrogen transport to shore is facilitated through offshore hydrogen pipelines. These pipelines enable efficient and secure transportation of hydrogen from the offshore electrolysers to onshore hydrogen facilities or other desired destinations.

The steps outlined depict the general process of producing hydrogen through electrolysis powered by offshore wind energy. In addition to the general process steps, there are several ancillary activities that support the offshore production of hydrogen, ensuring its efficient and sustainable operation. The following is a list of these ancillary activities:

- *Power control*: Managing and controlling the electrical power generated by the offshore wind turbines to ensure stable and efficient operation of the electrolysis process.
- *Water pumping*: Handling the movement and supply of water required for the electrolysis process.
- *System cooling*: Maintaining appropriate temperature levels within the electrolysis system to optimise its performance and prevent overheating.
- *Data communication*: Establishing reliable communication networks to monitor and control various components of the offshore hydrogen production system.
- *Brine disposal*: Properly managing and disposing of the brine or wastewater produced as a byproduct of the electrolysis process.

The ancillary activities are performed by the ancillary components, and they are required in every configuration. On the other hand, the general process steps take place in their respective associated components, but not all of these steps are required in every offshore wind-to-hydrogen configuration. Additionally, there are components that are not directly associated with the ancillary activities or general process steps, such as the hydrogen substations.

In this report, the components to the process steps and ancillary activities are further categorized and shown in Figure 2.1. The water treatment equipment, hydrogen purification equipment and system cooling system are grouped as part of the Balance of Plant (BOP), while the components for power transformation and power conversion are grouped within the electrical system. The hydrogen compressor component as well as the electrolyser stacks are treated as individual components. Moreover, the collective term used for the electrolysers, BOP, electrical system and compressors is the Hydrogen Production Unit (HPU). The HPU consists of all the components directly involved in the production and processing of hydrogen at the offshore hydrogen facility.

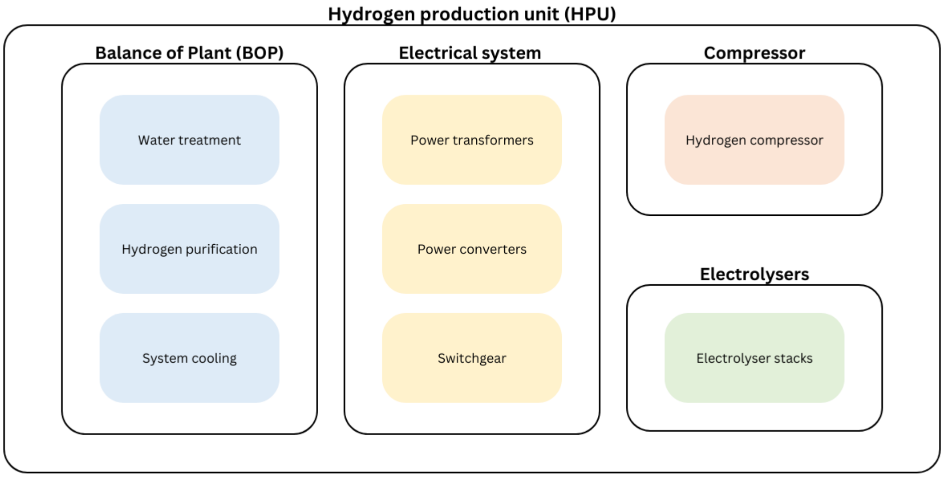

Figure 2.1: Schematic overview of the hydrogen production unit equipment.

Table 2.1 provides an overview of the components that are not common to all three configurations. The variations among the configurations primarily involve wind turbines, hydrogen wind turbines, inter-array cables, medium and high voltage (MD/HV) switchgear and transformers, and hydrogen substations. Infield flowlines, which are flexible hydrogen pipelines, and the manifold, an offshore substation for assembling hydrogen, are also not required in all three configurations.

Conversely, the electrolyser stacks, BOP, compressors, AC-DC converters, steel pipelines, and ancillary components remain consistent across all configurations, with the only difference being their installed capacity.

	Configuration		
Component	**Centralised**	**Semi-centralised**	**Decentralised**
Wind turbines	X	X	
Hydrogen wind turbines			X
Inter-array cables	X	X	
MD/HV switchgear	X	X	
MD/HV transformers	X	X	
Infield flowlines			X
Steel pipelines	X	X	X
Manifold			X
Hydrogen substations	X	X	

Table 2.1: Differences in components between the centralised, semi-centralised and decentralised offshore wind-to-hydrogen configurations.

The difference in components per configuration is important for the techno-economic comparison between the different offshore wind-to-hydrogen configurations. Therefore, the next sections describe the configuration-specific general process steps and components.

2.2. Centralised offshore wind-to-hydrogen

This section presents information on the centralised offshore wind-to-hydrogen configuration. A schematic system overview is discussed in subsection 2.2.1. Following that, subsection 2.2.2 provides an elaboration of the centralised offshore hydrogen substation.

2.2.1. Centralised offshore wind-to-hydrogen schematic overview

In centralised offshore wind-to-hydrogen, the hydrogen is produced in a single location in a wind farm. The installed hydrogen production unit capacity ranges from 900-1000MW for a 1GW wind farm, depending on the HPU sizing. In figure (2.2) a schematic overview of the centralised offshore wind-to-hydrogen configuration is provided. In this figure, an overview is given of the flow lines between the wind turbines, inter-array cables, electrical system, electrolysers, BOP and hydrogen pipelines. The flow lines include AC power, DC power, hydrogen, seawater and desalinated water. The electrolysers in the centralised offshore wind-to-hydrogen configuration are located offshore on single substation. This substation will have gigawatt scale electrolysis capacity to produce hydrogen and therefore a large jacket substructure similar to current existing oil and gas platforms is necessary.

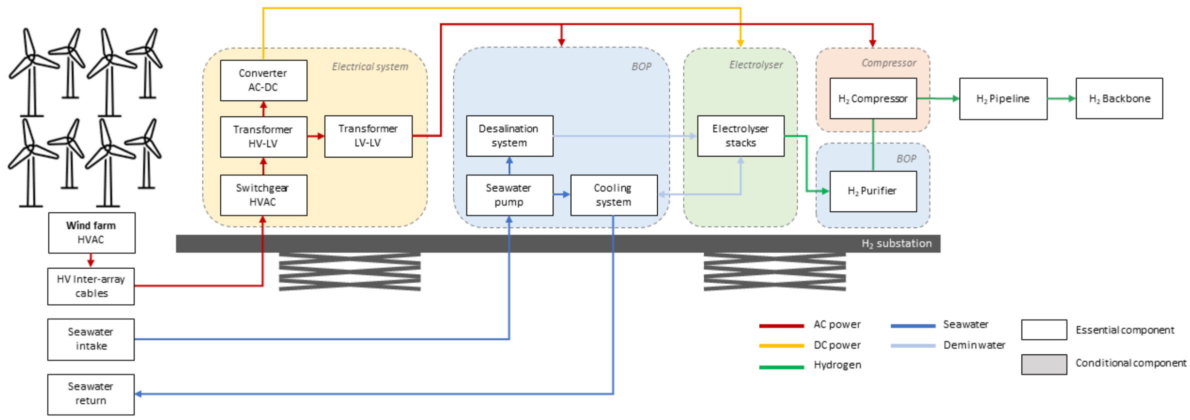

Figure 2.2: Schematic overview of centralised electrolysis in an offshore wind-to-hydrogen farm.

The electricity produced by the wind turbines is converted at the wind turbines from low voltage alternating current (LVAC) power to medium or high voltage alternating current (MDVA or HVAC) power and transmitted via inter-array cables to the centralised offshore hydrogen substation. The need for power transformation could be eliminated when employing low voltage electrical transmission. However, the generated electricity is transformed to HVAC which is necessary to minimise inter-array cable energy losses in the transmission process. Low voltage electrical transmission involves a substantial number of inter-array cables and results in high losses. Consequently, low voltage electrical transmission is not considered a viable option for the centralised offshore wind-to-hydrogen configuration.

At the centralised offshore hydrogen substation, the electrical system consists of medium or high voltage switch-gear, transformers and converters. In the electrical system, the MDAC or HVAC is first transformed to LVAC. The majority of LVAC electricity is then converted to low voltage direct current (LVDC), to power the electrolysers [41]. The remaining minority of the LVAC electricity further transformed to lower voltages and used to power the BOP. If required to meet the off-take pressure, the generated hydrogen is compressed and then transported through a single steel pipeline to a hydrogen backbone pipeline.

2.2.2. Centralised offshore hydrogen substation

Centralised electrolysis is conducted at the offshore hydrogen substation, as illustrated in Figure 2.2. The hydrogen conversion process implemented at this substation differentiates itself from decentralised electrolysis due to its larger scale. The substructure of the substation acts as the substructure for constructing the topside. In the context of the centralised offshore hydrogen substation, jacket substructures emerge as a viable option. These substructures are commonly employed in larger offshore installations, such as high voltage AC or DC substations. Jackets are steel structures characterized by a lattice framework supported by piles driven into the seabed. They offer several advantages over other types of substructures, including their ability to withstand heavy loads and support large structures. Consequently, jackets are considered a good option for accommodating large-scale centralised hydrogen substations. The specific size and type of jacket required for the substation depend on the weight and dimensions of the topside.

2.3. Decentralised offshore wind-to-hydrogen

In this section, information is provided about the decentralised electrolysis configuration. First a schematic system overview is discussed in subsection 2.3.1. Subsequently, in subsection 2.3.2, there is an elaboration of the offshore hydrogen wind turbine.

2.3.1. Decentralised offshore wind-to-hydrogen schematic overview

The electrolysers in the decentralised offshore wind-to-hydrogen configuration are placed at each wind turbine platform of the wind farm. No extra substructures besides the ones from the turbines, need to be drilled into the seabed because the electrolysers are placed on a redesigned platform below the turbine on the same monopile substructure. The decentralised configuration offers two system design options: the add-on system and the deep-integrated system. In the add-on system, the electrolysis system is added to a standard wind turbine requiring no modifications to a standard wind turbine except for an additional platform to the substructure. In the deep-integrated system, the HPU is directly connected to the electrical system of the wind turbine and placed at the additional wind turbine platform, optimising space utilization and eliminating the need for certain electrical components. For the decentralised configuration considered in this research, a deep-integrated system design is chosen, as it has the potential to reduce the overall cost of the decentralised configuration. In this report, the term ”hydrogen wind turbine” refers to the deep-integrated offshore hydrogen wind turbine.

A schematic overview of the decentralised configuration is given in Figure 2.3. In this figure, an overview is given of the flow lines between the wind turbines, inter-array cables, electrical system, electrolysers, BOP and hydrogen pipelines. The flow lines include AC power, DC power, hydrogen, seawater and desalinated water.

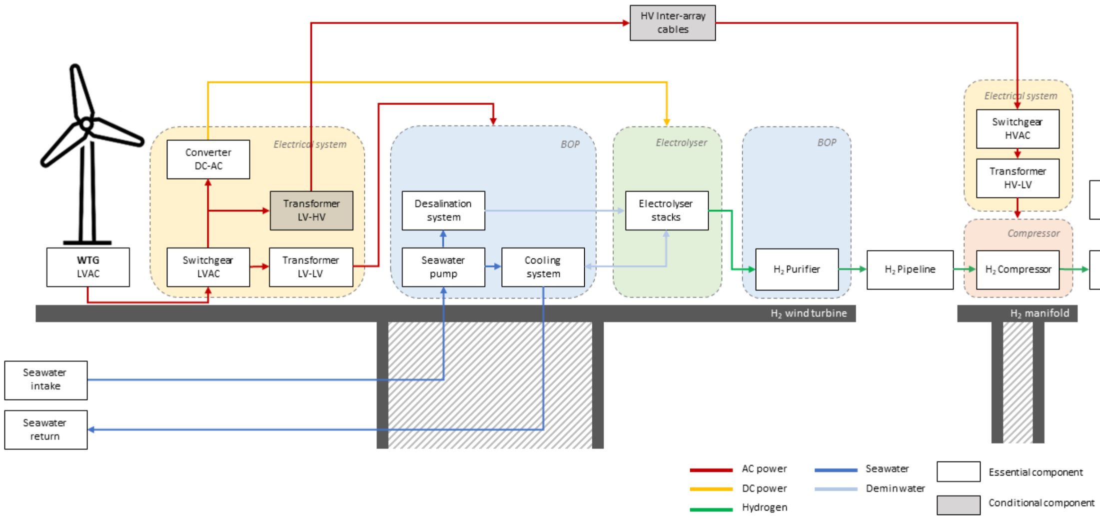

Figure 2.3: Schematic overview of decentralised electrolysis in an offshore wind-to-hydrogen farm.

The wind turbine generates LVAC power, which can be directly converted to LVDC power for the electrolysers as the generated electricity is not transmitted through inter-array cables. The AC power from the wind turbine is directly converted to DC power using a low voltage AC-DC converter. The DC power is then utilized in the electrolysers for hydrogen production. The deep-integrated decentralised electrolysis system eliminates the need for medium or high voltage transformers. After the electrolysis and purification, the hydrogen is transported from the wind turbines to the hydrogen manifold through hydrogen infield flowlines. At the hydrogen manifold, the hydrogen is collected and, if required, compressed. Subsequently, it is transmitted to the hydrogen backbone pipeline through a steel hydrogen pipeline for further distribution.

2.3.2. Offshore hydrogen wind turbine

The offshore hydrogen wind turbine is an offshore wind turbine equipped with a redesigned platform situated on top of the wind turbine substructure. This platform is specifically designed to accommodate the electrical system, electrolysers stacks and BOP components. When incorporating this platform, the increased weight on the substructure must be taken into account during the substructure design process. Currently, the most commonly used substructure type is the monopile substructure. However, ongoing research and projects focuses on exploring alternative wind turbine substructure options like jackets or floating substructures [39]. Nonetheless, for the purposes of this particular research, the focus will solely be on considering monopile substructures for both the wind turbines and the deep integrated decentralised offshore hydrogen turbine to limit the scope.

2.4. Semi-centralised offshore wind-to-hydrogen

This section presents information about the semi-centralised electrolysis configuration. Firstly, a schematic system overview is discussed in subsection 2.4.1. Following that, subsection 2.4.2 provides an elaboration of the semi-centralised offshore hydrogen substation.

2.4.1. Semi-centralised offshore wind-to-hydrogen schematic overview

Semi-centralised offshore wind-to-hydrogen falls between centralised and decentralised configurations. In this configuration, multiple electrolysis substations are present within a wind farm. Each hydrogen substation connects to a cluster of wind turbines. This research will evaluate multiple semi-centralised configurations containing different numbers of hydrogen substations. A schematic overview of a semi-centralised hydrogen substation is provided in Figure 2.4.

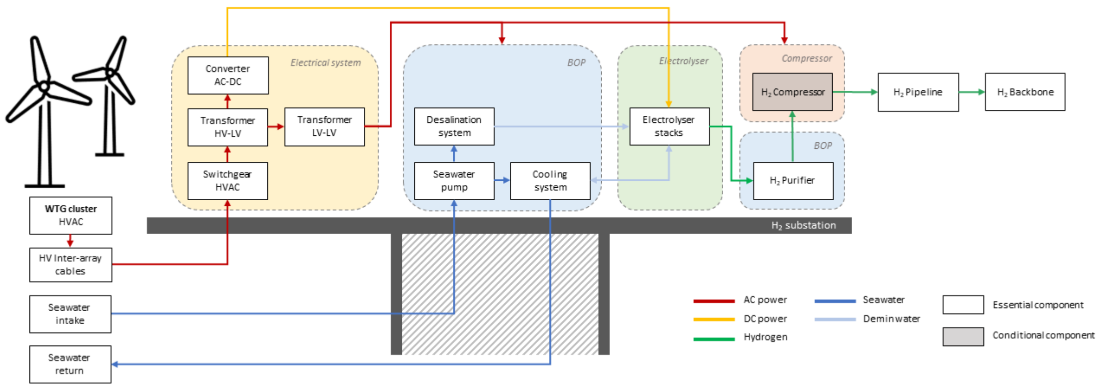

Figure 2.4: Schematic overview of semi-centralised electrolysis in an offshore wind-to-hydrogen farm.

The overall working principle of the semi-centralised configuration is similar to that of the centralised configuration. The main difference lies in the number of wind turbines connected to the substation, which impacts the capacity of the electrical system, electrolysers, and BOP. As a result, the size of the substation varies from the centralised platform, potentially influencing the type of substructure used. Furthermore, energy transmission takes place through both inter-array cables and hydrogen pipelines. The inter-array cables serve to connect the clusters of wind turbines to the substations. On the other hand, the hydrogen pipelines establish the connection between the substations and the hydrogen backbone pipeline.

2.4.2. Semi-centralised offshore hydrogen substation

Depending on the overall weight of the topside structure, the semi-centralised substation can be installed on either a monopile, jacket, or gravity-based substructures. However, for the sake of research scope limitation, gravity-based substructures are not taken into consideration. The weight of the topside is determined by factors such as the mass of the electrical system, electrolysers, BOP, and the support structure. The support structure serves the purpose of providing structural support to the topside components. By utilizing the same monopile substructure for both the substation and the wind turbines, cost-saving synergies can be achieved. However, if the topside's weight exceeds the capacity of a monopile substructure, a jacket substructure becomes necessary.

2.5. Qualitative configuration comparison

Comparing the different offshore wind-to-hydrogen configurations, a qualitative evaluation of their advantages and disadvantages is provided in this section. In Table 2.2, a high level qualitative comparison providing high, medium or low scores per aspect is provided. Hereafter, the various aspects will be discussed in the context of the centralised, semi-centralised, and decentralised offshore wind-to-hydrogen configurations.

	Configuration		
Aspect	**Centralised**	**Semi-centralised**	**Decentralised**
Economy of scale	High	Medium	Low
Synergies	Low	High	High
Maintainability	High	Medium	Low
Resilience	Low	Medium	High
Transport and installation	Low	Medium	High
Asset risk	Low	Medium	High
Complexity	High	Medium	Low
Energy transmission	Low	Medium	High

Table 2.2: Qualitative comparison of the system characteristics of the centralised, semi-centralised and decentralised offshore wind-to-hydrogen configurations.

- *Economy of scale*: The centralised configuration excels in this aspect, leveraging economies of scale to its advantage by consolidating all hydrogen production in one location, benefiting from a single electrical system and BOP. Semi-centralised configurations have potential cost efficiencies due to the economy of scale for the electrical system and BOP, whereas the decentralised configuration lacks economies of scale, requiring BOP equipment at each turbine and increasing costs.
- *Synergies*: There are no synergies to be gained for the substructure of the wind turbines and the hydrogen substations in the centralised configuration. However, both the semi-centralised and decentralised configurations offer notable synergies as the wind turbines and hydrogen production can share the same monopile, leading to potential cost reductions.
- *Maintainability*: The centralised configuration offers the advantage of streamlined and faster repair times and maintenance since all hydrogen-related activities are consolidated in one place. Semi-centralised configurations, while less streamlined than centralised systems, still manage to strike a balance. However, managing multiple independent units in the decentralised configuration can pose challenges in terms of operations and maintenance.
- *Resilience*: The centralised configuration faces challenges in the event of a failure as the impact can be significant. Conversely, both the semi-centralised and decentralised configurations offer a high level of resilience, as the failure of one unit does not impact the entire system.
- *Transport and installation*: The transportation and installation of the centralised substation may pose difficulties due to its size and weight. In the semi-centralised configuration, the process is more manageable as the size and weight of the substations are significant but smaller than centralised substations. The decentralised configuration offers the most efficiency in this aspect due to the smaller size of the installations.
- *Asset risk*: The concentration of electrolysers in a single location increases the asset risk for the centralised configuration. In the semi-centralised configuration, the risk is reduced as assets are distributed across various locations, while the decentralised configuration reduces asset risk the most due to its distributed nature.
- *Complexity*: The centralised configuration simplifies the system but it is complex in terms of the overall setup. The semi-centralised configurations fall in the middle range, less complex than centralised systems but more complex than decentralised systems. The decentralised configuration introduces more complexity into the system due to the distribution of assets across various locations.

- *Energy transmission*: The centralised configuration involves two infrastructures: inter-array cables and a hydrogen pipeline, which could be disadvantageous compared to a single energy transmission system. The semi-centralised configurations require both infrastructures, similar to the centralised system. The decentralised configuration stands out, eliminating the need for expensive inter-array cable infrastructure and high voltage transformation, resulting in reduced electrical losses and a simplified infrastructure setup.

In conclusion, each of the offshore wind-to-hydrogen configurations presents distinct advantages and trade-offs. The centralised configuration leverages economies of scale and streamlines maintenance but struggles with resilience and transport difficulties or cost. The decentralised configuration, while offering high resilience and cost efficient transport and installation, lacks the economies of scale and has higher complexity in terms of operations and maintenance. Meanwhile, the semi-centralised configuration aims to balance these extremes, achieving a blend of benefits across all aspects. However, based on the qualitative comparison, no configuration stands out significantly from the others.

3

Offshore wind-to-hydrogen component description

An offshore wind-to-hydrogen farm consists of various components for hydrogen production and energy transmission. The configurations discussed in Chapter 2 share similarities in terms of electricity and hydrogen generation and transmission. However, not all components are required in each configuration, and the specific types and sizes of these components vary depending on the configuration. This chapter provides information regarding the following components: the hydrogen production unit, inter-array cables, hydrogen pipelines, hydrogen substations and hydrogen wind turbines. The components involved in an offshore wind-to-hydrogen are compared across the three offshore wind-to-hydrogen configurations. Additionally, it explores different methods for offshore transport and installation.

Section 3.1 provides an overview of the components of the hydrogen production unit and describes the selected techniques for each component. Following that, Section 3.2 provides detailed information about the inter-array cables. The different types of hydrogen pipelines are discussed in Section 3.3, and Section 3.4 focuses on the substructure and superstructure of the hydrogen substations. Section 3.5 covers the topic of hydrogen wind turbines, while Section 3.6 discusses the offshore hydrogen manifold. Finally, Section 3.7 elaborates on the methods used for the transport and installation of offshore hydrogen facilities.

3.1. Hydrogen production unit

This section provides detailed information on the components of the HPU. The HPU includes the electrolyser, BOP, electrical system, and a hydrogen compressor if hydrogen compression is required. Subsection 3.1.1 focuses on the electrolyser technology, while Subsection 3.1.2 elaborates on the components of the BOP. The components of the electrical system are discussed in Subsection 3.1.3, and finally, Subsection 3.1.4 provides detailed information on the hydrogen compressor.

3.1.1. Electrolyser

Electrolysers are utilised to produce hydrogen from electricity and desalinated water. Therefore, background information regarding the electrolyser efficiencies, degradation and lifetime is provided, followed by the electrolyser technology comparison.

Efficiencies

The efficiency of the electrolyser is a crucial factor in determining the annual hydrogen production of a wind farm. Electrolysis efficiency can be divided into electrolyser stack efficiency, also known as DC efficiency, and electrolyser system efficiency, which takes into account selected components from the HPU [67]. The electrolyser stack efficiency refers to the efficiency of the electrolysis process within the stack itself. On the other hand, the system efficiency considers additional components such as the BOP (auxiliary equipment), stack energy losses, and electrical losses. The stack and electrolyser system efficiency are given in Figure 3.1.

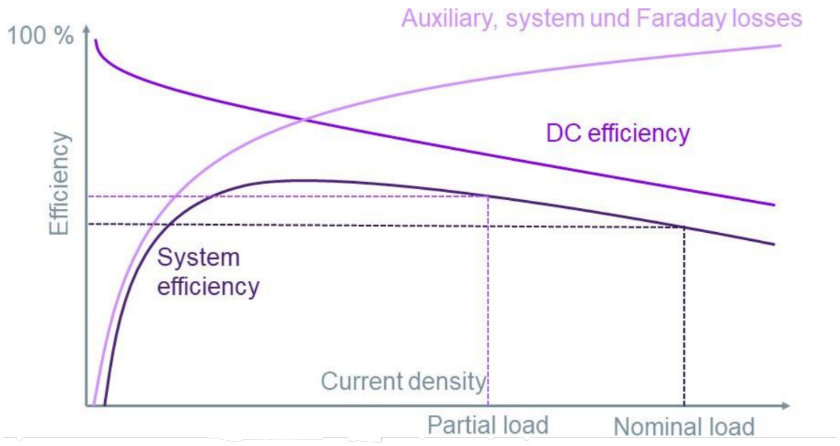

Figure 3.1: Electrolysis system efficiency and electrolyser stack efficiency (DC efficiency) [67].

Figure 3.1 illustrates that as the electrolyser power consumption (load) increases, the system efficiency undergoes a rapid rise. This is attributed to the significant auxiliary losses experienced at lower loads, despite having high DC efficiency. The operating point shifts along the x-axis as the load on the electrolyser grows, resulting in a corresponding change in system efficiency (shown by the black curve). The system efficiency reaches its optimal level, typically between 20-40% power consumption. As the power consumption continues to increase towards the nominal load (rated power), the system efficiency gradually declines due to the decrease in DC efficiency outweighing the efficiency gains from the auxiliary equipment [67].

In this study, the stack efficiency is utilized for calculating hydrogen production, as the BOP power consumption is calculated separately. In reality, the stack efficiency depends on the input power of the electrolyser stacks as can be seen in Figure 3.1. Additionally, the stack input power depends on the control strategy because the electrolyser stacks are modular designed. Therefore, in this research, the electrolyser stack efficiency is assumed to be independent of the input power and equal to the nominal load efficiency, as the control strategy of the electrolyser stacks is not in the scope of this research.

Degradation

Electrolyser degradation is a major challenge that must be addressed when designing and operating electrolysis systems for hydrogen production. Over time, the performance of an electrolyser degrades which result in decreased efficiency, decreased hydrogen production, and increased maintenance costs [56]. The electrolyser degradation rate is the rate at which the electrolyser degrades over time, typically measured in percentage points per full load hour [91]. The electrolyser degradation is calculated with an electrolyser degradation rate and the number of full load hours of the electrolyser. In this research, it is assumed that all electrolysers degrade simultaneously since the electrolyser system operation strategy is beyond the scope of this study. The full load hours are the number of hours that the electrolyser has been operating at full load.

Lifetime

The lifetime of an electrolyser is determined by its degradation and is measured in terms of the maximum number of full load hours of operation. The degradation rate of the electrolyser is currently defined as a linear relationship with the accumulated full load hours. Consequently, although a stack may still have some usability after reaching its lifetime, it becomes economically impractical to continue using it [41]. It is therefore crucial and advantageous for the annual hydrogen production to periodically replace the electrolyser stacks. By opting for equal full load hour distribution over the different stacks, the average electrolyser lifetime efficiency can be increased. Consequently, it is more advantageous to conduct replacements prior to the electrolysers reaching their end-of-life, enabling the utilization of new stacks in a similar manner.

Technology comparison

There are three main electrolysers types; Alkaline Electrolyser (AE), Proton Exchange Membrane Electrolyser (PEME) and Solid Oxide Electrolysers (SOE). AE and PEME are commercial available and only require electricity to produce hydrogen. SOE is relatively new, currently not commercially available and requires additional heat to produce hydrogen [17][90]. The SOE is a high temperature electrolyser operating at temperatures between 700-900°C. Besides, the SOE is still in early development phase. The use of SOE is therefore not preferable in offshore hydrogen electrolysis. For this reason, SOE is excluded further in this study.

PEME an AE are both modular designed system, meaning the electrolyser systems are made up of modules, also known as stacks, that can function independently of each other. To increase the capacity of the electrolyser system, electrolyser stacks can be added. The following sections describe the AE and PEME systems.

An AE electrolyser consist of an alkaline aqueous electrolyte, liquid water feed, monopolar or bipolar electrodes and a separation unit. The application of AE in various industries has spanned over a century, establishing it as a well-established and dependable technology [90][77].

A PEME consist of monopolar or bipolar electrodes, liquid water feed and a proton membrane electrolyte. In contrast to AE, PEME does not have a separation unit because H_2 and O_2 are formed at different electrodes [90]. Additionally, the development of PEME is still proceeding and therefore improvements in performance can be expected [62].

For offshore hydrogen production, a comparison is provided between AE and PEME. The comparison is made for the year 2019, 2030 and long term prediction data [55] [42].

	AE			PEME		
	2019	2030	Long term	2019	2030	Long term
Electrical efficiency (%)	50-68	65-71	>70	56-60	63-68	>80
Operating pressure (bar)	1-30			30-80		
Operating temperature (°C)	60-80			50-80		
Stack lifetime (Operating hrs.)	60 000 - 90 000	90 000 - 100 000	100 000 - 150 000	30 000 - 90 000	60 000 - 90 000	100 000 - 150 000
Load range (%, relative to nominal load)	10-110			0-160		
Plant footprint (m^2/kW_e)	0.095			0.048		

Table 3.1: AE and PEME specification comparison [42][90][66][77].

Weight and size are crucial considerations for the centralised, semi-centralised, and decentralised offshore wind-to-hydrogen configurations due to space limitations on the hydrogen substation and hydrogen wind turbine. In terms of electrolyser performance, several factors are significant, including electrical efficiency, cold start time, ramp-up and ramp-down time, and load range.

Table 3.1 demonstrates that PEME outperform AE counterparts in terms of plant footprint, load range, and comparable stack lifetime. Currently, the AE exhibits higher electrical efficiency compared to the PEME. However, it is anticipated that the PEME will eventually surpass the AE in terms of electrical efficiency.

The cold start time, ramp-up time, ramp-down time, and load range are particularly important due to the fluctuating input power generated by wind turbines. Alkaline electrolysers may face challenges in handling dynamic loads caused by fluctuating power in wind farms due to longer cold start time, narrower load range, and higher ramp-up and ramp-down times [15][62].

When comparing PEME and AE for offshore applications, the difference in output pressure becomes a crucial aspect to consider. Since hydrogen production takes place offshore, higher pressures are necessary for efficient hydrogen transmission. Therefore, a higher electrolyser output pressure offers advantages by reducing the need for extensive compression. In this regard, PEME outperform AE significantly in terms of output pressure.

Therefore, this report will exclusively focus on PEME, aligning with the electrolyser design choice made by Mehta et al. [51].

3.1.2. Balance of plant

In the three offshore wind-to-hydrogen configurations, the components and techniques used in BOP remain consistent, with the exception of their capacity, which is adjusted to the installed hydrogen production unit's capacity. The BOP consist of the water treatment and hydrogen purification. These components are critical for the successful functioning of the electrolysis plant as they enable the supply of high-quality water, necessary to obtain high quality hydrogen.

Water treatment

To facilitate the production of hydrogen using electrolysers, it is essential to use desalinated and deionized water because poor water quality is one of main reason for electrolyser stack failure [77]. Desalination, a process that removes salt and other impurities from seawater, plays a critical role in offshore hydrogen production systems. By integrating desalination technology within these systems, the need for an external water supply is eliminated. In this study, Seawater Reverse Osmosis (SWRO) is chosen as the desalination technology due to its widespread usage for seawater desalination [23][86]. The SWRO process involves the utilization of partially permeable membranes to selectively remove salt ions from water. Prior to entering the membrane units, the seawater is pressurized, and a portion of the pressure can be recovered to conserve energy. The SWRO system comprises two main outlets: a purified water stream and a brine disposal stream. Typically, the brine stream is three to four times larger than the purified water stream [23]. Following the desalination process, deionization is applied to further enhance the purity of the outlet stream from the reverse osmosis units.

Hydrogen purification

Hydrogen purification is a crucial process in offshore hydrogen production to ensure the purity and dryness of the hydrogen gas. It involves separating hydrogen from oxygen and subsequently purifying and drying the gas. Advanced technologies like membrane-based separation and Pressure Swing Adsorption (PSA) are employed for efficient and reliable gas treatment. In this study, the membrane-based separation and PSA methods are selected due to their efficiency, reliability, capability to meet purity requirements, flexibility, and compact design, making them well-suited for gas treatment in offshore wind-to-hydrogen [70].

3.1.3. Electrical system

The electrical system ensures the connection of the incoming electrical power from the wind turbine, wind turbine cluster or wind farm, to the electrolysers and the BOP. The electrical systems of centralised and semi-centralised electrolysis can be defined as high voltage electrical system and the electrical system of decentralised electrolysis as the low voltage electrical system as stated in Section 2.5.

High voltage electrical system

The electrical system of the centralised and semi-centralised configurations both consist of a switchgear, HVAC-LVAC transformer, AC-DC converter and a LV-LV transformer. The switchgear receives the incoming HVAC and connects the incoming power with the OHF. The switchgear functions as a safety barrier and could decouple the power form a wind turbine cluster or wind farm in case of power failures from the hydrogen substation or hydrogen platform respectively [77]. Hereafter, a HVAC-LVAC transformer is used to decrease the incoming HVAC power to LVAC power. The transformer is followed by a converter to convert the LVAC power to LVDC power necessary for the electrolysers [41]. Additionally, a LV-LV transformer is used to partly transform the LVAC power after the first transformer to LVAC power to power the BOP. The only difference between the electrical systems of centralised and semi-centralised electrolysis is the capacity of the components due to the difference in incoming power.

Low voltage electrical system

The electrical system of the decentralised configuration will be integrated in the wind turbine design due to the lack of electrical transmission. The electrical system of decentralised consist of a LV-LV transformer and an AC-DC converter. The incoming power from the wind turbine is LVAC power and the majority of power is converted to DC power by a AC-DC converter to power the electrolysers. The minority of LVAC power is transformed to a lower LVAC power by a LVAC-LVAC transformer to power the BOP. The capacity of the electrical components is scaled to the maximum capacity of the selected hydrogen wind turbine.

3.1.4. Hydrogen compressor

To ensure efficient hydrogen transmission to shore, hydrogen compression becomes necessary to overcome the pressure drop in a hydrogen pipeline. PEME typically generate hydrogen at a pressure output in the range of 30-35 bar, which serves as the starting point for hydrogen compression. Mechanical compressors are widely employed for this purpose, efficiently converting mechanical energy into compressed gas energy [46] [63]. Two common types of compressors are used for hydrogen compression: positive displacement compressors and dynamic compressors.

Positive displacement compressors operate by trapping a fixed volume of gas and subsequently reducing its volume to achieve compression. This process involves the use of pistons, screws, or other mechanisms that displace the gas, resulting in compression.

Dynamic compressors, on the other hand, leverage rotating impellers or blades to increase the kinetic energy of the gas. This heightened kinetic energy is then converted into pressure energy through a diffuser or volute.

When considering a compressor for offshore hydrogen compression, the following criteria are made; pressure range of 0 to 100 bar, high hydrogen flow rates and low maintenance requirements. When taking into account the criteria, a positive displacement compressor, specifically a reciprocating piston compressor, emerges as a suitable choice for the following reasons:

- Pressure Range: Reciprocating piston are well-equipped to handle the pressure range of 0 to 100 bar, making them suitable for the offshore wind-to-hydrogen configuration considered in this research.
- Reciprocating piston compressors excel at accommodating high hydrogen flow rates, making them highly suitable for effectively compressing the hydrogen flow required for megawatt-scale electrolysis and subsequent compression processes.
- Low Maintenance: Reciprocating piston compressors have a relatively simple design with fewer moving parts compared to some other compressor types. This simplicity contributes to lower maintenance needs and reduced downtime preferred in offshore systems.

While mechanical centrifugal compressors could also meet the selected criteria, their use may pose challenges due to high impeller tip speeds and the potential for hydrogen embrittlement [57]. Therefore, for all three offshore wind-to-hydrogen configurations, a reciprocating piston compressor is selected as the preferred choice.

3.2. Inter-array cables

The possible inter-array cables for energy transmission and differences per configuration are discussed in this section. In the decentralised configuration, the energy generated by the wind turbine is directly utilized by the electrolysers without the need for electrical cables. However, for both the centralised and semi-centralised configurations, medium or high voltage AC inter-array cables are required to transmit the electricity generated by the wind turbines to the centralised and semi-centralised substations.

In centralised and semi-centralised configurations, where wind turbines are connected in strings of multiple wind turbines at similar distances, the cable voltage capacity remains consistent. In the current design of offshore wind farms, inter-array cables are typically medium voltage (MV) cables with a voltage rating of 33kV or high voltage (HV) cables with a voltage rating of 66kV. By choosing 33kV cables instead of the standard 66kV AC inter-array cables, the need for larger transformers can be reduced. However, lowering the cable voltage restricts the maximum transmission power through the cables and increases cable losses. Therefore, careful consideration of cable voltage is essential during wind farm design.

3.3. Hydrogen pipelines

The possible hydrogen pipeline types for energy transmission and differences per configuration are discussed in this section. Hydrogen pipelines are essential for the transportation of hydrogen to shore in offshore wind-to-hydrogen configurations. The size of a pipeline depends on the flow characteristics of hydrogen, the friction factor of the pipeline and the pressure drop. This will be explained in detail in chapter 6.

The hydrogen pipelines can be divided into flexible infield flowlines and steel export pipelines. The difference between the pipelines relates mainly to the hydrogen transport capacity, structure and the flexibility and the cost of the pipeline.

Infield flowlines can be divided into bonded or unbonded flowlines. The primary distinctions among these flowline types lie in their relative roughness, which results in varying pressure drop per meter, different segment prices, and distinct stability characteristics. For unbonded flowlines that transport hydrogen, instability occurs on the seabed when their inner diameter exceeds four inches [22]. In this research, the maximum diameter assumed for bonded flowlines is six inches [36]. The flexible infield pipelines are well suited to connect small electrolyser facilities because of their plug and play principle and the flexibility to around monopile structures.

Steel export pipelines are well suited to transport large amount of hydrogen over larger distances because the diameter can easily be sized to gigawatt scale hydrogen transport [32] [82] [65]. It is preferable to use steel export pipelines if possible due to the lower price per meter of steel export pipelines compared to flexible infield pipelines [22]. For steel pipelines it is important to use internal coatings to prevent the pipelines from hydrogen embrittlement. Additionally, external corrosion protection is required to protect the steel pipeline from Galvanic corrosion [82].

In the centralised and semi-centralised configurations, steel export pipelines are used. A relatively large pipeline is required to transport all the hydrogen produced by the wind farm to the general hydrogen backbone pipeline. The flexibility of infield pipelines is not necessary for this large hydrogen transport and therefore steel export pipelines are preferable.

In the decentralised configuration, both infield flowlines and a single steel export pipeline are employed. The infield flowlines serve the purpose of transporting hydrogen from one decentralised offshore hydrogen turbine to another hydrogen wind turbine, as well as to the hydrogen assembly station. These flowlines are preferred due to their plug-and-play installation and flexible structure, which makes them well-suited for navigating around the monopiles, especially for difficult angles [74]. The hydrogen is then transported from the assembly station to the hydrogen backbone pipeline using a steel pipeline.

3.4. Hydrogen substation

This section relates to the hydrogen substations of the centralised and semi-centralised configurations. An overview of the hydrogen substation is given in Subsection 3.4.1. Hereafter, the substructures of the hydrogen substations are discussed in Subsection 3.4.2 followed by the superstructure in Subsection 3.4.3.

3.4.1. Hydrogen substation overview

A hydrogen substation consist of a substructure and the topside. The substructure functions as the base of the topside where the topside contains the HPU equipment and superstructure. The superstructure serves as the framework of the topside structure. Hydrogen substations in the centralised and semi-centralised configurations can be classified into two types: jacket substations and monopile substations. The distinction between these types is based on the substructure of the substations, and is determined by the mass of the substation topside. The substation topside comprises the superstructure and HPU equipment. Since the HPU equipment has already been discussed in Section 3.1, this section solely focuses on the substructure and the superstructure.

In Figure 3.2a and 3.2b, an example of both a jacket hydrogen substation and a monopile hydrogen substation is given showing the difference in scale.

(a) Jacket hydrogen substation

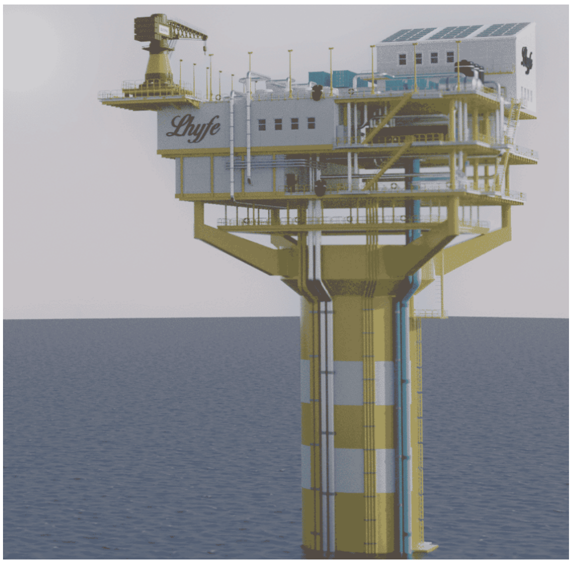

(b) Monopile hydrogen substation

Figure 3.2: Jacket and monopile hydrogen substation examples [58] [49].

3.4.2. Substructure

Currently, different substructure types are employed for offshore substations, including monopiles, jackets, floating and gravity-based structures (GBS). However, for the purpose of this research, the scope will be limited to monopiles and jacket substructures. In Figure 3.3, a schematic overview of a monopile and jacket substructure is given. Monopiles are commonly used in shallower to moderate water depths. These substructures consist of large steel cylindrical piles that are driven into the seabed. Monopiles are known for their excellent load-bearing capacity, making them suitable for supporting substations of relatively smaller sizes. Jacket structures, on the other hand, are frequently utilized in deeper waters. They feature lattice-like steel frames composed of vertical and diagonal members, providing support and stability to the substation. Jacket substructures offer enhanced strength and load-bearing capacity compared to monopiles, making them well-suited for larger and heavier substations.

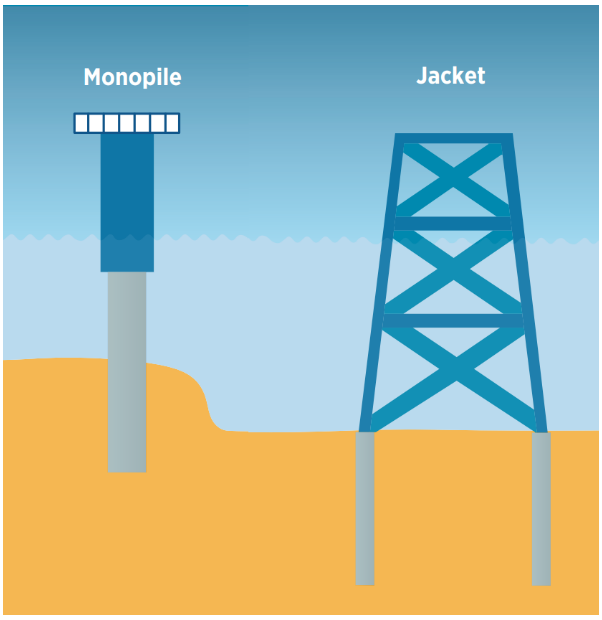

Figure 3.3: Monopile (left) and jacket (right) substructures [14].

To optimise synergies and reduce costs, utilizing the same monopile substructure for both the wind turbine and the substation is advantageous over the use of jacket substructures. This allows for shared infrastructure and construction processes. However, it is essential to ensure that the topside's mass remains within the maximum vertical load limit specified for the monopile substructure. The feasibility of using a monopile substructure for the substation depends on the installed electrolyser capacity, as it directly influences the topside's mass. Conversely, a jacket substructure can be adjusted to accommodate the topside mass of the substation and offers a higher maximum load capacity. The jacket substructure can be optimised within the feasible limits of transportation and installation to accommodate the maximum topside mass effectively.

3.4.3. Superstructure

The superstructure of a hydrogen substation is primarily constructed from steel and incorporates gratings as floors and claddings as walls. The superstructure serves as the framework for the topside as can be seen in Figure 3.2, providing housing and protection for the electrolysers, electrical equipment, and BOP components. The substation superstructure consists of multiple decks, varying in size based on the installed hydrogen production unit capacity [28]. These structures may also include features such as cranes, emergency shutdown systems, and fire protection systems to facilitate equipment movement, ensure safety, and prevent and manage fires on the substation.

3.5. Hydrogen wind turbine

This section provides detailed information about the offshore hydrogen wind turbine specifically for the decentralised configuration. First, an overview of a hydrogen wind turbine is given in Subsection 3.5.1. In Subsection 3.5.2, the substructure of a hydrogen wind turbine is discussed. Subsection 3.5.3, discuss the working platform superstructure.

3.5.1. Hydrogen wind turbine overview

The hydrogen wind turbine consists of two main elements: the substructure and the topside. The substructure serves as the foundation for the topside. The topside includes a working platform superstructure, which accommodates the HPU equipment, as well as the wind turbine tower and rotor nacelle assembly (RNA). In contrast to a conventional wind turbine, the distinguishing factor lies in the electrical system, as explained in Subsection 3.1.3 concerning the electrical systems. Figure 3.4 provides an illustration of a hydrogen wind turbine as an example.

Figure 3.4: Siemens Gamesa offshore hydrogen wind turbine [68].

It is worth noting that the wind turbine tower and RNA components in a hydrogen wind turbine are identical to those in a standard wind turbine. Therefore, the wind turbine tower and RNA components are not further discussed, as they do not differ from those found in standard offshore wind turbines.

3.5.2. Substructure

The substructure of an offshore wind turbine plays a vital role in providing the necessary foundation and stability for its operation in the marine environment. Various types of substructures are employed, such as monopile, jacket, and floating substructures. Monopile substructures consist of steel piles that are driven into the seabed and are commonly used in shallow waters. Jacket substructures are lattice-like steel structures assembled offshore, offering stability in deeper waters and challenging seabed conditions. Floating substructures are moored to the seabed, enabling the installation of wind turbines in deep waters. For the purpose of this research, only monopile substructures will be considered, aiming to establish synergies between the wind turbine and substation substructures, as outlined in the research scope (1.5).

3.5.3. Superstructure

The superstructure of the hydrogen wind turbine, referred to as the working platform, is primarily composed of steel material. It typically encompasses a single deck accompanied by protective walls to safeguard the HPU equipment, as indicated in [3]. The size of the working platform is contingent upon the specific installed capacity of the HPU. For an illustrative example of the working platform superstructure in an offshore hydrogen wind turbine, please refer to Figure 3.5.

Figure 3.5: Working platform superstructure of an offshore hydrogen wind turbine [68].

3.6. Hydrogen manifold

This section elaborates on the offshore hydrogen manifold in the decentralised configuration. The offshore hydrogen manifold primary function, is to act as a central hub for gathering hydrogen produced by the hydrogen wind turbines. Additionally, at the manifold, the collected hydrogen is compressed if necessary, and subsequent transported to the hydrogen backbone pipeline.

The manifold consists of two main components: the substructure and the topside. The substructure is designed as a monopile substructure, similar to that of the hydrogen wind turbines. This deliberate choice aims to create synergies between the manifold and the wind turbines, allowing for shared construction and installation methods, optimising efficiency, and reducing costs. The topside construction accommodates hydrogen infield flowline connections, hydrogen compressors and a battery system. The battery system serves as an energy storage solution which enables power supply to the hydrogen compressors during periods of low wind or varying demand. It stores excess electricity generated by the wind turbine, which can be utilized during temporary power shortfalls or peak demand periods. This enhances the overall stability and reliability of the manifold's operations.

To ensure sufficient power for the manifold's operations, it is supplied by the closest wind turbine connected by inter-array cables. This arrangement allows for a direct and efficient power supply, as the nearby wind turbine can provide the necessary electricity. This setup promotes energy efficiency and reduces the need for additional power generation at the manifold.

3.7. Offshore hydrogen facility transport and installation

This section relates to the transport and installation of a centralised substation, semi-centralised substation and decentralised offshore hydrogen turbine. For a decentralised offshore hydrogen turbine, regular wind turbine installation methods can be used with additional installation of the small scale electrolyser and BOP equipment. For the centralised and semi-centralised substations, large scale installation methods are required. For this, multiple methods exist for the transportation and installation of an offshore substation, and the choice depends on the substation's weight and size. Below, a method for the transport from the onshore construction side to the offshore substation sides is given. Followed by different possible installation methods.

Transport

Both the substructure and topside of a centralised and semi-centralised substation need to be transported from the onshore construction side to the offshore substation location. For both components, this can be done by a barge or a heavy transport vessel (HTV), depending on the distance of transportation. The selection between a barge or an HTV is influenced by factors such as distance and logistical considerations.

Installation

The installation process for a decentralised offshore hydrogen turbine, semi-centralised substation, and centralised substation begins with the installation of the substructures. For a monopile substructure, the foundation is drilled into the seabed. In the case of a jacket substructure, multiple pile foundations are drilled into the seabed, followed by the installation of the jacket substructure on top [28]. Once the substructure is placed, the topside of the substation can be installed.

The installation of the substructure and topside of an offshore decentralised offshore hydrogen turbine, semi-centralised substation or centralised substation, can be achieved through various methods, including a wind turbine installation vessel (WTIV), top lifting, gravity-based structures, float-over, and bottom lifting installation [9]. The main factor influencing the method selection is the maximum installation weight capacity. Here is a brief description of each method:

- WTIV: A WTIV is equipped with essential features such as a crane system, dynamic positioning, and onboard storage and workshop facilities [9]. The crane system of a WTIV provides the required lifting capacity and precision for installing various components, including wind turbine components, electrolysers, and BOP components for a decentralised offshore hydrogen turbine. Dynamic positioning ensures accurate positioning and stability during the installation process. Multiple WTIV vessels are available, with a maximum installation capacity of 1,500 tons [4].
- Top Lifting: In this method, a crane vessel is used to lift and install the substation module onto a pre-installed jacket. Semi-submersible crane vessels (SSCVs) such as SSCV Sleipnir, SSCV Thialf, and SSCV Saipem 7000 are commonly employed for this purpose. The maximum weight that can be handled by the crane vessel ranges from 4,000 to 18,000 tons [28].
- Gravity-Based Installation (GBS): GBS installations utilize gravity-based structures as the substructure for the offshore substations. These structures, constructed onshore or in dry docks, are then floated to the installation site and ballasted to sink onto the seabed. Tugboats or specialized vessels are typically involved in the towing and positioning of GBS structures.The maximum weight limit of the GBS installation methods is assumed to be 25,000 tons [13].
- Float-over: The float-over method involves transferring the substation module from a transport vessel to the jacket by aligning and sliding it onto the jacket. Barges or HTVs are typically employed for this procedure. The maximum weight that can be accommodated in a float-over installation is assumed to be 32,000 tons [76].
- Bottom Lifting: A specialized vessel equipped with a topside lifting system, such as Pioneering Spirit, is utilized in this method. The substation module is lifted and installed using this system. Pioneering Spirit, along with the barge Iron Lady or an HTV, is commonly involved in bottom lifting installations. Pioneering Spirit has a maximum lift capacity of 48,000 tons [6].

4
Model framework

The centralised, semi-centralised and decentralised offshore wind-to-hydrogen configurations are compared qualitatively in chapter 2 and 3 on their technical aspects and feasibility. In order to compare the configurations quantitatively on their technical and financial performance a financial metric will be used. The required inputs of the financial metrics are obtained from existing in-house Vattenfall models or new models developed for this research. This chapter provides an overview of the already existing models, required models and the workflow between the models will be provided. Additionally, the in-house vattenfall models will be discussed briefly in this chapter while the new developed models will be explained each in their own separate chapter. Moreover, this chapter selects and describes a financial matrix appropriate to the objective of this study to analyse the techno-economic feasibility of semi-centralised compared with centralised and decentralised hydrogen production. In section 4.1, an overview of the required models and the workflow between the different models will be given. Followed by Section 4.2, where the financial metric will be described. Hereafter, in Section 4.4, the layout optimisation model of Vattenfall is briefly explained. Finally, in Section 4.4, the model to obtain the wind farm cost is discussed.

4.1. Workflow description

This section describes the workflow between the different models used to calculate the required values for the financial metric described in section 4.2. In Figure 4.1, a schematic overview of the models is given. In this overview, the in-house Vattenfall models are depicted in yellow, the new developed models in green and the financial metric in blue. The arrows between the models denote main input and output relations between the models.

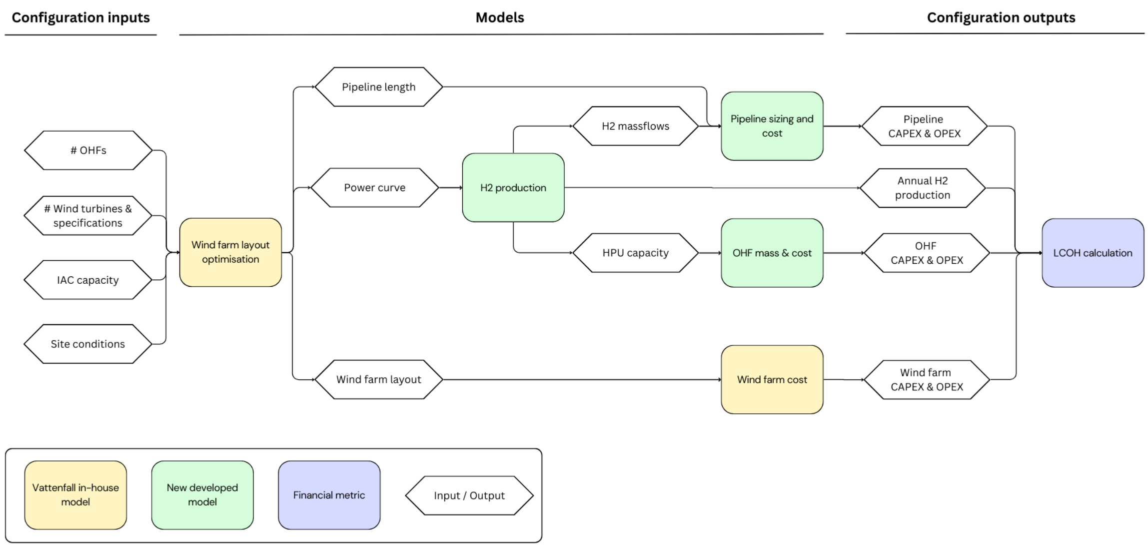

Figure 4.1: Schematic overview of the workflow between Vattenfall in-house models and new developed models.

The design of wind farm layouts with optimised electricity production and associated cost information is a key component to be able to compare different offshore wind-to-hydrogen configurations. Vattenfall incorporates an internal model known as FEPM to create optimised wind farm layouts and calculate the costs associated with them. As a result, the workflow overview includes a representation of both a wind farm layout optimisation model and a wind farm cost model. The wind farm layout optimisation model optimises wind farm layouts for specific sites, by placing offshore substations, wind turbines, and cable routing. The model is capable of creating layouts for a selected number and type of wind turbines and substations, with the aim of minimising the levelised cost of electricity. The wind farm cost model is used to calculate the non-hydrogen cost of the wind farm. Both the layout optimisation model and wind farm cost model will be further discussed in Section 4.3 and 4.4 respectively as they are existing models.

Hereafter, the hydrogen production model calculates the annual hydrogen production of the offshore wind-to-hydrogen configuration. The electrical wind farm power curve from FEPM is used to calculate the wind farm hydrogen flow rate curve based on the energy distribution, electrolyser efficiency, and different loss and availability factors. The hydrogen flow rate curve together with the wind speed distribution and degradation factors results in the annual hydrogen production.

Additionally, the pipeline lengths obtained from FEPM together with the hydrogen mass flow rates from the hydrogen production model, are used to calculate the optimal hydrogen pipeline diameters and the associated cost in the hydrogen pipeline sizing & cost model. First, the pipeline sizing model calculates the minimum pipeline diameter required for each pipeline segment based on two important inputs: pipeline segment length and maximum hydrogen mass flow rate. The length of the pipeline segment is important because it influences the pressure drop that occurs in the pipeline due to friction and other losses. The maximum hydrogen mass flow rate determines the maximum amount of hydrogen gas that needs to be transported through the pipeline at any given time. Once the pipeline length and maximum hydrogen mass flow rate have been obtained, the pipeline sizing model uses these inputs to calculate the minimum pipeline diameter required for each pipeline segment to overcome the pressure drop. This calculation takes into account factors such as flow velocity and pipe material properties to ensure that the pipeline is able to safely and efficiently transport the hydrogen gas. The hydrogen pipeline cost model calculates the pipeline cost based on the pipeline length, the pipeline diameters and associated procurement, logistic and non-material cost.

Hereafter, the hydrogen substation and hydrogen wind turbine cost are calculated by the offshore hydrogen facility mass & cost model. The model first calculates the topside mass of the substation or hydrogen wind turbine, using the installed HPU capacity. The mass of the topside determines the type of substation substructure type. Once the topside mass and the type of substructure have been established, the model calculates the breakdown of costs. These include expenses for HPU equipment, topside superstructure, substructure, non-material, manifold and transportation, installation and commissioning.

Finally, the annual hydrogen production, wind farm costs, offshore hydrogen facility costs, and hydrogen pipeline costs are utilized in the calculation of the Levelised Cost of Hydrogen (LCOH). This enables a comparison of various offshore wind-to-hydrogen configurations.

4.2. Levelised cost of hydrogen

The LCOH is used to quantitatively compare the different offshore wind-to-hydrogen configurations. The LCOH is a useful metric for comparing different offshore wind-to-hydrogen configurations because it provides a comprehensive assessment of the economic viability and competitiveness of each configuration over the project's lifecycle. The LCOH includes the capital expenditures (CAPEX), operational expenditures (OPEX) and hydrogen production. The CAPEX and OPEX represent the financial part of a wind-hydrogen configuration. The hydrogen production represents mostly the technical performance of the offshore wind-to-hydrogen configuration. The LCOH can be calculated with equation 4.1 [71].

$$\mathrm{LCOH} = \sum_{y=0}^{LT_y} \frac{\mathrm{CapEx}_{\mathrm{ELEN},y} + \mathrm{OpEx}_{\mathrm{ELEN},y} + \mathrm{CapEx}_{\mathrm{PtH},y} + \mathrm{OpEx}_{\mathrm{PtH},y}}{(1+\mathrm{DR})^y} / \sum_{y=0}^{LT_y} \frac{\mathrm{M}_{\mathrm{H}_2,y}}{(1+\mathrm{DR})^y} \tag{4.1}$$

This equation consist of the CAPEX and OPEX related to the electrical energy ($\mathrm{CapEx}_{\mathrm{ELEN}}$,$\mathrm{OpEx}_{\mathrm{ELEN}}$) and power to hydrogen ($\mathrm{CapEx}_{\mathrm{PtH}}$,$\mathrm{OpEx}_{\mathrm{PtH}}$). Additionally, in this equation, $\mathrm{M}_{\mathrm{H}_2}$ represents the annual hydrogen production mass, DR the discount rate, LT the lifetime of the wind-to-hydrogen farm and y is the production year ranging form 0 to LT.

The LCOH is used for the evaluation of potential profitability, informed investment decision-making, and assessment of project development opportunities. This metric enables the analysis and comparison of the cost-effectiveness of various hydrogen production pathways, providing valuable insights into the market competitiveness of hydrogen as an energy carrier.

4.3. Wind farm layout optimisation

This section provides a brief explanation of Vattenfall's in-house model for optimising the layout of wind farms. The objective is to maximize the energy production of the wind farm while minimising costs associated with the installation, maintenance, and operation of wind turbines and related infrastructure. Vattenfall's model employs a systematic approach to this optimisation process, consisting of three main steps: substation positioning, substation connection, and unified wind turbine positioning and cable routing. The inputs to the model include the wind farm's expected lifetime, site data, the number and specifications of wind turbines, as well as the specifications of inter-array cables.

The first step involves optimising the positioning of substations to minimise the total length of cables required for efficient power transmission. The optimal positions are determined by considering the wind farm's site data and the number of offshore substations. The model selects locations where the sum of distances from each substation to the wind turbines is minimised.

In the substation connection step, the connections between substations, as well as the connection between a substation and the backbone pipeline using hydrogen pipelines, are established manually. Optimal pipeline routes are determined based on minimising the total length of pipelines. This approach aims to reduce overall installation and maintenance costs by minimising the total pipeline length.

The final step involves unifying the positioning of wind turbines and cable routing [18]. The model iteratively places the turbines to maximize energy production while minimising wake losses and the levelized cost of electricity. The model takes into account wind direction and speed frequency distributions. Simultaneously, cable routing is optimised to efficiently connect turbines to substations. The model ensures that the cable routes are as short as possible while adhering to given restrictions, such as avoiding cable crossings.

4.4. Wind farm cost

The wind farm cost relates to all cost in a wind-to-hydrogen farm except for the cost associated directly to hydrogen, namely; the offshore hydrogen facility, hydrogen pipelines and hydrogen manifold cost. Additionally, this study combines the different cost components of the wind farm cost, such as wind turbines, foundations, cables, transport, installation, and other project-related expenses, in order to calculate one single total CAPEX value and one single total OPEX value per year over the lifespan of the wind farm. The costs of the wind farm components will be aggregated due to the confidentiality of Vattenfall's internal models. However, this information is still useful to determine the wind farm cost for each offshore wind-to-hydrogen configuration in the offshore wind-to-hydrogen farm. The research focuses on analysing the cost values that vary per offshore wind-to-hydrogen configuration, specifically the expenses related to cables, transport and installation, and decommissioning of the wind farm.

For both the centralised and semi-centralised configuration, the cost estimates for standard wind farm are directly derived from the in-house Vattenfall model, which provides the CAPEX and OPEX associated with building and running the wind farm. However, it's important to note that the costs associated with the hydrogen infrastructure components, namely the OHFs and the Hydrogen pipelines, are not included in the Vattenfall model.

For the decentralised configuration, the wind farm cost can not directly be obtained from the in-house Vattenfall model. Therefore, modifications need to be made because of the significant differences in design compared to a stand wind farm.

5 Hydrogen production modeling

This chapter focuses on the hydrogen production of an offshore wind-to-hydrogen farm. To determine the LCOH for an offshore wind-hydrogen farm, the annual hydrogen production must be calculated. Therefore, the primary objective of this model is to estimate the hydrogen production of a specific offshore wind-to-hydrogen farm configuration. The method used to calculate the annual hydrogen production is similar for different configurations. The primary distinctions arise from the configuration-specific energy loss factors. The model overview is given in Section 5.1 together with the annual hydrogen production equation. Section 5.2 provides insights into the HPU input power, while Section 5.3 elaborates on the power distribution. Section 5.4 outlines the hydrogen flow rate calculations. Finally, Section 5.5 elaborates on the intermediate results of the hydrogen production model taking into account the assumed constants for the model.

5.1. Hydrogen production model overview

This section provides an overview of the hydrogen production model for hydrogen production through electrolysis powered by offshore wind energy. The hydrogen production model calculates the annual hydrogen production for an offshore hydrogen facility. The annual hydrogen production per OHF can be calculated by considering the annual wind speed distribution and the hydrogen flow rate curve per OHF, which incorporates the power distribution factors, electrolyser efficiency (including degradation), electrolyser replacements and availability factors. By multiplying the annual probability per wind speed by the total hours per year and the hydrogen flow rate per wind speed, the hydrogen production per wind speed can be determined. The total annual hydrogen production per OHF is calculated with Equation 5.1, summing the annual hydrogen production per wind speed for year y.

$$\mathrm{AHP}_{\mathrm{OHF},y} = \sum_{i=1}^{N} \left(\mathrm{p}_{i,y} \cdot 8760 \cdot \mathrm{HFR}_{i,y} \cdot \mathrm{AF}_{\mathrm{HPU}} \right) \tag{5.1}$$

In this equation, $\mathrm{AHP}_{\mathrm{OHF},y}$ represents the total annual hydrogen production per OHF, N represents the number of wind speed data points considered, $\mathrm{p}_{i,y}$ represents the annual probability associated with wind speed bin i, $\mathrm{HFR}_{i,y}$ represents the hydrogen flow rate corresponding to wind speed bin i in year y and $\mathrm{AF}_{\mathrm{HPU}}$ is the availability factor of the HPU. The multiplication by 8760 represents the total number of hours in a year.

The availability factor is a critical parameter for assessing the operational reliability and performance of offshore wind-to-hydrogen configurations. To simplify the analysis, the availability factors of the electrolyser stacks, BOP and OHF electrical system components are combined into a single value representing the annual availability of the entire HPU. It quantifies the percentage of time that the HPU is available and operational. Given the nascent stage of OHF designs and the scarcity of accessible data, it’s currently assumed that the availability factor of the HPU remains constant across different offshore wind-to-hydrogen configurations. However, it is important to note that although this assumption is reasonable, there are potential factors that could result in different availabilities. For instance, in a centralised OHF design, if there is a failure in the centralised substation, the entire wind farm would be affected, compared to a decentralised case where only one hydrogen wind turbine would be impacted. Furthermore, safety considerations may require the shutdown of the entire centralised substation during maintenance due to explosion risks and other safety concerns. These factors could potentially lead to variations in the availability of the OHF configurations.

The total annual hydrogen production of a wind-to-hydrogen configuration is calculated by summing the annual hydrogen production of all OHFs within a wind-to-farm. Equation 5.2, calculates the offshore wind-to-hydrogen annual hydrogen production (AHP_{OWHF}).

$$\text{AHP}_{\text{OWHF},y} = \sum_{\text{OHF}} \text{AHP}_{\text{OHF},y} \tag{5.2}$$

To calculate the annual hydrogen production, the model utilizes an integration approach, specifically the integration of the hydrogen flow rate curve (HFR_i), the probability density function of the wind speed distribution (p_i), and the differential wind speed (d_i). This integration allows for a comprehensive evaluation of the hydrogen production potential based on the available wind resources.

To determine the hydrogen flow rate curve, the electrical power curve from FEPM is used, representing the power produced by the wind turbines. The model first takes into account the power curtailment, which represents the maximum input power of the hydrogen production units. This functionality is required to size the hydrogen production unit versus the installed wind turbine capacity and to create an adjusted electrical power curve. This adjusted power curve is the input to the hydrogen production unit. Hereafter, the power distribution is determined by calculating the power demand per component. Hereby, the percentage of power available for electrolysis is determined. This is followed by the electrolyser efficiency and degradation calculation. The power distribution and the electrolyser annual efficiency together with the overall annual wind farm degradation are used to convert the electrical power curve into a hydrogen flow rate curve for each year during the lifetime of the wind-to-hydrogen farm.

5.2. Hydrogen production unit input power

The annual hydrogen production per OHF can be calculated using the HPU input power. The HPU input power is derived from the electrical power curve per OHF and the curtailment factor. The wind turbine specifications, wake losses, wind farm availability and electrical losses regarding power conversion, transformation and transmission, are included in the electrical power curve for an OHF. The wind farm degradation and the electrical system at the OHF are not included and will be added separately.

The HPU electrical input power for each year of operation is determined by multiplying the initial electrical power curve with the wind farm degradation factor and the OHF electrical system efficiency. The HPU input power curve per year for an OHF, considering degradation and electrical system efficiency, is calculated using Equation 5.3.

$$P_{\text{HPU},i,y} = P_{\text{OHF},i} \cdot (1 - \text{DR}_{\text{WF}})^y \cdot \eta_{\text{OHF,ES}} \tag{5.3}$$

In this Equation, ($P_{\text{HPU},i,y}$) represents the HPU input power for an OHF per wind speed bin i and year y. $P_{\text{OHF},i}$ denotes the initial OHF electrical input power at that particular wind speed bin without considering degradation effects and OHF electrical system losses. DR_{WF} represents the wind farm degradation rate, which captures the gradual reduction in power generation capability over time. The symbol $\eta_{\text{OHF,ES}}$ represents the electrical system efficiency of the OHF for both the high voltage and low voltage electrical systems ($\eta_{\text{OHF,HV-ES}}$ & ($\eta_{\text{OHF,LV-ES}}$)). The efficiency of the high voltage electrical system differs from that of the low voltage electrical system due to the inclusion of an additional power transformation step in the high voltage system.

5.3. Power distribution

The power distribution at the OHF involves the allocation of electrical power from the wind turbines to various systems required for hydrogen production and processing. This section provides information regarding the power distribution overview in Subsection 5.3.1. Additionally, the subsequent subsections provide information on the power demand per component of the HPU.

5.3.1. Power distribution overview

The electrical power is first transmitted through cables to the electrical systems, as explained in Section 2. Once the electrical power reaches the substation, the electrical system transforms and converts the HVAC power to LVDC power with a specific efficiency of the OHF electrical equipment components. Following the electrical system, power is allocated to the electrolyser stacks, BOP equipment, and compressors based on their respective power requirements for hydrogen production and processing. The ancillary step of water pumping, which involves supplying sea water to the desalination unit and circulating cooling water through the electrolysis process, consumes a specific amount of power, and is duly considered in the power distribution analysis. Furthermore, it is assumed that the power demand associated with ancillary steps such as power control and data communication is negligible and can be disregarded in the overall power distribution.

To ensure efficient power distribution, the power demand of each system is determined by evaluating the power demand necessary for the production and processing hydrogen. The total power demand of the HPU to process and produce hydrogen (P_{HPU}) is given in Equation 5.4.

$$P_{\text{HPU}} = P_{\text{electrolyser}} + P_{\text{desalination}} + P_{\text{compression}} + P_{\text{purification}} + P_{\text{pump}} \tag{5.4}$$

This equation includes the power demand of the electrolyser ($P_{\text{electrolyser}}$), desalination unit ($P_{\text{desalination}}$), compression system ($P_{\text{compression}}$), hydrogen purification ($P_{\text{purification}}$) and water pump system (P_{pump}). The following subsections provide further details on the power demand per component, elaborating on their respective contributions to the overall power demand to produce and process hydrogen.

5.3.2. Electrolysis

The power demand of the electrolyser stacks can be calculated with the Higher Heating Value (HHV) of hydrogen and the electrolyser efficiency ($\eta_{\text{electrolyser},y}$) in year y [67]. The HHV of hydrogen refers to the heat released per kilogram (originally at 25 °C) when it undergoes complete combustion, with the resulting products returning to a temperature of 25 °C. The HHV takes into account the latent heat of vaporization of water that is formed during the combustion process [10]. The annual electrolyser efficiency ($\eta_{\text{electrolyser},y}$) refers to the percentage of input electrical energy that is converted to hydrogen gas output in year y. The power demand of the electrolyser can be calculated with Equation 5.5 [71]. Where $\dot{m}_{\text{H}_2}$ is the hydrogen mass flow rate.

$$P_{\text{electrolyser}} = \dot{m}_{\text{H}_2} \cdot \frac{\text{HHV}_{\text{H}_2}}{\eta_{\text{electrolyser},y}} \tag{5.5}$$

The annual electrolyser efficiency plays a significant role in determining the annual hydrogen production of the wind farm, as discussed in Subsection 3.1.1. Over time, the electrolyser efficiency degrades and eventually reaches its maximum lifespan. The annual electrolyser degradation is calculated with an electrolyser degradation rate and the number of full load hours of the electrolyser per year. The full load hours represent the cumulative number of operating hours for the electrolyser, considering both full load hours and partial-load hours.

The number of electrolyser full load hours per year (FLH_y) is calculated with equation 5.6. In this equation, $E_{\text{electrolyser},y}$ is the electrolyser input energy in year y and $P_{\text{electrolyser},rated}$ is the electrolyser installed capacity.

$$\text{FLH}_y = \frac{E_{\text{electrolyser},y}}{P_{\text{electrolyser},rated}} \tag{5.6}$$

By multiplying the full load hours in year y (FLH_y) with the degradation rate ($\text{DR}_{\text{electrolyser}}$), the annual electrolyser degradation ($\text{AD}_{\text{electrolyser}y}$) in year y, is calculated with Equation 5.7.

$$\text{AD}_{\text{electrolyser},y} = \text{DR}_{\text{electrolyser}} \cdot \text{FLH}_y \tag{5.7}$$

The electrolyser end-of-year efficiency ($\eta_{\text{electrolyser-end},y}$) in year y is then calculated by subtracting the annual degradation from the electrolyser efficiency at the start of year y ($\eta_{\text{electrolyser-start},y}$) in Equation 5.8. Hereafter, the average electrolyser efficiency ($\eta_{\text{electrolyser},y}$) in year y is calculated from the start and end-of-year efficiency with Equation 5.9.

$$\eta_{\text{electrolyser-end},y} = \eta_{\text{electrolyser-start},y} - \text{AD}_{\text{electrolyser},y} \tag{5.8}$$

$$\eta_{\text{electrolyser},y} = \frac{\eta_{\text{electrolyser-start},y} + \eta_{\text{electrolyser-end},y}}{2} \tag{5.9}$$

By employing the average electrolyser efficiency, the calculation of the annual hydrogen production becomes more straightforward, as it does not involve complex iterative processes or detailed analysis of degradation dynamics. However, it is important to acknowledge that this assumption may not capture the exact efficiency variations throughout the year, particularly in cases where non-linear degradation patterns or significant variations exist.

In order to calculate the electrolyser efficiency accurately during the lifetime of the wind-to-hydrogen farm, it is necessary to consider the number of electrolyser stack replacements. By taking into account the number of electrolyser stack replacements, the impact of new stacks with higher efficiencies replacing older ones is taken into account. The minimum number of electrolyser stack replacement (N_{minSR}) during the lifetime of the wind-to-hydrogen farm is determined with the maximum stack lifetime (LT_{stack}) and the sum of the annual full load hours (FLH_y) during the lifetime. Equation 5.10 is used to calculate the minimum number of stack replacements.

$$N_{\text{minSR}} = \frac{\sum \text{FLH}_y}{\text{LT}_{\text{stack}}} - 1 \tag{5.10}$$

5.3.3. Desalination

The power demand of the desalination unit to produce desalinated water as input for the electrolyser stacks is calculated with equation 5.11 [71].

$$P_{\text{desalination}} = \dot{m}_{\text{H}_2} \cdot \frac{DWC_{\text{electrolysers}} \cdot e_{\text{desalination}}}{\eta_{\text{desalination}}} \tag{5.11}$$

In this equation, the desalinated water consumption of electrolysers is given as $DWC_{electrolysers}$. Additionally, the energy to process seawater in the desalination unit is given as $e_{desalination}$ and an efficiency factor denoted as $\eta_{desalination}$ is applied [69]. The efficiency factor is applied because during the desalination process, not all seawater is transformed into desalinated water due to inevitable water losses [42][69].

5.3.4. Hydrogen compression

The power demand of the compressors depends on the desired hydrogen pressure of the hydrogen substation. The power demand of the compressors can be calculated with the adiabatic compression equation 5.12 [52].

$$P_{compressor} = \dot{m}_{\text{H}_2} \cdot \frac{c_{\text{comp},1} \cdot T_{MEAN}}{\eta_{COMP} \cdot G_{H_2} \cdot c_{\text{comp},2}} \cdot \left(\frac{\gamma \cdot N_{ST}}{\gamma - 1}\right) \cdot \left[\left(\frac{p_{COMP,OUT}}{p_{COMP,IN}}\right)^{\frac{\gamma-1}{\gamma \cdot N_{ST}}} - 1\right] \tag{5.12}$$

This equation involves several variables and constants that are important for calculating the power required to compress hydrogen gas. The compression efficiency is denoted as η_{COMP}. The specific heat capacities of hydrogen gas are represented by the ratio $\gamma = c_v/c_s$. The value of γ depends on factors such as the temperature and pressure of the gas. The mean temperature, denoted as T_{MEAN}, is assumed to be constant and represents the average temperature during the compression process. The gas gravity of hydrogen gas is denoted as G_{H2}. The input pressure of the compressor is denoted as $p_{COMP,IN}$, while the output pressure is indicated as $p_{COMP,OUT}$. The number of compressor stages is denoted as N_{ST} and can be calculated with equation 5.13, where r_{stage} is the compression ratio per stage [35].

$$N_{ST} = \frac{ln(\frac{p_{COMP,OUT}}{p_{COMP,IN}})}{ln(r_{stage})} \tag{5.13}$$

In this study, most variables remain constant except for the input and output pressure, which play a significant role in determining the compressor power demand. The specific input and output pressure settings of the compressors directly affect the power demand during the compression process.

5.3.5. Water pump system

To provide water to the desalination unit and the cooling system, a water pump system is necessary. In this study, a simplified calculation method is employed to estimate the power demand of the pump system, considering its minimal impact on the overall power distribution.

The pump system for the desalination unit is assumed to be an open loop system, while the pump system for the cooling system is considered a closed loop system. To determine the power demand of the open loop system, the hydraulic power required to pump seawater to a specific height is calculated, considering the energy efficiency of the pump [79]. In the closed loop system, the pump power demand is mainly caused by friction losses. For simplicity, it is assumed that the power demand caused by friction losses, is a fraction of the power demand of an open loop system and therefore is determined using a friction loss factor. By applying this simplified method, the losses due to friction within the closed loop system are taken into account [35]. Since it is anticipated that the pump power demand of the closed loop system is not significant, it is deemed possible to use this assumption. The equation for the power demand of pumping seawater to an offshore substation located at a certain height above sea level can be determined using equation (5.14) [79].

$$P_{\text{pump}} = \frac{\rho_{\text{seawater}} \cdot g \cdot Q_{\text{desalination}} \cdot H}{\eta_{\text{pump}}} + \frac{\mu_{\text{closed-loop}} \cdot \rho_{\text{seawater}} \cdot g \cdot Q_{\text{cooling}} \cdot H}{\eta_{\text{pump}}} \tag{5.14}$$

In this equation, P_{pump} represents the power demand of the pump system (in kW) required to supply the desalination and cooling system with the amount of water necessary to produce and process hydrogen. Additionally, $\mu_{\text{closed-loop}}$ is the friction factor for the open loop system, ρ_{seawater} is the density of seawater, g is the gravity constant, $Q_{\text{desalination}}$ is the volumetric flow rate of seawater for desalination, Q_{cool} is the volumetric flow rate of seawater for cooling, H is the total head between the sea level and the substation, and η_{pump} is the efficiency of the pump.

The volumetric flow rate of the water supply for the desalination system and the water input of the cooling system are calculated with the equation 5.15 and 5.16 respectively. In both equations, Q represents the volumetric flow rate of the desalination and cooling respectively. SWC_{cooling} represents the seawater water consumption for cooling.

$$Q_{\text{desalination}} = \dot{m}_{\text{H}_2} \cdot \frac{DWC_{\text{electrolysers}}}{\eta_{\text{desalination}}} \tag{5.15}$$

$$Q_{\text{cooling}} = \dot{m}_{\text{H}_2} \cdot SWC_{\text{cooling}} \tag{5.16}$$

5.3.6. Hydrogen purification

The process of hydrogen purification involves the utilization of Pressure Swing Adsorption (PSA) as discussed in Section 3.1.2. The amount of power consumed by PSA is influenced by various factors, including the rate at which hydrogen flows, the operating pressure, the desired level of hydrogen purity, and the specific power demand of the PSA system. To simplify matters, we assume a constant specific power demand of hydrogen processed in the PSA system [50]. Since it is anticipated that the power demand of the hydrogen purification process are small, it is deemed possible to use this assumption. Therefore, the power demand of gas separation and hydrogen purification system can be estimated using equation 5.17 [50]. $P_{\text{purification}}$ is the PSA system power demand and $p_{\text{purification}}$ is the specific power demand of the purification.

$$P_{\text{purification}} = \dot{m}_{\text{H}_2} \cdot p_{\text{purification}} \tag{5.17}$$

5.4. Hydrogen flow rate

In Section 5.2, an electrical power curve is given. This power curve can be used to estimate the amount of hydrogen that could be produced at different wind speeds. The electricity production is converted into hydrogen production estimates, taking into account the HPU installed capacity, the electrolyser efficiency and the power distribution given in Section 5.3.1. The equation to translate the electrical power curve into a hydrogen flow rate curve in year y, is given in equation 5.18.

$$\text{HFR}_{i,y} = \frac{P_{\text{HPU},i,y} \cdot pd_{\text{electrolyser},i,y} \cdot \eta_{\text{electrolyser},y}}{\text{HHV}_{H_2}} \tag{5.18}$$

In this equation, $\text{HFR}_{i,y}$ is the hydrogen flow rate per wind speed bin i per year y, $P_{\text{HPU},i,y}$ is the HPU input power per wind speed bin i per year y, $pd_{\text{electrolyser}}$ is the electrolyser power distribution factor and HHV_{H_2} is the higher heating value of hydrogen.

To calculate the electrolyser power distribution factor, equation 5.19 is utilized. In this equation, $P_{\text{electrolyser},i,y}$ represents the power demand of the electrolysers, while $P_{\text{HPU},i,y}$ represents the total power demand of the HPU, taking into account the electrolysers efficiency, compressor input pressure, and compressor output pressure.

$$pd_{\text{electrolyser},i,y} = \frac{P_{\text{electrolyser},i,y}}{P_{\text{HPU},i,y}} \tag{5.19}$$

5.5. Hydrogen production model demonstration

This section aims to demonstrate the functionality of the hydrogen production model. First the constants used are given in Subsection 5.5.1. Hereafter, the hydrogen production unit input power is analysed in Subsection 5.5.2. Furthermore, the power distribution is discussed in Subsection 5.5.3, followed by the hydrogen flow rate in Subsection 5.5.4. Finally, in Subsection 5.5.6, the annual hydrogen production is given.

5.5.1. Hydrogen production model constants

The constants used in the hydrogen production model are depicted in Table 5.1.

Parameter	**Symbol**	**Value**	**Unit**	**Source**
HPU input				
Wind farm degradation rate	$\text{DR}_{\text{WF},y}$	X	%/yr	[72]
OHF HV-electrical system efficiency	$\eta_{\text{OHF,HV-ES}}$	96.2	%	[38]
OHF LV-electrical system efficiency	$\eta_{\text{OHF,LV-ES}}$	96.4	%	[38]
Electrolysis				
Initial PEME stack efficiency	$\eta_{\text{electrolyser}}$	80.0	%	[41]
Hydrogen higher heating value	HHV_{H2}	39.4	kWh/kg	[21]
Electrolyser degradation rate	$\text{DR}_{\text{electrolyser}}$	0.1	%./1000 FLH	[91]
Electrolyser stack lifetime	LT_{stack}	80000	FLH	[27][42]
Desalination				
Desalinated water consumption	$DWC_{\text{electrolysers}}$	15	l/kg	[80, 69]
Desalination energy	$e_{\text{desalination}}$	0.0035	kWh/l	[42, 69]
Seawater desalination efficiency	$\eta_{\text{desalination}}$	60.0	%	[69]
Compression				
Compressor constant 1	$c_{\text{comp},1}$	286.76	-	[52]
Compressor constant 2	$c_{\text{comp},2}$	$3.6 \cdot 10^9$	-	[52]
Mean compression temperature	T_{MEAN}	285.15	Kelvin	[87]
Gas gravity of hydrogen gas	G_{H_2}	0.0696	-	[71]
Compression ratio per stage	r_{stage}	2	-	[2]
Compression efficiency	$\eta_{\text{CO M P}}$	50	%	[81]
H_2 specific heat capacities ratio	γ	1.41	-	[30]
Pumping				
Cooling sea water consumption	$SWC_{\text{electrolysers}}$	15	l/kg	[80, 69]
Seawater density	μ_{pump}	1027	kg/m^3	[16]
Head height	H	20	m	Estimate
Gravity constant	g	9.81	m/s^2	
Closed loop pump friction factor	μ_{pump}	1	%	[35]
Purification				
Specific power demand for PSA system	$p_{\text{purification}}$	1800	kW/kgH_2s^{-1}	[50]
HPU availability				
HPU availability factor	AF_{HPU}	97.5	%	[37]

Table 5.1: Hydrogen production model constants.

5.5.2. Hydrogen production unit input power

An OHF electrical power curve example for a 1GW wind farm is shown in Figure 5.1. In this figure, the wind farm power output and HPU input power including high voltage and low voltage electrical system efficiency are depicted. The shape of the curves are related to the specifications of the wind turbines connected to the OHF. Additionally, the size of the power curve is related to the amount of wind turbines connected to the OHF.

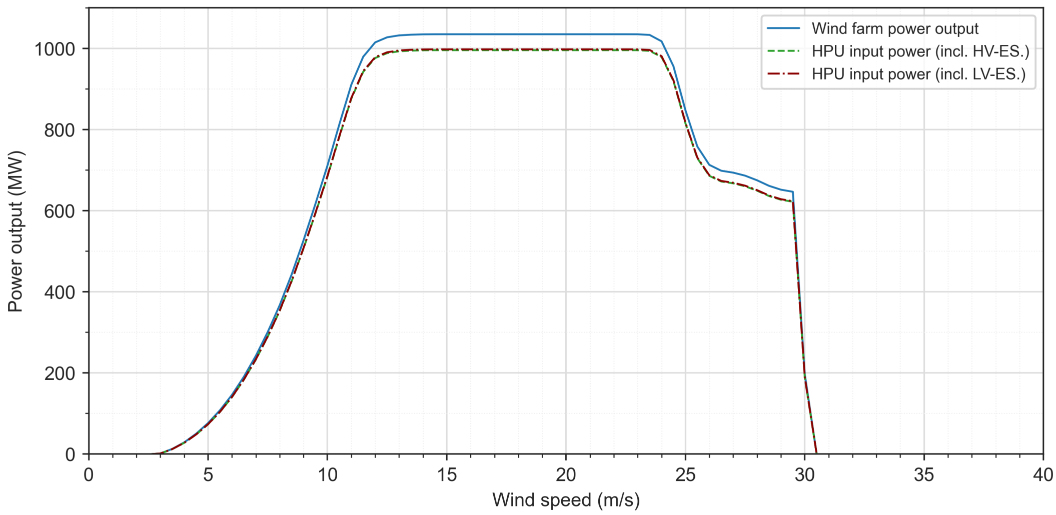

Figure 5.1: Wind farm power curve before electrical system (Wind farm power curve), HPU input power including HV-electrical system efficiency (HPU input power (incl. HV-ES.)) and HPU input power including LV-electrical system efficiency (HPU input power (incl. HV-ES.)).

Taking into account the electrical system efficiency of the centralised configuration and the degradation rate of the wind farm, the hydrogen production unit input power is determined with equation 5.3.

5.5.3. Power distribution overview

The power demand for the HPU components to reach a specific hydrogen flow rate is calculated for the initial year.

Electrolysis

The power demand of the electrolyser stacks for a range of hydrogen mass flows is given in Figure 5.2.

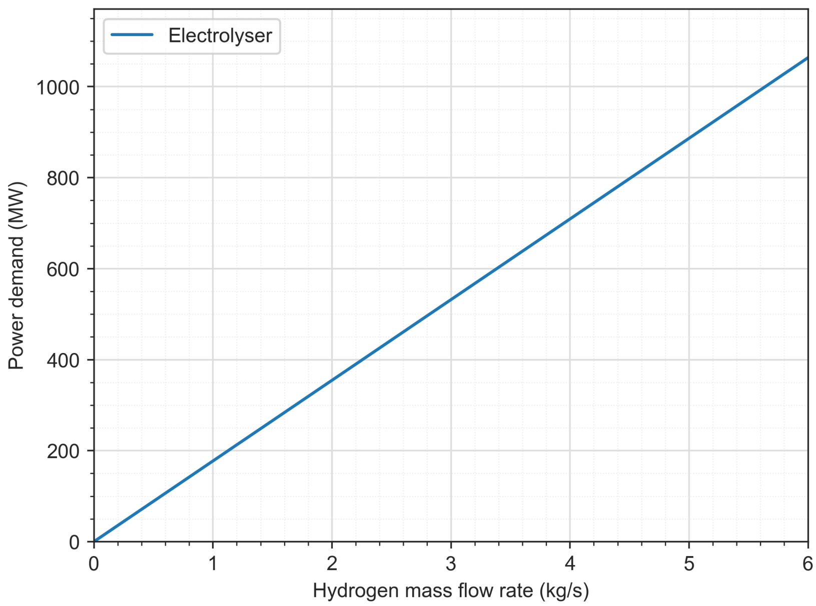

Figure 5.2: Electrolyser power demand for hydrogen mass flow rates (0-6 kgH_2/s).

Balance of Plant

The power demand of the BOP components for a range of hydrogen mass flows is given in Figure 5.3. It can be noticed that the power demand of the BOP components is a fraction of the electrolyser stacks power demand.

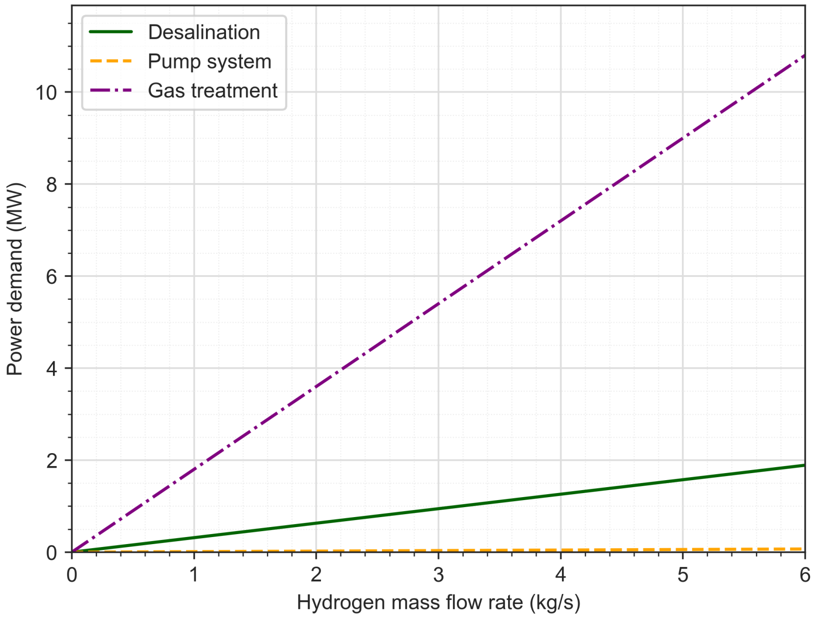

Figure 5.3: BOP component power demand for hydrogen mass flow rates (0-6 kgH_2/s)

Hydrogen compression

Figure 5.4 illustrates the energy consumption of the compressor when compressing 1kg hydrogen for a range of input pressures (1-35 bar), to a range of output pressures (1-200 bar). Notably, the energy consumption is influenced by the pressure ratio between the input and output pressure. Therefore, it is advantageous to start with a relatively higher input pressure, such as the 35 bar input pressure from the electrolyser, to minimise the energy required for compression.

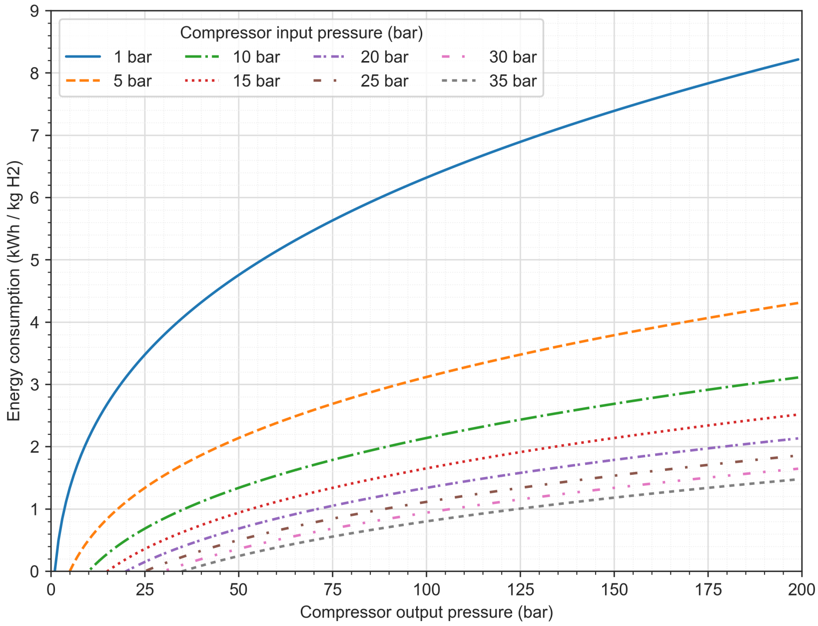

Figure 5.4: Compressor energy consumption for a range of input pressures (1-35 bar), to a range of output pressures (1-200 bar)

To connect the offshore wind-to-hydrogen farm to a hydrogen backbone pipeline an output pressure of 50 bar will be considered. Figure 5.5 illustrates the power demand of the compressor when compressing hydrogen from 10.0, 15.0, 20.0, 25.0, 30.0 and 35.0 bar input pressure to 50.0 bar output pressure.

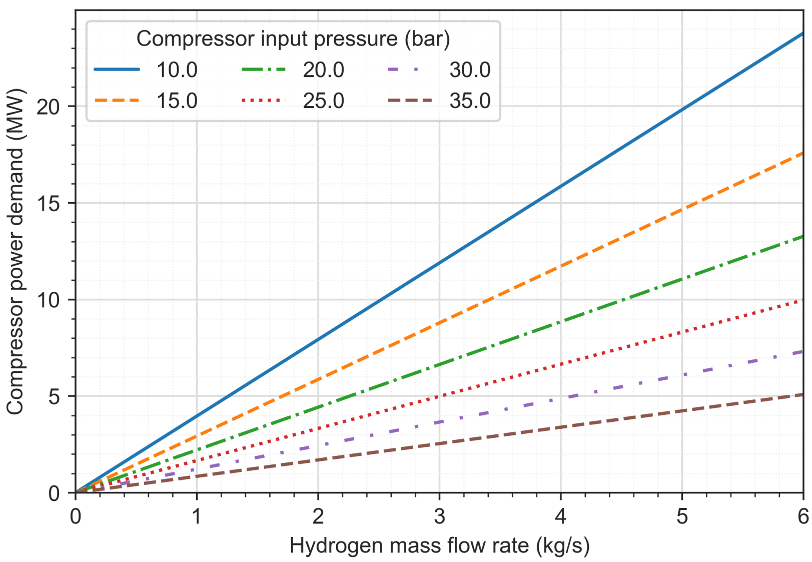

Figure 5.5: Compressor power demand versus hydrogen mass flow rates, when compressing hydrogen from 10.0, 15.0, 20.0, 25.0, 30.0 and 35.0 bar input pressure to 50.0 bar output pressure.

Notably, the power demand of the compressor is fraction of the electrolyser stack power consumption, especially when compressing form 35.0 bar to 50.0 bar.

Hydrogen production unit power demand

Considering the hydrogen production model constants in 5.5.1, the initial PEME stack efficiency, a compressor input pressure of 35.0 bar and output pressure of 50.0 bar, the total HPU power demand for a range of hydrogen mass flow rates is given in Figure 5.6.

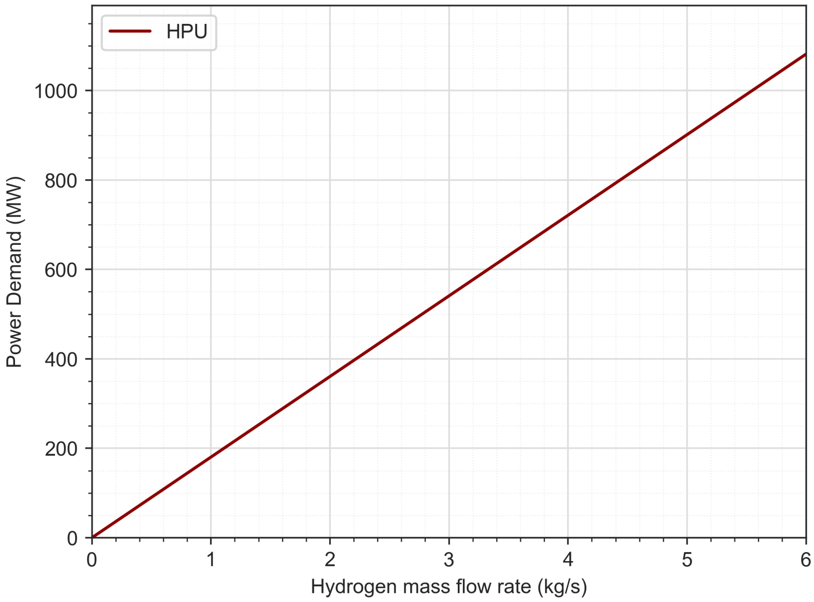

Figure 5.6: Total HPU power demand for a range of hydrogen mass flow rates (0-6 kgH_2/s), considering a compressor input and output pressure of 35.0 and 50.0 bar respectively.

The relative electrolyser stack power demand of the total HPU power demand is 98.35% when an input and output pressure of 35.0 and 50.0 bar respectively, are considered. This also leads to the conclusion that the electrolyser stack efficiency is a key factor for the total hydrogen production as it directly impacts the electrolyser hydrogen output.

Due to the linear relation between the HPU power demand and the hydrogen mass flow rate, a linear relation between the installed HPU capacity and annual hydrogen production is obtained.

5.5.4. Hydrogen flow rate curve

Figure 5.7 shows an example of a hydrogen flow rate curve based on the electrical power curve given in Subsection 5.5.2 and hydrogen production model constants given in Table 5.1. This hydrogen flow rate curve relates to the first year of operation including the initial electrolyser efficiency. To determine the annual hydrogen production during the lifetime of the offshore wind-to-hydrogen farm, a hydrogen flow rate curve will be generated for each year, incorporating the effects of degradation and availability factors.

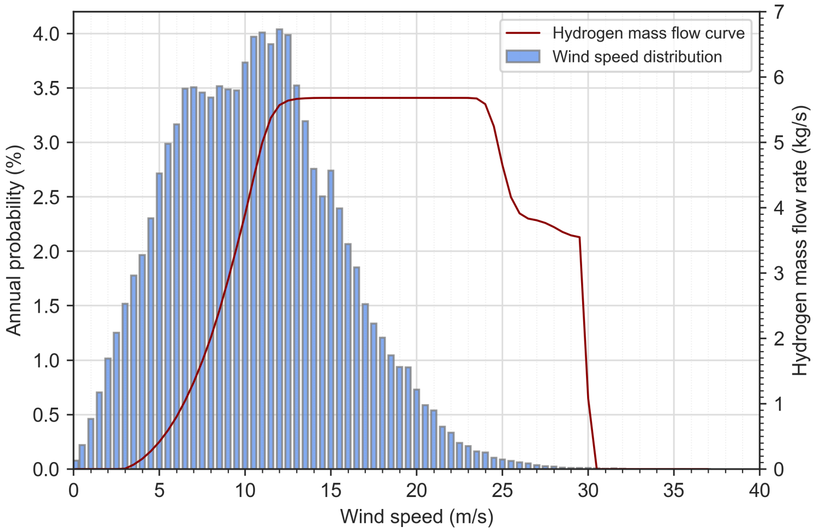

Figure 5.7: Hydrogen mass flow rate curve and wind speed probability distribution (example).

5.5.5. Electrolyser stack replacements

In figure 5.8, an example of the average electrolyser efficiency per year is provided for 0-4 electrolyser replacements. Replacements of the electrolysers increase the average efficiency over the lifetime of the wind farm. In this example, the average electrolyser efficiency for 0-4 replacements during the lifetime of the wind farm, is respectively; 72.4%, 76.3%, 77.5%, 78.1% and 78.5%.

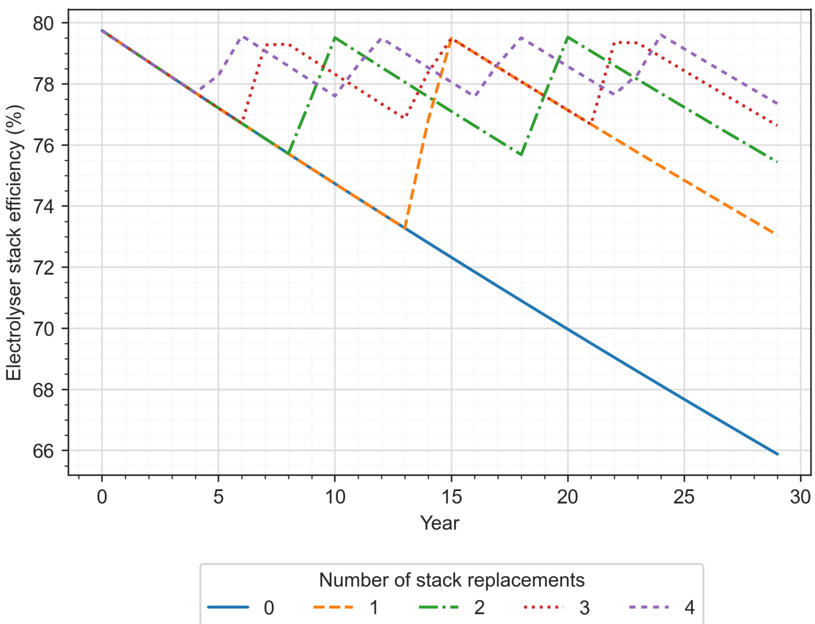

Figure 5.8: Electrolyser stack efficiency including degradation for 0-4 electrolyser stack replacements.

In this example, the option of not replacing the electrolyser stack is not feasible because the stack's lifetime is surpassed by the high number of full load hours it has already operated. The total full load hours accumulated by the electrolyser stack over the lifetime of the offshore wind-to-hydrogen farm are nearly 150,000 hours while its maximum capacity is assumed to be 80,000 full load hours. This indicates that at least one replacement of the electrolyser stack is necessary, and multiple replacements are optional to sustain operations effectively.

The optimal number of electrolyser replacements is not solely determined by the lifetime efficiency of the electrolyser and the electrolyser maximum full load hours. Other factors, such as the cost of the electrolysers and the impact of decreased availability during the replacement of electrolyser stacks, also play significant roles. Therefore, finding the optimal number of replacements requires careful consideration of these factors in addition to the electrolyser lifetime efficiency.

5.5.6. Annual hydrogen production

Figure 5.9 provides an example of the annual hydrogen production of a centralised offshore wind-to-hydrogen farm for scenarios involving 1 and 2 electrolyser replacements. In this figure, the impact of electrolyser degradation and wind farm degradation on hydrogen production is noticeable. The degradation of the wind farm leads to linear overall decrease in hydrogen production. Furthermore, the figure illustrates that stack replacements occur during specific years. During this specific replacement year, there will be a portion of the year where old degraded stacks are in operation, followed by another portion of the year where new electrolyser stacks are utilized. As a result, the average efficiency during this period is lower compared to the first full year with new electrolyser stacks.

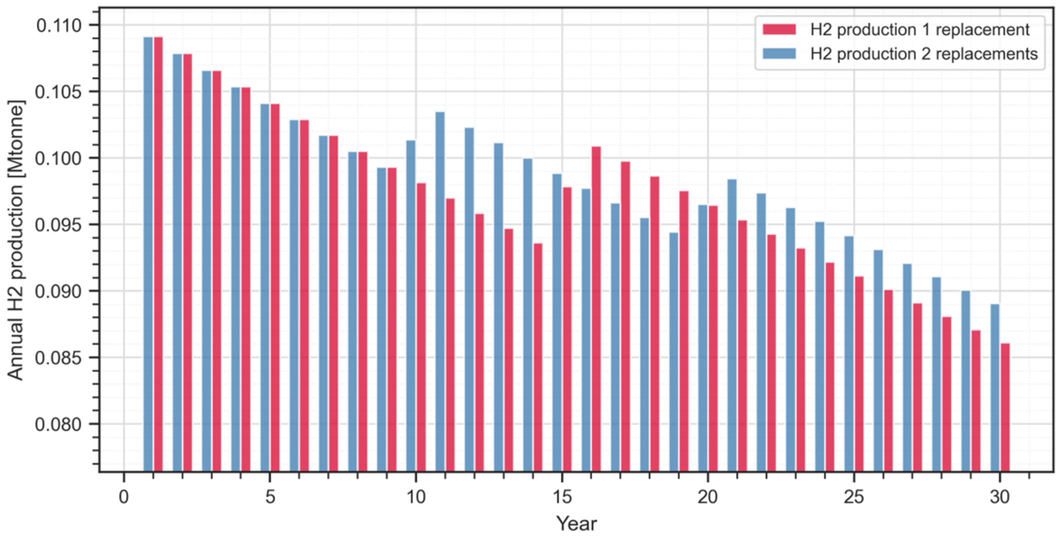

Figure 5.9: Annual hydrogen production for 1 and 2 electrolyser stack replacements.

Lastly, the annual hydrogen production represents the cumulative hydrogen production of the offshore wind-to-hydrogen farm throughout its entire lifetime.

6 Hydrogen pipeline sizing & cost modeling

When designing a hydrogen pipeline system, it is important to determine the appropriate diameter of the pipeline to ensure the safe and efficient transport of the required amount of hydrogen but also to minimise the hydrogen pipeline cost. This chapter aims to elaborate on the hydrogen pipeline sizing and cost modeling. First the flow characteristics of hydrogen are discussed in Section 6.1. Subsequently, Section 6.2 presents a comprehensive explanation of the methodology employed to calculate the diameter of a hydrogen pipeline. Hereafter, the cost modeling of a hydrogen pipeline is explained in Section 6.3. Finally, in Section 6.4, the hydrogen sizing and cost modeling intermediate results are given.

6.1. Hydrogen flow characteristics

Hydrogen gas has several flow characteristics that are important to consider in the design and operation of hydrogen pipeline systems. The key characteristics include a relative low density, high compressibility and low viscosity which depend on the temperature and pressure of the hydrogen gas as well as the specific characteristic of hydrogen. The density, compressibility and viscosity are determined with the CoolProp function in python [11]. The density is discussed in Subsection 6.1.1, the compressiblity in Subsection 6.1.2 and the viscosity in Subsection 6.1.3.

6.1.1. Low density

The density of hydrogen gas for different pressures and temperatures can be seen in Figure 6.1. Hydrogen has a low density compared to other gasses such as methane. For a temperature of 283.15 Kelvin and a pressure of 35.0 bar, hydrogen has a density of 2.934 kg/m^3 and methane 25.694 kg/m^3 [60]. The low density can make it more difficult to transport and store in large quantities. However, the advantage of a low density is the lower mass flow rate for a given volumetric flow rate. This can result in lower pressure drops and lower energy losses during the transport of hydrogen gas in hydrogen pipelines.

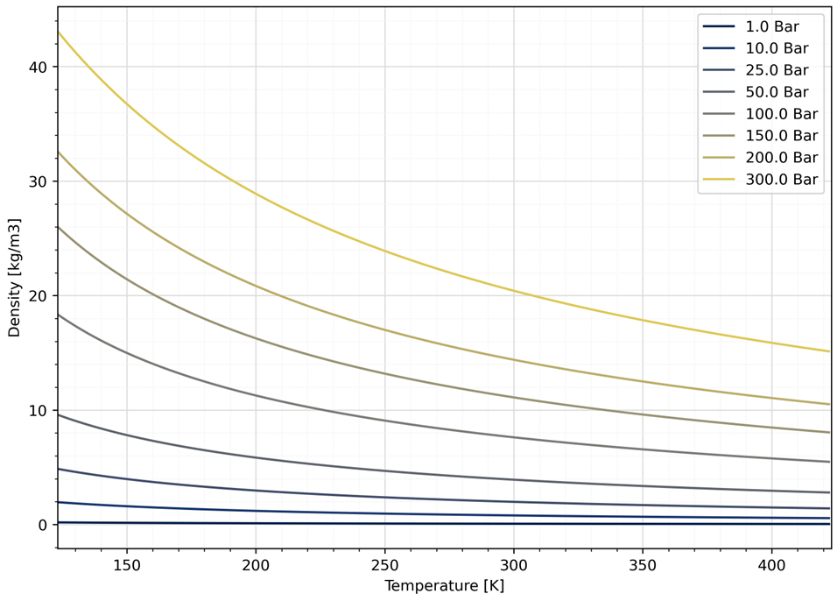

Figure 6.1: Density of hydrogen gas for different temperature and pressure.

The low density of hydrogen gas poses a challenge in offshore wind-to-hydrogen projects where space is often limited. To store the same amount of energy, larger volumes of hydrogen gas are needed compared to denser gases. This necessitates careful design of storage systems that can accommodate the larger volume of hydrogen. One approach is to use larger tanks or storage facilities to meet the storage requirements. Additionally, alternative storage methods like underground caverns or offshore tanks can be explored as viable options to overcome space limitations effectively. By carefully considering storage solutions, offshore wind-to-hydrogen projects can optimise the use of available space and ensure efficient storage of hydrogen gas.

6.1.2. High compressibility

Figure 6.2 illustrates the compressibility factor of hydrogen gas at varying pressures and temperatures. Hydrogen gas is relatively compressible, which means that its volume can change significantly in response to changes in pressure. This can be both an advantage and a disadvantage in different applications, as it allows for efficient storage and transportation of hydrogen but can also result in significant changes in density and viscosity under varying conditions [29].

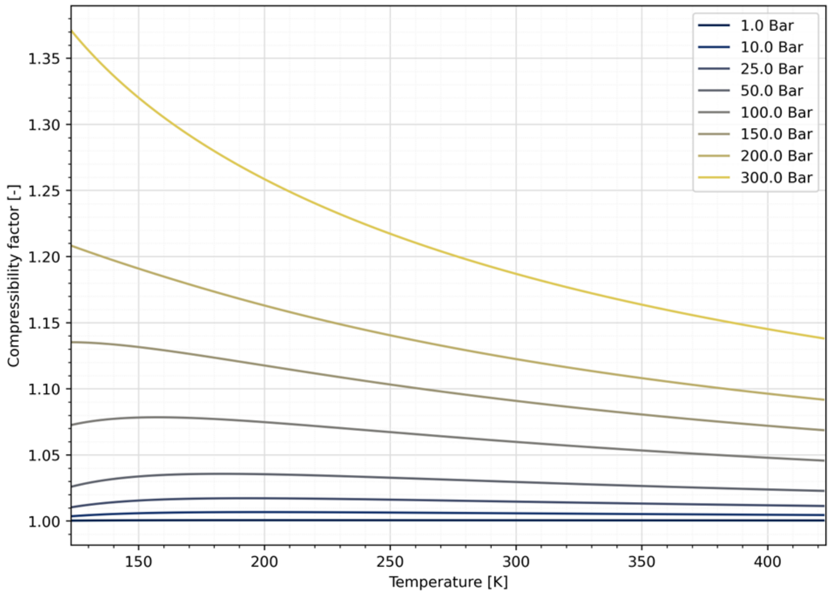

Figure 6.2: Compressibility factor of hydrogen gas for different temperature and pressure.

The high compressibility of hydrogen enables efficient compression, which is vital for offshore applications involving hydrogen transportation to shore. This compression process increases the energy density of hydrogen, allowing for the storage of more energy in a given volume. Efficient compression also reduces energy consumption when overcoming pressure drops during transport. However, it is important to note that the high compressibility of hydrogen results in significant pressure changes during pipeline transport. Therefore, optimising the compression and decompression processes is essential to maximise energy storage, minimise energy losses, and achieve overall efficiency in offshore wind-to-hydrogen configurations.

6.1.3. Low viscosity

The dynamic viscosity of hydrogen gas is given in Figure 6.3 at different pressures and temperature. Hydrogen gas has a very low dynamic viscosity, which increases the Reynolds number and decreases the friction losses [83]. This low viscosity can be an advantage in terms of minimising pressure drop and energy loss during transport, but it can also lead to vibration-induced fatigue in the pipeline if flow velocities are too high [45].

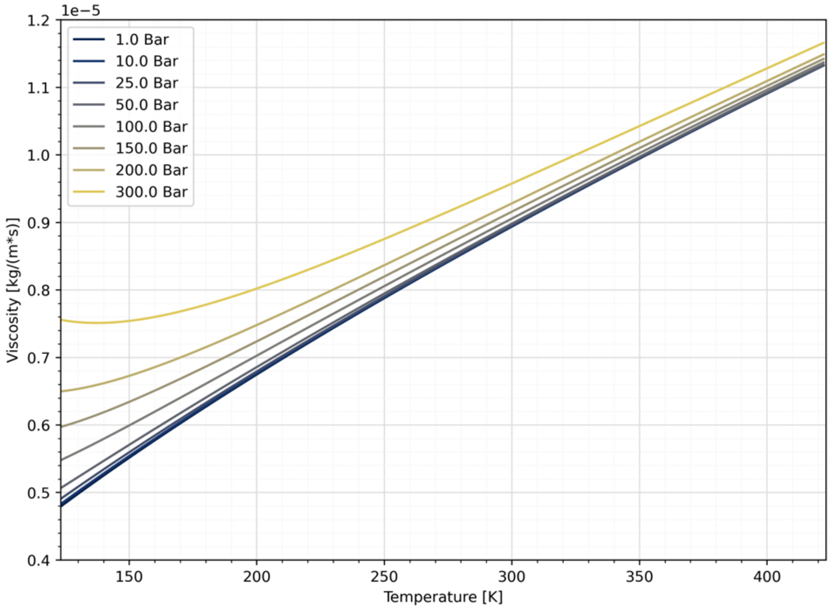

Figure 6.3: Viscosity of hydrogen gas for different temperature and pressure.

The low viscosity of hydrogen gas reduces friction losses and pressure drops during transport. This property minimises energy losses due to friction as hydrogen flows through pipelines or other transportation systems. In the context of offshore wind-to-hydrogen configurations, where the distance between the wind turbines and the hydrogen production facility can be significant, minimising energy losses during transport is crucial for overall system efficiency. The low viscosity of hydrogen gas favors the design of pipeline systems with larger diameters or smoother inner surfaces. These features help reduce friction and maintain optimal flow rates, minimising pressure drop along the pipeline. However, proper consideration of vibration-induced fatigue is essential during pipeline design to ensure the safe transport of hydrogen.

Overall, the flow characteristics of hydrogen gas can have both advantages and disadvantages in different applications. Proper consideration of these characteristics is essential in the design and operation of hydrogen pipeline systems to ensure safe and efficient transport of hydrogen.

6.2. Methodology pipeline diameter sizing

This section provides an overview of the methodology employed for determining the minimum pipeline diameter required to transport hydrogen over a specified distance, while accounting for a designated pressure drop, velocity limit and maximum hydrogen mass flow rate. The methodology is based on a method from Engineers Edge [31] and the work of E. Craye [22]. However, the exact methodology and friction factor calculation are different compared to Craye's work. In Subsection 6.2.1, an overview of the pipeline diameter sizing method is given. Hereafter, Subsections 6.2.2 and 6.2.3 offer detailed explanations of the pressure drop and the associated friction factor.

6.2.1. Methodology overview

The pipeline diameter is determined based on the pipeline length, desired pressure drop, velocity limit and maximum hydrogen mass flow rate.

- The *pipeline length* represents the distance between the hydrogen inlet point and the outlet point of the hydrogen pipeline. It is the specific distance for which the calculation of pressure drop is determined.
- To mitigate vibration-induced fatigue, the *velocity limit* must be considered in hydrogen pipelines. Excessive flow velocities in these pipelines can induce vibrations that lead to cracks and leaks over time. The risk of VIF is influenced by factors such as vibration frequency, intensity, pipe geometry, material properties, and operating conditions [61][45]. Therefore, it is crucial to restrict the flow velocity of hydrogen within the pipeline as a preventive measure against VIF.

- The *maximum hydrogen mass flow rate* corresponds to the highest amount of hydrogen entering the pipeline per unit time. This value is determined by the hydrogen production capacity of the HPU.
- The *pressure drop* in a pipeline is the difference between the inlet and outlet pressure of a pipeline. The pressure drop is caused by friction losses in the pipeline and is therefore affected by the pipeline diameter. The desired pressure drop is the predetermined difference between the input pressure and output pressure of a pipeline.

The method used to calculate the pressure drop over a pipeline with certain diameter is a numerical integration method. By employing this method, the pressure drop in a pipeline with a certain diameter and length is determined taking into account a velocity limit and maximum hydrogen mass flow rate. To determine the minimum pipeline diameter, the pressure drop in a pipeline is calculated for a range of pipeline diameters. The goal is to find the smallest diameter that meets the desired pressure drop criteria.

The pipeline pressure drop can not be directly calculated for the total length of a pipeline because the change in pressure, changes the density, viscosity and compressibility factor of the hydrogen gas. This results in a change in hydrogen flow velocity, Reynolds number and friction factor which all influence the pressure drop in the pipeline. Therefore, a numerical integration method is used. In the numerical integration method, the pressure drop over a pipeline for a diameter is calculated for segments of 250 meter. Due to the short length and thus the minimal difference in pressure between the inlet and outlet of the segment, it is not necessary to know the average pressure within the segment to estimate the viscosity, density and compressibility factor. The minimal pressure difference in the segment leads to negligible changes in viscosity, density, and compressibility. Consequently, the pressure at the outlet of the segment is sufficient for calculating the corresponding friction factor and hydrogen flow velocity. The values that need to be calculated are presented in Figure 6.4, alongside a schematic overview of the pipeline segment.

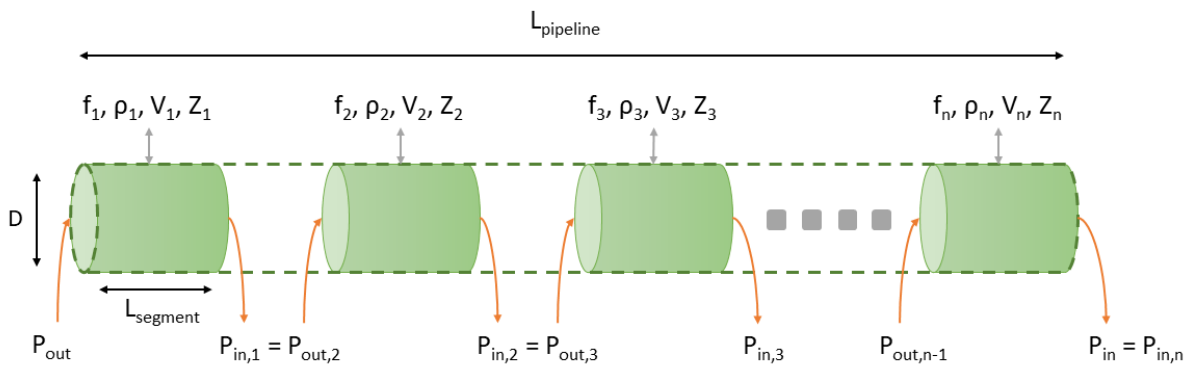

Figure 6.4: Numerical integration method for hydrogen pipeline diameter sizing [36]).

The pressure drop calculation begins with the segment closest to the pipeline outlet. The inlet pressure of this segment, located 250 meters from the outlet, is calculated using the pressure drop equation. Subsequently, the calculated pressure serves as the outlet pressure for the next segment, which is 500 meters from the pipeline outlet. This process continues for each segment until reaching the pipeline inlet, allowing the determination of the required inlet pressure at the beginning of the pipeline to reach a selected outlet pressure. For pipelines shorter then 250 meters, only one integration step is performed. During each iteration, several parameters need to be recalculated as they vary throughout the flow in the pipeline. These parameters include:

- Density
- Dynamic viscosity
- Compressibility factor
- Reynolds number
- Hydrogen flow velocity

- Friction factor

To simplify the pressure drop calculations, two main assumptions are made regarding the hydrogen flow. First, an isothermal flow is assumed, meaning that the hydrogen's temperature is presumed constant throughout the pipeline. Second, no elevation changes are considered, and therefore, any pressure drop resulting from height differences is disregarded.

6.2.2. Pressure drop

When the hydrogen molecules are transported through pipelines, they experience frictional resistance, resulting in energy losses that can be quantified as pressure drops along the pipeline. This means that energy needs to be supplied to maintain a steady flow of gas through the pipeline. The pressure drop over a pipeline can be calculated with Equation 6.1, which is obtained from the general flow equation [89].

$$\frac{P_{\text{in}}^2 - P_{\text{out}}^2}{2 \times P_{\text{in}}} = f \times \frac{L}{D} \times \rho \times \frac{V^2}{2} \times \frac{T_{\text{avg}}}{T_1} \tag{6.1}$$

This equation can be rewritten as Equation 6.2 and is used to calculate the inlet pressure of a pipeline for a specified output pressure (P_{out}), compressibility factor (Z), friction factor (f), pipeline length (L), pipeline diameter (D), hydrogen density (ρ) and flow velocity (V). Besides, isothermal flow is assumed and therefore, $\frac{T_{\text{avg}}}{T_1} = 1$ [31].

$$P_{\text{in}} = \sqrt{2 \cdot P_{\text{out}} \cdot Z \cdot f \cdot \frac{L}{D} \cdot \rho \cdot \frac{V^2}{2} \cdot 1 + P_{\text{out}}^2} \tag{6.2}$$

6.2.3. Friction factor

The friction factor of the hydrogen pipeline is calculated with Equation 6.3 also known as the Colebrook-White equation [89]. The Colebrook-White equation is an empirical formula that relates the friction factor to the Reynolds number and the relative roughness of the pipe.

$$\frac{1}{\sqrt{f}} = -2 \cdot \log_{10}\left(\frac{\epsilon}{3.7 \cdot D} + \frac{2.51}{Re \cdot \sqrt{f}}\right) \tag{6.3}$$

In this equation; f is the friction factor, ϵ is the pipe roughness, D is the diameter of the pipe and Re is the Reynolds number. The Reynolds number is a dimensionless quantity that describes the ratio of inertial forces to viscous forces in a fluid. The Reynolds number is calculated with Equation 6.4, where ρ is the density of the fluid, V is the velocity of the fluid, D is the diameter of the pipeline and μ is the dynamic viscosity of the fluid [34]. The velocity of the fluid is calculated with Equation 6.5, where $\dot{m}$ is the mass flow rate, ρ the density and D the diameter [34].

$$Re = \frac{\rho \cdot V \cdot D}{\mu} \tag{6.4}$$

$$V = \frac{\dot{m}}{\rho\pi(\frac{D}{2})^2} \tag{6.5}$$

The Colebrook-White equation is an implicit equation, which means that it cannot be solved directly for f. Instead, it is typically solved iteratively using numerical methods. Equation 6.6 calculates $factor$ based on a guessed friction factor f_{guess}. This factor is then used in Equation 6.7 to calculate an estimate of the friction factor [31].

$$\text{factor} = -2 * \log_{10}\left(\frac{\epsilon}{3.7 * D} + \frac{2.51}{Re * \sqrt{f_{\text{guess}}}}\right) \tag{6.6}$$

$$f = \left(\frac{1}{\text{factor}}\right)^2 \tag{6.7}$$

6.3. Hydrogen pipeline cost modeling

This section elaborates upon the hydrogen pipeline cost, taking into account the pipeline diameter from the pipeline sizing model. The cost components can be categorized into procurement, logistic and pipeline non-material cost in Subsections 6.3.1, 6.3.2 and 6.3.3 respectively. Because the procurement and logistic cost modeling differs for the infield flow lines and the steel pipelines, a distinction in these subsection is made between the type of hydrogen pipelines.

The cost associated with the hydrogen pipelines can be divided into two categories: capital expenditures (CAPEX) and operational expenditures (OPEX). In this research, the cost functions denoted by $C_{\text{component}}$ refer to the CAPEX values incurred before operation of the wind-to-hydrogen farm starts. On the other hand, the OPEX values represent the costs incurred during each year of the facility's lifetime and are denoted as $C_{\text{OPEX,component}}$. The OPEX values are calculated by multiplying the CAPEX of a specific component by its corresponding OPEX factor, indicated as $f_{\text{OPEX,component}}$. The OPEX of hydrogen pipelines are specifically associated with the pipeline procurement.

This hydrogen pipeline cost modeling is based on the work of E. Craye regarding hydrogen pipeline cost modeling [22].

6.3.1. Procurement

Procurement costs include expenses related to acquiring raw material, fabrication of the pipeline and cost related to support structures such as valves. Regarding the infield flowlines, specific procurement cost assumptions per meter are obtained within Vattenfall. For steel pipelines, the costs are estimated based on the raw material cost and fabrication rates.

Support Structures

Support structures include various connection components for the pipeline system, such as isolation valves and check valves. Check valves regulate pressure at each turbine, with in-string turbines having three isolation valves and end-of-string turbines having one. Valve costs scale with pipeline diameter, using a relation derived from the oil and gas industry.

Infield flowlines

The infield flowline (IF) network consists of bonded and unbonded flowlines, both proposed as feasible solutions but with a different price per meter. Additionally, the network incorporates flanges at the end of each pipeline segment, diverless connections, risers for turbine connection and check and isolation valves. Check valves regulate pressure at each turbine, with in-string turbines having three isolation valves and end-of-string turbines having one. Valve costs scale with pipeline diameter, using a relation derived from the oil and gas industry. The total procurement cost of the flowlines is determined with Equation 6.8 [22]. In this equation, $C_{\text{IF,pc}}$ represents the total procurement cost of the flowlines. c_{IF} denotes the segmental cost per meter, L_{IF} represents the flowline length, c_{flange} is the cost of each flange, $N_{\text{IF,seg}}$ represents the number of flowline segments, c_{dc} denotes the cost of each diverless connection, and c_{riser} represents the cost of each riser. N_{turbines} denotes the number of turbines connected to the network and c_{valves} represent the cost of the valves per IF segment.

$$C_{\text{IF,pc}} = c_{\text{IF}} \cdot L_{\text{IF}} + c_{\text{flange}} \cdot 2 \cdot N_{\text{IF,seg}} + c_{\text{dc}} \cdot N_{\text{IF,seg}} + c_{\text{riser}} \cdot N_{\text{turbines}} + N_{\text{IF,seg}} \cdot c_{\text{valves}} \tag{6.8}$$

The unbonded and bonded infield flowline cost per meter for a given diameter can be determined with Equation 6.9 [36]. In this equation, D_{IF} is the inner diameter of the infield flowline and $c_{\text{IF},1}$, $c_{\text{IF},2}$ and $c_{\text{IF},3}$ are the specific cost constants related to an unbonded or bonded flowline.

$$c_{\text{IF}} = c_{\text{IF},1} \cdot D_{\text{IF}}^2 + c_{\text{IF},2} \cdot D_{\text{IF}} + c_{\text{IF},3} \tag{6.9}$$

The cost of the valves, flanges and diverless connections can be determined with Equations 6.10, 6.11 and 6.12 respectively [36]. The cost of a riser is a constant.

$$c_{\text{valves}} = c_{\text{valves},1} \cdot D_{\text{IF}} + c_{\text{valves},2} \tag{6.10}$$

$$c_{\text{flange}} = c_{\text{flange},1} \cdot D_{\text{IF}} - c_{\text{flange},2} \tag{6.11}$$

$$c_{\text{dc}} = c_{\text{dc,1}} \cdot c_{\text{flange}} \tag{6.12}$$

In the equations above, C_{valves} represents the cost of the valves, with $c_{\text{valves,1}}$ and $c_{\text{valves,2}}$ being the associated cost coefficients. C_{flange} represents the cost of the flange, with $c_{\text{flange,1}}$ and $c_{\text{flange,2}}$ being the associated cost coefficients. C_{dc} represents the cost of the diverless connection, with $c_{\text{dc,1}}$ being the associated cost coefficient.

Steel pipeline

The total procurement cost of the steel pipeline (SP) is determined by combining the raw material cost and the fabrication cost, as described in Equation 6.13 [22]. In this equation, $C_{\text{SP,pc}}$ represents the total procurement cost of the steel pipeline, $C_{\text{SP,mat}}$ denotes the cost of raw materials for the steel pipeline, and $C_{\text{SP,fab}}$ represents the cost of fabrication for the steel pipeline.

$$C_{\text{SP,pc}} = C_{\text{SP,mat}} + C_{\text{SP,fab}} \tag{6.13}$$

The pipeline's raw material cost is influenced by its steel composition, as the cost scales with the specific mass of the pipeline segment (Γ_{SP}) and the specific price of steel (c_{steel}). The mass of a pipeline depends on the diameter (D), the wall thickness (T_{wall}) and the steel density (ρ). The pipeline thickness is determined with Equation 6.14, where a relationship between pipeline inner diameter and pipeline thickness was established through logarithmic curve fitting [22].

$$T_{wall} = 0.0021 \cdot \log(D) + 0.021 \tag{6.14}$$

Equations 6.15 and 6.16 are used to determine the pipeline specific mass [22]. Hereafter, a pressure scale factor (P_{scale}) from Equation 6.17 is used to take into account the maximum pressure in the pipeline (p_{max}) [22].

$$A = \frac{\pi}{4} \cdot ((D + 2 \cdot T)^2 - D^2) \tag{6.15}$$

$$\Gamma_{\text{SP}} = A \cdot \rho \tag{6.16}$$

$$P_{\text{scale}} = 1 - \frac{(D/0.0245 - 1) \cdot (50 - 50/35 \cdot p_{\text{max}}/10^5)}{5000} \tag{6.17}$$

The material cost per meter of the hydrogen steel pipeline is calculated with Equation 6.18 [22]. In this equation, $C_{\text{SP,mat}}$ represents the material cost per meter of the hydrogen steel pipeline. P_{scale} denotes the scaling factor, Γ_{SP} represents the weight factor for the steel material, c_{steel} denotes the specific cost of steel material per unit weight, cf_{SP} represents a fixed cost per meter steel pipeline and $cf_{\text{SP,support}}$ denotes a fixed cost per pipeline which represents the additional cost for support structures of the steel pipeline.

$$C_{\text{SP,mat}} = (P_{\text{scale}} \cdot \Gamma_{\text{SP}} \cdot c_{\text{steel}} + cf_{\text{SP}}) \cdot L_{\text{SP}} + cf_{\text{SP,support}} \tag{6.18}$$

The fabrication of the steel pipeline is calculated with a fixed fabrication rate per meter ($c_{\text{SP,fab}}$) and the pipeline length (L_{SP}). Additionally, depending on the diameter and thickness of the pipeline, a spool is required. For every l_{spool} meter pipeline, a spool need to be fabricated. The total hydrogen steel pipeline fabrication cost can be calculated by the Equation 6.19 [22].

$$C_{\text{SP,fab}} = c_{\text{SP,fab}} \cdot L_{\text{SP}} + c_{\text{spool}} \cdot \frac{L_{\text{SP}}}{l_{\text{spool}}} \tag{6.19}$$

In this equation, $C_{\text{SP,fab}}$ represents the total fabrication cost of the steel pipeline. $c_{\text{SP,fab}}$ denotes the fixed fabrication rate per meter, L_{SP} represents the pipeline length, c_{spool} denotes the cost of each spool, and l_{spool} represents the maximum pipeline length per spool.

Operation and maintenance

To estimate the operation and maintenance costs of the hydrogen pipelines, which are referred to as the OPEX of pipelines in this study, a simplified method is employed. In this approach, the OPEX values are assumed to be a percentage of the procurement cost of the hydrogen pipeline. The OPEX values for the hydrogen pipeline are calculated using Equation 6.20, where $C_{\text{OPEX,pipeline}}$ represents the total OPEX of the pipelines, C_{pc} denotes the procurement cost of either the infield flowlines or steel pipelines, and $f_{\text{OPEX,pipeline}}$ represents the OPEX factor associated with the pipelines. By using this equation, the ongoing operation and maintenance costs can be estimated based on the initial procurement cost and the specified OPEX factor.

$$C_{\text{OPEX,pipeline}} = C_{\text{pc}} \cdot f_{\text{OPEX,pipeline}} \tag{6.20}$$

6.3.2. Logistics

The model approach for the transport and installation cost, referred to as logistic cost (C_{log}), of both hydrogen infield flowlines and steel pipelines is determined by the pipeline's length and diameter. The installation procedure takes into account weather allowance, mobilization, demobilization, initiation, laydown, and interim mobilization expenses. The total cost of installing an infield flowline or steel pipeline is calculated by multiplying the overall timeline required for the export pipeline with either the Reel-lay vessel day rate or the S-lay vessel day rate [22]. It is important to note that the fixed cost for mobilization of a pipeline is assumed to be divided by the number of pipeline segments and does not increase with the number of segments.

Infield flowlines

Infield flowlines, which always have an outer diameter equal or smaller than 6 inches, are installed using Reel-lay vessels. Each trip of a Reel-lay vessel can accommodate up to 75 km of infield flowline [22]. The installation speed depends on the type of flowline, with bonded flowlines being installed at half the speed of unbonded flowlines. Additionally, the installation process includes the time required for support structure installation.

Steel pipelines

The choice of installation vessel for steel pipelines depends on the outer diameter. For pipelines with outer diameters less than 16 inches, Reel-lay vessels are utilized. These vessels have a daily laying capacity of up to 10 km and can carry up to 20 km of pipeline per trip. On the other hand, for pipelines with outer diameters larger than 16 inches, Reel-lay vessels are not suitable, and S-lay vessels are required. In the case of S-lay installation, the laying speed decreases to 3 km per day as the steel pipeline segments are welded together offshore [22]. Additionally, support structures need installation time.

6.3.3. Non-material

The non-material cost relate to the cost of site preparation, FEED studies, company costs and Project Management & Engineering (PME). Equation 6.21 is used to calculate both the steel pipeline and infield flowline non-material cost [22]. In this equation, f_{SP} denotes the site preparation cost, L the infield flowline or steel pipeline length, f_{CC} represents the company cost factor, f_{FS} the FEED studies factor, and the PME factor is denoted with f_{PME}. The total project cost ($PC + LC$) encompasses both the procurement cost and the logistic costs associated with the hydrogen pipeline project.

$$C_{\text{NM}} = (f_{\text{FS}} + f_{\text{CC}} + f_{\text{PME}}) \cdot (C_{\text{pc}} + C_{\text{log}}) + f_{\text{SP}} \cdot L \tag{6.21}$$

6.4. Hydrogen pipeline sizing & cost model demonstration

This section aims to demonstrate the hydrogen pipeline sizing & cost model. Subsection 6.4.1 provides the constants used in the hydrogen pipeline sizing and cost model. Additionally, Subsection 6.4.2 gives the demonstration results of the pipeline diameter sizing and Subsection 6.4.3 discuss the hydrogen pipeline cost demonstration results.

6.4.1. Hydrogen pipeline sizing & cost model constants

The constants utilized in the Hydrogen pipeline sizing & cost model are summarized in Table 6.1. These constants serve as key parameters for the accurate estimation of hydrogen pipeline sizing and associated cost.

Parameter	Symbol	Value	Unit	Source
Pipeline sizing				
Steel pipeline inner roughness	ϵ_{SP}	X	μm	[22]
Unbonded infield flowline inner roughness	ϵ_{UBIF}	X	μm	[22]
Bonded infield flowline inner roughness	ϵ_{BIF}	X	μm	[22]
Hydrogen flow velocity limit	V_{lim}	X	m/s	[36]
Infield flowline procurement cost				
Unbonded IF segment cost coefficient 1	$c_{\text{IF},1}$	X	€$/inch^2$	[36]
Unbonded IF segment cost coefficient 2	$c_{\text{IF},2}$	X	€/inch	[36]
Unbonded IF segment cost coefficient 3	$c_{\text{IF},3}$	X	€	[36]
Bonded IF segment cost coefficient 1	$c_{\text{IF},1}$	X	€$/inch^2$	[36]
Bonded IF segment cost coefficient 2	$c_{\text{IF},2}$	X	€/inch	[36]
Bonded IF segment cost coefficient 3	$c_{\text{IF},3}$	X	€	[36]
Riser cost	c_{riser}	X	€	[36]
Valves cost coefficient 1	$c_{\text{valves},1}$	X	€/inch	[36]
Valves cost coefficient 2	$c_{\text{valves},2}$	X	€	[36]
Flange cost coefficient 1	$c_{\text{flange},1}$	X	€/inch	[36]
Flange cost coefficient 2	$c_{\text{flange},2}$	X	€	[36]
Diverless connection cost coefficient 1	$c_{\text{dc},1}$	X	€	[36]
Infield flowline OPEX factor	$f_{\text{OPEX,IF}}$	2.0	%	[8]
Steel pipeline procurement cost				
Steel density	ρ	7850	kg/m^3	
Specific cost of steel material per unit weight	c_{steel}	X	€/kg	[22]
Fixed cost per meter of steel pipeline	cf_{SP}	X	€/m	[22]
Fixed cost per pipeline for support structures	$cf_{\text{SP,support}}$	X	€/pipeline	[22]
Fabrication rate per meter	F_{SP}	X	meters/day	[22]
Spool length	l_{spool}	20	km	[22]
Steel pipeline OPEX factor	$f_{\text{OPEX,SP}}$	2.0	%	[8]
Pipeline logistics cost modeling				
Offshore service vessel day rate		X	€/day	[22]
Reel-lay Vessel day rate		X	€/day	[22]
S-lay vessel day rate		X	€/day	[22]
Jet trenching vessel day rate		X	€/day	[22]
Multi services vessel day rate		X	€/day	[22]
Pipeline non-material cost modeling				
Site preparation factor	f_{SP}	X	€/m	[22]
Company cost factor	f_{CC}	10	%	[22]
FEED studies factor	f_{FS}	1	%	[22]
PME factor	f_{PME}	7	%	[22]

Table 6.1: Hydrogen pipeline sizing & cost model constants.

6.4.2. Hydrogen pipeline diameter sizing

The goal of the pipeline diameter sizing is to find the minimum diameter to overcome the pressure drop in the pipeline while adhering to the hydrogen flow velocity limit. Figure 6.5 illustrates the relationship between pressure drop and hydrogen velocity increase for two pipelines, each with a length of 200km, hydrogen mass flow rate of 2 kg/s, and an input pressure of 35 bar and 24 bar. Additionally, the outlet pressure is limited to 20.0 bar, and the maximum allowable hydrogen flow velocity is denoted as *X* m/s. The selected input pressures, combined with the specified output pressure, massflow, velocity limit, pipeline length, and inner roughness, lead to pipeline diameters of 12 inches and 16 inches for input pressures of 35 bar and 24 bar, respectively.

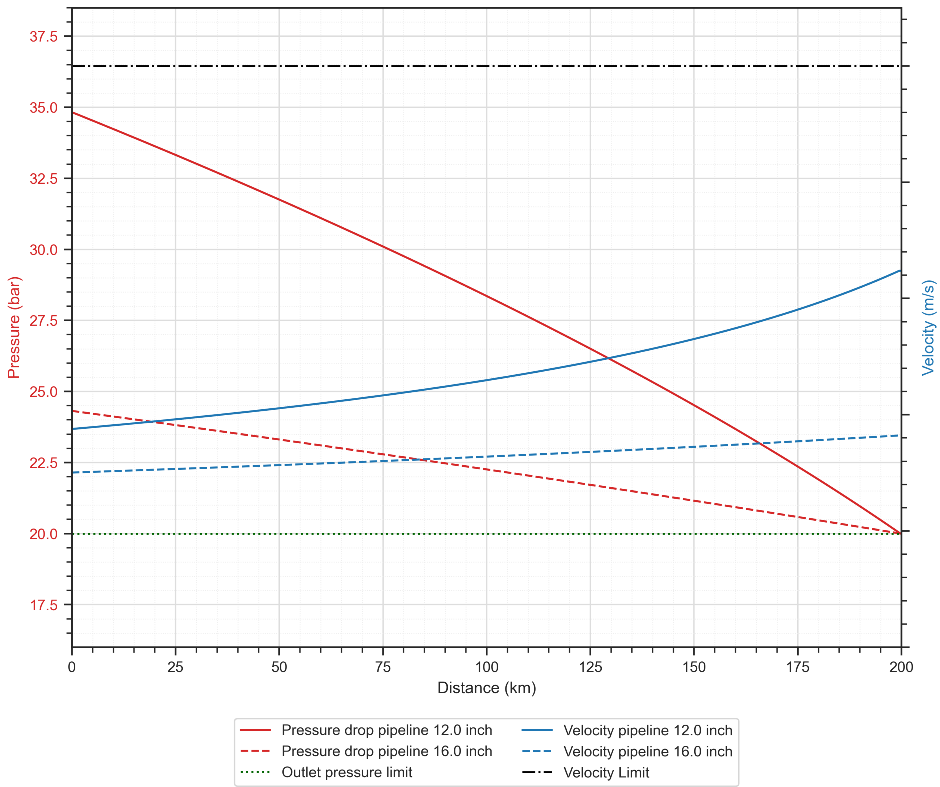

Figure 6.5: Hydrogen pressure drop and flow velocity increase for two hydrogen pipelines with input pressures: 35 bar and 24 bar, output pressure: 20 bar, length: 200km, massflow: 2 kg/s, velocity limit: *X*, inner roughness: *X*, diameters: 16 inch and 12 inch.

The graph reveals that as the pressure decreases, the hydrogen flow velocity increases. Larger pressure drops correspond to greater increases in hydrogen flow velocity. This trend is evident when comparing the pressure drop and hydrogen flow velocity increase for the two pipelines. The 12-inch pipeline experiences a pressure drop from 35 bar to 20 bar, while the 16-inch pipeline undergoes a pressure drop from 24 bar to 20 bar, accompanied by a hydrogen flow velocity increase that is five times smaller than that of the 12-inch pipeline.

To mitigate pressure drop in a pipeline, increasing its diameter is necessary, as evidenced by the difference in pressure drop and flow velocity increase between the 12-inch and 16-inch pipelines. This difference emphasizes the balance that must be maintained when sizing hydrogen pipelines, between the pipeline diameter, pressure drop, and hydrogen flow velocity increase.

The optimal input pressure and resulting pipeline diameter are dependent on several factors, including pipeline cost, compressor cost, and the impact of compression on hydrogen production losses. As a result, the optimal input pressure and corresponding pipeline diameter will be further assessed during the preliminary optimisation phase of the case study.

6.4.3. Hydrogen pipeline cost

In Figure 6.6, the hydrogen pipeline cost per meter for a range of diameters is given for a steel pipeline, bonded infield flow line and unbondend infield flowline.

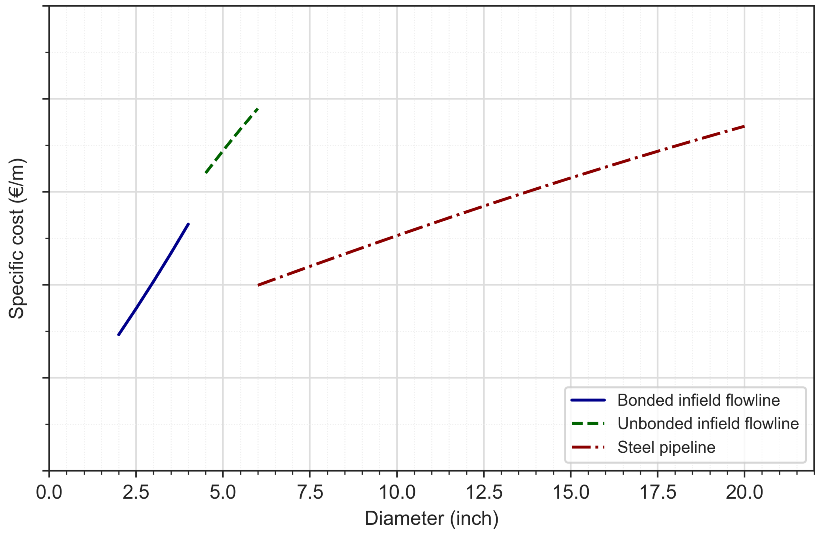

Figure 6.6: Procurement specific cost for infield flowlines and steel pipeline.

Increasing the hydrogen pipeline diameter results in a higher specific cost, as evident from Figure 6.6. Conversely, reducing the pipeline diameter leads to a larger pressure drop, which in turn may necessitate additional compression, incurring associated costs and power consumption. This scenario introduces a trade-off, necessitating a careful balance between opting for minimal compression with larger pipeline diameters or increased compression with smaller pipeline diameters.

7

Offshore hydrogen facility mass & cost modeling

This chapter delves into the mass and cost modeling associated with an OHF and discusses the various assumptions made, along with their applicability to different configurations. Comparing the mass and cost of OHFs is crucial due to the differences in their capacities within offshore wind-to-hydrogen systems. The modeling of OHF mass is addressed in Section 7.1, followed by the modeling of OHF cost in Section 7.2. Following that, in Section 7.3, the intermediate results of the OHF mass and cost modeling are presented to demonstrate the models.

7.1. Mass modeling

This section provides an elaboration on the mass modeling of OHFs, which is required for the cost calculations of the different OHF compositions in the various offshore wind-to-hydrogen configurations. In Subsection 7.1.1, an overview is presented, covering the different components involved in mass modeling for various OHF compositions. Following that, Subsection 7.1.2 discusses topside mass modeling. Subsection 7.1.4 focuses on the modeling of jacket substructure mass, while Subsection 7.1.5 provides an elaboration on the modeling of monopile substructure mass.

7.1.1. Mass modeling overview

The mass of an OHF consist of the topside and substructure mass. The topside mass is important to determine the substructure type while both the topside and substructure type are important to eventually determine the transport and installation cost. Table 7.1 provides an overview of the mass modeling components for different OHF compositions. The table distinguishes between jacket and monopile substructures, as well as centralised, semi-centralised, and decentralised offshore wind-to-hydrogen configurations. Consequently, the following OHF compositions are derived: centralised jacket, semi-centralised jacket, semi-centralised monopile, and decentralised monopile. This overview serves as a guideline for the mass modeling of OHFs, and the specific components will be further discussed in the subsequent subsections.

Section	Component	Symbol	Cen. Jacket	Semi-cen. Jacket	Semi-cen. MP	Decen. MP
Topside (M_{topside})	HPU HV	$M_{\text{HPU,HV}}$	X	X	X	
	HPU LV	$M_{\text{HPU,LV}}$				X
	Compressor	M_{comp}	X	X	X	
	Superstructure	M_{super}	X	X	X	
	Supportstructure	M_{support}	X	X	X	
	Working platform	M_{WP}				X
	H_2 wind turbine	M_{HWT}				X
Substructure: Jacket (M_{jacket})	Primary steel	M_{ps}	X	X		
	Secondary steel	M_{ss}	X	X		
	Anode	M_{anode}	X	X		
	Piles	M_{pile}	X	X		
Substructure: Monopile (M_{MP})	Foundation	$M_{\text{MP,fou}}$			X	X
	Transition piece	$M_{\text{MP,tp}}$			X	X

Table 7.1: Offshore hydrogen facility mass components per configuration.

Based on the provided table, two equations for the topside mass of the OHF and two equations for the substructure mass of the OHF can be derived. They are presented below.

The topside mass of a centralised jacket, semi-centralised jacket, and semi-centralised monopile OHF, known as the topside of an offshore hydrogen substation, is determined using a similar approach as described in Equation 7.1 [28].

$$M_{\text{Topside,substation}} = M_{\text{HPU,HV}} + M_{\text{comp}} + M_{\text{super}} + M_{\text{support}} \tag{7.1}$$

The topside mass of a decentralised OHF, also known as the topside of an offshore hydrogen wind turbine, is calculated with Equation 7.2.

$$M_{\text{Topside,HWT}} = M_{\text{HPU,LV}} + M_{\text{WP}} + M_{\text{HWT}} \tag{7.2}$$

The substructure mass of the jacket founded substations is determined with Equation 7.3 [28] [53]. This equation applies for the centralised jacket and semi-centralised jacket OHF composition.

$$M_{\text{Jacket}} = M_{\text{ps}} + M_{\text{ss}} + M_{\text{anode}} + M_{\text{pile}} \tag{7.3}$$

The substructure mass of a monopile founded substation and hydrogen wind turbine is determined with Equation 7.4. This equation applies for the semi-centralised monopile and decentralised monopile OHF composition.

$$M_{\text{MP}} = M_{\text{MP,fou}} + M_{\text{MP,tp}} \tag{7.4}$$

7.1.2. Topside hydrogen substation

The substation topside mass equation (Equation 7.1), is derived from a high-level study conducted by DNV for substations ranging from 100MW to 2GW [28]. It is important to note that the equations assume a linear relation between the mass and the installed hydrogen production unit capacity, without considering any scaling benefits and include an uncertainty of 25%. The substation topside mass is important because it determines the substation substructure type. The topside mass of a substation is determined by the combined mass of the HPU components, compressor mass, superstructure and auxiliary equipment.

$M_{\text{HPU,HV}}$ represents the mass of the high voltage HPU equipment. This can be calculated using Equation 7.5, where $\Gamma_{\text{HPU,HV}}$ represents the HPU high voltage specific mass per installed HPU capacity.

$$M_{\text{HPU,HV}} = \Gamma_{\text{HPU,HV}} \cdot P_{\text{HPU}} \tag{7.5}$$

The mass of the compressor is determine with Equation 7.6, where the compressor installed capacity is denoted with $P_{\text{compressor}}$ and the compressor's specific mass with $\Gamma_{\text{compressor}}$.

$$M_{\text{comp}} = \Gamma_{\text{compressor}} \cdot P_{\text{compressor}} \tag{7.6}$$

The superstructure mass is calculated with Equation 7.7. In this equation, M_{super} refers to the superstructure mass and Γ_{super} represents the specific mass of the superstructure per unit HPU equipment mass.

$$M_{\text{super}} = \Gamma_{\text{super}} \cdot M_{\text{HPU}} \tag{7.7}$$

The supporting infrastructure mass (M_{support}) can be calculated using Equation 7.8, where Γ_{support} represents the specific mass of the supporting infrastructure per unit HPU equipment mass.

$$M_{\text{support}} = \Gamma_{\text{support}} \cdot M_{\text{HPU}} \tag{7.8}$$

7.1.3. Topside hydrogen wind turbine

The topside mass of the hydrogen wind turbine is calculated with Equation 7.2 [3]. The mass of a hydrogen wind turbine consist of the turbine mass, HPU low voltage equipment mass and working platform mass. The turbine mass is supplied by Vattenfall and depends on type of turbine used [48].

The low voltage HPU equipment denoted with $M_{\text{HPU,LV}}$, can be calculated using Equation 7.9, where $\Gamma_{\text{HPU,LV}}$ represents the HPU low voltage specific mass per installed HPU capacity.

$$M_{\text{HPU,LV}} = \Gamma_{\text{HPU,LV}} \cdot P_{\text{HPU}} \tag{7.9}$$

The working platform mass of the hydrogen wind turbine can be calculated with Equation 7.10 [3] [28]. In this equation, M_{WP} represents the mass of the working platform, P_{turbine} is the rated power of the turbine, A_{HPU} is the area of the HPU equipment. The constant values are coefficients derived from fitting the historical data [3].

$$M_{\text{WP}} = \left[\left(\sqrt{\frac{P_{turbine}}{0.00031}} \cdot 0.0368 + 3 \right) + A_{HPU} \right] \cdot 0.25 \tag{7.10}$$

7.1.4. Jacket substructure

Equation 7.11 is used to calculate the mass of the jacket substructure (M_{Jacket}) [28]. The jacket substructure mass is determined by the sum of four components: primary steel mass (M_{ps}), superstructure mass (M_{ss}), anode mass (M_{anode}) and pile mass (M_{pile}).

$$M_{\text{Jacket}} = M_{\text{ps}} + M_{\text{ss}} + M_{\text{anode}} + M_{\text{pile}} \tag{7.11}$$

M_{ps} is calculated using Equation 7.12, where Γ_{ps} represents the specific mass of the primary steel per unit topside mass, cf_{ps} is a correction factor and D_{water} is the water depth [28].

$$M_{\text{ps}} = (\Gamma_{\text{ps}} \cdot M_{\text{Topside}} - cf_{ps}) \cdot D_{\text{water}} \tag{7.12}$$

M_{anode} is determined by Equation 7.13, which incorporates the specific mass of the anode per unit primary steel mass (Γ_{anode}) and a correction factor cf_{anode} [28].

$$M_{\text{anode}} = \Gamma_{\text{anode}} \cdot M_{\text{ps}} + cf_{anode} \tag{7.13}$$

The secondary steel mass (M_{ss}) is calculated using Equation 7.14, where Γ_{ss} represents the specific mass of the superstructure per unit HPU capacity, and cf_{ss} is a correction factor [28].

$$M_{\text{ss}} = \Gamma_{\text{ss}} \cdot P_{\text{HPU}} + cf_{ss} \tag{7.14}$$

The mass of the piles can be calculated using Equation 7.15. In this equation, M_{pile} represents the mass of the piles, which is determined by raising the mass of the jacket (M_{Jacket}) to the power of Γ_{pile} and multiplying it by 8 [53].

$$M_{\text{pile}} = 8 \cdot M_{\text{Jacket}}^{\Gamma_{\text{pile}}} \tag{7.15}$$

7.1.5. Monopile substructure

The mass of a monopile substructure consists of the foundation and the transition piece. These components depend on the specific mass per meter of a monopile, the length of the monopile, and the transition piece mass, which are obtained from a Vattenfall substructure expert. The monopile substructure mass can be calculated using Equation 7.16 [48].

$$M_{\text{MPsub}} = M_{\text{MPfou}} + M_{\text{MPtp}} \tag{7.16}$$

In Equation 7.16, M_{MPsub} represents the mass of the monopile substructure, M_{MPfou} represents the mass of the monopile foundation, and M_{MPtp} represents the mass of the transition piece. The mass of the monopile foundation can be calculated using Equation 7.17.

$$M_{\text{MPfou}} = \Gamma_{\text{MPfou}} \cdot (D_{\text{water}} + D_{\text{embedded}} + D_{\text{elevation}}) \tag{7.17}$$

In Equation 7.17, Γ_{MPfou} represents the specific mass of the monopile foundation, D_{water} represents the water depth, D_{embedded} represents the embedded depth into the soil and $D_{\text{elevation}}$ represents the distance between the water level and the top of the monopile foundation [48].

7.2. Cost modeling

This section focuses on cost modeling for OHFs, which is crucial due to variations in OHF compositions across different offshore wind-to-hydrogen configurations. Subsection 7.2.1 provides an overview of the cost modeling components for different OHF compositions. Subsection 7.2.2 discusses hydrogen production unit (HPU) equipment costs, while Subsection 7.2.3 elaborates on superstructure cost modeling. Subsection 7.2.4 addresses substructure cost modeling, followed by an explanation of transport, installation, and commissioning cost modeling in Subsection 7.2.5. Subsection 7.2.6 explores non-material cost modeling, and finally, Subsection 7.2.7 delves into manifold cost modeling.

7.2.1. Cost modeling overview

This section provides an overview of the cost modeling components for the different OHF composition. A distinction is made between the jacket and monopile substructure as well as the centralised, semi-centralised and decentralised offshore wind-to-hydrogen configurations. This leads to the following OHF compositions:

- Centralised jacket
- Semi-centralised jacket
- Semi-centralised monopile
- Decentralised monopile

Table 7.2 depicts the cost modeling components. The cost associated with the OHFs can be divided into two categories: capital expenditures (CAPEX) and operational expenditures (OPEX). In this research, the cost functions denoted by $C_{\text{component}}$ refer to the CAPEX values incured before operation of the wind-to-hydrogen farm starts. On the other hand, the OPEX values represent the costs incurred during each year of the facility's lifetime and are denoted as $C_{\text{OPEX,component}}$. The OPEX values are calculated by multiplying the CAPEX of a specific component by its corresponding OPEX factor, indicated as $f_{\text{OPEX,component}}$. These OPEX costs are specifically associated with the HPU equipment, substation superstructure, substation substructure and hydrogen manifold.

Section	Component	Symbol	Cen. Jacket	Semi-cen. Jacket	Semi-cen. MP	Decen. MP
HPU ($C_{\text{HPU,HV}}$) or ($C_{\text{HPU,LV}}$)	Electrolyser stacks	C_{stacks}	X	X	X	X
	BOP	C_{BOP}	X	X	X	X
	Compressor	$C_{\text{compressor}}$	X	X	X	X
	Electrical HV	$C_{\text{HV-electrical}}$	X	X	X	
	Electrical LV	$C_{\text{LV-electrical}}$				X
Superstructure ($C_{\text{super,substation}}$) or ($C_{\text{super,HWT}}$)	Superstructure steel	$C_{\text{steel-super}}$	X	X	X	
	Grating	C_{grating}	X	X	X	
	Cladding	C_{cladding}	X	X	X	
	Coating	C_{coating}	X	X	X	
	Working platform	C_{WP}				X
Substructure (C_{jacket}) or (C_{MP})	Jacket primary steel	C_{ps}	X	X		
	Jacket anode	C_{anode}	X	X		
	Jacket secondary steel	C_{ss}	X	X		
	Jacket pile	C_{pile}	X	X		
	MP Foundation	$C_{\text{Mp,fou}}$			X	X
	MP Transition piece	$C_{\text{MP,tp}}$			X	X
TIC ($C_{\text{TIC,substation,jacket}}$) ($C_{\text{TIC,substation,MP}}$) ($C_{\text{TIC,HWT,MP}}$)	Jacket substation T&I	$C_{\text{T\&I,substation,jacket}}$	X	X		
	MP substation T&I	$C_{\text{T\&I,substation,MP}}$			X	
	MP HWT T&I	$C_{\text{T\&I,HWT,MP}}$				X
	HPU installation	$C_{\text{HPU,I}}$	X	X	X	X
	Commissioning	C_{com}	X	X	X	X
	Decommissioning	C_{decom}	X	X	X	X
Non-material ($C_{\text{non-material}}$)	EPC	C_{EPCm}	X	X	X	X
	Owner	C_{owner}	X	X	X	X
	Contingencies	C_{cont}	X	X	X	X
Tower & RNA ($C_{\text{Tower\&RNA}}$)	Tower	C_{Tower}				X
	Rotor nacelle assembly	C_{RNA}				X
Manifold (C_{MF})	Procurement	$C_{\text{MF,pc}}$				X
	T&I	$C_{\text{MF,T\&I}}$				X
	IAC	$C_{\text{MF,IAC}}$				X

Table 7.2: Offshore hydrogen facility cost components per configuration.

From this table, the OHF cost equation for each wind-to-hydrogen farm can be derived. Important to mention is that that the Tower and Rotor Nacelle Assembly (RNA) costs are incorporated only in the calculations for the decentralised OHF cost because in the decentralised configuration, they share the same monopile as the HPU equipment.

In addition to the discussion of the OHF cost, this cost section also covers the manifold cost for the decentralised configuration. The costs associated with the Manifold, while listed in the table, are calculated independently from the decentralised OHF in Subsection 7.2.7. This separate calculation is due to the Manifold being a distinct offshore substation construction.

The CAPEX of the centralised jacket and semi-centralised jacket OHF, known as jacket substation, is calculated with Equation 7.18.

$$C_{\text{OHF,jacket-substation}} = C_{\text{HPU,HV}} + C_{\text{super,substation}} + C_{\text{jacket}} + C_{\text{TIC}} + C_{\text{non-material}} \tag{7.18}$$

The CAPEX of the semi-centralised monopile OHF, known as a monopile substation, is determined with Equation 7.19.

$$C_{\text{OHF,MP-substation}} = C_{\text{HPU,HV}} + C_{\text{super,substation}} + C_{\text{MP}} + C_{\text{TIC}} + C_{\text{non-material}} \tag{7.19}$$

The CAPEX of the decentralised monopile OHF, known as a monopile hydrogen wind turbine, is calculated with Equation 7.20. The costs for the wind turbine tower and RNA ($C_{\text{Tower\&RNA}}$) are sourced internally from Vattenfall. These costs are fixed for the chosen type of wind turbine and do not include high voltage electrical equipment [48].

$$C_{\text{OHF,MP-HWT}} = C_{\text{HPU,LV}} + C_{\text{super,HWT}} + C_{\text{MP}} + C_{\text{TIC,MP}} + C_{\text{non-material}} + C_{\text{Tower\&RNA}} \tag{7.20}$$

The overall OPEX of an OHF can be determined using Equation 7.21. This equation incorporates the OPEX values associated with the HPU equipment, superstructure, and substructure. The superstructure OPEX can pertain to either the substation superstructure or the working platform superstructure of the hydrogen wind turbine. Similarly, the substructure OPEX can be associated with either a monopile or jacket substructure.

$$C_{\text{OPEX,OHF}} = C_{\text{OPEX,stacks}} + C_{\text{OPEX,BOP}} + C_{\text{OPEX,compressor}} + C_{\text{OPEX,superstructure}} + C_{\text{OPEX,substructure}} \quad (7.21)$$

7.2.2. Hydrogen production unit equipment

The cost of the HPU equipment comprises the combined cost of the electrolyser stacks, BOP, compressor, and electrical equipment. The HPU equipment cost modeling for the centralised jacket and semi-centralised jacket and monopile OHF, differs compared to the decentralised monopile OHF. The difference lies in the electrical system cost, which is dependent on the incoming voltages. Specifically, the electrical system cost varies based on whether the incoming voltages are high voltage or low voltage.

The high voltage HPU equipment CAPEX can be calculated with Equation 7.22. The low voltage HPU equipment CAPEX is determined with Equation 7.23. Important to mention is that the compressor CAPEX $C_{\text{compressor}}$ only applies when there is a compressor present in the OHF.

$$C_{\text{HPU,HV}} = C_{\text{stacks}} + C_{\text{BOP}} + C_{\text{compressor}} + C_{\text{HV-electrical}} \quad (7.22)$$

$$C_{\text{HPU,LV}} = C_{\text{stacks}} + C_{\text{BOP}} + C_{\text{compressor}} + C_{\text{LV-electrical}} \quad (7.23)$$

The cost functions assume a scaling of HPU cost with installed capacity. The scaling of cost is obtained from the Danish Energy Agency and DNV [3]. This assumption is based on the limited economies of scale above 100MW [88]. The economy of scale of the electrolyser stacks is limited due to the modular design of electrolyser stacks.

The CAPEX of the electrolyser stacks within the HPU can be calculated using Equation 7.24. Here, C_{stacks} represents the CAPEX of the electrolyser stacks, P_{HPU} is the power of the HPU, and c_{stacks} is the specific cost of the electrolyser stacks. It is assumed that the electrolyser stack cost scale non-linear with the installed HPU capacity [3].

$$C_{\text{stacks}} = P_{\text{HPU}} \cdot c_{\text{stacks}} \cdot \left(\frac{(P_{\text{HPU}})^{SF_{\text{stacks}}}}{P_{\text{HPU}}} \right) \quad (7.24)$$

The specific cost of the stacks is calculated with Equation 7.25[3]. This is done to take into account the economy of scale of the electrolyser stacks. In this equation, $c_{\text{stacks,ref}}$ is the reference specific cost of the electrolyser stacks, $P_{\text{HPU,ref}}$ is the associated reference HPU capacity and SF_{stacks} is the scale factor of the electrolyser stacks.

$$c_{\text{stacks}} = c_{\text{stacks,ref}} \cdot \left(\frac{P_{\text{HPU,ref}}}{(P_{\text{HPU,ref}})^{SF_{\text{stacks}}}} \right) \quad (7.25)$$

The OPEX associated with the electrolyser stacks are determined using Equation 7.26, where $C_{\text{OPEX,stacks}}$ denotes the OPEX of the electrolyser stacks. The OPEX factor of the electrolyser stacks is represented by $f_{\text{OPEX,stacks}}$.

$$C_{\text{OPEX,stacks}} = C_{\text{stacks}} \cdot f_{\text{OPEX,stacks}} \quad (7.26)$$

The BOP CAPEX (without compressor) (C_{BOP}), can be calculated with Equation 7.27 [41]. In this equation, (c_{BOP}) presents the specific cost of the BOP. It is assumed that the cost of the BOP scales non-linear with the HPU installed capacity.

$$C_{\text{BOP}} = P_{\text{HPU}} \cdot c_{\text{BOP}} \cdot \left(\frac{(P_{\text{HPU}})^{SF_{\text{BOP}}}}{P_{\text{HPU}}} \right) \quad (7.27)$$

The specific cost of the BOP is calculated with Equation 7.28 [3]. This is done to take into account the economy of scale of the BOP equipment. In this equation, $c_{\text{BOP,ref}}$ is the reference specific cost of the BOP equipment, $P_{\text{HPU,ref}}$ is the associated reference HPU capacity and SF_{BOP} is the scale factor of the BOP equipment.

$$c_{\text{BOP}} = c_{\text{BOP,ref}} \cdot \left(\frac{P_{\text{HPU,ref}}}{(P_{\text{HPU,ref}})^{SF_{\text{BOP}}}} \right) \quad (7.28)$$

The OPEX associated with the BOP are determined using Equation 7.29, where $C_{\text{OPEX,BOP}}$ denotes the OPEX of the BOP. The OPEX factor of the BOP is represented by $f_{\text{OPEX,BOP}}$.

$$C_{\text{OPEX,BOP}} = C_{\text{BOP}} \cdot f_{\text{OPEX,BOP}} \tag{7.29}$$

The compressor CAPEX, can be calculated with Equation 7.30 [57]. In this equation, $C_{\text{compressor}}$ represents the CAPEX of the compressor. The cost factors for the compressor are denoted as $c_{1-\text{compressor}}$ and $c_{2-\text{compressor}}$. The power of the compressor is represented by $P_{\text{compressor}}$. It can be noted that besides a cost component which scales with the installed compressor capacity, a fixed cost is associated independent from the installed capacity.

$$C_{\text{compressor}} = P_{\text{compressor}} \cdot c_{1-\text{compressor}} + c_{2-\text{compressor}} \tag{7.30}$$

The OPEX associated with the compressor are determined using Equation 7.31, where $C_{\text{OPEX,compressor}}$ denotes the OPEX of the compressor. The OPEX factor of the compressor is represented by $f_{\text{OPEX,compressor}}$.

$$C_{\text{OPEX,compressor}} = C_{\text{compressor}} \cdot f_{\text{OPEX,compressor}} \tag{7.31}$$

The high voltage electrical equipment CAPEX ($C_{\text{HV-electrical}}$) scales non-linear with the installed HPU capacity and is adapted from an internal Vattenfall source and the gigawatt scale study of Hydrohub [41]. The high voltage electrical equipment CAPEX for a range of HPU installed capacities is given in Figure 7.1. This cost function stems from a list of electrical components per installed capacity, as provided by an in-house expert at Vattenfall [48]. Major contributors to this function are the step-down transformers and high voltage switchgears. The significant cost hike around 330, 660, and 990MW is attributable to the step-down transformers, as an additional one becomes necessary after a specific capacity. The same applies to high voltage switchgears, albeit with smaller capacity increments. This stepped function is especially disadvantageous for the smaller OHFs capacities within the semi-centralised configuration, as it could raise their specific cost significantly. Nevertheless, fully utilising the electrical equipment capacity of the primary contributors is more critical in order to decrease the specific electrical equipment cost.

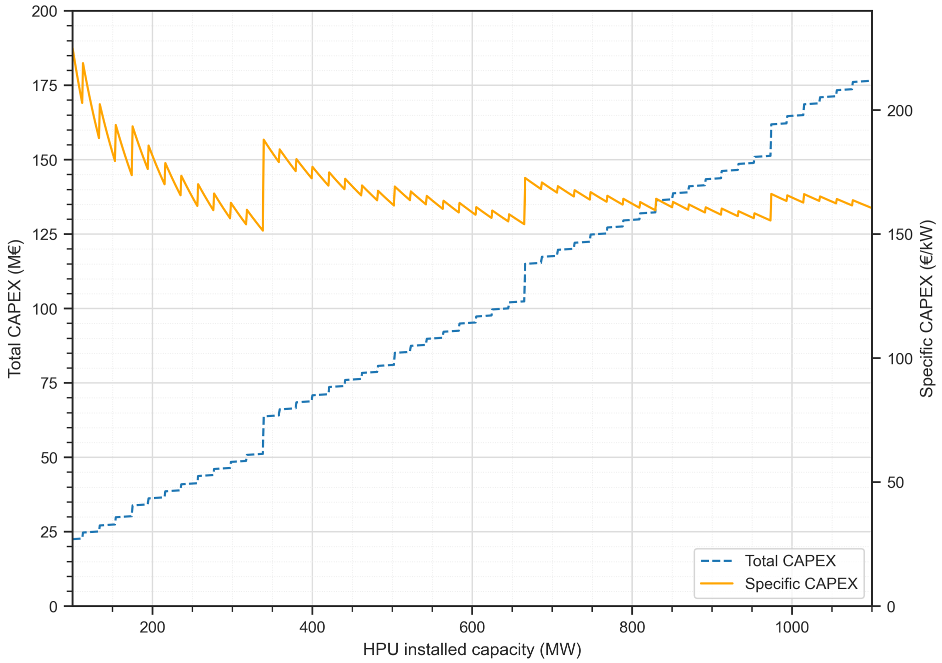

Figure 7.1: Total and specific electrical equipment CAPEX per HPU installed capacity.

The OPEX associated with the high voltage electrical equipment are determined using Equation 7.32, where $C_{\text{OPEX,HV-electrical}}$ denotes the OPEX of the high voltage electrical equipment. The OPEX factor of the high voltage electrical equipment is represented by $f_{\text{OPEX,HV-electrical}}$.

$$C_{\text{OPEX,HV-electrical}} = C_{\text{HV-electrical}} \cdot f_{\text{OPEX,HV-electrical}} \tag{7.32}$$

The low voltage electrical equipment CAPEX ($C_{\text{LV-electrical}}$) scales linear with the installed HPU capacity and calculated with Equation 7.33. In this equation, $c_{\text{LV-electrical,1}}$ represents the fixed cost coefficient and $c_{\text{LV-electrical,2}}$ the variable cost coefficient of the LV electrical equipment. Additionally, P_{turbine} represents the rated power of the hydrogen wind turbine.

$$C_{\text{LV-electrical}} = c_{\text{LV-electrical,1}} \cdot P_{\text{turbine}} + c_{\text{LV-electrical,2}} \tag{7.33}$$

The OPEX associated with the low voltage electrical equipment are determined using Equation 7.34, where $C_{\text{OPEX,LV-electrical}}$ denotes the OPEX of the low voltage electrical equipment. The OPEX factor of the low voltage electrical equipment is represented by $f_{\text{OPEX,LV-electrical}}$.

$$C_{\text{OPEX,LV-electrical}} = C_{\text{LV-electrical}} \cdot f_{\text{OPEX,LV-electrical}} \tag{7.34}$$

The cost of replacing the electrolyser stack is expected to be lower than the initial stack cost, as it is assumed that the stack cost reduces over time due to learning rates [38]. The formula to calculate the replacement cost ($C_{\text{stacks,y}}$) for the electrolyser stack in year y can be determined using Equation 7.35. This equation involves several variables: P_{HPU}, which represents the installed capacity of the HPU; c_{stacks}, the cost per unit of electrolyser stack capacity; f_{SCR}, the stack replacement cost coefficient; and $C_{\text{TIC,replacement}}$, an additional cost component covering the transport and installation of the stack replacement.

$$C_{\text{stacks,y}} = P_{\text{HPU}} \cdot c_{\text{stacks}} \cdot f_{\text{SCR}} + C_{\text{TIC,replacement}} \tag{7.35}$$

The calculation of the stack cost decrease is based on a simplified approach, assuming that the electrolyser stack cost decreases by the same percentage with each replacement. Furthermore, it is assumed that the transport and installation expenses for the stack replacement amount to a percentage of the stack cost [3]. This transport and installation of a stack replacement can be calculated with Equation 7.36, where $f_{\text{TIC,replacement}}$ represents the transport and installation cost coefficient.

$$C_{\text{TIC,replacement}} = f_{\text{TIC,replacement}} \cdot P_{\text{HPU}} \cdot c_{\text{stacks}} \cdot f_{\text{SCR}} \tag{7.36}$$

7.2.3. Superstructure

The superstructure CAPEX of the centralised jacket, semi-centralised jacket and semi-centralised monopile OHF, consist of the substation superstructure CAPEX and is depicted as $C_{\text{super,substation}}$ [28]. The superstructure CAPEX of the decentralised monopile OHF, known as the monopile hydrogen wind turbine, consist only of the working platform CAPEX denoted as $C_{\text{super,HWT}}$ [3].

The cost of the substation superstructure is primarily influenced by the HPU installed capacity. In literature, a linear relation between the topside superstructure cost and the HPU installed capacity is found [28]. The substation superstructure CAPEX, is obtained by summing the CAPEX of the individual components steel ($C_{\text{steel-super}}$), grating (C_{grating}), cladding (C_{cladding}) and coating (C_{coating}). Equation 7.37 is used to calculate the substation superstructure CAPEX [28].

$$C_{\text{super,substation}} = C_{\text{steel-super}} + C_{\text{grating}} + C_{\text{cladding}} + C_{\text{coating}} \tag{7.37}$$

The superstructure steel CAPEX is determined using Equation 7.38, where c_{steel} represents the specific cost of steel [28].

$$C_{\text{steel-super}} = M_{\text{super}} \cdot c_{\text{steel}} \tag{7.38}$$

The grating CAPEX in the substation superstructure is estimated using Equation 7.39, with c_{grating} representing the cost of grating surface [28].

$$C_{\text{Grating}} = V_{\text{Topside}} \cdot c_{\text{grating}} \tag{7.39}$$

The cladding CAPEX in the substation superstructure, is estimated using Equation 7.40, where c_{cladding} represents the specific cost of cladding in per unit support infrastructure mass [28].

$$C_{\text{cladding}} = M_{\text{support}} \cdot c_{\text{cladding}} \tag{7.40}$$

The coating CAPEX in the substation superstructure is calculated using Equation 7.41, with c_{coating} representing the specific cost of coating per unit mass of both the support infrastructure and superstructure steel [28].

$$C_{\text{coating}} = (M_{\text{support}} + M_{\text{super}}) \cdot c_{\text{coating}} \tag{7.41}$$

The OPEX associated with the substation superstructure are determined using Equation 7.42, where $C_{\text{OPEX,super,substation}}$ denotes the OPEX of the substation superstructure. The OPEX factor of the superstructure is represented by $f_{\text{OPEX,super,substation}}$.

$$C_{\text{OPEX,super,substation}} = C_{\text{super,substation}} \cdot f_{\text{OPEX,super,substation}} \tag{7.42}$$

The CAPEX of the superstructure working platform of the hydrogen wind turbine is calculated with Equation 7.43 [3]. The cost scales with the mass of the working platform (M_{WP}) determined with Equation 7.10, and the specific cost of the working platform (c_{WP}).

$$C_{\text{WP}} = M_{\text{WP}} \cdot c_{\text{WP}} \tag{7.43}$$

The OPEX associated with the working platform are determined using Equation 7.44, where $C_{\text{OPEX,WP}}$ denotes the OPEX of the working platform. The OPEX factor of the working platform is represented by $f_{\text{OPEX,WP}}$.

$$C_{\text{OPEX,WP}} = C_{\text{WP}} \cdot f_{\text{OPEX,WP}} \tag{7.44}$$

7.2.4. Substructure

The cost of the OHF substructure is influenced by the type of substructure used, which is directly impacted by the topside weight. The cost for a jacket substructure or monopile substructure is calculated using different equations.

The CAPEX of a jacket substructure, denoted as C_{Jacket}, can be determined by Equation 7.45. The jacket substructure CAPEX consist of the primary steel CAPEX (C_{ps}), anode CAPEX (C_{anode}), secondary steel CAPEX (C_{ss}) and pile CAPEX (C_{pile}).

$$C_{\text{Jacket}} = C_{\text{ps}} + C_{\text{anode}} + C_{\text{ss}} + C_{\text{pile}} \tag{7.45}$$

The primary steel CAPEX is calculated using Equation 7.46, where M_{ps} represents the mass of the primary steel and c_{ps} is the cost per unit mass of primary steel [28].

$$C_{\text{ps}} = M_{\text{ps}} \cdot c_{\text{ps}} \tag{7.46}$$

The anode CAPEX is determined by Equation 7.47, which incorporates the mass of the anode (M_{anode}) and the cost per unit mass of the anode material (c_{anode})[28].

$$C_{\text{anode}} = M_{\text{anode}} \cdot c_{\text{anode}} \tag{7.47}$$

The secondary steel CAPEX is calculated using Equation 7.48, where M_{ss} represents the mass of the secondary steel and c_{ss} is the cost per unit mass of secondary steel [28].

$$C_{\text{ss}} = M_{\text{ss}} \cdot c_{\text{ss}} \tag{7.48}$$

The pile CAPEX is calculated using Equation 7.49. In this equation, M_{pile} denotes the mass of the piles, and c_{pile} represents the cost per unit mass of the piles.

$$C_{\text{pile}} = M_{\text{pile}} \cdot c_{\text{pile}} \tag{7.49}$$

The OPEX associated with the jacket substructure are determined using Equation 7.50, where $C_{\text{OPEX,Jacket}}$ denotes the OPEX of the jacket substructure. The OPEX factor of the jacket substructure is represented by $f_{\text{OPEX,Jacket}}$.

$$C_{\text{OPEX,Jacket}} = C_{\text{Jacket}} \cdot f_{\text{OPEX,Jacket}} \tag{7.50}$$

For semi-centralised monopile and decentralised monopile OHFs, the CAPEX of the monopile substructure, denoted as C_{MP}, is determined using Equation 7.51. The CAPEX of the monopile substructure consist of the monopile foundation CAPEX and the monopile transition piece CAPEX [48].

$$C_{\text{MP}} = M_{\text{MPfou}} \cdot c_{\text{MP,fou}} + M_{\text{MP,tp}} \cdot c_{\text{tp}} \tag{7.51}$$

In this equation, $M_{\text{MP,fou}}$ represents the mass of the monopile foundation and $c_{\text{MP,fou}}$ represents the cost per unit mass of the monopile foundation. $M_{\text{MP,tp}}$ represents the total transition piece mass, and $c_{\text{MP,tp}}$ represents the cost per unit mass of the transition piece.

The OPEX associated with the monopile substructure are determined using Equation 7.52, where $C_{\text{OPEX,monopile}}$ denotes the OPEX of the monopile substructure. The OPEX factor of the monopile substructure is represented by $f_{\text{OPEX,monopile}}$.

$$C_{\text{OPEX,monopile}} = C_{\text{monopile}} \cdot f_{\text{OPEX,monopile}} \tag{7.52}$$

7.2.5. Transport, installation and commissioning

The cost of transport, installation and commissioning (TIC) represents the total expenditure required for the entire process from transporting the hydrogen related components from an onshore yard to the offshore location and associated commissioning. The TIC differs for the different OHF compositions due to the different types of substructures and the difference in topside mass.

For a centralised jacket and semi-centralised jacket substation, the TIC costs are calculated with Equation 7.53. In this equation $C_{\text{T\&I,substation,jacket}}$ represents the jacket substation transport and installation cost. The HPU equipment installation cost are depicted as $C_{\text{HPU,inst}}$ and the commissioning cost as C_{com}.

$$C_{\text{TIC,substation,jacket}} = C_{\text{T\&I,substation,jacket}} + C_{\text{HPU,inst}} + C_{\text{com}} \tag{7.53}$$

The TIC of a semi-centralised monopile substation, denoted as $C_{\text{TIC,substation,MP}}$, can be calculated using Equation 7.54. In this equation, $C_{\text{T\&I,substation,MP}}$ represents the transport and installation cost of a monopile substation.

$$C_{\text{TIC,substation,MP}} = C_{\text{T\&I,substation,MP}} + C_{\text{HPU,inst}} + C_{\text{com}} \tag{7.54}$$

The TIC of a decentralised monopile hydrogen wind turbine is determined using Equation 7.55. In this equation, $C_{\text{T\&I,HWT,MP}}$ represents the transport and installation cost of a monopile hydrogen wind turbine.

$$C_{\text{TIC,HWT,MP}} = C_{\text{T\&I,HWT,MP}} + C_{\text{HPU,inst}} + C_{\text{com}} \tag{7.55}$$

The cost of transport and installation (T&I) for an OHF substructure and topside is determined by the specific method of T&I, as described in Section 3.7. The choice of T&I method is influenced by the topside mass of the OHF, which in turn depends on the installed capacity of the HPU.

For the substation jacket composition, there are no synergies in T&I, necessitating a separate T&I procedure that does not consider the transport and installation of wind turbines. The T&I cost for a jacket substation ($C_{\text{T\&I,substation,jacket}}$) is estimated using data from Vattenfall's internal sources. Due to the inherent uncertainty, a simplified and conservative cost function is employed. This function incorporates both transport and installation costs, represented by a fixed cost per T&I method, determined by the topside's mass. This approach results in the step function observed in Figure 7.2.

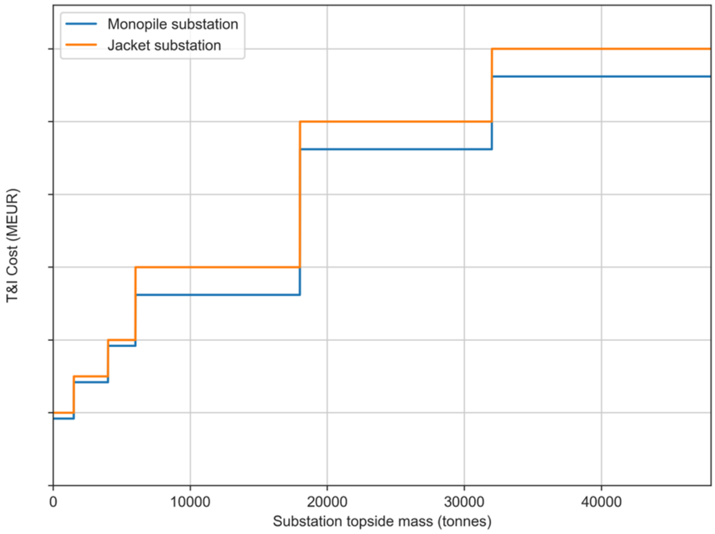

Figure 7.2: Total transport and installation cost function for jacket and monopile substations for a range of topside masses [73].

The step function of the monopile substation is depicted in Figure 7.2 as well. The T&I cost for the monopile substation differs from the jacket substation OHF due to the synergies created by sharing the monopile foundations with the wind turbines. Similar to the jacket substation, Vattenfall provides a cost estimate for the monopile substation T&I cost, as depicted in the figure. This cost function incorporates both transport and installation costs, with a fixed cost per T&I method determined by the topside's mass.

The hydrogen wind turbine's T&I cost ($C_{\text{T\&I,HWT,MP}}$) encompasses the expenses associated with both the transport and installation of the working platform on the hydrogen wind turbine, as well as the T&I operations specific to the hydrogen wind turbine itself. The calculation of $C_{\text{T\&I,HWT,MP}}$ can be achieved using Equation 7.56, where $C_{\text{T\&I,WP}}$ represents the T&I cost of the working platform, and $C_{\text{T\&I,HWT}}$ denotes the transport and installation cost of the hydrogen wind turbine. The T&I of the offshore hydrogen wind turbine includes the standard T&I cost for a wind turbine, substructure, and foundation, and is determined using Vattenfall's in-house model. The transport and installation cost for the hydrogen wind turbine is a fixed constant per turbine.

$$C_{\text{T\&I,HWT,MP}} = C_{\text{T\&I,WP}} + C_{\text{T\&I,HWT}} \tag{7.56}$$

The cost of the HPU equipment installation scales with the HPU equipment cost and is calculate with Equation 7.57 [3]. In this equation, $C_{\text{HPU,installation}}$ represents the HPU equipment installation cost. The component specific cost coefficients of the stacks, BOP, electrical equipment and compressor are denoted with $c_{\text{inst,stacks}}$, $c_{\text{inst,BOP}}$, $c_{\text{inst,electrical}}$ and $c_{\text{inst,comp}}$ respectively.

$$C_{\text{HPU,inst}} = C_{\text{stacks}} \cdot c_{\text{inst,stacks}} + C_{\text{BOP}} \cdot c_{\text{inst,BOP}} + C_{\text{electrical}} \cdot c_{\text{inst,electrical}} + C_{\text{comp}} \cdot c_{\text{inst,comp}} \tag{7.57}$$

The commissioning cost of the offshore substation can be determined using Equation 7.58 [5]. This equation, commonly utilized in the oil and gas industry, calculates the commissioning cost as a percentage of the total HPU equipment CAPEX. In this equation, C_{com} represents the commissioning cost, C_{HPU} denotes the total equipment CAPEX (including the HPU), and cf_{com} is the commissioning cost factor expressed as a percentage.

$$C_{\text{com}} = C_{\text{HPU}} \cdot cf_{\text{com}} \tag{7.58}$$

The decommissioning cost (C_{decom}) at the end of the lifetime of the OHF is calculated using Equation 7.59 [5]. In this equation, C_{TIC} represents the combined cost of construction, transport, installation, and commissioning of the OHF, and c_{decom} is the decommissioning cost factor.

$$C_{\text{decom}} = C_{\text{TIC}} \cdot c_{\text{decom}} \tag{7.59}$$

7.2.6. Non-material

The Non-material costs refer to expenses that are not directly attributed to the physical components of the hydrogen substation but still hold significant importance in the overall cost estimation. The calculation of non-material costs remains consistent across all OHF compositions. These costs, denoted as $C_{\text{non-material}}$, can be determined using Equation 7.60, which involves the summation of engineering, procurement, project and construction management costs (C_{EPCm}), owner's costs (C_{owner}), and contingency costs (C_{cont}) [41].

$$C_{\text{non-material}} = C_{\text{EPCm}} + C_{\text{owner}} + C_{\text{cont}} \tag{7.60}$$

Engineering, procurement, project and construction management (EPCm) costs (C_{EPCm}) can be calculated using Equation 7.61. In this equation, C_{HPU}, C_{sub}, and C_{super} represent specific material cost components, while cf_{EPCm} denotes the cost factor associated with EPCm [41]. It is essential to note that, for the non-material cost calculation, a cost scaling factor of 1 is used to determine the HPU equipment cost C_{HPU} because it is assumed that the non-material costs do not scale with the HPU installed capacity.

$$C_{\text{EPCm}} = (C_{\text{HPU}} + C_{\text{sub}} + C_{\text{super}}) \cdot cf_{\text{EPCm}} \tag{7.61}$$

Owner's costs (C_{owner}) refers to expenses incurred by the owner of the OHF, such as legal fees, permitting, and insurance costs. These costs can be calculated using Equation 7.62, where C_{HPU}, C_{sub}, and C_{super} represent material cost components, and f_{owner} denotes the cost factor associated with owner's costs [41].

$$C_{\text{owner}} = (C_{\text{HPU}} + C_{\text{sub}} + C_{\text{super}}) \cdot c_{\text{owner}} \tag{7.62}$$

Contingency costs (C_{cont}) account for unforeseen events or circumstances that may arise during the construction or operation of the OHF. These costs can be calculated using Equation 7.63, where C_{HPU}, C_{sub}, C_{super} relate to the material cost, C_{EPCm} represent EPCm cost, C_{owner} the owner's cost and cf_{cont} denotes the contingency cost factor [41]. The total contingency costs are determined by adding the costs of these components and multiplying the sum by the contingency cost factor.

$$C_{\text{cont}} = (C_{\text{HPU}} + C_{\text{sub}} + C_{\text{super}} + C_{\text{EPCm}} + C_{\text{owner}}) \cdot cf_{\text{cont}} \tag{7.63}$$

7.2.7. Manifold

The cost modeling of the hydrogen manifold specifically pertains to the decentralised configuration. Since it the manifold is a separate construction, it is not included in the overall cost of the OHFs. The manifold CAPEX comprises the procurement cost, installation cost, substructure cost, and compressor cost, which can be calculated using Equation 7.64 [36]. It is crucial to note that this equation represents a simplified method, incorporating case-specific values obtained within Vattenfall.

$$C_{\text{MF}} = C_{\text{MF,procurement}} + C_{\text{MF,T\&I}} + C_{\text{MF,substructure}} + C_{\text{compressor}} + C_{\text{MF,IAC}} \tag{7.64}$$

The manifold procurement cost ($C_{\text{MF,procurement}}$) and transport and installation cost ($C_{\text{MF,T\&I}}$) are fixed cost. The manifold substructure cost ($C_{\text{MF,substructure}}$) is determined with monopile cost Equation 7.51. The compressor cost ($C_{\text{compressor}}$) is determined with Equation 7.30. Finally, the cost and length of the IAC connecting the closest wind turbine to the manifold ($C_{\text{MF,IAC}}$), necessary for supplying power to the compressors, are calculated using the in-house Vattenfall model.

The OPEX associated with the manifold are determined using Equation 7.65, where $C_{\text{OPEX,MF}}$ denotes the OPEX of the manifold. The OPEX factor of the manifold is represented by $f_{\text{OPEX,MF}}$.

$$C_{\text{OPEX,MF}} = C_{\text{MF}} \cdot f_{\text{OPEX,MF}} \tag{7.65}$$

7.3. Mass & cost model demonstration

This section aims to demonstrate the functioning of the OHF mass & cost modeling. First the constants used are given in Subsection 7.3.1. Hereafter, the OHF mass modeling demonstration results are given in Subsection 7.3.2. Hereafter, in Subsection 7.3.3, the OHF cost modeling demonstration results are elaborated.

7.3.1. Offshore hydrogen facility constants

In Table 7.3, the constants used for the mass modeling of the OHF are given. Additionally, in Table 7.4, the cost constants used for the OHF cost modeling for the centralised and semi-centralised configurations are given.

Parameter	Symbol	Value	Unit	Source
Hydrogen production unit				
Compressor specific mass	$\Gamma_{\text{compressor}}$	X	tonne/MW	[57]
HPU HV specific mass	Γ_{HPU}	12.8	tonne/MW	[28]
HPU LV specific mass	Γ_{HPU}	9	tonne/MW	[3]
Superstructure				
Superstructure specific mass	Γ_{super}	1.035	tonne/tonne$_{\text{HPU}}$	[28]
Supporting infrastructure specific mass	Γ_{support}	0.515	tonne/tonne$_{\text{HPU}}$	[28]
HPU area decentralised configuration	A_{HPU}	577	m^2	[3]
Substructure				
Jacket primary steel specific mass	Γ_{ps}	0.0184	%	[28]
Jacket secondary steel specific mass	Γ_{ss}	0.085	tonne/tonne$_{\text{HPU}}$	[28]
Jacket primary steel mass correction factor	cf_{ps}	15.79	tonne	[28]
Jacket secondary steel mass correction factor	cf_{ss}	88.7	tonne	[28]
Jacket Anode mas correction factor	cf_{anode}	7.5	tonne	[28]
Jacket Anode specific mass	Γ_{anode}	0.0095	tonne/tonne$_{\text{PS}}$	[28]
Jacket pile mass factor	Γ_{pile}	0.5574	-	[53]
Monopile foundation mass	$M_{\text{MP,fou}}$	X	tonne	[48]
Monopile transition piece mass	$M_{\text{MP,tp}}$	X	tonne	[48]

Table 7.3: Offshore hydrogen facility mass constants.

Parameter	Symbol	Value	Unit	Source
Hydrogen production unit equipment				
Electrolyser stacks specific cost (1000MW)	$c_{\text{stacks,ref}}$	154000	€/MW	[41]
Electrolyser stack scale factor	SF_{BOP}	0.95		[3]
Electrolyser stack OPEX factor	$_{\text{OPEX,BOP}}$	2.0	%	[77]
BOP specific cost (1000MW)	$c_{\text{BOP,ref}}$	54000	€/MW	[41]
BOP scale factor	SF_{BOP}	0.75		[3]
BOP OPEX factor	$f_{\text{OPEX,BOP}}$	3.0	%	[71]
Compressor specific cost	$c_{\text{1-compressor}}$	X	€/MW	VF
Compressor fixed cost	$c_{\text{2-compressor}}$	X	€	VF
Compressor OPEX factor	$f_{\text{OPEX,compressor}}$	8.0	%	[26]
Stack replacement cost coefficient	f_{SCR}	90.0	%	[38]
Stack replacement TIC cost coefficient	$f_{\text{TIC,replacement}}$	50.0	%	[3]
Superstructure				
Superstructure steel specific cost	c_{steel}	4042.1	€/tonne	[28]
Grating specific cost	c_{grating}	21.1	€/m^2	[28]
Cladding specific cost	c_{cladding}	3464.7	€/tonne	[28]
Coating specific cost	c_{coating}	138.6	€/tonne	[28]
Substation Superstructure OPEX factor	$f_{\text{OPEX,super,substation}}$	2.0	%	[39]
Working platform specific cost	c_{WP}	7500	€/tonne	[3]
Working platform OPEX factor	$f_{\text{OPEX,WP}}$	2.0	%	[39]
Substructure				
Jacket primary steel specific cost	c_{ps}	2309.8	€/tonne	[28]
Jacket Anode specific cost	c_{anode}	7506.9	€/tonne	[28]
Jacket secondary steel specific cost	c_{ss}	2887.3	€/tonne	[28]
Jacket OPEX factor	$f_{\text{OPEX,Jacket}}$	2.0	%	[54]
Monopile foundation specific cost	$c_{\text{MP,fou}}$	X	€/tonne	[48]
Monopile transition piece specific cost	$c_{\text{MP,tp}}$	X	€/tonne	[48]
Monopile OPEX factor	$f_{\text{OPEX,monopile}}$	2.0	%	[54]
Transport and installation				
Stack installation cost coefficient	$c_{\text{inst,stacks}}$	50.0	%	[3]
BOP installation cost coefficient	$c_{\text{inst,BOP}}$	10.0	%	[3]
Electrical equipment installation cost coefficient	$c_{\text{inst,electrical}}$	30.0	%	[3]
Compressor installation cost coefficient	$c_{\text{inst,comp}}$	30.0	%	[3]
Commissioning OHF cost factor	cf_{comm}	10.0	%	[5]
T&I cost of working platform	$C_{\text{T\&I,WP}}$	95,000	€ /turbine	[3]
Non-material				
EPCm OHF cost factor	cf_{EPCm}	23.0	%	[41]
Contingency OHF cost factor	cf_{cont}	35.0	%	[41]
Owner cost factor	cf_{owner}	16.0	%	[41]
Decommissioning cost factor	cf_{decom}	50.0	%	[35]
Manifold				
Manifold procurement cost	$C_{\text{MF,procurement}}$	X	€	[36]
Manifold transport and installation cost	$C_{\text{MF,T\&I}}$	X	€	[36]
Manifold OPEX factor	$f_{\text{OPEX,MF}}$	X	%	[36]

Table 7.4: Offshore hydrogen facility cost constants.

7.3.2. Mass model demonstration results

The topside mass of the substation determines the appropriate substructure type and is thus vital for the overall system design of the substation. Additionally, the substructure mass is of significant importance as it directly influences the selection of the transport and installation method for the substation. In Figure 7.3, the hydrogen substation topside and substructure mass per installed HPU capacity are depicted. It can be observed from this figure that the substructure's mass remains constant between 0-300MW. Moreover, it's apparent that there's a linear relationship between the topside and substructure mass and the installed HPU capacity after 300MW. The transition point around 300MW, signifies the shift from a monopile substructure to a jacket substructure, determined based on the analysis of the topside mass and the monopile's load capacity.

The monopile mass remains constant for the HPU installed capacity before the transition point. The assumption here is that the monopiles utilized for offshore wind turbines are also employed for the hydrogen substations. As a result, the monopile's load capacity is not fully utilized below the HPU installed capacity of the transition point between the monopile and jacket. This conservative decision guarantees that the monopiles are sufficiently robust to handle the maximum load of both the wind turbines and the topsides of the hydrogen substations. While optimising the monopiles for the specific HPU installed capacity could reduce costs, it would also lead to fewer synergies between the monopiles of the wind turbines and the hydrogen substations.

Conversely, for jacket substructures, the mass does increase with a rise in topside mass, as the jacket is designed to specifically accommodate the corresponding topside weight.

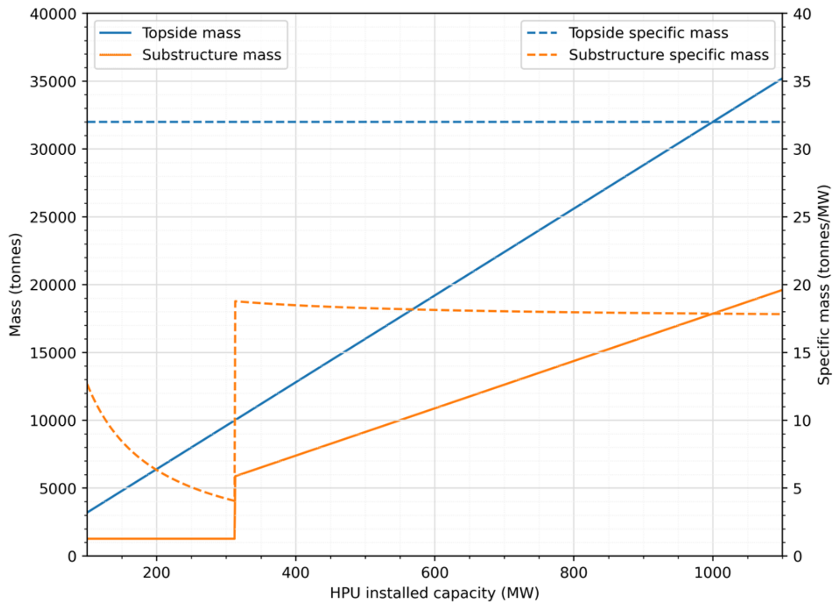

Figure 7.3: The total and specific mass of a hydrogen substation topside and substructure, plotted against the HPU installed capacity for HPU capacities exceeding 100MW.

The determination of the substructure, whether a jacket or a monopile, can be achieved by referring to the values provided in the figure above and considering the load capacity of the monopile. Specifically, for a 15MW wind turbine using a monopile substructure with an 8-meter diameter, it is noted that the vertical load capacity is 10,000 tons [7]. In cases where the installed HPU capacity leads to a topside weight surpassing 10,000 tons, a jacket substructure will be chosen for the semi-centralised substation. Similarly, for the centralised configuration, a jacket substructure is preferred for the centralised substation due to the anticipated topside weight, which is not suitable for a monopile substructure.

In this research, the topside and substructure mass of the offshore hydrogen wind turbine is presented as two single values since only one offshore wind turbine with a constant capacity is selected. Considering a 15MW hydrogen wind turbine, the topside mass and substructure mass are 1,903 and 1,280 tonne respectively.

7.3.3. Cost model demonstration results

The aggregate cost of a hydrogen substation can be determined by summing up the individual cost components for each HPU installed capacity. Figure 7.4 illustrates both the total CAPEX and specific CAPEX per HPU installed capacity. The plot demonstrates an evident economy of scale, aligning with the cost scaling observed for electrolyser stacks, BOP equipment, and electrical equipment. Furthermore, cost steps can be observed in the total and specific CAPEX graph, which correspond to changes in transport and installation expenses, as well as shifts in the substructure type. Notably, the transition from a monopile to a jacket substructure, occurring at around the 300MW mark, triggers a significant surge in costs.

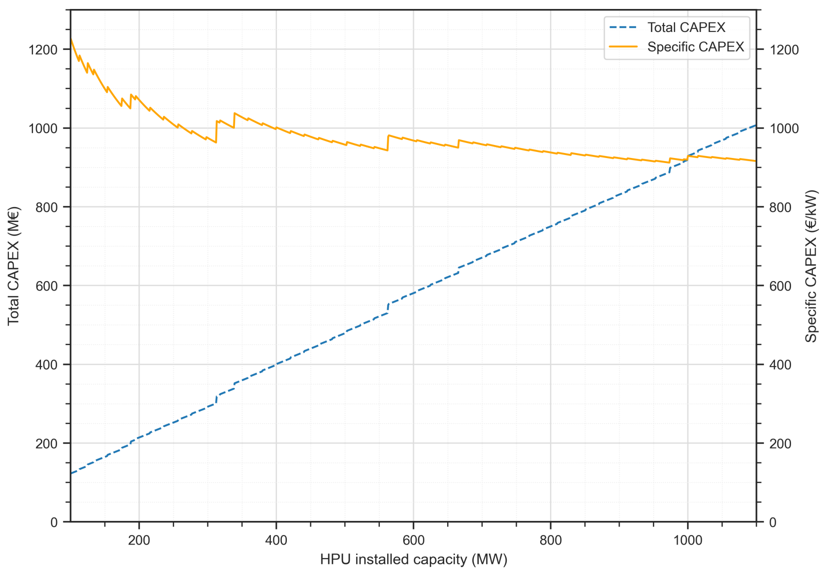

Figure 7.4: Hydrogen substation total and specific CAPEX vs. HPU installed capacity for HPU installed capacity above 100MW.

The total and specific OPEX of a hydrogen substation for a range of installed HPU capacities is depicted in Figure 7.5. The substation OPEX consist largely of HPU equipment cost, therefore a significant economy of scale is observed when looking at the specific OPEX line in the figure.

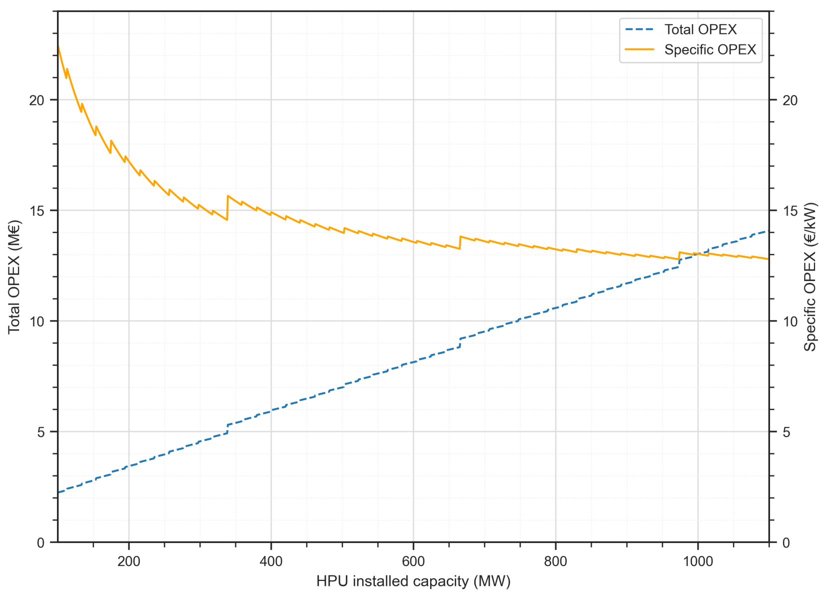

Figure 7.5: Hydrogen substation total and specific OPEX vs. HPU installed capacity for HPU installed capacity above 100MW.

When determining the offshore hydrogen turbine cost, a single CAPEX value and a single OPEX value is obtained by using Equation 7.20. For this particular example, undersizing is not considered. As a result, the capacity of the HPU is equivalent to the input power capacity of the HPU. This results in a total CAPEX of 27.5 million euros and an OPEX value of 0.48 million euros per year. However, it's important to note that the CAPEX and OPEX values of the hydrogen wind turbine cannot be directly compared with the substation CAPEX and OPEX. This is because the CAPEX and OPEX value of the hydrogen turbine includes the cost of the wind turbine, whereas the hydrogen substation CAPEX and OPEX does not incorporate the wind turbine cost.

8 Case study

The primary objective of this chapter is to conduct a comparative analysis of various offshore wind-to-hydrogen configurations, employing a case study approach. The case study involves several steps, including a site selection, the creation of wind-to-hydrogen farm layouts, modeling the cost of the wind farm excluding hydrogen components and calculating the hydrogen production, hydrogen pipeline diameters and associated costs, as well as the mass and cost of the offshore hydrogen facilities. These steps are executed by utilizing the in-house Vattenfall model combined with newly developed model, specified in this report. Section 8.1 provides an overview of the key characteristics of the case study. Hereafter, the wind-to-hydrogen farm layouts are created. Subsequently, the components of the wind-to-hydrogen farm need to be sized to achieve the lowest LCOH for each individual configuration. This is done in Section 8.2, which presents the preliminary optimisation results for the wind-to-hydrogen farm designs. Section 8.3 explains the process of selecting the semi-centralised configuration which is then used for the comparison of the centralised, semi-centralised, and decentralised configurations in Section 8.4. This comparison focuses on the LCOH and identifies the key drivers affecting the configurations. Moving forward, Section 8.5 conducts a sensitivity analysis to evaluate the potential impact of variations in the key drivers of LCOH. This is followed by Section 8.6, where a more in-depth evaluation of different assumptions and scenario sensitivities is conducted. Finally, Section 8.7 presents a discussion of the case study results.

8.1. Case description

This section presents background information on the selected case study, needed for evaluating various offshore wind-to-hydrogen configurations. It encompasses site selection, project specifications and component capacity determination. Subsection 8.1.1 provides an overview of the case study site and selected parameters. The rationale behind the site selection is discussed in Subsection 8.1.2. In Subsection 8.1.3, the project specifications are discussed, while Subsection 8.1.4 elaborates on the determination of wind turbine capacity, number of wind turbines, number of OHFs, inter-array cable capacity, and electrolyser stack capacity.

8.1.1. Case description overview

The case-specific parameters relevant to component specifications, project specifications, site conditions and configuration specifications are summarized in Table 8.1. The table provides an overview of the key parameters associated with the case study, facilitating a deeper understanding of the subsequent analysis and discussions.

Parameters	Value	Unit
Site conditions and specifications		
Mean wind speed	10.6	m/s
Range water depth	25-35	m
Estimated Weibull scale factor	11.9779	m/s
Estimated Weibull shape factor	2.3682	-
Estimated Weibull mean wind speed	10.61	m/s
Distance of site to shore	100	km
Distance of site to backbone pipeline	7	km
Project specifications		
Commissioning year	2030	-
Project lifetime wind-to-hydrogen farm	30	year
Discount rate	10.0	%
Component specification		
Wind turbine rated capacity	15	MW
Inter-array cable voltage rating	66	kV
Inter-array cable type 1: cross sectional area	X	mm^2
Inter-array cable type 2: cross sectional area	X	mm^2
Electrolyser min. stack capacity	0.1	MW
Electrolyser max. stack capacity	10.0	MW
Configuration specifications		
Number of OHF centralised	1	-
Number of OHF semi-centralised	2 - 8	-
Number of OHF decentralised	70	-

Table 8.1: Case specific parameters regarding component specifications, project specifications, site conditions and configuration specifications.

8.1.2. Site selection

The site selected for the wind-to-hydrogen farm in this case study is a planned all-electric wind farm location in the North Sea with an intended electrical wind farm capacity of 1000MW. This location is selected because of the available resources within Vattenfall, regarding site conditions such as wind speed, wave height, water depth and geographical obstacles. This location is considered ideal for offshore wind farms due to its high wind resources and the presence of consistently calm and predictable sea conditions [19]. Additionally, the location consists of water depths ranging from 25-35 meters, making it suitable for ground-based wind turbines and substations [14]. Furthermore, the intended electrical capacity of the wind farm site, set at 1000MW, aligns with the capacities observed in literature for wind-to-hydrogen farms [28][3][24].

The selected site is assumed to be more than 100km away from shore, where energy transmission via pipelines is considered advantageous compared to high voltage DC cables, reducing transportation costs [3]. Therefore, a wind-to-hydrogen farm at this site will be ideal for the integration with the future European hydrogen backbone network [88].

The shape of the selected site together with the location of the assumed hydrogen backbone pipeline connection, denoted with "**x**", is given in Figure 8.1. The figure depicts possible locations for wind turbines or hydrogen substations, represented by blue dots. The center bottom of the figure, depicted in white and surrounded by blue dots and the lower boundary, indicates an area where neither wind turbines nor substations can be placed but permits the crossing of cables or pipelines. For the hydrogen backbone pipeline connection, it is assumed that the location is situated 7 km from the site boundary at UTM X and Y coordinates of [redacted] and [redacted] respectively.

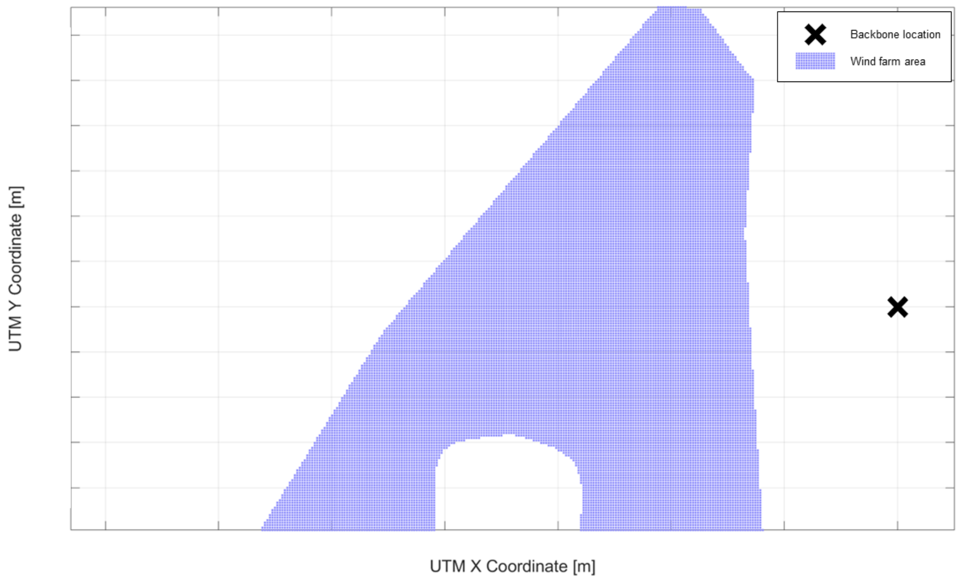

Figure 8.1: Shape of selected site and the assumed location for hydrogen backbone connection (depicted with: "**X**").

The wind speed probability distribution for the specific location, provided by Vattenfall, is presented in Figure 8.2. By combining this data with the hydrogen flow rate curve, the annual hydrogen production can be computed, as explained in Chapter 5. To facilitate future research or replication of this work, a Weibull fit is incorporated. Additionally, the corresponding scale factor, shape factor, and mean wind speed are calculated and provided in Table 8.1.

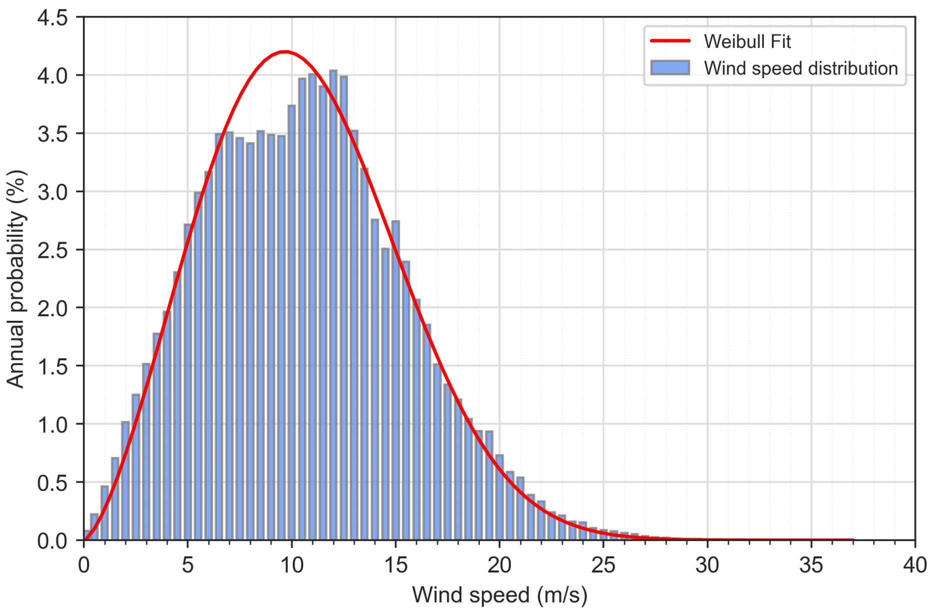

Figure 8.2: Wind speed probability distribution and Weibull fit [1].

8.1.3. Project specifications

The commissioning year of the wind-to-hydrogen farm is assumed to be 2030. This is inline with the current expectations of green hydrogen production in the North Sea area [59]. Furthermore, the project lifetime for this specific site is provided by the national government, which is approximately 30 years [48].

The discount rate, also referred to as the Weighted Average Cost of Capital (WACC), plays a critical role in determining the LCOH and has a significant impact on the final results. Jansen et al. conducted an analysis of country-specific data on offshore wind projects within Europe [44]. Their study revealed that, historically, most countries have used a WACC of 6-8% for offshore wind projects. However, it's important to note that their research predates a recent increase in interest rates, which has substantial implications for financial investment markets. Consequently, it is reasonable to consider an increase in the WACC.

Recent findings from a DNV study on hydrogen backbone pipeline projects have already reflected this trend, using a nominal discount rate of 10% [3]. Therefore, a discount rate of 10% will be adopted for this project to account for the evolving financial landscape and its potential impacts on the investment scenario.

8.1.4. Component capacities

The choice of technology for the wind-to-hydrogen components is already addressed in chapter 3. This subsection selects the capacities for the wind turbines, inter-array cables, and electrolyser stacks.

- *Wind turbine capacity*: The case study employs a standard 15MW wind turbine. Given that the current offshore wind farm development for the commissioning year 2030 often assumes the use of 15MW turbines as a standard, the same type of turbines is considered in this context. Increasing the wind turbine capacity augments the monopile's maximum vertical load capacity, thereby enabling a higher maximum electrolyser installed capacity on a hydrogen substation that uses the same monopile [7].

  Furthermore, choosing 15MW wind turbines over smaller ones offers additional advantages. Firstly, larger wind turbines can capture higher wind speeds at greater heights, leading to increased annual energy production and more efficient use of low-wind areas [12]. Secondly, larger turbines benefit from economies of scale, reducing costs per megawatt and improving the economic viability of wind energy projects [43]. Additionally, their increased inertia results in slower short-term power fluctuations, which is advantageous for electrolysers, especially in decentralised configurations. In such configurations, electrolysers are directly connected to a single wind turbine without power aggregation [78] [35].

  For projects further in the future, even larger wind turbines could be considered, as the trend toward increased turbine capacity is expected to continue [43].
- *Number of wind turbines*: The offshore wind-to-hydrogen farm comprises 70 wind turbines, resulting in a combined installed capacity of 1045MW. This capacity aligns with the observed range for wind-to-hydrogen farms, as discussed in Subsection 8.1.2.
- *Inter-array cable capacity*: Two different inter-array cables with a voltage capacity of 66kV are used to transport electricity. 66kV is required to transmit the produced energy from the 15MW wind turbines to an OHF. 33kV inter-array cable is not considered viable because only two turbines could be connected to an OHF due to cable capacities and a significant increase in energy losses in the cables. By combining the two 66kV cables, it is possible to connect a string of five wind turbines to an OHF [48]. The distinction between the two 66kV inter-array cables lies in their cross-sectional areas. Opting for a larger cross-sectional, enables the cable it to accommodate a higher capacity of electrical current. This capability proves advantageous but is also required for increased power transmission. Moreover, the larger cross-sectional area cable leads to lower power losses during transmission due to a lower cable resistance. However, it is important to consider the financial aspect associated with a larger cross-sectional area. As the cross-sectional area increases, the price per meter of the cable also rises. Both technical and cost considerations are taken into account during the cable routing of the wind farm layout optimisation, to ensure optimal performance and economic feasibility of the electrical energy transmission.
- *Electrolyser stack capacity*: The capacity of the electrolyser stacks is selected within the range of 0.1MW to 10MW for the PEM electrolyser stacks. This range allows for a more specific optimisation of the HPU capacity with steps of 0.1MW, aiming to optimise the LCOH for the wind-to-hydrogen farm. This level of steps is particularly important for offshore hydrogen turbines because they have a relatively small electrolyser capacities. In future electrolysis installations, there is a preference for large-scale electrolyser stacks due to their anticipated higher performance compared to smaller-scale stacks, as well as their reduced physical footprint [77] [41].

8.2. Preliminary optimisation

Before comparing the different offshore wind-to-hydrogen configurations, a preliminary optimisation of four design parameters will be conducted for each configuration. This section begins by providing an overview of the preliminary optimisation process in Subsection 8.2.1. Hereafter, an explanation of the four preliminary optimisations is given. The preliminary optimisations cover the following aspects: the adjustment of the compressor input pressure (Subsection 8.2.2), the determination of the number of electrolyser stack replacements (discussed in Subsection 8.2.3), the adjustment of the compressor output pressure to meet the requirements of the backbone pipeline (elaborated in Subsection 8.2.4), and the sizing of the HPU capacity in relation to the HPU input power (outlined in Subsection 8.2.5).

8.2.1. Preliminary optimisation overview

In order to optimise the key design parameters for the offshore wind-to-hydrogen configurations, the constants provided in Table 5.1, 6.1, 7.3, and 7.4 from the modeling chapters, are utilised. The key design parameters for optimisation, namely the compressor input pressure, number of stack replacements, compressor output pressure, and HPU installed capacity, need to be determined to calculate the optimal LCOH for each configuration. The following points are important to consider during the preliminary optimisations:

- *Optimisation applicability*: The compressor input pressure optimisation is exclusively applicable to the semi-centralised and decentralised configurations. In the case of the centralised configuration, the compressor input pressure is predetermined as it aligns with the constant output pressure of the electrolysers. On the other hand, the optimisation of the compressor output pressure, number of stack replacements and HPU capacity sizing is applicable to all three offshore wind-to-hydrogen configurations.
- *Placement of compressor*: The placement of the compressor within an offshore wind-to-hydrogen farm is important to understand how the input and output pressure of the compressor could be optimised. Each offshore wind-to-hydrogen configuration consist of one compressor location which is located at the beginning of the steel hydrogen pipeline connected to the hydrogen backbone pipeline. This means that for the centralised configuration, the compressor is located at the centralised hydrogen substation, for the decentralised at the hydrogen manifold and for the semi-centralised at the last hydrogen substation that connects the wind-to-hydrogen farm to the hydrogen backbone pipeline.
- *Steel pipeline arrangement*: For the semi-centralised configurations, the steel hydrogen pipelines connecting the hydrogen substations can be arranged in parallel or in series, which impacts the allowed pressure drop in the pipeline. The specific layout dictates the type of connection used and varies between different semi-centralised configurations. Figure 8.3 provides an example of the parallel and series arrangement for the semi-centralised configuration with 3 hydrogen substations.
- *Approach to allowed pressure drop*: The approach used to determine the allowed pressure drop within the steel hydrogen pipelines previous to the compressor, in relation to the compressor input pressure, is the same for each semi-centralised configuration. For hydrogen pipelines in series, the pressure drop within a steel pipeline segment is the difference between the electrolyser output pressure and the compressor input pressure, divided by the number of steel pipeline segments between the farthest hydrogen substation and the compressor. For hydrogen pipelines in parallel, the pressure drop within a steel pipeline segment is the difference between the electrolyser output pressure and the compressor input pressure. As an example, for a semi-centralised configuration with three hydrogen substations, a compressor input pressure of 30 bar and electrolyser output pressure of 35 bar, the allowed pressure drop in the pipelines prior to the compressors is 2.5 bar for series and 5 bar for parallel. This example is shown in Figure 8.3.

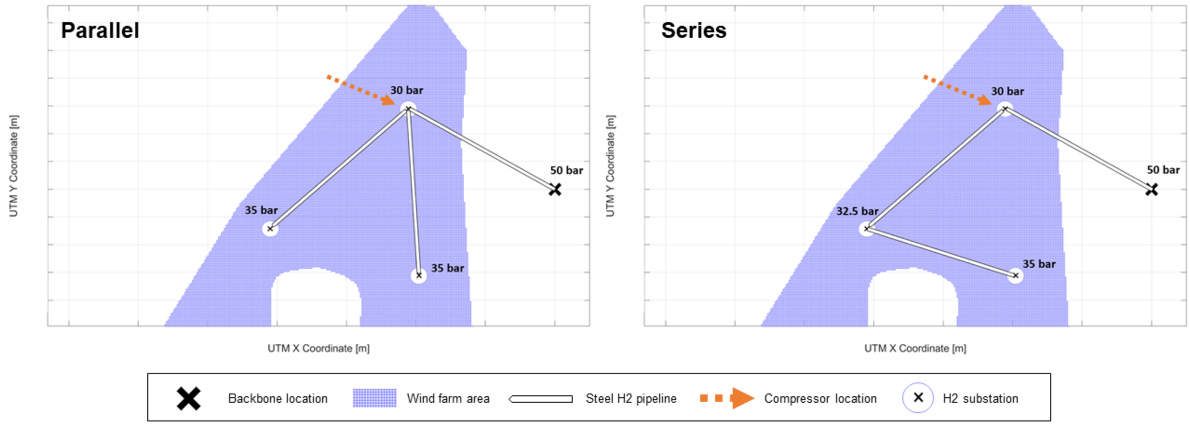

Figure 8.3: Steel pipeline arrangement example for both parallel and series for the semi-centralised configuration consisting of 3 hydrogen substations.

An individual key design parameter is considered optimal when its value leads to the lowest LCOH for a particular configuration. Consequently, the optimal values of the four key design parameters result in the lowest LCOH for a specific wind-to-hydrogen configuration. Each preliminary optimisation parameter involves certain trade-offs, and the explanation of these trade-offs, along with the optimisation range, is provided as follows:

- **Compressor input pressure**: The compressor input pressure determines the allowed pressure drop within the hydrogen pipelines previous to the compressor, subsequently impacting the required diameters of the pipelines and the associated costs. Moreover, the compressor input pressure affects the installed capacity of the compressor and the electrolyser, thus influencing the overall cost of the system and the total hydrogen production. This results in a trade-off between the cost of the steel hydrogen pipelines previous to the compressor, the cost of the compressors, the cost of the electrolysers and the total hydrogen production. Given that the electrolyser output pressure is 35 bar, the considered range of compressor input pressures for the semi-centralised configurations is between 27 and 34.5 bar. For the decentralised configuration, only two compressor input pressures are considered, namely 25 and 30 bar. This is done to simplify the calculations and only to show the impact of the compressor input pressure.
- **Number of stack replacements**: The optimal number of electrolyser stack replacements is determined by balancing the increase in hydrogen production with the cost of the stack replacements. Additional stack replacements lead to improved average electrolyser stack efficiency over the lifespan of the wind-to-hydrogen farm. The considered range of electrolyser stack replacements is between 1 and 4. No stack replacement is not an option as the maximum lifetime of the stacks is exceeded.
- **Compressor output pressure**: The compressor output pressure determines the allowed pressure drop within the steel hydrogen pipeline after the compressor, subsequently impacting the required diameter of the pipeline and the associated costs. This is the pipeline connecting the wind-to-hydrogen farm to the backbone pipeline. Additionally, the compressor output pressure affects the installed capacity of the compressor and the electrolyser, thus influencing the overall cost of the system and the total hydrogen production. This results in a trade-off between the cost of the steel hydrogen pipeline after the compressor, the cost of the compressors, the cost of the electrolysers and the total hydrogen production. Given that the inlet pressure of the backbone pipeline is 50 bar, the compressor's output pressure must exceed 50 bar to compensate for the pressure drop that occurs in the pipeline, as explained in Chapter 6. The considered range for optimising the compressor output pressure is between 51 and 59 bar.
- **HPU capacity sizing**: Optimisation of HPU installed capacity versus the HPU input power impacts the hydrogen production and the cost of the HPU. By evaluating different HPU installed capacities, the goal is to find the optimal balance between the HPU installed capacity to produce hydrogen and the cost associated with the HPU installed capacity. The HPU is CAPEX-intensive and usually operates at full rated power continuously. However, in wind farms, its capacity factor

is around 40-50% due to the variable nature of wind energy. Reducing the HPU installed capacity could therefore increase the HPU capacity factor [37]. The relationship between HPU installed capacity sizing and HPU input power can be represented by a factor known as the HPU sizing factor, denoted as $f_{\text{HPU-sizing}}$. This factor captures the correlation between the installed capacity of the HPU and its corresponding input power. In general, there are three sizing options:

- *Matching,* $f_{\textit{HPU-sizing}} = 1$: Matching HPU capacity means that the installed HPU capacity is the same as the maximum HPU input power. This means that the HPU can utilize all the available wind power without any restrictions. The HPU will have a similar capacity factor as the wind farm since it can fully utilize the available power.
- *Undersizing,* $f_{\textit{HPU-sizing}} < 1$: Undersizing the HPU installed capacity means that its capacity is smaller than the maximum HPU input power. This leads to an increase HPU capacity factor and thus an increase in full load hours because a larger period of the year the HPU produces hydrogen at rated capacity. An increase in the number of full load hours will increase the annual degradation of the electrolyser. The total hydrogen production will be reduced compared to a matched sizing scenario because the HPU rated capacity is limited. Undersizing the HPU installed capacity can result in cost savings since a smaller installed capacity would require a lower upfront investment.
- *Oversizing,* $f_{\textit{HPU-sizing}} > 1$: Oversizing the HPU means that its capacity exceeds the maximum HPU input power. Oversizing the HPU would decrease the capacity factor and the full load hours since the HPU would not be able to operate at full capacity for extended periods. However, when the variable HPU efficiency curve is considered, the hydrogen production may increase when the HPU operate below nominal load because of an increased HPU efficiency. However, a variable efficiency curve of the HPU is not considered in the modeling of this research and therefore oversizing will not be discussed further.

The considered range for the HPU capacity sizing factor is between 0.90 and 1.0.

When investigating the interaction between the four key design parameters, it was discovered that the optimal values of the number of stack replacement, compressor output pressure and HPU capacity sizing are not affected by the compressor input pressure within the range. As a result, the compressor input pressure was initially optimised separately, also due to its inapplicability to each of the three configurations. To determine an optimal value for the compressor input pressure, a base value of 51 bar was considered for the compressor output pressure, along with one stack replacement and a HPU capacity sizing factor of 1.0.

Subsequently, the optimisation process focused on the number of stack replacements, compressor output pressure, and HPU installed capacity. These parameters were optimised together as they are applicable to each configuration and demonstrate interaction. The LCOH is determined for each combination of the three parameters within their specified range for the centralised, semi-centralised, and decentralised configurations. The objective was to identify the combination of these design parameters that results in the lowest LCOH.

In the following subsections, the optimisation of the four key design parameters is discussed sequentially. However, to demonstrate the interaction between the HPU sizing factor, the number of stack replacements, and the compressor input pressure, the optimal values for the number of stack replacements and compressor output pressure will be presented for different HPU sizing factors within their respective ranges.

8.2.2. Compressor input pressure

Figure 8.4 illustrates the relationship between the LCOH and the compressor input pressure for the semi-centralised configurations. For each configuration, the LCOH initially decreases as the compressor input pressure increases, reaching a minimum at the optimal compressor input pressure. The minimum values vary slightly across configurations, approximately falling between 32 and 34.8 bar. The decrease in LCOH is attributed to the reduction in compressor cost, which outweighs the increase in pipeline cost at higher compressor input pressures. However, as the pressure approaches 35 bar, the LCOH starts increasing again due to the rising cost of hydrogen pipelines, outweighing the reduced compressor cost.

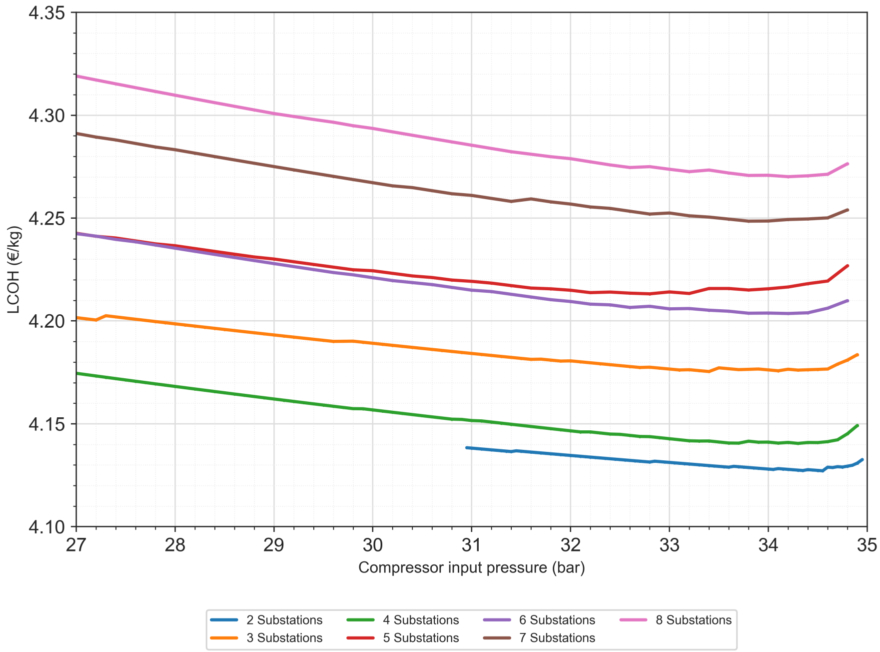

Figure 8.4: LCOH vs. a range of compressor input pressures for semi-centralised offshore wind-to-hydrogen configurations. For the 2 substation configuration (blue line), the LCOH for input pressures smaller than 30.9 bar is not calculated due to the large amount of calculations and because lower input pressures are assumed to be less economically viable considering the trend of the other semi-centralised configurations.

Figure 8.5 displays the relationship between the diameter of the largest hydrogen pipeline in a configuration and the compressor input pressure. Initially, the largest pipeline diameter increases gradually with the increasing compressor input pressure. However, a notable increase is observed when reaching a compressor input pressure of 35 bar. This suggests that a small pressure difference between the electrolyser and the compressor input pressure necessitates relatively larger pipeline diameters to avoid exceeding the allowed pressure drop.

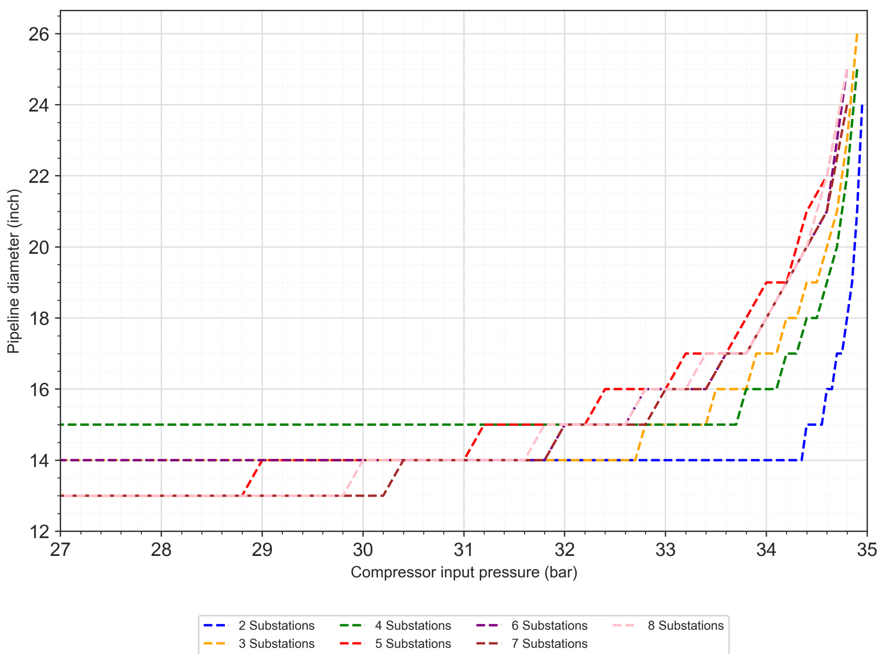

Figure 8.5: The largest steel pipeline diameter of a configuration vs. a range of compressor input pressures for semi-centralised offshore wind-to-hydrogen configurations.

To facilitate the comparison of the semi-centralised configurations, a uniform compressor input pressure is chosen for each semi-centralised configuration. This compressor input pressure must take into account the assumed maximum allowed steel pipeline diameter of 16 inch [36]. Therefore, the highest compressor input pressure that can be used is 33 bar. With this standardised pressure of 33 bar, the LCOH values for each semi-centralised configuration differ from their optimal LCOH by a maximum of 0.01€/kg. A compressor input pressure of 33 bar will be used further in this case study for the semi-centralised offshore wind-to-hydrogen configurations.

In contrast, for the decentralised configuration, the LCOH outcome is compared for two different compressor input pressures: 25 bar and 30 bar. The results indicate that when the compressor input pressure is set to 25 bar, the decentralised configuration yields a lower LCOH of 3.91€/kg, whereas it rises to 3.94€/kg with the compressor input pressure set to 30 bar. Therefore, for the decentralised configuration, a compressor input pressure of 25 bar is selected and will be used further in this case study.

8.2.3. Number of electrolyser stack replacements

Figure 8.6 presents the LCOH for varying numbers of stack replacements, considering HPU sizing factors from 0.9 to 1, and using a compressor output pressure of 51 bar for the centralised, decentralised, and semi-centralised configurations. Because the effect of different number of stack replacements is similar within the range of compressor output pressures, the choice of a fixed compressor output pressure of 51 bar is sufficient to demonstrate the impact of different stack replacements across a range of HPU sizing factors. The semi-centralised configuration with four hydrogen substations serves as an illustrative example for all semi-centralised configurations.

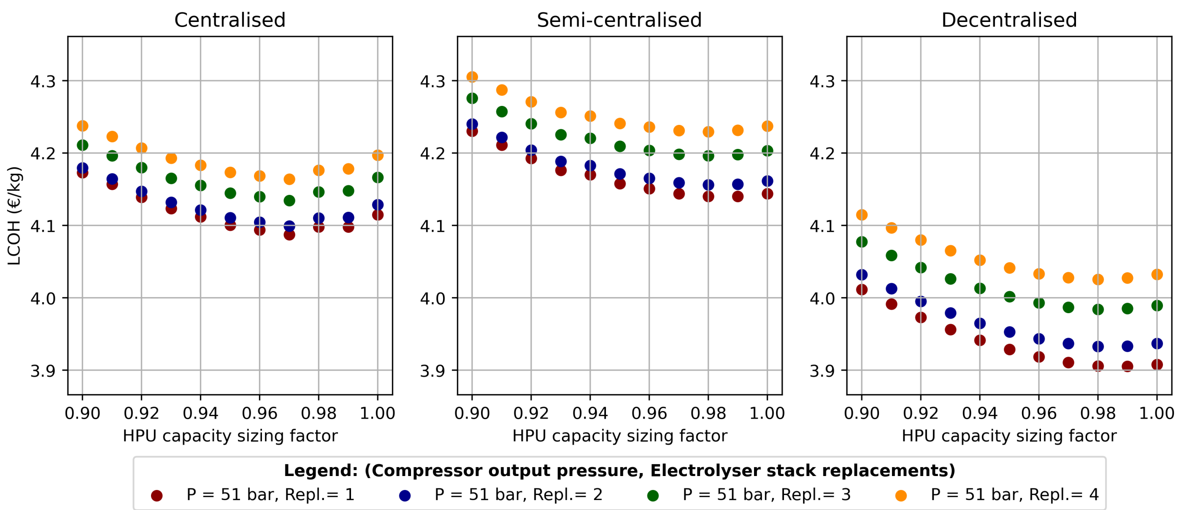

Figure 8.6: Preliminary optimisation: LCOH versus the HPU capacity sizing factor (0.9-1.0) for a range of stack replacements (1-4) in the centralised, semi-centralised (4 hydrogen substations), and decentralised configurations. (Fixed compressor output pressure = 51 bar)

The figure clearly indicates that the lowest LCOH is achieved when there is only one stack replacement, represented by the color red, for all three configurations. If an additional stack replacement does not lead to a decrease in LCOH, it means that the cost incurred by the extra stack replacement outweighs the increase in hydrogen production.

Moreover, the figure shows that as the HPU capacity sizing factor increases, the distances between the different color dots also increase. This suggests that with a higher HPU capacity sizing factor, adding an extra stack replacement results in a larger increase in LCOH compared to smaller HPU capacity sizing factors. This effect arises from the higher number of full load hours per year associated with a decreasing HPU sizing factor, leading to increased electrolyser stack degradation. Consequently, for smaller HPU capacity sizing factors, replacing the electrolyser stacks results in a more significant overall increase in hydrogen production throughout the wind-to-hydrogen farm's lifespan than with larger HPU capacity sizing factors. Additionally, with an increasing number of full load hours during the lifespan, there may be a need for a second electrolyser stack replacement once the maximum stack lifetime is exceeded for the second time.

Additionally, the figure highlights a variability in the impact of electrolyser stack replacements among different configurations. The distance between the dots representing different stack replacements, increases from the centralised to the semi-centralised and then to the decentralised configuration. This increase is due to the rise in electrolyser stack cost with the decrease in HPU installed capacity from the centralised to the decentralised configuration, caused by the cost scaling factors. Consequently, replacing the electrolyser stack in the centralised configuration would result in lower costs compared to the decentralised configuration.

Taking into account a range of HPU sizing factors between 0.9 and 1, based on the constants and assumptions outlined in the previous chapters, it can be concluded that the optimal number of stack replacements for the various wind-to-hydrogen configurations is one. This value for stack replacements will be further utilized in the subsequent sections for the centralised, semi-centralised and decentralised offshore wind-to-hydrogen configurations.

8.2.4. Compressor output pressure

Figure 8.7 illustrates the LCOH for different compressor input pressures (ranging from 51 to 59 bar), one stack replacement and various HPU capacity sizing factors for the centralised, semi-centralised, and decentralised configurations. The semi-centralised configuration with four hydrogen substations is used as an illustrative example for all semi-centralised configurations. For each compressor input pressure, the diameter of the steel hydrogen pipeline that connects the wind-to-hydrogen farm to the backbone pipeline is optimised to ensure the hydrogen reaches 50 bar at the backbone pipeline.

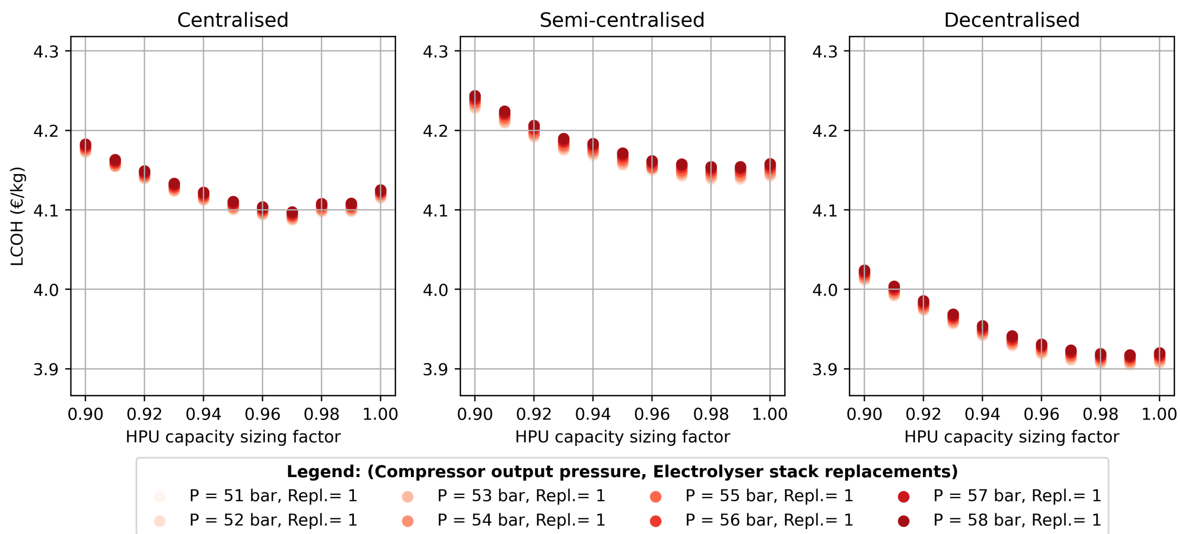

Figure 8.7: Preliminary optimisation: LCOH versus the HPU capacity sizing factor (0.9-1.0) for a range of compressor output pressures (51-59 bar) in the centralised, semi-centralised (4 hydrogen substations), and decentralised configurations.

The analysis reveals that the lowest LCOH is attained when the compressor output pressure is set to 51 bar. Increasing the compressor output pressure beyond this value leads to an increase in the LCOH. This indicates that above 51 bar, the cost associated with an increasing compressor output pressure and the decrease in hydrogen production due to less installed electrolyser capacity, outweigh the cost savings of a smaller steel hydrogen pipeline diameter.

Additionally, for practical reasons and limited expected decrease in LCOH, it was chosen not to decrease the compressor output pressure below 51 bar. This decision was made to avoid potential issues arising from very small differences between the 50 bar backbone pressure and the compressor output pressure, which could lead to impracticality's in case of minor errors with the compressor.

8.2.5. Hydrogen production unit sizing

Figure 8.8, presents the LCOH for HPU installed capacity sizing factors ranging from 0.9 to 1.0, considering one stack replacement and a compressor output of 51 bar from the previous optimisations. The semi-centralised configuration with four hydrogen substations is used as an illustrative example for all semi-centralised configurations.

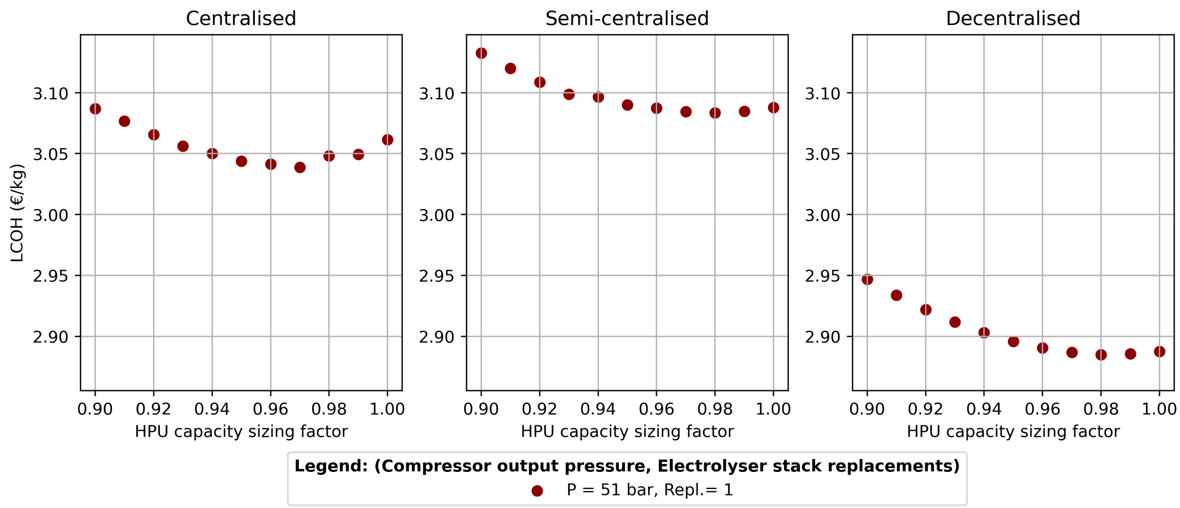

Figure 8.8: Preliminary optimisation: LCOH versus the HPU capacity sizing factor (0.9-1.0) for a single compressor output pressures (51 bar) and stack replacement (1), in the centralised, semi-centralised (4 hydrogen substations), and decentralised configurations.

The figure illustrates that a certain degree of undersizing results in a decrease in the LCOH for the various configurations. However, it can be concluded that the disparity between matching sizing and optimal undersizing remains relatively small for each configuration. Furthermore, notable differences in the impact of undersizing can be observed among the centralised, semi-centralised, and decentralised configurations. With an increasing number of OHFs, the beneficial influence of undersizing on the LCOH diminishes. This finding can be explained by the growing significance of the BOP and electrolyser cost scale factors as the number of OHFs increases. Undersizing the HPU with a small installed capacity results in a relatively larger impact of the BOP and electrolyser cost scale factors. Consequently, the potential cost reduction due to undersizing becomes limited in this context.

From the figure, it is possible to identify the optimal sizing factor per configuration. The optimum sizing factor differs per configuration and therefore the sizing of all the different semi-centralised configurations is included in Figure A.3 in Appendix A.1. The optimal HPU sizing factors lie between 0.95 and 1.0. To be able to compare the configurations on their total hydrogen production and cost, the average optimal HPU sizing factor is selected of 0.97. The average HPU sizing factor may not be ideal for all configurations, but the variances in LCOH are relatively small (<0.02€/kg). Consequently, these differences do not significantly impact the selection of the optimal wind-to-hydrogen configuration.

8.3. Semi-centralised configuration selection

To facilitate a comparison between the centralised, semi-centralised and decentralised wind-to-hydrogen configurations, the first step is to identify the optimal semi-centralised configuration that yields the lowest LCOH. This section focuses on the selection of the optimum number of hydrogen substations within the semi-centralised configuration, aiming to minimise the LCOH. The selection process involves considering the semi-centralised configurations, ranging from to 2 to 8 hydrogen substations. By evaluating and comparing the LCOH values for different numbers of hydrogen substations within this range, the optimal semi-centralised configuration can be identified. In Subsection 8.3.1, an overview will be presented regarding the selection of the semi-centralised configuration, along with the primary factors that influence the optimal number of substations. This will be followed by a comparison of the energy transmission infrastructure in Subsection 8.3.2. Subsequently, in Subsection 8.3.3, a comparison of the hydrogen substations within the semi-centralised configurations is elaborated.

8.3.1. Optimum semi-centralised configuration selection overview

The layouts of the semi-centralised configurations are created according to the method discussed in Section 4.3. The semi-centralised layouts consisting of 3 and 7 hydrogen substations are shown in Figure 8.9, to function as examples. The layouts consisting of 2,4,5,6 and 8 substations are included in Figure A.4 and Figure A.5 of Appendix A.2. In the figures, the blue area represents the site available for wind turbine and hydrogen substation placement, the dark blue and red lines depict the inter-array cables, the white bars present the hydrogen steel pipelines and the wind turbines are numbered. The wind-to-hydrogen layouts exhibit a strategic arrangement with wind turbines positioned along the site's borders to reach the highest energy yield. Moreover, the hydrogen substations do not each require their own hydrogen steel pipeline connected directly to the backbone pipeline. Instead, the hydrogen is initially conveyed from the substations to another substation. At the last substation before the backbone pipeline, the hydrogen is compressed and subsequently transported to the hydrogen backbone pipeline via a single pipeline. This approach of not connecting every substation to the hydrogen backbone pipeline serves to minimise space constraints and the total length of the inter-array cables and the pipelines.

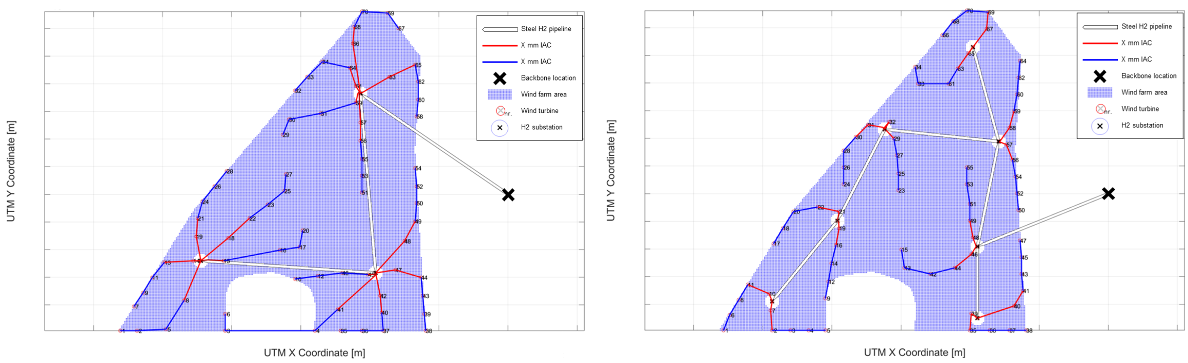

(a) H_2 substations: 3 **(b)** H_2 substations: 7

Figure 8.9: Semi-centralised offshore wind-to-hydrogen farm layouts including 3 and 7 offshore hydrogen substations.

A comparison of the semi-centralised configurations based on their LCOH is conducted. Figure 8.10 presents the LCOH values for the semi-centralised configurations. Among them, the configuration with 2 hydrogen substations achieves the lowest LCOH of 4.13 €/kg. Hereafter, the configuration consisting of 4 hydrogen substations achieves the lowest LCOH of 4.14 €/kg. These two configurations differ in terms of substation substructure type. The 2 substation configuration features a jacket substructure, while the 4 substation configuration utilizes monopile substructures for the OHFs. Since the resulting LCOH is almost similar for both configurations, the 4 substation configuration with monopile substructures is selected for the overall configuration comparison.

The selection of the 4 substation configuration with monopile substructures over the 2 jacket substation configuration is supported by several practical reasons. Firstly, opting for monopile substructures allows for the use of the same contractors responsible for wind turbine installations. This streamlines the project management process and fosters collaboration among teams with expertise in offshore wind projects, reducing complexities and potential delays.

Secondly, 4 smaller monopile substations generally require smaller construction and installation vessels compared to the installation of 2 larger jacket substations. The availability of smaller vessels is more abundant in the market, which decreases the risk related to project logistics and scheduling and has the potential to reduce overall costs.

By considering these practical aspects, the 4 monopile hydrogen substation configuration emerges as a favorable choice. Consequently, the 4 substation semi-centralised configuration is compared with the centralised and decentralised configurations in Section 8.4.

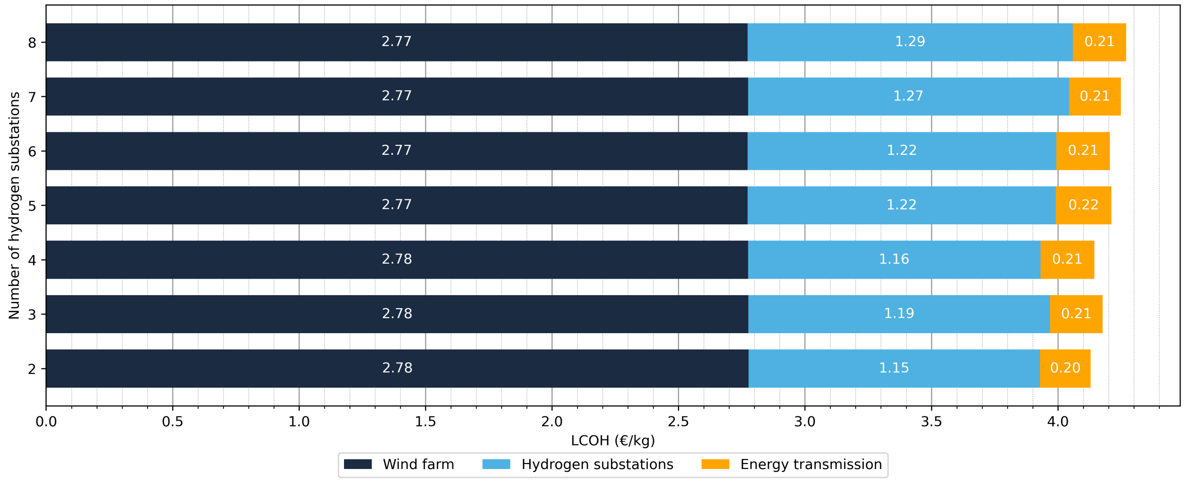

Figure 8.10: LCOH breakdown for semi-centralised configurations comprising 2-8 hydrogen substations (2-3 substations = Jacket substructure, 4-8 substations = monopile substructure). The LCOH is categorized into three components: wind farm, hydrogen substation, and energy transmission.

Next to the overall LCOH, Figure 8.10 illustrates the contribution to the LCOH from the wind farm, energy infrastructure, and hydrogen substations. The wind farm contribution includes the costs associated with all components of the wind-to-hydrogen farm, excluding the hydrogen pipelines, inter-array cables, and hydrogen substations.

There is a significant disparity observed in the contribution of hydrogen substations between the semi-centralised configurations. Furthermore, a minor difference arises in the contribution of energy transmission to the LCOH, which encompasses the costs of the hydrogen pipelines and inter-array cables.

Since the variations in LCOH among the semi-centralised configurations are primarily attributed to the hydrogen substations and energy infrastructure, the subsequent subsections will provide a detailed analysis of these components.

Furthermore, variations in hydrogen production arise throughout the lifetime of the semi-centralised configurations due to discrepancies in inter-array cable losses. Table 8.2, provides an overview of the maximum total HPU input capacity and maximum inter-array cable power loss. The variances in inter-array cable power loss can be attributed to differences in inter-array cable type and length. For the maximum current, the smaller diameter inter-array cable leads to a significant higher power loss then the larger inter-array cable [48].

Parameter	**Unit**	**Semi-centralised**						
Number of hydrogen substations	#	2	3	4	5	6	7	8
Maximum total HPU input power	MW	1036.75	1037.37	1038.02	1038.26	1038.95	1038.57	1038.86
Maximum power loss inter-array cables	MW	*X*	*X*	*X*	*X*	*X*	*X*	*X*

Table 8.2: Maximum HPU input power and power loss inter-array cables for semi-centralised wind-to-hydrogen configurations.

Figure 8.11 depicts the total hydrogen production over the lifetime for the semi-centralised configurations. A slight increase in hydrogen production is observed due to the reduction in power loss resulting from inter-array cables. However, the hydrogen production shows a decrease from 6 to 7 hydrogen substations and then increases from 7 to 8 hydrogen substations. This is because the power loss in the inter-array cables for the 7 substations is larger compared to the losses for the 6 and 8 substations. Nevertheless, the differences in hydrogen production among the configurations are not significant, with the maximum variance being only 0.2%.

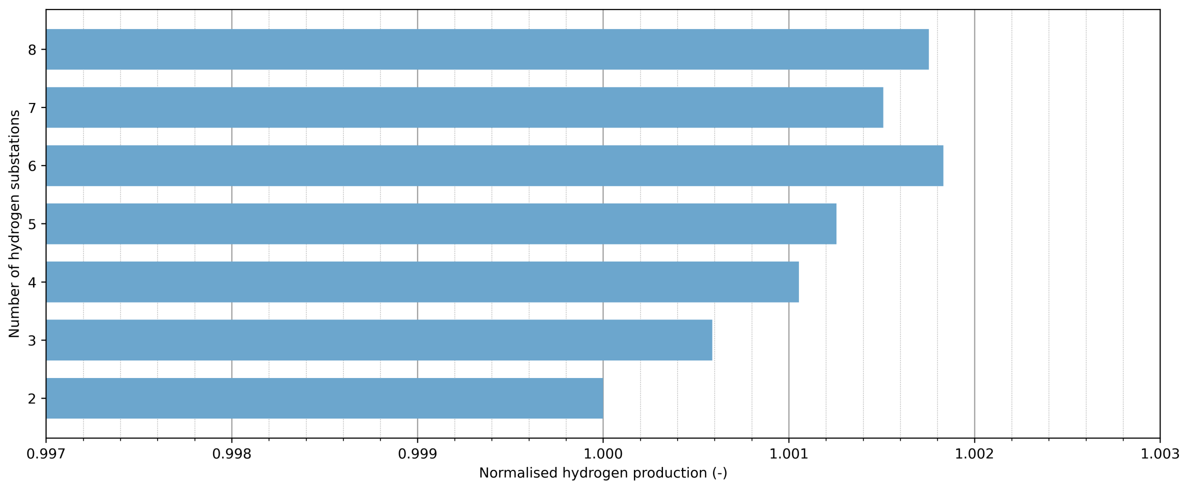

Figure 8.11: Normalised hydrogen production during lifetime for semi-centralised configurations comprising 2-8 hydrogen substations.

8.3.2. Energy transmission infrastructure

Within the semi-centralised configurations, the energy infrastructure differs due to the different number and positioning of hydrogen substations, the different positioning of the wind turbines as well as the associated inter-array cable and hydrogen pipeline routing. The resulting difference affecting the energy infrastructure contribution to the LOCH relates to the total length of the inter-array cables and the total length of the hydrogen pipelines.

It is important to note that the total length and CAPEX of the energy infrastructure are highly dependent on the specific case study and site dimensions. However, the results obtained from the analysis can provide insights into the relation between length and cost of the energy infrastructure. Additionally, the specific CAPEX values of the energy infrastructure are included for comparison with existing literature.

Figure 8.12a presents the total length of inter-array cables and hydrogen pipelines for the different number of substations. The graph demonstrates that as the number of substations rises, the total length of inter-array cables decreases, with a maximum reduction of 8% observed between two substations and seven substations. On the contrary, the length of hydrogen pipelines generally expands as the number of substations increases. However, this growth tapers off after five substations, reaching a maximum difference in total pipeline length of 143% between two substations and five substations.

Figure 8.12a illustrates the total CAPEX of the energy infrastructure for each configuration. It is apparent that the pattern of total CAPEX differs from that of the total length of the energy infrastructure. This suggests variations in the specific CAPEX values for the energy infrastructures. Regarding the inter-array cables, the total CAPEX decreases similar to the decrease in total length. However, when examining the hydrogen pipelines, a relatively larger difference in total CAPEX becomes apparent. This indicates that the costs associated with the hydrogen pipelines have a more significant impact on the overall CAPEX of the energy infrastructure compared to the inter-array cables.

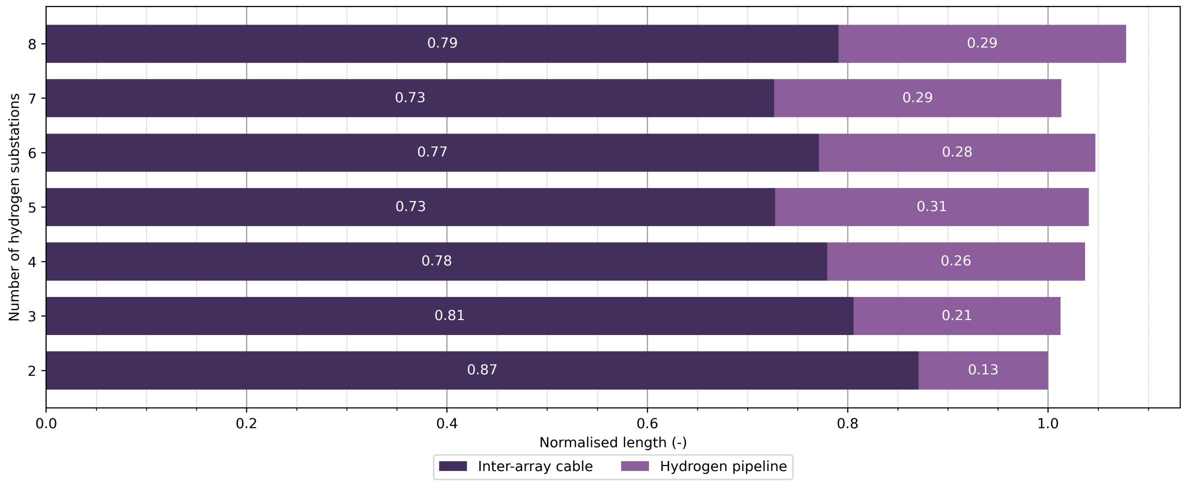

(a) Normalised energy infrastructure length.

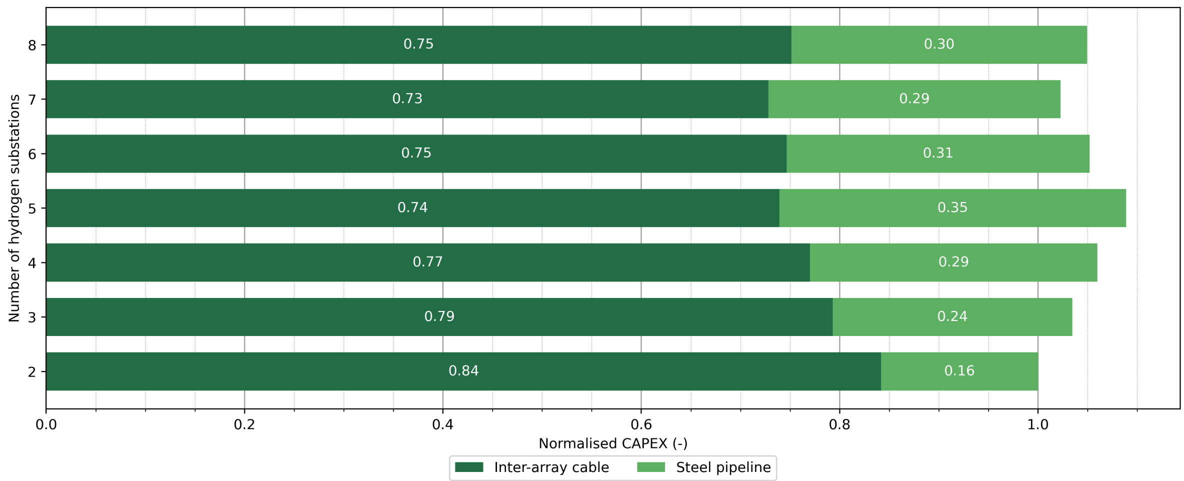

(b) Normalised energy infrastructure CAPEX.

Figure 8.12: Normalised length and CAPEX of inter-array cables and hydrogen pipelines for each semi-centralised configuration.

Figure 8.13 presents specific CAPEX information for steel hydrogen pipelines and inter-array cables. Analysis of the figure reveals that the specific price of inter-array cables does not vary significantly across different configurations. The small differences can be attributed to the varying lengths and costs of the two types of inter-array cables. The decrease in specific CAPEX for the pipelines is a result of the number of segments and pipeline diameters. Generally, an increase in the number of segments and total pipeline length leads to a decrease in specific CAPEX for hydrogen pipelines. The reason why there is a decrease in the specific CAPEX when the number of segments and total pipeline length increases is because their are several fixed cost associated with the transport and installation of the hydrogen pipelines. Furthermore, the specific hydrogen pipeline CAPEX is influenced by the average pipeline diameter. When the number of pipelines increases within a wind-to-hydrogen farm, the average pipeline diameter decreases. This is because with more pipelines, each pipeline needs to transport a smaller flow rate, allowing the usage of smaller pipeline diameters, and as a result, the average pipeline diameter decreases.

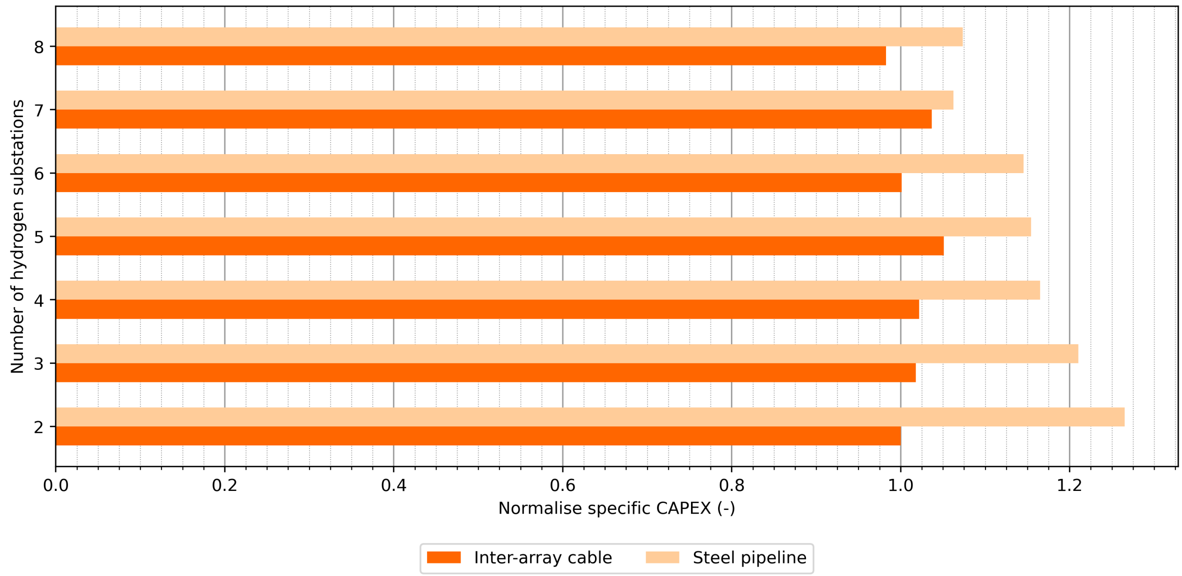

Figure 8.13: Normalised specific CAPEX of energy infrastructure for semi-centralised configurations (2-8 substations), divided into steel pipeline and inter-array cables.

Based on the figure, it can be inferred that there is no significant difference in the specific CAPEX between the inter-array cables and hydrogen pipelines. This finding contradicts the initial assumption that pipelines are less expensive than electrical cables. The main reason for this is the lower energy transmission capacity required and the relatively short distances involved in this particular context. Pipelines are typically well-suited for the transmission of large amounts of energy over long distances, but in this case, the distances are short, and the amount of energy in the form of hydrogen is relatively small.

8.3.3. Offshore hydrogen facilities

Table 8.3 displays the specifications of various semi-centralised configurations, including their HPU rated capacity per substation, substation topside mass, topside specific mass and substructure type. As the number of substations increases, both the HPU rated capacity per substation and the substation topside mass decrease. The table also indicates the type of substructure used, which will be further explained below.

Parameter	**Unit**	**Semi-centralised**						
Hydrogen substations	#	2	3	4	5	6	7	8
HPU rated capacity per substation	MW	502	336	252	202	168	144	126
Substation topside mass	tonne	15,617	10,418	7,818	6,256	5,217	4,470	3,912
Substation specific topside mass	tonne/MW	31.1	31.0	31.0	31.0	31.1	31.1	31.0
Substation substructure type	-	Jacket	Jacket	MP	MP	MP	MP	MP

Table 8.3: Offshore hydrogen facility specifications for semi-centralised (2-8 substations) wind-to-hydrogen configurations (Substructure types: MP = monopile, Jacket).

Figure 8.14 illustrates the topside mass of the semi-centralised hydrogen substations per configuration. Additionally, a line in the figure represents the load capacity of the monopile, thereby indicating whether a substation utilizes a monopile substructure. By considering a maximum vertical load capacity of 10,000 tonnes, the boundary between a monopile and jacket substructure can be determined. For semi-centralised configurations with up to three hydrogen substations, jacket substructures are utilized, whereas in semi-centralised configurations with 4 or more substations, monopile substructures are employed.

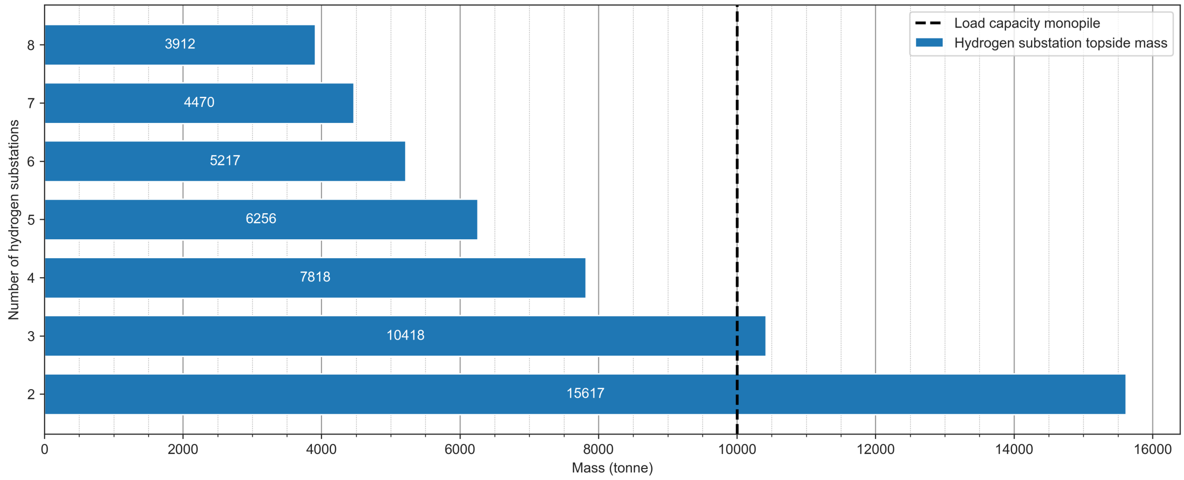

Figure 8.14: Topside mass of hydrogen substations for semi-centralised wind-to-hydrogen configurations (2-8 substations) including the monopile load capacity. (2-3 substations = Jacket substructure, 4-8 substations = monopile substructure).

Figure 8.15 provides a comparison of specific CAPEX among the hydrogen substations in the semi-centralised configurations. The specific CAPEX is of the hydrogen substations is the total CAPEX divided by the HPU installed capacity. The figure displays the specific costs of different components, such as HPU equipment, superstructure, substructure, transport and installation, and non-material expenses, for each configuration. It is important to note that the substructure type differs across configurations. Specifically, the configurations with two and three substations utilize jacket substation substructures, while configurations with 4 or more substations employ monopile substructures.

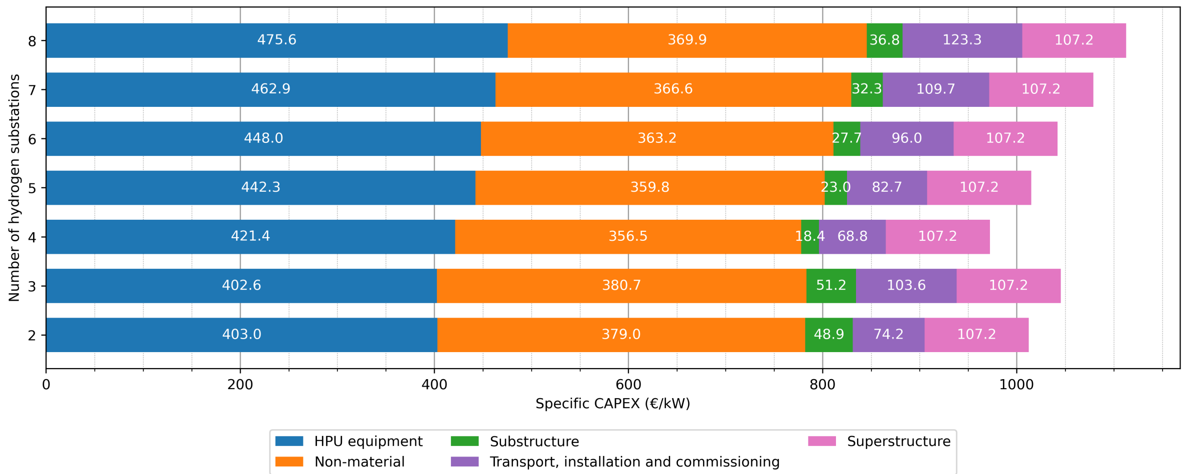

Figure 8.15: Specific CAPEX of hydrogen substation components for semi-centralised configurations (2-3 substations = Jacket substructure, 4-8 substations = monopile substructure).

Distinct variations in specific costs can be observed for the HPU equipment, substructure, and transport and installation in the semi-centralised configurations. The specific cost of HPU equipment is influenced by scaling, resulting in higher costs when the HPU installed capacity per substation decreases. It is of significance to emphasize that the electrolyser replacement costs are not incorporated in the specific HPU equipment CAPEX, as they are considered part of the HPU's OPEX. Differences in non-material costs arise from the increase in material cost, as non-material costs scale with material costs. The superstructure cost remains similar across different configurations, as it scales linearly with the installed HPU capacity.

Variations in substructure and transport, installation and commissioning costs primarily stem from the topside weight, which determines the type of substructure and the method of transport, installation, and commissioning used. Notably, a significant difference in substructure cost and transport, installation, and commissioning cost can be observed between configurations with three and 4 substations, representing the boundary between jacket and monopile substructures. This suggests that substantial cost reductions are achieved through the synergies offered when using monopiles substructures both for wind turbines and hydrogen substations. However, it is important to mention that the specific cost of the substructure and transport, installation, and commissioning increases from 4 to 8 substations. This can be attributed to the fixed cost component associated with monopiles, as the same monopile is used for configurations with 4 to 8 substations, resulting in increased costs as the number of substations rises.

8.4. Offshore wind-to-hydrogen configuration comparison

In this section, the economic feasibility of the centralised, semi-centralised, and decentralised offshore wind-to-hydrogen configurations is compared within the specific case study. The evaluation focuses on the economic viability by examining the created layouts and their LCOH in Subsection 8.4.1. Subsequently, a detailed analysis of the energy infrastructures and offshore hydrogen facilities is presented in Subsections 8.4.2 and 8.4.3 respectively. The main objective of these analyses is to determine the optimal configuration for offshore hydrogen production within an offshore wind farm based on LCOH. Additionally, the goal is to identify the key factors that influence the selection of the optimal configuration. Once these factors are identified, a sensitivity analysis can be performed to assess their individual impacts more specifically.

8.4.1. Offshore wind-to-hydrogen configuration comparison overview

The wind-to-hydrogen farm layout for the centralised, semi-centralised and decentralised configurations are depicted in Figure 8.16, 8.17 and 8.18 respectively. The centralised configuration consist of one hydrogen substation while the semi-centralised configuration consist of 4 hydrogen substations, chosen based on the semi-centralised configuration selection. On the other hand, the decentralised configuration consist of 70 hydrogen wind turbines. In the centralised and semi-centralised layouts, the blue area represents the site available for wind turbine placement, the dark blue and red lines depict the two different inter-array cable types, the white bars present the hydrogen steel pipelines and the wind turbines are presented by small red circles with a specific number. In the decentralised layout, the green, blue and red lines depict the infield flowlines, the white bar represents the steel hydrogen pipeline, the central circle is the hydrogen manifold and the wind turbines are depicted with a small "x".

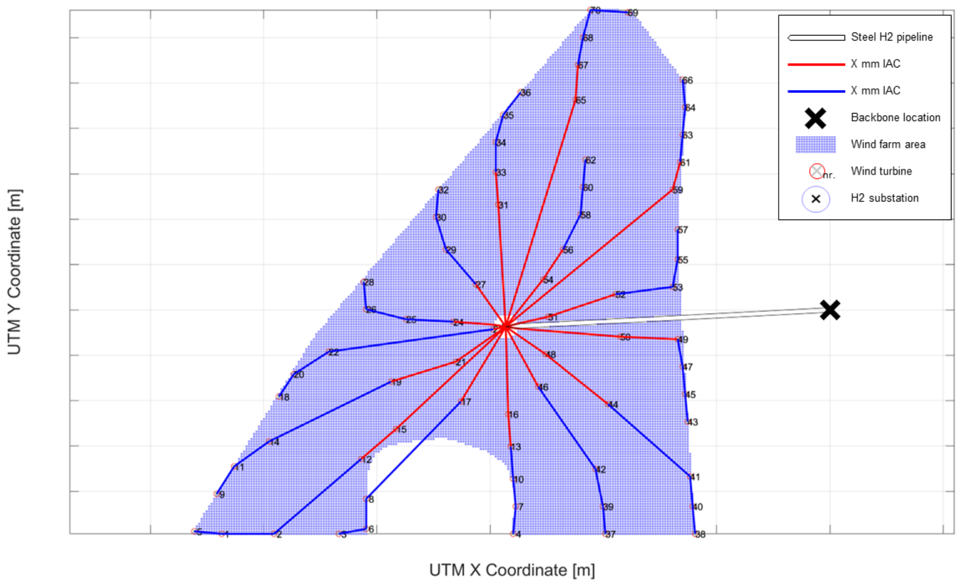

Figure 8.16: Centralised offshore wind-to-hydrogen farm layout.

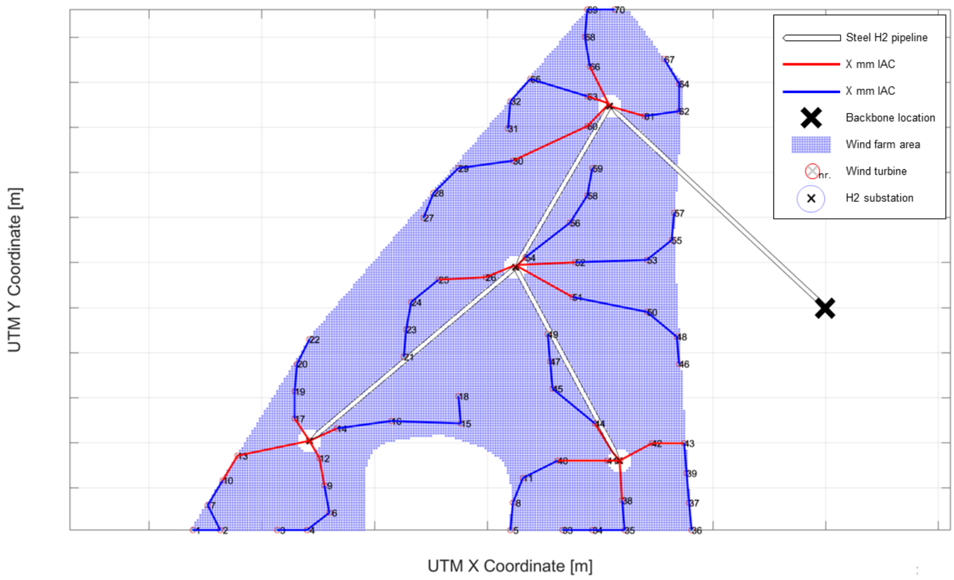

Figure 8.17: Semi-centralised (4 hydrogen substations) offshore wind-to-hydrogen farm layout.

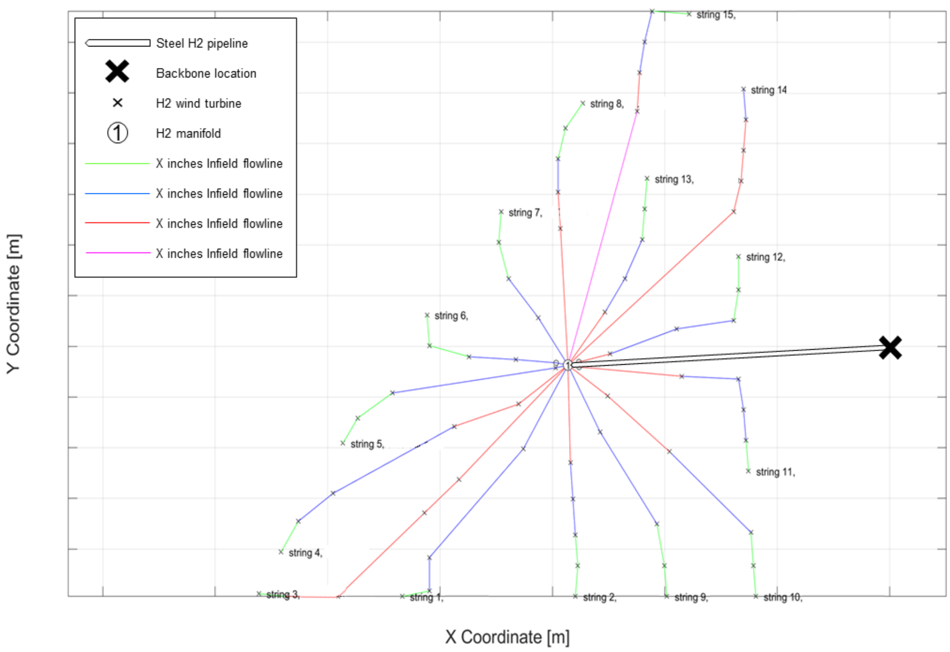

Figure 8.18: Decentralised offshore wind-to-hydrogen farm layout.

The wind-to-hydrogen farm layout in the centralised configuration follows a similar arrangement to an all-electric wind farm. It includes a single offshore electrical substation and adopts the same placement of wind turbines and substations. In the decentralised configuration, the layout is the same as for the centralised configuration, as it shares the optimised substation position, steel pipeline substation-backbone connection, wind turbine positions, and cable routing. The main differences lie in the replacement of standard wind turbines with hydrogen wind turbines, the substitution of the substation with a manifold, and the use of infield flowlines instead of inter-array cables.

Furthermore, in all three configurations, the positioning of wind turbines along the borders of the site is notable. This arrangement is strategically designed to minimise wake losses and maximize power output. While this placement increases the length of inter-array cables, the overall focus is on augmenting power output, which carries greater significance. This strategic arrangement of wind turbines along the site's borders demonstrates consistency across different offshore wind-to-hydrogen configurations.

The offshore wind-to-hydrogen configurations are compared on their LCOH taking into account the preliminary optimisations of Section 8.2. The LCOH of the configurations is depicted in Figure 8.19. From this figure, the conclusion can be drawn that the decentralised configuration results in the lowest LCOH of 3.91 €/kg.

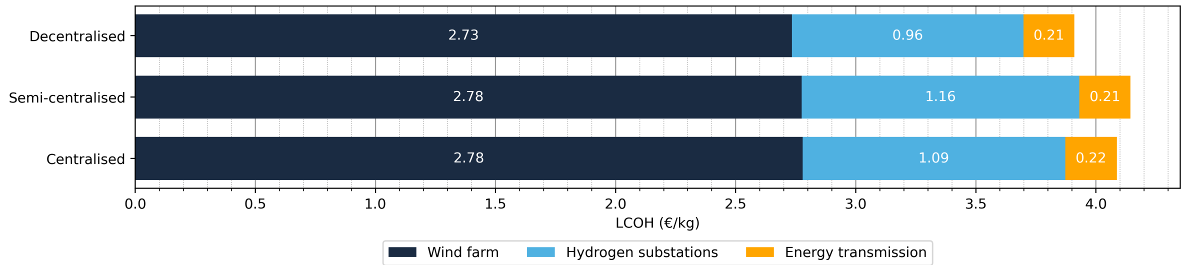

Figure 8.19: LCOH breakdown for the centralised, semi-centralised and decentralised configurations. The LCOH is categorized into three components: wind farm, hydrogen substation, and energy transmission.

Figure 8.19 provides an illustration of the contribution to the LCOH from the wind farm, energy infrastructure, and hydrogen substations or hydrogen wind turbines. The wind farm contribution encompasses the costs associated with all components of the wind-to-hydrogen farm, excluding the hydrogen pipelines, inter-array cables, and hydrogen substations. This component represents a significant portion of the LCOH and varies among the different configurations.

In the decentralised configuration, notable cost savings can be observed due to the absence of high voltage transformers in the electrical system of hydrogen wind turbines. This leads to a cost saving of 0.38M€ compared to a standard wind turbine. The cost advantage in the decentralised configuration is a direct result of this design choice.

The contribution of hydrogen substations to the LCOH exhibits considerable variation among the configurations. It is important to consider that the substructures of the hydrogen wind turbines are included as part of the wind farm contribution since they are already installed for the wind turbines. This distinction should be taken into account when analysing the LCOH contribution of the hydrogen substations.

Additionally, the LCOH contribution of energy transmission, which incorporates the expenses associated with hydrogen pipelines and inter-array cables, differs across the configurations. The specific costs for these components vary among the configurations, influencing their contribution to the overall LCOH.

Since the differences in LCOH related to the energy infrastructure and offshore hydrogen facilities among the configurations are influenced by multiple factors and not just one, the upcoming subsections will delve into an analysis of these components.

Furthermore, variations in total hydrogen production throughout the lifespan occur due to disparities in electrical power losses. The total hydrogen production during the lifetime for the centralised, semi-centralised and decentralised configuration is given in Figure 8.20. The variances in inter-array cable power loss can be attributed to differences in inter-array cable length and causes the differences in hydrogen production during lifetime.

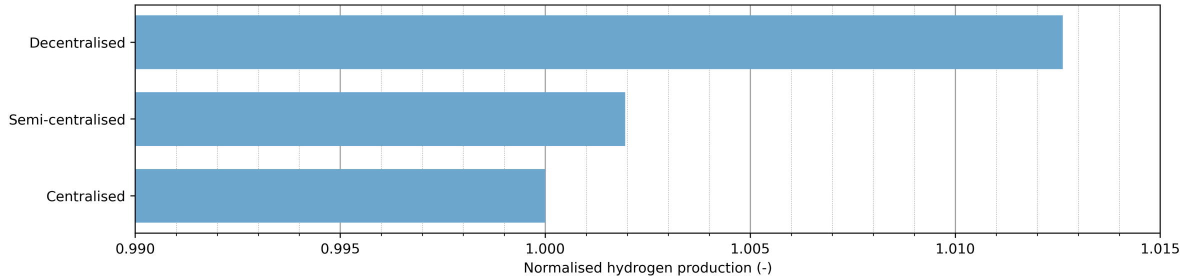

Figure 8.20: Normalised hydrogen production during lifetime for the centralised, semi-centralised and decentralised configurations.

Table 8.4 offers an overview of the maximum total input capacity of the HPU and total electrical power loss for the centralised, semi-centralised and decentralised configurations. The differences in electrical power loss are caused by the differences in inter-array cable length. The decentralised configuration generates a greater amount of hydrogen throughout its lifetime compared with the centralised and semi-centralised configuration. This can be attributed to the absence of inter-array cables and the high voltage power transformer steps present in the configuration. These factors contribute to improved efficiency and reduced power losses, resulting in higher hydrogen production compared to the other configurations.

However, it's important to consider the simplification of the efficiency curve of the electrolysers when interpreting these results. The current analysis assumes a constant efficiency curve for the electrolysers, which may not fully capture the actual performance variations among different configurations. The impact of this simplification on hydrogen production will differ per configuration due to the varying capacities of the electrolysers. Specifically, the decentralised configuration is expected to be more affected by a variable efficiency curve since there is less power aggregation leading to relatively large power fluctuations which could affect the hydrogen production negatively [37] [35].

Parameter	**Unit**	**Centralised**	**Semi-centralised**	**Decentralised**
OHFs	#	1	4	70
Wind farm HPU maximum input power	MW	1034.6	1038.0	1041.4
Maximum inter-array cable power loss	MW	X	X	-

Table 8.4: Centralised, semi-centralised and decentralised wind-to-hydrogen configuration specifications.

8.4.2. Energy transmission infrastructure

The energy transmission infrastructures of the three configurations are compared based on their type, length, and associated cost. Figure 8.21 provides a visual representation of the offshore wind-to-hydrogen configurations' energy transmission infrastructure type, length and total CAPEX.

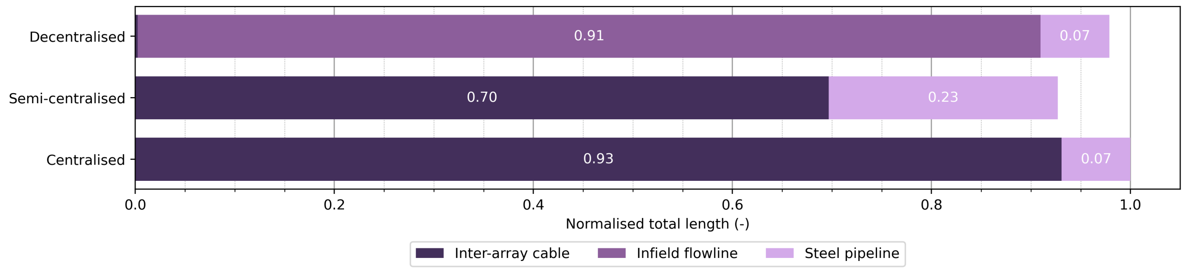

(a) Normalised energy infrastructure length.

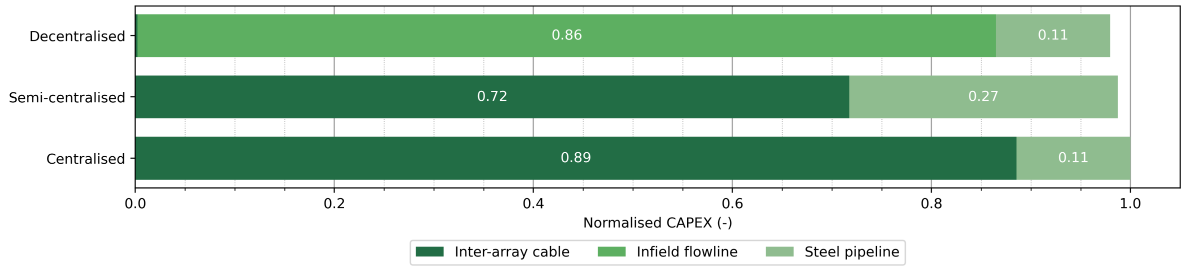

(b) Normalised energy infrastructure CAPEX.

Figure 8.21: Length and CAPEX of inter-array cables, steel hydrogen pipelines and hydrogen infield flowlines for the centralised, semi-centralised and decentralised configurations.

Figure 8.21a demonstrates that the semi-centralised configuration exhibits a shorter total length of energy transmission infrastructure compared to the centralised and decentralised configurations. The centralised and decentralised configurations share the same cable or pipeline layout and, therefore, should have identical total energy infrastructure lengths. However, the disparity in infield flowline length and inter-array cable length between the centralised and decentralised configurations can be attributed to the inclusion of spare length in the inter-array cable. In the case of the decentralised configuration, the inter-array cable length specifically refers to the cable connecting the turbine nearest to the manifold, responsible for supplying the required power for compression. However, due to the relatively short length of the inter-array cables (approximately X km), their impact on the overall length and CAPEX is not easily observable in the figure.

Figure 8.21b shows the total CAPEX of the energy infrastructures of the three configurations. It can be seen that the total energy infrastructure CAPEX of the semi-centralised and decentralised is similar and is marginally lower compared to the centralised configuration. The difference in total CAPEX is mainly caused by the variation in specific CAPEX between inter-array cables, steel pipelines, and infield flowlines.

Figure 8.22 presents specific CAPEX information for hydrogen pipelines and infield flowlines. Analysis of the figure reveals that the specific CAPEX of inter-array cables does not vary significantly across different configurations. The minor differences can be attributed to the varying lengths and costs of the two types of inter-array cables. For the steel pipeline, a notable disparity can be observed. The decrease in specific CAPEX for the pipelines is a result of the number of segments and pipeline diameters. Generally, an increase in the number of segments and total pipeline length leads to a decrease in specific CAPEX for hydrogen pipelines. The specific price of infield flowlines is comparable to the specific price of the inter-array cables.

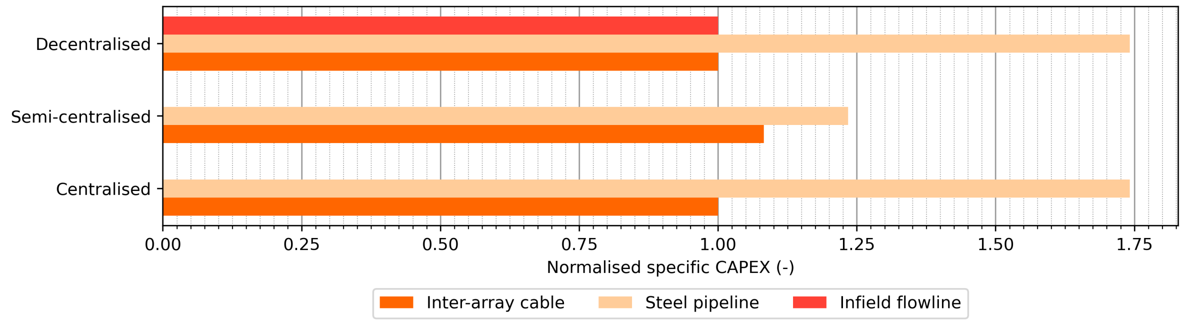

Figure 8.22: Normalised specific CAPEX of energy infrastructure for the centralised, semi-centralised and decentralised configurations, divided into steel pipelines, infield flowlines and inter-array cables.

As discussed in the semi-centralised energy infrastructure specific CAPEX, it becomes apparent that there exists a disparity in the specific CAPEX between inter-array cables and hydrogen pipelines, resulting in a higher cost for the pipelines. As explained before, this finding contradicts the initial assumption that pipelines are typically less expensive than electrical cables.

8.4.3. Offshore hydrogen facilities

Table 8.5 provides insights into the specifications of the OHFs in the configurations, displaying the HPU rated capacities, topside masses, specific topside mass, and substructure types for the substation or hydrogen wind turbines. It is evident from the table that the specific topside mass of the decentralised configuration is significantly higher than that of the other configurations. This is primarily due to the additional mass of the wind turbines.

Parameter	**Unit**	**Centralised**	**Semi-centralised**	**Decentralised**
OHFs	#	1	4	70
OHF HPU rated capacity	MW	1002	252	14.4
OHF topside mass	tonne	31,234	7,818	1,880
OHF Specific topside mass	tonne/MW	31.1	31.0	130.6
OHF Substructure type	-	Jacket	Monopile	Monopile

Table 8.5: Offshore hydrogen facility specifications for centralised (1 hydrogen substation), semi-centralised (4 hydrogen substations) and decentralised (70 hydrogen wind turbines) wind-to-hydrogen configurations.

Figure 8.23 offers a comparison of the specific CAPEX for offshore hydrogen facilities across the different configurations. The figure presents a breakdown of specific costs for various components, including HPU equipment, superstructure, substructure, transport, installation and commissioning, and non-material expenses, for each configuration. It is important to note that in the decentralised configuration with 70 OHFs, the CAPEX of hydrogen wind turbines and substructures are not included as explained before.

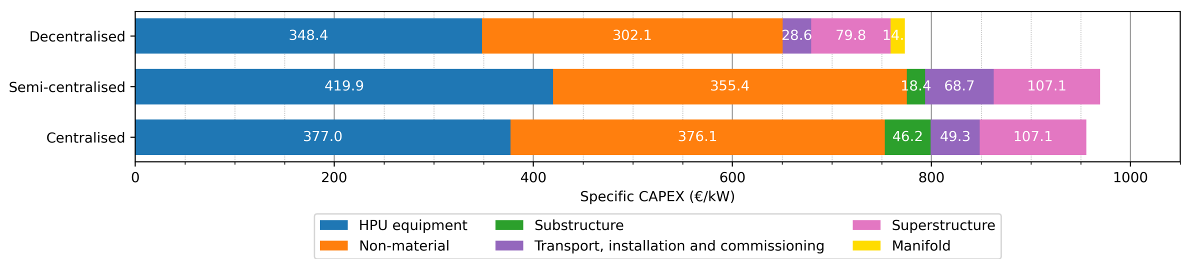

Figure 8.23: Specific CAPEX of hydrogen substation components for the centralised, semi-centralised and decentralised configurations.

Distinct variations in specific CAPEX are apparent for HPU equipment, non-material, substructure, transport, installation, and commissioning, and superstructure.

The specific CAPEX of HPU equipment is influenced by scaling, resulting in higher CAPEX when the HPU installed capacity decreases. This discrepancy can be observed between the centralised and semi-centralised configurations,where the semi-centralised setup exhibits a higher HPU equipment specific CAPEX value because of its lower HPU installed capacity per hydrogen substation. However, the HPU equipment specific CAPEX in the decentralised configuration is significantly lower, due to the cost savings of not requiring high voltage electrical equipment.

Differences in non-material CAPEX arise because these costs are calculated as a percentage of the material CAPEX, and thus, they scale with the HPU equipment, substructure, and superstructure CAPEX. However, the non-material CAPEX is based on the HPU equipment cost without considering the cost scaling factors of the electrolyser stacks and BOP. For the semi-centralised configuration, the HPU equipment cost used for calculating non-material costs is the same as in the centralised configuration. Additionally, the substructure cost is lower for the semi-centralised configuration than for the centralised configuration. Consequently, the total non-material CAPEX in the semi-centralised configuration is lower compared to the centralised configuration.

Disparities in substructure and transport and installation CAPEX primarily stem from variations in topside weight, influencing the selection of substructure type and the method of transport and installation. Where the centralised hydrogen substation contains a jacket substructure, the semi-centralised hydrogen substation contain monopile substructures. Additionally, for the decentralised configuration, no substructure cost is included since the substructure is already installed for the wind turbine and included in the wind farm cost.

The superstructure specific CAPEX in the centralised and semi-centralised configurations is similar as the cost scales linearly with the installed capacity of HPUs. In contrast, the superstructure specific CAPEX in the decentralised configuration is significantly lower, as it requires a simpler construction in the form of a working platform.

8.5. Sensitivity Analysis

This section provides a sensitivity analysis, aiming to understand how varying key parameters can influence the overall system performance and cost of offshore wind-to-hydrogen configurations. First in Subsection 8.5.1, an overview of the high-level and low-level parameters is given together with the method used to conduct the sensitivity analysis. Hereafter, in Subsection 8.5.2, the sensitivity analysis is provided of the high-level parameters. Finally, in Subsection 8.5.3, the sensitivity analysis regarding low-level parameters is given. Both the high-level and low-level parameter sensitivities are used to compare the impact on the different configurations.

8.5.1. Sensitivity analysis overview

The sensitivity analysis methodology, designed to highlight the sensitivities concerning the LCOH of different offshore wind-to-hydrogen configurations, incorporates the extraction of key parameters for the LCOH from previously discussed sections. Subsequently, a sensitivity analysis of these parameters is conducted. The procedure entails altering the input parameters by -20%, -10%, +10%, and +20%, and subsequently calculating the consequent LCOH. This mechanism facilitates the identification and comparative evaluation of the impacts invoked by variations in the defined parameters. This strategy is uniformly executed across the centralised, semi-centralised, and decentralised. As a result, differences in sensitivity across these configurations become evident.

The first step involves conducting a sensitivity analysis on the high-level parameters, which are presented in Table 8.6, along with an explanation for each parameter. Important note is that for the centralised and semi-centralised configuration, the OHF total CAPEX and OHF total OPEX are represented by *Substation* total CAPEX and *Substation* total OPEX. For the decentralised configuration, the OHF total CAPEX and OPEX are represented by Hydrogen wind turbine (*HWT*) total CAPEX and *Substation* total OPEX.

In the HPU in-efficiency and HPU in-availability parameters, the emphasis is placed on inefficiency and in-availability rather than efficiency and availability. This decision was made to ensure that the parameter values remain within realistic bounds. Increasing efficiency or availability by 20% would exceed physical limits [35]. Since efficiency and availability are capped at 100%, extending them beyond this threshold can lead to unrealistic results that violate fundamental principles. On the other hand, by focusing on inefficiency and in-availability, a more practical range of values is obtained for sensitivity analyses. This range includes variations of ±20%. As an example, let's examine the impact of a 20% increase in the HPU inefficiency parameter. If the initial inefficiency of the HPU is 10%, a 20% increase would raise it to 12%. On the other hand, if the original efficiency is 90%, a 20% increase would result in an efficiency value of 108%. Therefore, selecting inefficiency and in-availability helps maintain the feasibility and validity of the analysis.

High-level parameters	**Description**
Wind farm CAPEX	CAPEX of wind farm excluding cost related to offshore hydrogen facilities, hydrogen pipelines and inter-array cables.
OHF total CAPEX	CAPEX of HPU equipment, substructure, superstructure, transport, installation and commissioning and decommissioning. For decentralised, this does not included the wind turbines and monopile substructure.
Energy transmission CAPEX	CAPEX of the inter-array cables and hydrogen pipelines.
Wind farm OPEX	OPEX of wind farm excluding cost related to offshore hydrogen facilities, hydrogen pipelines and inter-array cables.
OHF total OPEX	OPEX of all components of the offshore hydrogen facilities. For decentralised, this does not included the wind turbines and monopile substructure.
Energy transmission OPEX	OPEX of the inter-array cables and hydrogen pipelines.
Discount rate	Discount rate
HPU in-efficiencies	Initial in-efficiency electrolyser stacks, electrical equipment, desalination, hydrogen purification and compression.

Table 8.6: High-level parameters for the sensitivity analysis.

In the second step, a more detailed sensitivity analysis is conducted on low-level parameters. This analysis aims to provide a deeper understanding of the key factors influencing the LCOH. The low-level parameters are defined in Table 8.7. By examining these specific components, it becomes possible to identify the main drivers behind the variations in LCOH across different configurations. It is important to note that the low-level parameters considered for the sensitivity analysis do not include parameters related to the wind farm CAPEX and OPEX. This deliberate choice is made to align with the focus of this study, which centers on the hydrogen components. Furthermore, the analysis of the LCOH has indicated that the contribution of the wind farm to the LCOH is similar across all configurations.

Important note is that for the centralised and semi-centralised configuration, the OHF parameters are represented by *Substation* parameters. For the decentralised configuration, the OHF parameters are represented by Hydrogen wind turbine (*HWT*) parameters.

Low-level parameter	Description
HPU equipment CAPEX	CAPEX of the electrolyser stacks, BOP equipment, electrical system and compressor.
OHF non-material CAPEX	CAPEX of EPCm, owner and contingencies.
Inter-array cable CAPEX	CAPEX of inter-array cables.
Hydrogen pipeline CAPEX	CAPEX of steel hydrogen pipelines and infield flowlines.
OHF superstructure CAPEX	CAPEX of substation superstructure.
OHF substructure CAPEX	CAPEX of substation jacket or monopile substructure.
OHF TIC CAPEX	CAPEX of substation transport, installation and commissioning.
Manifold total CAPEX	CAPEX of manifold.
Cost scaling factor electrolyser stacks	Scaling factor electrolyser stacks and BOP.
Cost scaling factor BOP	Scaling factor electrolyser stacks and BOP.
Degradation rate wind farm	Degradation rate power conversion wind farm.
Degradation rate electrolyser stacks	Degradation rate electrolyser stacks.
Initial in-efficiency electrolyser stacks	Initial in-efficiency electrolyser stacks.
HPU in-availability	HPU in-availability.
monopile load	monopile load.
Mass OHF topside	Mass of HPU equipment and superstructure.

Table 8.7: Low-level parameters for the sensitivity analysis.

8.5.2. LCOH high-level parameter sensitivities

Figure 8.24 illustrates the influence of high-level parameters on the LCOH for the centralised configuration. The parameters are ranked based on their impact of uncertainty or change. The results reveal that changes in the wind farm CAPEX have a significant effect on the overall system cost. Thus, initiatives aimed at reducing the wind farm CAPEX can result in substantial cost savings. It could be stated that the wind farm CAPEX is crucial for different offshore wind-to-hydrogen configurations. However, it is worth noting that the uncertainty associated with the wind farm CAPEX is relatively small compared to the hydrogen-related parameters, as the wind farm CAPEX is well-established.

Additionally, the discount rate and the inefficiencies of the HPU significantly contribute to the variations in the LCOH. Changes in the discount rate impact the time value of money, while alterations in HPU inefficiencies directly affect the hydrogen production over the wind-to-hydrogen farm's lifetime. Therefore, it is important to evaluate the uncertainties associated with these parameters to enhance the certainty and accuracy of the LCOH results. This evaluation can bring to light any challenges in accurately estimating their values or models.

Moreover, investigating the potential changes in these parameters over time or in different locations can provide valuable insights. For instance, variations in discount rates or HPU efficiencies might arise due to evolving market conditions, technological advancements, or regional differences. Understanding the dynamics and possible fluctuations in these key parameters can enable more informed decision-making and robust planning for the design of cost-effective offshore wind-to-hydrogen configurations.

In contrast, the impact of changes in hydrogen substation OPEX and energy infrastructure CAPEX and OPEX on the LCOH appears to be relatively limited. While they influence the overall system performance, their direct influence on the LCOH is less pronounced compared to the wind farm CAPEX, discount rate, and HPU inefficiencies.

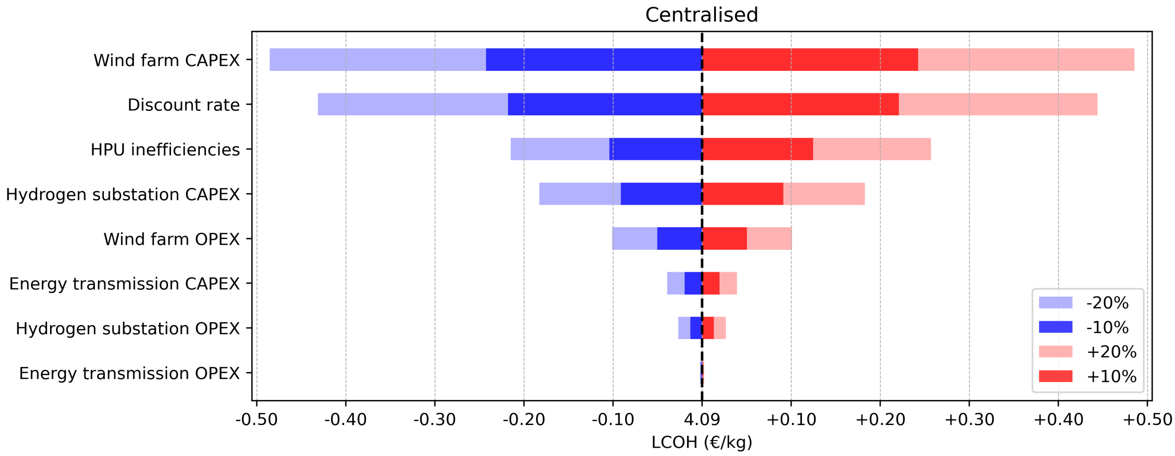

Figure 8.24: Tornado plot illustrating the high-level parameter sensitivity analysis of LCOH for the centralised offshore wind-to-hydrogen configuration.

In Figure 8.25, the influence of the high-level parameters on the LCOH for the semi-centralised configuration is presented. The parameters are ranked in the same order as for the centralised configuration for comparison purposes. The shape of the tornado plot is similar to the shape of the tornado plot of the centralised configuration. This similarity in the shape of the tornado plots indicates that the high-level parameters, such as wind farm CAPEX, discount rate, and HPU inefficiencies, have a similar influence on the LCOH in both the centralised and semi-centralised configurations.

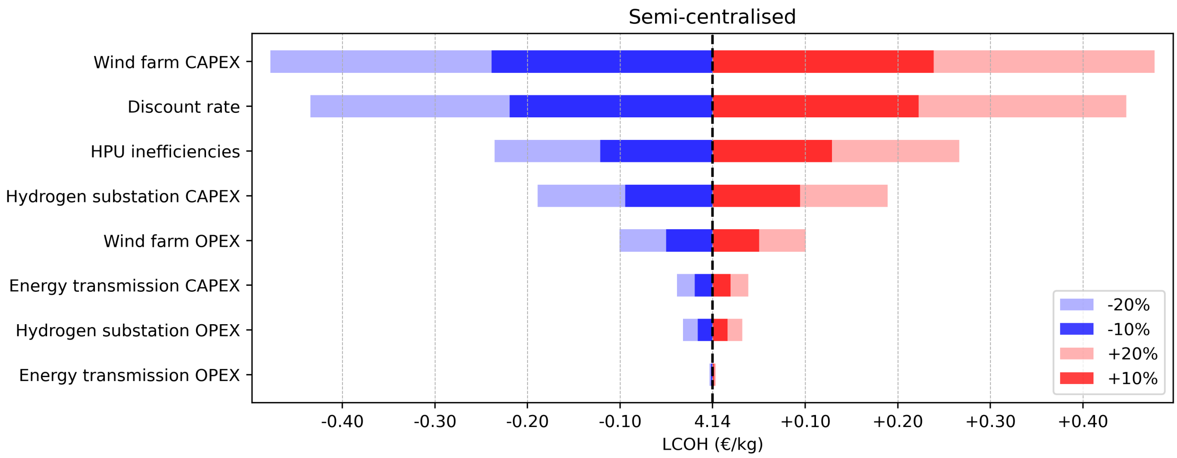

Figure 8.25: Tornado plot illustrating the high-level parameter sensitivity analysis of LCOH for the semi-centralised offshore wind-to-hydrogen configuration consisting of 4 hydrogen substations.

In Figure 8.25, the influence of the high-level parameters on the LCOH for the decentralised configuration is presented. The parameters are ranked in the same order as for the centralised configuration for comparison purposes. The shape of the tornado plot is almost similar to the shape of the tornado plot of the centralised and semi-centralised configuration. The only difference relates to the impact of the hydrogen substation CAPEX and OPEX. This can be declared by the significantly lower specific OHF CAPEX of the decentralised configuration due to fact that the substructure cost are not included as well as the lack of high voltage electrical equipment.

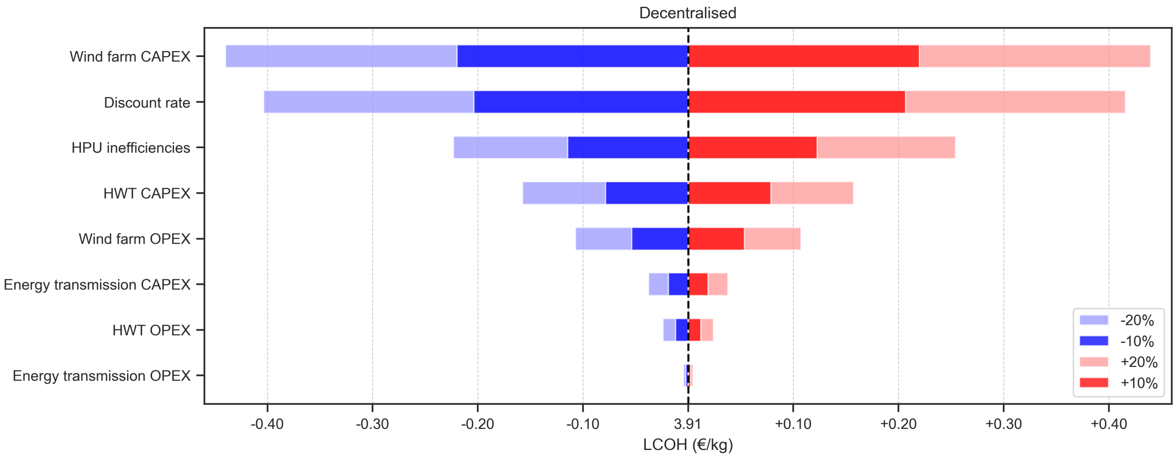

Figure 8.26: Tornado plot illustrating the high-level parameter sensitivity analysis of LCOH for the decentralised offshore wind-to-hydrogen configuration.

In all configurations, the wind farm CAPEX, discount rate, and HPU inefficiencies have significantly impact on uncertainty and change. The energy infrastructure has a comparatively limited influence.

Regarding the decentralised configuration, it is observed that its advantage lies in having significantly lower OHF specific CAPEX due to the exclusion of substructure costs and high voltage electrical equipment. However, this advantage might not be fully reflected in the tornado diagrams, as these diagrams primarily show the sensitivity of the LCOH to changes in parameters rather than comparing absolute differences in LCOH between configurations.

Additionally, in the sensitivity study, the difference in the decentralised configuration compared to the other two configurations may be related to the fact that the centralised and semi-centralised configurations have more potential for cost reductions through further improvements to the hydrogen substation, while the decentralised configuration already exhibits lower costs. Therefore, the potential for additional cost reduction in the decentralised configuration might be limited compared to the other configurations.

Overall, these findings emphasize the importance of reducing the values and reducing the uncertainty of the wind farm CAPEX, discount rate, and HPU in-efficiency to achieve cost-effective offshore wind-to-hydrogen systems.

8.5.3. LCOH low-level parameter sensitivities

Figure 8.27 presents the low-level parameter sensitivities for the centralised configuration. Similar to the high-level parameter tornado plot, the parameters are ranked based on their impact on uncertainty and change. The same order of parameters is maintained for the semi-centralised and decentralised configuration tornado plots for the low-level parameter sensitivities.

The analysis reveals that the primary parameters affect by uncertainty and change within the centralised configuration are the initial inefficiency of the electrolyser stacks and the CAPEX of the HPU equipment. Conversely, the impact of scaling factors is zero in the centralised configuration since no scaling occurs.

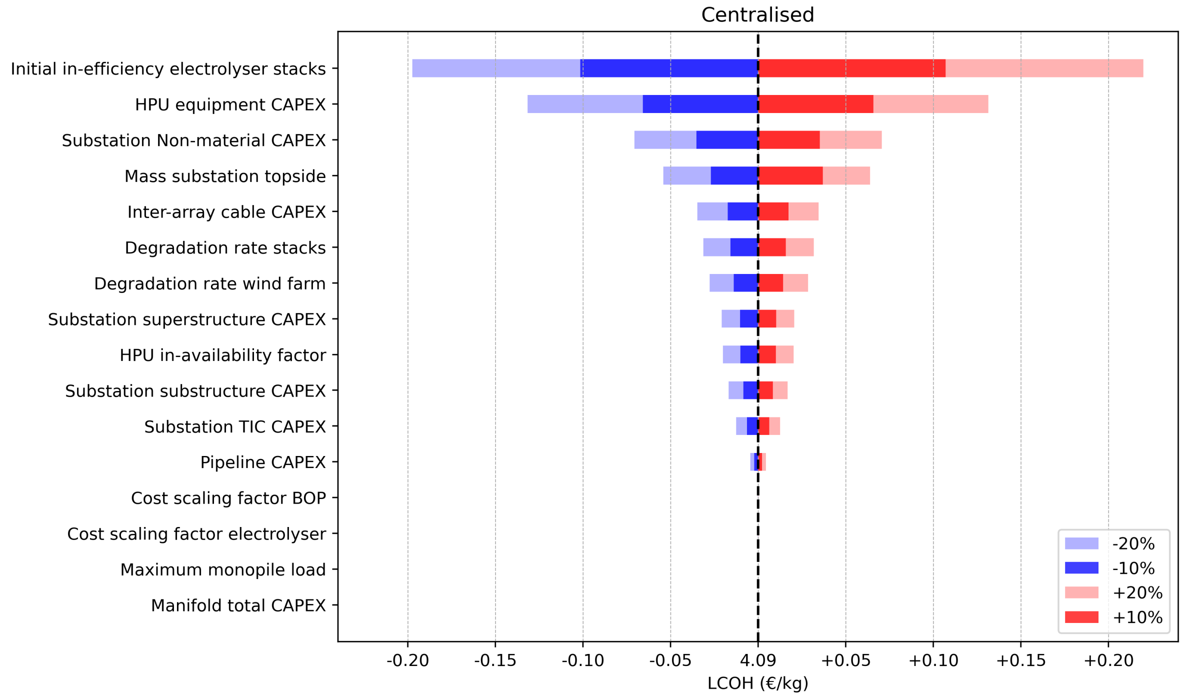

Figure 8.27: Tornado plot illustrating the low-level parameter sensitivity analysis of LCOH for the centralised offshore wind-to-hydrogen configuration.

For the semi-centralised configuration, the low-level parameter sensitivity is depicted in Figure 8.28. As in the centralised configuration, the impact of the initial in-efficiency of the electrolyser stacks and the HPU equipment CAPEX is the most significant. However, there a some differences compared to the specific parameter sensitivity of the centralised configuration. The influence of the substation topside mass and substructure is relatively smaller. Additionally, the impact of the BOP and electrolyser stack cost scaling factors is visible, albeit limited.

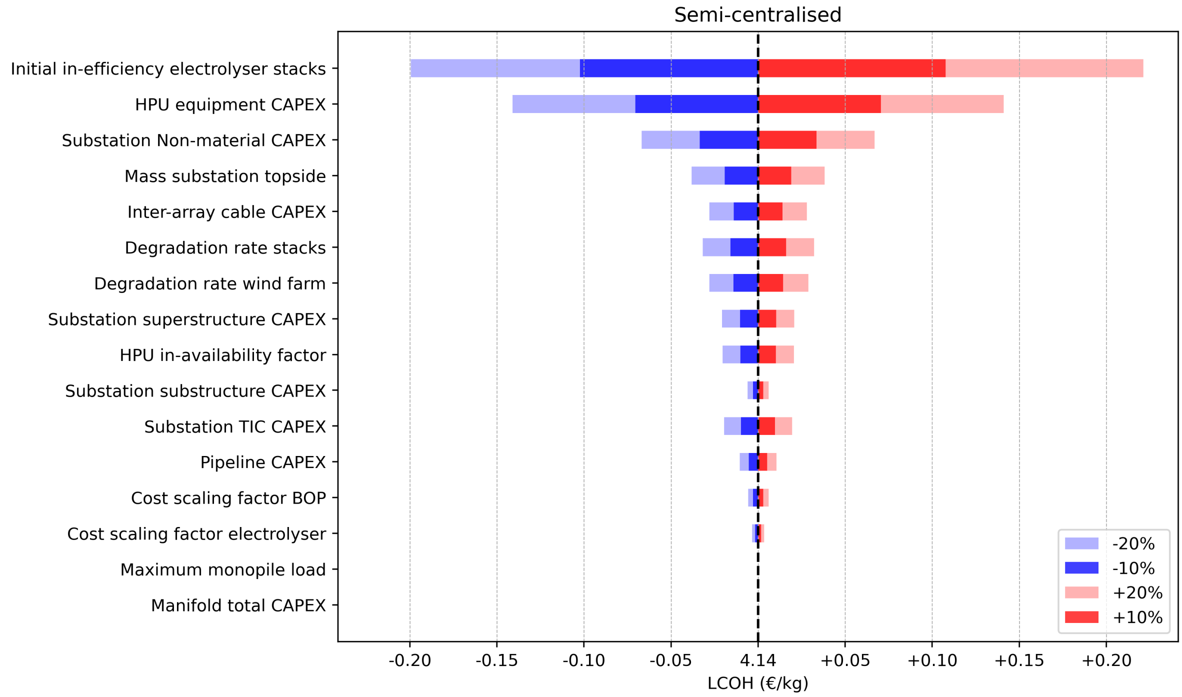

Figure 8.28: Tornado plot illustrating the low-level parameter sensitivity analysis of LCOH for the semi-centralised offshore wind-to-hydrogen configuration.

In the decentralised configuration, the low-level parameter sensitivity is depicted in Figure 8.29. Similar to the centralised and semi-centralised configurations, the impact of the initial inefficiency of the electrolyser stacks and HPU equipment CAPEX remains significant. However, there are notable differences compared to the other configurations. The mass of the substation topside and substation substructure have negligible impact in the decentralised configuration. This suggests that these factors have less influence on the LCOH within this configuration. On the other hand, the decentralised configuration shows a larger impact of pipeline CAPEX and manifold CAPEX. This indicates that the cost of the hydrogen pipelines and manifold significantly affects the LCOH in the decentralised setup. Additionally, the cost scaling factor of the electrolyser and the BOP have a more prominent influence in the decentralised configuration. This can be explained by relative small scale HPU installed capacities thus leading to a greater impact of the cost scale factors.

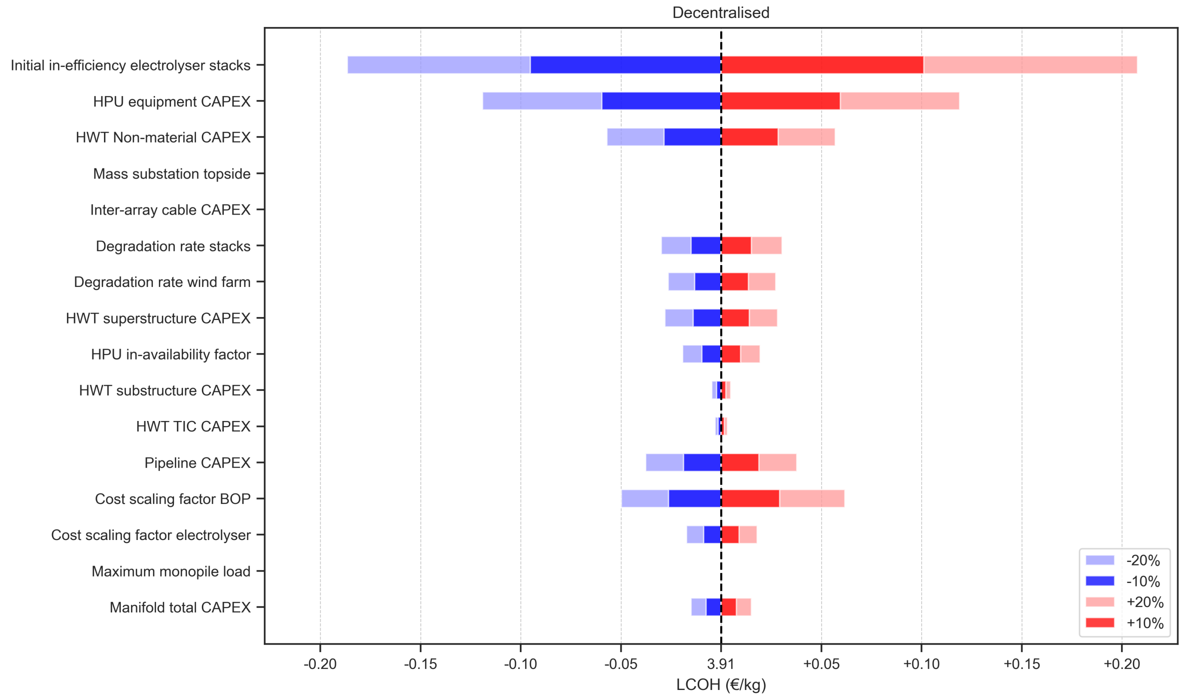

Figure 8.29: Tornado plot illustrating the low-level parameter sensitivity analysis of LCOH for the decentralised offshore wind-to-hydrogen configuration.

Parameters such as the initial stack in-efficiency and the stack degradation rate are considered uncertain due to the limit knowledge about their offshore working. Changes in these parameter will largely affect the LCOH.

Moreover, the sensitivity of several parameters varies across the three configurations, potentially leading to a different optimal offshore wind-to-hydrogen configuration. For instance, the HPU equipment CAPEX is subject to uncertainty and will likely change over time. Depending on the cost scale factors, this could result in different optimal configurations in terms of LCOH.

Overall, the low-level sensitivity analysis provides valuable insights into the impact of uncertainty and change to the parameters of the wind-to-hydrogen configurations. In addition to optimising the parameters, it is important to consider the uncertainty associated with these parameters and evaluate the accuracy of the models used to estimate them.

8.6. Assumption and scenario sensitivity analysis

This section examines the influence of assumptions made prior to the LCOH calculations, which may vary for the different offshore wind-to-hydrogen configurations. Different assumptions for the three configurations may yield different optimal configuration results. For instance, Subsection 8.6.1 analyses the load capacity of the monopile to understand its impact on determining the optimal number of hydrogen substations in the semi-centralised configuration. Moreover, Subsection 8.6.2 investigates whether significant differences in electrolyser stack CAPEX, combined with the cost scale factors, could lead to alternative optimal configuration outcomes. Subsection 8.6.3 assesses a scenario where different HPU availabilities and OPEX factors are considered for each configuration. Subsection 8.6.4, delves into the effect of different degradation rates on the optimal number of electrolyser replacements. Lastly, Subsection 8.6.5 evaluates the effect of different discount rates on the different configurations.

8.6.1. Monopile load capacity

The determination of the monopile load capacity is a critical factor in selecting the appropriate substructure type for different semi-centralised configurations within a substation. Previous chapters have presented findings regarding the relationship between the number of hydrogen substations, the HPU sizing factor, and the monopile load capacity, resulting in distinct substructure types.

Specifically, when considering a monopile load capacity of 10,000 tonnes, semi-centralised configurations comprising 2 and 3 hydrogen substations, along with an HPU sizing factor of 0.97, consistently led to the adoption of jacket substructures. On the other hand, for semi-centralised configurations with 4 or more hydrogen substations, monopile substructures were utilized as their topside did not exceed the load capacity of 10,000 tonnes.

The assumed monopile load capacity of 10,000 may be uncertain as it is based on simplified load capacity and lacks a detailed structural analysis. To assess the influence of different monopile load capacities, various capacities were considered to calculate the corresponding LCOH. For each capacity, it was determined whether the number of substations could be accommodated on monopiles or if jackets were required. The LCOH was then calculated based on these potentially new substructures. Figure 8.30 presents an overview of the LCOH for different semi-centralised configurations across a range of monopile load capacities. Please note that the centralised configuration was excluded from the monopile consideration because the 33,000 ton topside was assumed to be out of the range of a monopile substructure. Similarly, the decentralised configuration was not considered as the hydrogen wind turbines already utilise monopile substructures. The figure includes both the LCOH values for the base case centralised and decentralised configurations as reference.

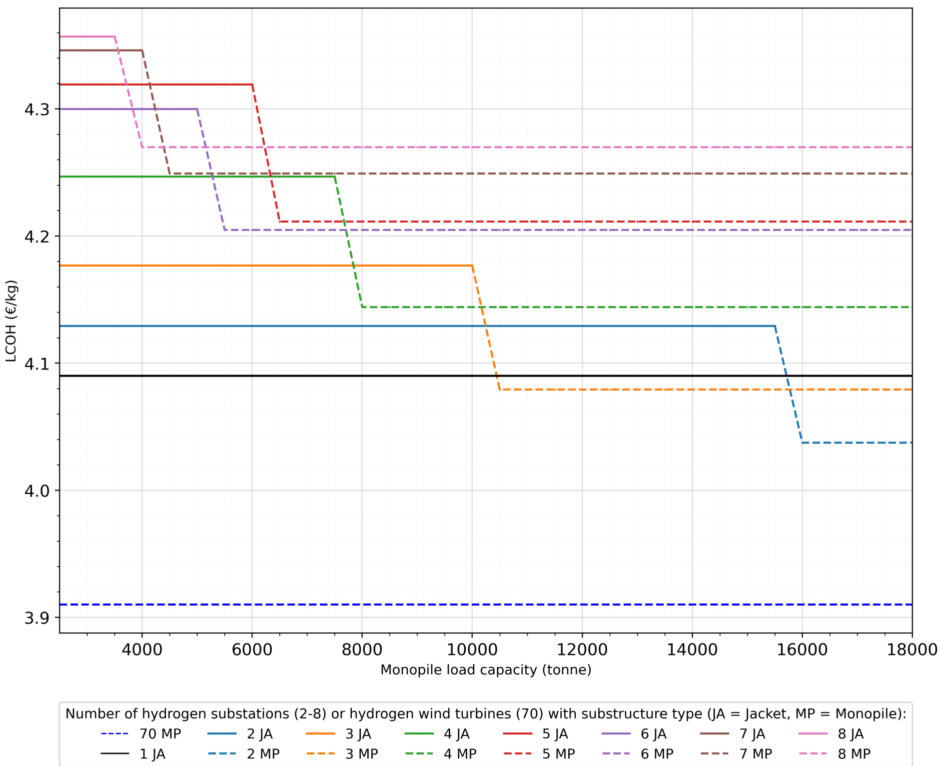

Figure 8.30: LCOH versus monopile load capacity for semi-centralised configurations. Figure indicates the transition point from jacket to monopile substructure, represented by a solid (Jacket) to dashed (Monopile) line.

In the presented figure, a distinct reduction in LCOH can be observed for each configuration at a specific monopile load capacity. This reduction signifies the transition from a jacket substructure to a monopile substructure. Notably, immediately following this drop, when the monopile load capacity is fully utilized by the hydrogen substation in the corresponding configuration, the LCOH is lower compared to the configuration with one fewer substation. These findings highlight the potential for achieving significant cost reductions by an increased monopile load capacity.

8.6.2. Electrolyser stack cost

The electrolyser stack cost assumed in this research is based on large cost reductions between now and 2030 due to electrolyser development [41]. However, one can argue that the electrolyser stack cost do not reduce as much as assumed in the coming years. Therefore, the LCOH is determined for a range of electrolyser stack CAPEX.

Figure 8.31 illustrates the LCOH for different configurations, including the centralised configuration, semi-centralised configurations with 4 hydrogen substations, and the decentralised configuration. The graph shows that an increase in electrolyser CAPEX has a more significant impact on the LCOH of the decentralised configuration compared to the centralised and semi-centralised configurations. Notably, at an electrolyser stack CAPEX of 550€ /kW, which is over three times the assumed electrolyser stack CAPEX for the base case, the centralised configuration achieves a lower LCOH than the decentralised configuration.

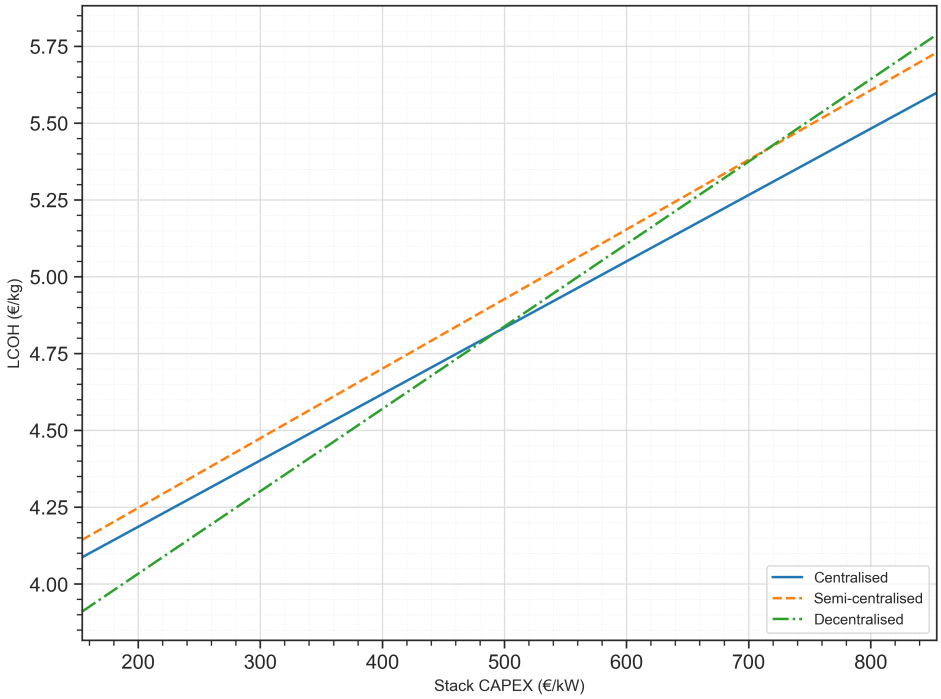

Figure 8.31: LCOH versus stack CAPEX for centralised, semi-centralised (4 substations) and decentralised offshore wind-to-hydrogen configurations.

The reason why an increase in electrolyser stack CAPEX leads to different optimal wind-to-hydrogen configuration can be attributed to the cost scaling factor of the electrolyser stacks. An increase in electrolyser stack CAPEX does increase the LCOH of the decentralised configuration significantly more then for the centralised configuration. Overall, it can be stated that the electrolyser stack CAPEX has influence on the optimal offshore wind-to-hydrogen configuration when cost scaling factors are considered. However, it is worth considering that the cost scaling factors may be closer to 1 than initially assumed in this study, mainly because of the modular design of the stacks. In scenarios where the cost scaling factors approach 1, the influence of stack cost on the various configurations may become negligible.

8.6.3. Availability and maintenance cost

In this report, it is assumed that the availability and maintenance costs are equal for the centralised, semi-centralised, and decentralised offshore wind-to-hydrogen configurations. However, it is plausible to consider that there might be differences across these configurations. For instance, during maintenance of the HPU in the centralised configuration, the entire HPU installation must be turned off for safety reasons, potentially leading to decreased HPU availability. Conversely, the maintenance cost of the decentralised configuration could be considerably higher due to the distributed HPU installations. Therefore, three scenarios: Base case, Middle and High are applied to each configuration. The scenarios represent the optimistic values (Base case), pessimistic values (High) and the values in between (Middle), for the availability and maintenance. The parameters and associated values are given in Table 8.8.

Parameter	Symbol	Unit	Base case	Middle	High
HPU availability factor	AF_{HPU}	%	97.5	93.75	90.0
Electrolyser OPEX factor	$f_{\text{OPEX,stacks}}$	%/CAPEX	2.0	11.0	20.0
BOP OPEX factor	$f_{\text{OPEX,BOP}}$	%/CAPEX	3.0	11.5	20.0
Electrical system OPEX factor	$f_{\text{OPEX,ES}}$	%/CAPEX	3.0	11.5	20.0

Table 8.8: Scenario availability and maintenance cost parameters for the base case and the centralised, semi-centralised and decentralised offshore wind-to-hydrogen configurations.

It is important to note that the values used are assumptions and can be considered as extreme values for illustrative purposes. They have been chosen to demonstrate the potential impact but are not derived from literature values.

Figure 8.32 displays the resulting LCOH for both the base case and the availability and maintenance cost scenario.

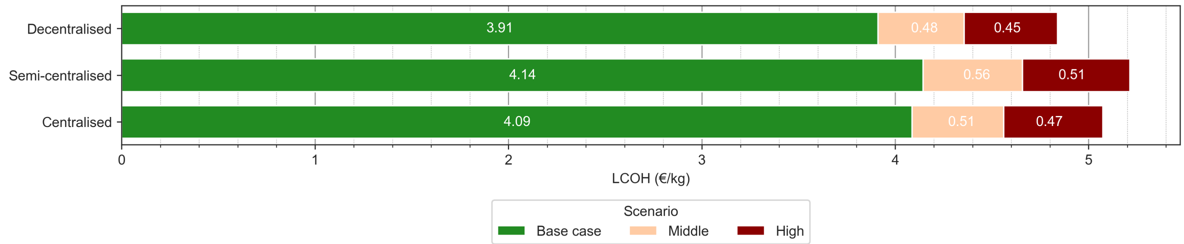

Figure 8.32: Availability and maintenance scenarios: LCOH of centralised, semi-centralised (4 substations) and decentralised offshore wind-to-hydrogen configurations for the Base case, Middle and High scenario. Base case: OPEX factors = 2.0 or 3.0%, HPU availability = 97.5%, Middle: OPEX factors = 11.0 or 11.5%, HPU availability = 97.5%, High: OPEX factors = 20.0%, HPU availability = 97.5%.

In each configuration, the LCOH experiences an increase. However, the magnitude of this increase varies depending on the configuration. This highlights the significance of accounting for availability and maintenance costs across the different configurations.

8.6.4. Stack degradation rate

The stack degradation assumed in this research may be considered optimistic. Hence, in this subsection, an evaluation of stack degradation is conducted to assess its impact on the preliminary optimisation of stack replacements. Figure 8.33 presents the LCOH as a function of a range of stack degradation rates for the centralised, semi-centralised, and decentralised configurations, considering various numbers of electrolyser stack replacements.

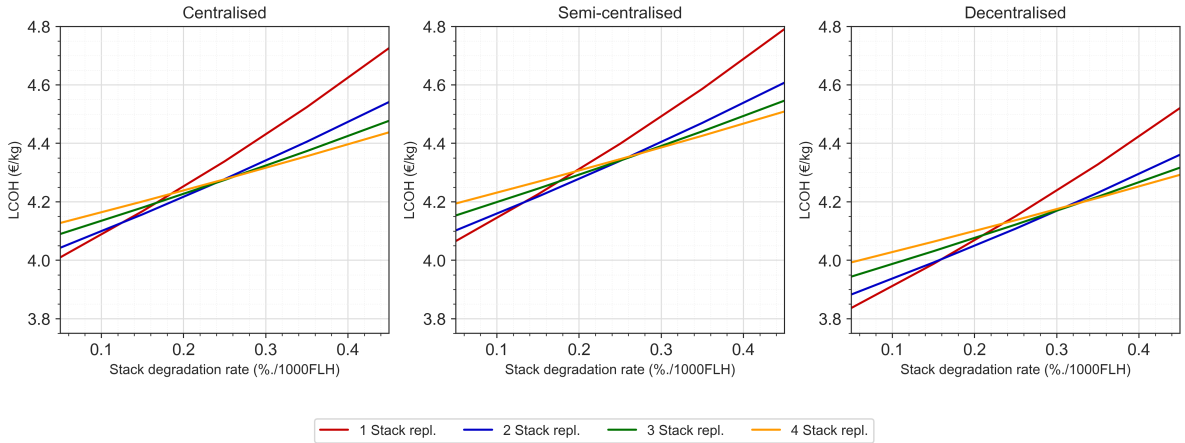

Figure 8.33: LCOH versus stack degradation rates for centralised, semi-centralised (4 substations) and decentralised offshore wind-to-hydrogen configurations. (base case degradation rate = 0.1 %./1000FLH)

The figure demonstrates that the optimal number of stack replacements is heavily influenced by the stack degradation rate. Additionally, the variations observed across the configurations can be attributed to the different electrolyser stack CAPEX due to cost scaling effects. These findings underscore the significance of accurately accounting for stack degradation rates in determining the optimal number of replacements, and how this impacts the cost-effectiveness of each configuration.

8.6.5. Discount rate

The discount rate has a significant impact on uncertainty and variation, as indicated in the sensitivity analysis. Moreover, the choice of discount rate may differ depending on the specific configuration being considered, mainly due to variations in associated project risks. These risks encompass both technical difficulties and asset-related uncertainties.

Consequently, it becomes imperative to conduct an analysis that explores different discount rates for each configuration, specifically focusing on identifying the optimal setup that results in the lowest LCOH. Therefore, it is chosen to calculate the LCOH for a range of discount rates for the different offshore wind-to-hydrogen configurations. By taking into account a range of discount rates, an assessment of the economic viability and cost-effectiveness of possible combination of discount rates is achieved.

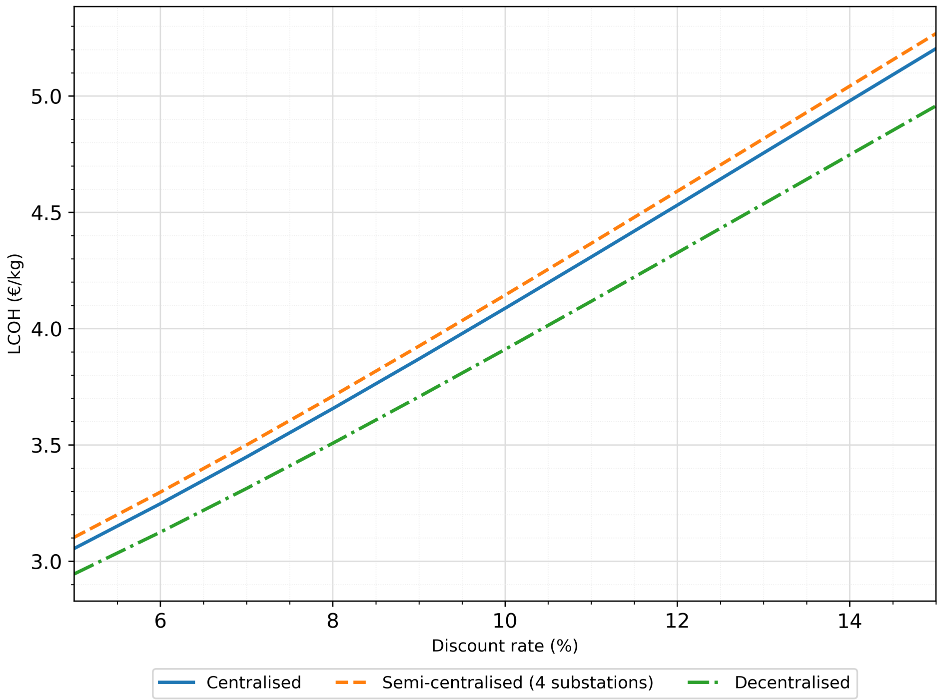

Figure 8.34: LCOH versus discount rates for centralised, semi-centralised (4 substations) and decentralised offshore wind-to-hydrogen configurations.

The figure illustrates that altering the discount rate results in a comparable increase in LCOH for each configuration. Nevertheless, when the discount rates vary per configuration, certain combinations of discounts may favor the centralised or semi-centralised configuration over the decentralised one.

8.7. Discussion case study

In this section, the findings of the case study are discussed in order to contextualise them appropriately. This includes an interpretation of the results in Subsection 8.7.1, a comparison with existing literature in Subsection 8.7.2, an acknowledgment of the limitations in Subsection 8.7.3 and implications of the case study results in Subsection 8.7.4.

8.7.1. Interpretation of results

The findings from the case study can be grouped into four main categories: preliminary optimisation, selection of semi-centralised configuration, configuration comparison, and sensitivity. Each category will be discussed in the subsequent paragraphs, providing valuable insights into the techno-economic aspects of offshore wind-to-hydrogen configurations.

Preliminary optimisation

- The optimal compressor input pressure is determined by striking a balance between the compressor cost, pipeline cost, and hydrogen production. In this specific case, the compressor cost plays a more substantial role than the hydrogen pipeline cost, making it advantageous to prioritize minimising compression and opting for larger pipeline diameters.
- The number of stack replacements influences the LCOH, with the optimal number being the minimum required. However, the number of stack replacement is highly dependent on electrolyser stack cost and the stack degradation rate.
- The undersizing of the HPU can lead to a decrease in the LCOH, depending on the scaling factors of the electrolyser and BOP. For larger HPU installed capacities with less influence from scaling factors, undersizing leads to a larger reduction in LCOH. However, undersizing also results in reduced hydrogen production. It is essential to consider the connection to revenue, especially when hydrogen prices are high. In such cases, undersizing may decrease the LCOH but also

have a negative impact on the Net Present Value (NPV) over the project's lifetime, making it an unfavorable choice. Therefore, when the total hydrogen production is the key performance indicator, undersizing is not preferred.

Semi-centralised configuration selection

- The LCOH of the semi-centralised configurations does not vary significantly, but the configurations with 2 and 4 substations yield the lowest LCOH. This is caused by the lowest energy transmission CAPEX and relatively low specific CAPEX of the hydrogen substations. An increase in number of hydrogen substations leads to higher cost.
- For the semi-centralised configurations with 2 and 3 hydrogen substations, jacket substructures are selected, because the topside mass of the substations exceeds the assumed load capacity of the monopile. The configurations with 4 to 8 hydrogen substations use monopile substructures, which offer cost savings in substructure, transport, and installation.
- Within a semi-centralised configuration consisting of a specific number of hydrogen substations, the use of monopile substructures is advantageous over jacket substructures as long as the load capacity of the monopile is not exceeded.
- The switch from a jacket to monopile substructure is advantageous if the monopile's load capacity is fully utilized. When transitioning from a semi-centralised configuration with 3 jacket substructures to a configuration with 4 monopile substructures, adding an additional hydrogen substation leads to a decrease in LCOH, due to the cost savings from using a monopile instead of jackets.
- After reaching 4 hydrogen substations, adding further substations leads to an increase in LCOH. This increase is primarily driven by the additional cost associated with installing extra offshore substations beyond the initial 4, offsetting the initial cost advantage of using monopiles over jackets.
- Increasing the monopile load capacity beyond the topside mass of the 3-substation configuration results in a new optimal semi-centralised configuration due to significant cost reductions when monopiles could be used in the semi-centralised configuration with 3 hydrogen substations.
- The total length of the energy infrastructure of the 2 substation semi-centralised configuration is the smallest. The total energy infrastructure CAPEX of the semi-centralised configuration with 4 substations is the highest due the high cost of the steel pipelines connecting the substations and because the inter-array cable cost are reduced further for 5 hydrogen substations. Nonetheless, the differences in energy transmission costs between these configurations are relatively small, falling within the range of 0-5%.
- Surprisingly, the specific cost of the hydrogen pipelines is higher than that of the inter-array cables. This is likely due to the relatively short length of the hydrogen pipelines. Furthermore, hydrogen pipelines with a relatively large diameter are chosen, despite the higher specific cost, because this reduces the need for compression and ultimately lowers the LCOH.
- The semi-centralised configuration consisting of 6 hydrogen substations yields the highest hydrogen production due to the lowest inter-array cable energy losses.

Configuration comparison

- The decentralised configuration demonstrates the lowest LCOH, primarily attributed to higher total hydrogen production during the lifetime and reduced costs.
- The absence of inter-array cables in the decentralised configuration eliminates inter-array cable power losses, resulting in increased hydrogen production throughout the lifetime.
- Cost savings in the decentralised configuration arise from the lack of high voltage electrical equipment and the absence of additional substations, except for the manifold. These factors significantly reduce costs compared to the semi-centralised and centralised configurations.
- The impact of the energy infrastructure varies minimally across the configurations. The hydrogen infield flowlines as well as the steel pipelines between the hydrogen substations exhibit higher costs than the inter-array cables. The pipelines do not have economic benefits over the inter-array cables due to their small energy volumes.

Sensitivity

- Sensitivity analysis reveals differences between the configurations. While influential high-level parameters like wind farm CAPEX and HPU inefficiency show similar impacts across configurations, low-level parameters demonstrate varying effects. For instance, changes in cost scaling factors have a greater impact on the decentralised configuration.
- A change in monopile load capacity leads to a different optimal semi-centralised configuration. When the monopile load capacity and the substation topside mass of a configuration are matched, a significant reduction in LCOH is achieved.
- Considering different electrolyser stack CAPEX values due to significant uncertainties could potentially result in different optimal wind-to-hydrogen configurations. This effect is primarily driven by the cost scaling of the electrolyser stacks, which becomes more pronounced with increasing electrolyser stack CAPEX.
- The availability and maintenance cost scenario analysis highlights the significance of considering availability and maintenance costs across different configurations. Specifically, in this scenario, the centralised configuration appears to be the preferred option, demonstrating a lower LCOH compared to the semi-centralised and decentralised configurations.
- The evaluation of stack degradation rate highlights its potential optimistic assumption and its significant impact on the preliminary optimisation of the number of stack replacements. The optimal number of stack replacements is highly dependent on the stack degradation rate, with variations observed across different configurations due to differing electrolyser stack CAPEX caused by cost scaling effects.
- The variation in discount rates among configurations, stemming from differences in risk levels, may result in distinct optimal offshore wind-to-hydrogen configurations. The considerable influence of the discount rate on uncertainty or change plays a significant role in this outcome.

8.7.2. Comparisons with previous research

The results of the case study will be compared with literature to explore if they support or challenge existing literature results. This will be done for the overall LCOH of the different configurations, the specific CAPEX of the offshore hydrogen facilities and the specific cost of energy infrastructure.

Levelised cost of hydrogen

To begin with, it is important to compare the LCOH obtained in this study with findings from existing literature. This comparison serves to validate the methodology employed in the case study and establish a benchmark for evaluating the competitiveness of offshore wind-to-hydrogen configurations. Several LCOH values for offshore wind-to-hydrogen production can be found in the literature.

According to the International Energy Agency (IEA), the projected LCOH range for offshore wind in 2030 is between 1.9€ /kg and 4.3€ /kg, where the spread is caused by regional variations in costs and renewable resource conditions [40]. DNV, a leading authority in the field, estimates a LCOH of 4.56€ /kg to be achieved by 2030 [3]. Another study by Singlitico et al. reports a LCOH of 2.5€ /kg for centralised considering a median range of 0.5 to 12GW of installed electrolyser capacity [71], and 3.2€ /kg for in-turbine electrolysis using a discount rate of 5%. Interestingly, this contradicts the findings of our research, where the decentralised configuration resulted in a lower LCOH compared to the centralised configuration.

However, Singlitico et al. mention that the higher LCOH for the decentralised configuration, as opposed to the centralised configuration, can be attributed to economies of scale. Their study emphasizes that economies of scale related to electrolysers and pipelines become more pronounced for smaller sizes. In the case of decentralised electrolysers, which have capacities below the size of the wind turbines, they are more strongly affected by economies of scale. Additionally, increasing the diameter of pipelines for a given length leads to a decrease in cost per capacity. Consequently, in the context of small-scale decentralised placement, the decentralised configuration with a large number of pipelines from the hydrogen wind turbines to the manifold is associated with a higher LCOH [71].

Compared to the study from Singlitico et al, this current study, limits the impact of economies of scale, and the costs of infield flowlines are comparable to the inter-array cable costs. As a result, the decentralised configuration yields a lower LCOH compared to both the semi-centralised and decentralised configurations in this research.

Specific cost substations

The specific cost of offshore hydrogen jacket substations is important for evaluating the feasibility and cost-effectiveness of offshore wind-to-hydrogen configurations. This current study found that the specific cost of the offshore hydrogen jacket substations ranged from 970€/kW to 1150€/kW. In contrast, DNV estimates the specific cost for 100-1000MW jacket hydrogen substations between 1330€/kW and 1380€/kW. The differences in costs arise from the relatively low assumed stack cost in this research, based on the cost reduction assumptions from the Institute for Sustainable Process Technology (ISPT), as compared to the findings in the DNV studies [28].

Energy transmission specific cost

The specific cost of inter-array cables remained consistent across the different configurations, with variations attributed solely to the two cable types employed. The specific cost of inter-array cables was deemed highly reliable, due to the available resources within Vattenfall.

In contrast, the specific cost of hydrogen pipelines exceeded that of inter-array cables, particularly for configurations with relatively shorter total pipeline lengths. The average specific cost of steel hydrogen pipelines across the three configurations was determined to be 1.4 million €/km, featuring an average diameter of 14 inches and an average total length of 51km. A noticeable disparity emerged when comparing this specific cost to the figures reported in literature. According to Khan et al., a specific cost of 0.39 million €/km was documented for a 36 inch steel offshore hydrogen pipeline spanning 1500km [47].

For the decentralised configuration, the specific cost of infield flowlines was estimated at *X* million €/km, with an average diameter of *X* inches and a total length of *X* km. Once again, a substantial deviation from the figures in literature was observed. DEA's report indicates a specific cost of 0.562 million €/km for 2-6 inch infield flowlines with a total length of 34km [3].

These findings highlight significant disparities in specific costs when compared to literature. The cost calculations for hydrogen pipelines in this study are considered conservative.

8.7.3. Limitations

This case study presents valuable insights, but it is important to acknowledge several limitations:

- *Specific site focus:* The case study focuses on a specific offshore wind-to-hydrogen site, which may not fully represent all possible scenarios. A different site could lead to a different optimal number of hydrogen substations for the semi-centralised configuration. However, the main conclusions drawn from this work would be similar as the impact of the specific layouts is limited.
- *Simplified efficiency curve for electrolysers:* In this study, the electrolyser's efficiency curve is represented by a single efficiency value. However, in reality, the efficiency curve can significantly influence hydrogen production. As mentioned earlier, this effect is more pronounced in smaller electrolyser facilities with limited power aggregation. Consequently, the decentralised configuration will be more sensitive to hydrogen production calculations when this simplification is not considered.
- *Substation design:* The study's examination of hydrogen substation design is limited. Particularly, the assumption that the topside area is not the limiting factor for using monopiles may not hold true in reality. Moreover, the evaluation of monopile substructures does not include an assessment of the substation's structural dynamics, which could potentially result in variations in the load capacities of the substructures. This limitation will mainly affect the configurations consisting of monopile substructures as jacket substructures are commonly used.
- *Simplified OPEX model:* The reliance on a simplified OPEX model based on CAPEX values introduces potential inaccuracies in the cost analysis. The operation and maintenance of offshore wind-to-hydrogen farms will be complex and challenging what could lead to a significant increase in cost. Additionally, the effect on the different offshore wind-to-hydrogen configuration is also not yet clear. Where the centralised configuration benefits from a single location for operation and maintenance and thus decrease complexity, the decentralised benefits from lower risk due to multiple locations for operation and maintenance and thus lower impacts of failures.
- *Offshore working of HPU equipment:* The case study's scope does not encompass the effects of offshore operation of hydrogen production unit equipment. Offshore operation may affects the

efficiency, degradation and therefore availibility and cost of the electrolysers, purifiers, desalination units and compressors. Vibrations caused by waves could potentially impacts the working of such components. This limitation will especially impact smaller hydrogen substations or offshore hydrogen wind turbines as they are assumed to be more affected by offshore conditions.

- *Regulatory and policy considerations:* The case study does not account for potential regulatory or policy changes that could influence the economic viability and feasibility of offshore wind-to-hydrogen configurations. The effect on different offshore wind-to-hydrogen configurations is unknown but and is highly depended on the regulation or policy.

Acknowledging these limitations is essential for understanding the scope and applicability of the case study findings. Addressing these limitations through further research will enhance the accuracy and comprehensiveness of future analyses in the field of offshore wind-to-hydrogen systems.

8.7.4. Implications

The findings of this case study have important implications for policy, practice, and further research in the field of offshore wind-to-hydrogen systems. The insights gained from the study can guide decision-making processes, optimisation strategies, and future investigations.

- *Optimisation strategies:* The preliminary optimisation findings highlight the significance of considering multiple factors, such as compressor cost, pipeline diameter, and stack replacements, when designing offshore wind-to-hydrogen systems. These insights provide valuable guidance for optimising configurations, minimising costs, and enhancing system performance.
- *Configuration selection:* The semi-centralised configuration selection findings offer practical implications for choosing the most suitable configuration. Moreover, the impact of inter-array cable length and monopile load capacity on cost reduction and hydrogen production is emphasized, aiding in configuration decision-making.
- *Comparison and validation:* Comparisons with existing literature validate the methodology employed in this study and establish benchmarks for offshore wind-to-hydrogen configurations. The findings both support and challenge previous research, particularly regarding LCOH estimates. Understanding these discrepancies contributes to a better understanding of cost drivers and provides insights for future investigations.
- *Consideration of multiple factors:* The case study underscores the importance of considering multiple factors, including HPU availability, hydrogen production efficiencies, cost sensitivities, and mass assumptions, when designing offshore wind-to-hydrogen configurations. By incorporating these factors, policymakers, industry practitioners, and researchers can make informed decisions to reduce the LCOH and improve overall system performance.
- *Further research opportunities:* The case study identifies several areas for further research. For example: Exploring the impact of structural analysis for substation design, developing more more accurate OPEX models, conducting studies across a broader range of sites, and considering potential regulatory and policy scenarios are important research opportunities. A more elaborate discussion of recommendations for future work will is given in Chapter 10.

In summary, the implications of this case study provide valuable insights for policymakers, industry practitioners, and researchers. By leveraging these findings, stakeholders can make informed decisions, optimise configurations, and drive the development of cost-effective offshore wind-to-hydrogen systems.

9 Conclusion

This research aimed to evaluate the techno-economic feasibility of the semi-centralised offshore wind-to-hydrogen configuration compared to centralised and decentralised configurations. By addressing the research gap regarding semi-centralised offshore wind-to-hydrogen electrolysis, the study examined its feasibility in an offshore wind farm context. The main research question was formulated as follows:

"What is the techno-economic feasibility of the semi-centralised offshore wind-to-hydrogen configuration compared with the centralised and decentralised offshore wind-to-hydrogen configurations?"

The analysis revealed the technical feasibility of a wind-to-hydrogen farm with multiple hydrogen substations utilizing monopile substructures. By addressing technical aspects related to offshore electrolysis, desalination, purification, and compression, alongside monopile load capacity and hydrogen transmission through pipelines, the semi-centralised offshore wind-to-hydrogen configuration demonstrated viability. However, it is important to acknowledge that, for all three offshore wind-to-hydrogen configurations, the analysis was limited to literature research and modeling, and did not encompass detailed technical considerations such as variable loads, structural dynamics, and the impact of offshore conditions on the hydrogen production unit equipment. These limitations could potentially influence the outcomes of this research if their implications differ per configuration.

Furthermore, the case study findings demonstrated the economic viability of the semi-centralised configuration when compared to the centralised and decentralised configurations. The difference in levelised cost of hydrogen (LCOH) between the centralised and semi-centralised configurations was minimal, while the decentralised configuration exhibited a 5% lower LCOH. Although the semi-centralised configuration offered CAPEX reductions through synergies between monopile substations and wind turbines, the additional costs associated with multiple substations outweighed the savings compared to the centralised configuration.

The study has identified the technical distinctions among the centralised, semi-centralised, and decentralised offshore hydrogen production configurations. These technical differences center around the energy transmission infrastructure, high voltage electrical system and substation substructure type. The energy transmission infrastructure of the centralised and semi-centralised consist of inter-array cables and one or multiple steel hydrogen pipelines, whereas the decentralised configuration consists of infield hydrogen flowlines and a single steel hydrogen pipeline. This approach eliminates the need for inter-array cables and high voltage electrical equipment, which leads to less electrical power losses and potential cost savings in the decentralised configuration. The substation substructure of the centralised configuration is a jacket, the substructure of the hydrogen wind turbines in the decentralised configuration are monopiles and the substation substructure type of the semi-centralised configuration can either be a jacket or monopile depending on the topside weight. Throughout the research, the monopile substructure demonstrated advantages over the jacket substructure.

Variations in energy conversion efficiency, hydrogen transmission, and electrical cable infrastructure were observed across the configurations. The centralised configuration, consisting of a large-scale inter-array cable infrastructure, experienced higher inter-array cable losses, the semi-centralised configuration, consisting of a decreased inter-array cable infrastructure, incurred slightly fewer inter-array energy losses, and the decentralised configuration benefited from the absence of inter-array cables and high voltage energy transformers, resulting in the highest electrical efficiency leading to the highest hydrogen production during lifetime. However, it's important to note that the difference in hydrogen production during the lifetime of these configurations was found to be only around 1.25% between the centralised and decentralised setups. Considering the inherent inaccuracies and uncertainties in the assumptions, these differences can be considered small. Additionally, the simplified electrolyser efficiency further contributed to the advantages of the decentralised configuration. Taking all factors into account, the total hydrogen production is not expected to differ significantly among the various configurations.

The sensitivity analysis identified the main cost and performance drivers, influencing the LCOH for each configuration. The wind farm cost, excluding hydrogen components, remained consistent across all configurations and served as the primary cost driver. As a result, the differences in LCOH between the offshore wind-to-hydrogen configurations were relatively small, with variations mainly caused by the hydrogen substation and energy transmission cost.

The disparities emerged in the hydrogen substation and hydrogen wind turbine cost, specifically related to substructure, transport, installation, and high voltage electrical equipment. On the other hand, the infield energy transmission cost among the different configurations was comparable and did not lead to significant variations in LCOH.

Concerning the performance drivers, the primary factor influencing hydrogen production is the initial efficiency of the electrolyser stack. Additionally, the stack degradation rate has a large impact on the LCOH and on the number of stack replacements. It's important to note that in this analysis, the initial electrolyser stack efficiency and degradation rate were assumed to be equal in each configuration. In reality, these values could vary among the configurations, but further research is needed to determine their actual differences.

Furthermore, the optimal number of hydrogen substations within a semi-centralised wind-to-hydrogen farm depends on the load capacity of the monopile as well as the substructure-related costs. The monopile substructure proves to be the most advantageous option when using the minimum number of substations that can still be accommodated by them.

Overall, the decentralised configuration outperformed the centralised and semi-centralised configurations in terms of LCOH. This was primarily attributed to the absence of high voltage electrical equipment and the absence of extra substructures, leading to cost reductions in substation substructures, as well as their transport, installation, and commissioning. Additionally, as stated above, the decentralised configuration achieved only a minor increase in hydrogen production due to the lack of electrical power loss in inter-array cables, resulting in a minor decrease in LCOH.

To conclude, this research provided comprehensive insights into the key technical parameters, energy efficiency, cost drivers, optimal substation numbers, and LCOH comparisons for centralised, decentralised, and semi-centralised offshore wind-to-hydrogen configurations. The findings contribute to understanding the techno-economic feasibility of these configurations and highlight the potential for further investigation and development in the field.

10 Recommendations for future work

This chapter presents a set of recommendations for future research and development in the field of offshore wind-to-hydrogen configurations. These recommendations aim to address key areas that require further research to advance development of offshore hydrogen production powered by wind energy. The recommendations are categorized into methodology related and content related topics. First the methodology related recommendations will be discussed in Subsection 10.1, followed by the recommendations related to the content in Subsection 10.2.

10.1. Methodology

The recommendations regarding the methodology apply on the wind farm layout optimisation, the number of case studies and a number of simplifications and are given as follows:

- This research utilized wind farm layouts optimised for electricity production in the offshore wind-to-hydrogen configuration. For further research, it is recommended to design *optimisation models specifically for offshore wind-to-hydrogen farms* because different cost and performances associated with offshore wind-to-hydrogen farms could influence the optimal positioning of wind turbines, hydrogen wind turbines, hydrogen substations and hydrogen pipeline routing.
- The number of case studies conducted is limited, which means the findings of this particular study may heavily rely on the specific parameters of this case study. *Conducting additional case studies* encompassing various wind farm shapes, diverse locations, various wind turbine capacities, and different wind farm capacities, will validate the proposed hydrogen production models and evaluate their applicability in different contexts.

The research methodology incorporated certain simplifications. These are enumerated below, along with suggestions to enhance the research's precision:

- The *electrolyser stack efficiency curve* is simplified in the hydrogen production model by using a fixed electrolyser efficiency value. A more detailed hydrogen production model including a dynamic electrolyser efficiency curve will enhance the accuracy of the hydrogen production and show the differences per offshore wind-to-hydrogen configuration.
- The *electrolyser stack degradation rate* is assumed to be constant for the different offshore wind-to-hydrogen configurations in this research. However, it can be argued that the electrolyser degradation rate varies per configuration as it depends on several factors such as the turn-on and turn-off ratio and the ramp-up and ramp-down speed. Advisory control strategies can significantly affect these factors [36]. As such, exploring the impacts of distinct advisory control strategies on various offshore wind-to-hydrogen configurations is highly recommended.
- The *modeling of the hydrogen substation mass and size* is simplified in this research. While this study emphasized the energy transmission system by sizing the hydrogen pipeline diameters, delving deeper into the structures of the hydrogen substations could enhance the precision of the work as the contribution of the substations to the LCOH is more significant than the energy

transmission. For example, a more detailed analysis and modeling of the hydrogen substation will decrease the uncertainty of the maximum installed capacity on a jacket or monopile substructure.

- The *transport and installation model for the hydrogen substations* was simplified in this research. A more detailed transport and installation model that could be used across different wind-to-hydrogen farms, could lead to a more precise rendering of the final results.
- The *OPEX* are considered as a percentage of the CAPEX. This simplification does not allow for optimisations within the operation and maintenance costs. Therefore, creating detailed OPEX models that are independent of CAPEX will enable a more accurate assessment of the economic viability of the offshore wind-to-hydrogen configurations.
- The *HPU availability* is simplified and considered equal for the different offshore wind-to-hydrogen configurations. However, it can be argued that the HPU availability depends on several factors such as the HPU capacity and number of hydrogen substations or hydrogen wind turbines. Therefore, investigating and developing models to accurately predict the availability of hydrogen production units will enhance the accuracy of the hydrogen production per configuration.

10.2. Content

The following content-related recommendations for future research could enhance development in the field of offshore hydrogen production powered by wind energy:

- *Dynamic behavior analysis:* Analyse the dynamic behavior of hydrogen production equipment under varying load conditions, with a particular focus on the difference between the centralised, semi-centralised, and decentralised configurations. Understanding and optimising the performance and efficiency of hydrogen production equipment in response to fluctuating loads will contribute to achieving stable and reliable hydrogen production processes, while also providing insights into the variations across different configurations. A viable approach would be to start with a lab-scale examination, simulating varying load conditions, and based on the findings, move towards setting up a testing facility.
- *Impact of offshore conditions on HPU equipment:* Investigate the impact of offshore deployment of HPU equipment, such as electrolysers, compressors, purifiers, and desalination units. This research will address the considerations and requirements for offshore hydrogen production, enabling safe and efficient operation of HPU equipment in offshore environments. Collaborative field studies, possibly in partnership with equipment manufacturers, can shed light on offshore operational challenges and solutions.
- *Floating offshore wind:* Examine the feasibility and technological requirements for implementing floating offshore wind-to-hydrogen systems in deeper waters. By expanding the potential areas for offshore hydrogen production, this research will contribute to leveraging offshore wind resources and enabling the sustainable production of hydrogen in regions with deeper waters. Pilot projects in select deeper water regions can validate findings and offer firsthand experience.
- *Salt water electrolysis:* Research to potential of salt water electrolysis to remove the desalination step from the offshore facilities. This could decrease cost but also system complexity as a process step will be removed. Conducting experimental setups in controlled environments can validate the efficacy and scalability of this method.
- *Hydrogen storage in pipelines:* Explore the possibility and potential benefits of hydrogen storage in hydrogen pipelines. This could potentially improve the business case of offshore wind-to-hydrogen facilities as the additional storage facilities onshore could be removed. Mathematical and computational modeling can be employed initially, followed by on-site testing for more comprehensive validation.
- *Integration with offshore floating solar:* Consider the combination of offshore wind and floating solar platforms for a steadier hydrogen output. This approach could lead to more consistent energy sourcing and hydrogen production. Prototype installations can be a practical way to evaluate the synergistic benefits of such an integrated system.

By addressing these topics, future research can significantly contribute to advancing the field of offshore hydrogen production powered by wind energy.

References

[1] 4C Offshore. *4C Offshore Wind Speed Data - 2023*. 4C Offshore Website. Accessed on August 2, 2023. 2023. URL: https://www.4coffshore.com/windfarms/windspeeds.aspx.

[2] Timothy Ablondi and Mark Barton. *Compressor Technology 2: Article - Hydrogen Compressor Selection*. Online. Siemens Energy, Oct. 2022. URL: https://assets.siemens-energy.com/siemens/assets/api/uuid:0aa6df14-ed53-4f63-9407-9bcec22d8e7e/comptech2-article-h2compressor-selection-oct2022.pdf.

[3] Danish Energy Agency. *Cost and performance data for offshore hydrogen production*. Tech. rep. Denmark: DNV, Mar. 2023.

[4] Dang Ahn et al. “Comparative evaluation of different offshore wind turbine installation vessels for Korean west–south wind farm”. In: *International Journal of Naval Architecture and Ocean Engineering* 9.1 (2017), pp. 45–54. ISSN: 2092-6782. DOI: https://doi.org/10.1016/j.ijnaoe.2016.07.004. URL: https://www.sciencedirect.com/science/article/pii/S209267821630437X.

[5] Uchenna O. Ajator. “Costing of Oil and Gas Projects for Efficient Management and Sustainability”. In: *IOSR Journal of Environmental Science, Toxicology and Food Technology* 8.12 (2014), pp. 70–84. DOI: 10.9790/2402-081217084. URL: http://dx.doi.org/10.9790/2402-081217084.

[6] Allseas. *Pioneering Spirit Offshore Construction Vessel*. Website. 2021. URL: https://allseas.com/equipment/pioneering-spirit-offshore-construction-vessel/.

[7] J.K.F. Andersen. *Vattenfall internal contact, expert view*. Personal communication. 2023.

[8] Jean André et al. “Time development of new hydrogen transmission pipeline networks for France”. In: *International Journal of Hydrogen Energy* 39.20 (2014), pp. 10323–10337. DOI: 10.1016/j.ijhydene.2014.04.190. URL: http://dx.doi.org/10.1016/j.ijhydene.2014.04.190.

[9] Yong Bai and Qiang Bai. “5 - Installation and Vessels”. In: *Subsea Engineering Handbook (Second Edition)*. Ed. by Yong Bai and Qiang Bai. Second Edition. Boston: Gulf Professional Publishing, 2019, pp. 123–141. ISBN: 978-0-12-812622-6. DOI: https://doi.org/10.1016/B978-0-12-812622-6.00005-1. URL: https://www.sciencedirect.com/science/article/pii/B9780128126226000051.

[10] Prabir Basu. “Chapter 2 - Biomass Characteristics”. In: *Biomass Gasification and Pyrolysis*. Ed. by Prabir Basu. Boston: Academic Press, 2010, pp. 27–63. ISBN: 978-0-12-374988-8. DOI: https://doi.org/10.1016/B978-0-12-374988-8.00002-7. URL: https://www.sciencedirect.com/science/article/pii/B9780123749888000027.

[11] Ian H. Bell et al. “Pure and Pseudo-pure Fluid Thermophysical Property Evaluation and the Open-Source Thermophysical Property Library CoolProp”. In: *Industrial & Engineering Chemistry Research* 53.6 (2014), pp. 2498–2508. DOI: 10.1021/ie4033999. eprint: http://pubs.acs.org/doi/pdf/10.1021/ie4033999. URL: http://pubs.acs.org/doi/abs/10.1021/ie4033999.

[12] Partha Biswas, Ponnuthurai Suganthan, and Gehan Amaratunga. “Optimization of Wind Turbine Rotor Diameters and Hub Heights in a Windfarm Using Differential Evolution Algorithm”. In: Apr. 2017, pp. 131–141. ISBN: 978-981-10-3324-7. DOI: 10.1007/978-981-10-3325-4_13.

[13] Boskalis. *Project Sheet Dolwin 2 Transport and Installation of the Dolwin Beta HVDC Platform*. Project Sheet. 2014.

[14] Engineering consultancy Boslan. *The next generation monopile foundations for offshore wind turbines: Manufacturing, design and handling challenges*. Technical Report. 2022.

[15] Jörn Brauns and Thomas Turek. “Alkaline Water Electrolysis Powered by Renewable Energy: A Review”. In: *Processes* 8.2 (2020). ISSN: 2227-9717. DOI: 10.3390/pr8020248. URL: https://www.mdpi.com/2227-9717/8/2/248.

[16] Wendell S. Brown. “Physical Properties of Seawater”. In: *Springer Handbook of Ocean Engineering*. Ed. by Manhar R. Dhanak and Nikolaos I. Xiros. Cham: Springer International Publishing, 2016, pp. 101–110. ISBN: 978-3-319-16649-0. DOI: 10.1007/978-3-319-16649-0_5. URL: https://doi.org/10.1007/978-3-319-16649-0_5.

[17] Gonçalo Calado and Rui Castro. “Hydrogen Production from Offshore Wind Parks: Current Situation and Future Perspectives”. In: *Applied Sciences* 11 (June 2021), p. 5561. DOI: 10.3390/app11125561.

[18] Davide Cazzaro. “Unified Optimization for Offshore Wind Farm Design”. English. PhD thesis. 2022.

[19] Ana-Maria Chirosca, Liliana Rusu, and Anca Bleoju. “Study on wind farms in the North Sea area”. In: *Energy Reports* 8 (2022). Selected papers from 2022 7th International Conference on Advances on Clean Energy Research, pp. 162–168. ISSN: 2352-4847. DOI: https://doi.org/10.1016/j.egyr.2022.10.244. URL: https://www.sciencedirect.com/science/article/pii/S2352484722021795.

[20] Clean Energy States Alliance. *Offshore Wind to Green Hydrogen: Insights from Europe*. Online. Report on Europe’s approach to green hydrogen development. Oct. 2021. URL: %7BURL%20of%20the%20report%7D.

[21] National Research Council and National Academy of Engineering. *The Hydrogen Economy: Opportunities, Costs, Barriers, and Needs*. Washington, DC: The National Academies Press, 2004. ISBN: 978-0-309-09163-3. DOI: 10.17226/10922.

[22] Emile Craye. *The Sizing and Costing of Hydrogen Pipelines for Offshore Wind Farms*. Internship Project, SET3080, Delft University of Technology. Supervisors: Michiel Zaayer, Hans van Heemst, Octavian Partenie. Nov. 2022.

[23] Domenico Curto, Vincenzo Franzitta, and Andrea Guercio. “A Review of the Water Desalination Technologies”. In: *Applied Sciences* 11.2 (2021). ISSN: 2076-3417. DOI: 10.3390/app11020670. URL: https://www.mdpi.com/2076-3417/11/2/670.

[24] Danish Energy Agency (DEA). *Screening of Possible Hub Concepts to Integrate Offshore Wind Capacity in the North Sea*. Tech. rep. DNV, 2022. URL: URL.

[25] Sandra Dermühl and Uwe Riedel. “A comparison of the most promising low-carbon hydrogen production technologies”. In: *Fuel* 340 (2023), p. 127478. ISSN: 0016-2361. DOI: https://doi.org/10.1016/j.fuel.2023.127478. URL: https://www.sciencedirect.com/science/article/pii/S0016236123000911.

[26] J. R. Diez et al. *Technical assessment of Hydrogen transport, compression, processing offshore*. Tech. rep. 2020. URL: https://north-sea-energy.eu/static/7ffd23ec69b9d82a7a982b828be04c50/FINAL-NSE3-D3.1-Final-report-technical-assessment-of-Hydrogen-transport-compression-processing-offshore.pdf.

[27] DNV. *Hydrogen Forecast To 2050*. Tech. rep. 2022.

[28] DNV-GL. *Power-to-Hydrogen IJmuiden Ver*. Technical Report. DNV-GL, 2018. URL: https://tennet-drupal.s3.eu-central-1.amazonaws.com/default/2022-07/P2H_IJmuiden_Ver_-_Final_Report_-_Public.pdf.

[29] Ahmed M. Elberry et al. “Large-scale compressed hydrogen storage as part of renewable electricity storage systems”. In: *International Journal of Hydrogen Energy* 46.29 (2021), pp. 15671–15690. ISSN: 0360-3199. DOI: https://doi.org/10.1016/j.ijhydene.2021.02.080. URL: https://www.sciencedirect.com/science/article/pii/S0360319921005838.

[30] Engineering Toolbox. *Specific Heat Ratio*. Website. Accessed 2023. URL: https://www.engineeringtoolbox.com/specific-heat-ratio-d_608.html.

[31] Engineers Edge. *Pressure Drop Along Pipe Length - Fluid Flow Hydraulic and Pneumatic*. Website. Unknown. URL: https://www.engineersedge.com/fluid_flow/pressure_drop/pressure_drop.htm.

[32] European Hydrogen Backbone Initiative. *The European Hydrogen Backbone (EHB) Initiative*. Report. Online. European Hydrogen Backbone Initiative, 2022. URL: URL%20not%20provided.

[33] Matteo Genovese et al. "Power-to-hydrogen and hydrogen-to-X energy systems for the industry of the future in Europe". In: *International Journal of Hydrogen Energy* 48.44 (2023), pp. 16545–16568. ISSN: 0360-3199. DOI: https://doi.org/10.1016/j.ijhydene.2023.01.194. URL: https://www.sciencedirect.com/science/article/pii/S0360319923003889.

[34] N. González Díez et al. *D1E.1 Impact of high speed hydrogen flow on system integrity and noise*. Online. Dit project is medegefinancierd door TKI Nieuw Gas | Topsector Energie uit de PPS-toeslag onder referentienummer TKI2020-HyDelta, Jan. 2022. URL: https://doi.org/10.5281/zenodo.5901833.

[35] Simon Hammecher. "Centralised Offshore Hydrogen Production: Techno-Economic Optimisation and Assessment of the Benefit of Aggregated Power Supply". MA thesis. MSc Thesis Sustainable Energy Technology, 2023.

[36] T. Helgason. *Vattenfall internal contact, expert view*. Personal communication. 2023.

[37] Thorkell Helgason. "System Design and Advisory Control Strategy For an Offshore Stand-Alone Hydrogen-Only Wind Turbine". MA thesis. MSc Thesis Sustainable Energy Technology, 2022.

[38] Joachim Holst and et al. *Cost forecast for low-temperature electrolysis - technology driven bottom-up prognosis for PEM and alkaline water electrolysis systems*. Tech. rep. Fraunhofer Institute for Solar Energy Systems, 2021.

[39] Omar S. Ibrahim et al. "Dedicated large-scale floating offshore wind to hydrogen: Assessing design variables in proposed typologies". In: *Renewable and Sustainable Energy Reviews* 160 (2022), p. 112310. ISSN: 1364-0321. DOI: https://doi.org/10.1016/j.rser.2022.112310. URL: https://www.sciencedirect.com/science/article/pii/S1364032122002258.

[40] IEA. *Global Hydrogen Review 2022*. IEA, Paris. License: CC BY 4.0. 2022. URL: https://www.iea.org/reports/global-hydrogen-review-2022.

[41] Institute for Sustainable Process Technology. *A One-GigaWatt Green-Hydrogen Plant: Advanced Design and Total Installed-Capital Costs*. Technical Report. Institute for Sustainable Process Technology, 2022. URL: https://ispt.eu/media/Public-report-gigawatt-advanced-green-electrolyser-design.pdf.

[42] International Energy Agency. "The Future of Hydrogen: Seizing today's opportunities". In: (June 2019), p. 203. URL: https://www.iea.org/reports/the-future-of-hydrogen.

[43] IRENA. *FUTURE OF WIND: Deployment, investment, technology, grid integration and socio-economic aspects*. A Global Energy Transformation paper. 2019.

[44] Jacob L.L.C.C. Janssen et al. "Country-specific cost projections for renewable hydrogen production through off-grid electricity systems". In: *Applied Energy* 309 (2022), p. 118398. ISSN: 0306-2619. DOI: https://doi.org/10.1016/j.apenergy.2021.118398. URL: https://www.sciencedirect.com/science/article/pii/S0306261921016342.

[45] Arvind Keprate, R.M. Chandima Ratnayake, and Shankar Sankararaman. "Minimizing hydrocarbon release from offshore piping by performing probabilistic fatigue life assessment". In: *Process Safety and Environmental Protection* 106 (2017), pp. 34–51. ISSN: 0957-5820. DOI: https://doi.org/10.1016/j.psep.2016.11.019. URL: https://www.sciencedirect.com/science/article/pii/S0957582016302890.

[46] M.A. Khan et al. *The Techno-Economics of Hydrogen Compression*. Tech. rep. Transition Accelerator, 2021. URL: https://transitionaccelerator.ca/wp-content/uploads/2021/12/1_TA-Brief_-TEEA-Hydrogen-Compression-PUBLISHED-print-UST-THIS-ONE-Dec-2021.pdf.

[47] M.A. Khan, C. Young, and D.B. Layzell. "The Techno-Economics of Hydrogen Pipelines". In: *Transition Accelerator Technical Briefs* 1.2 (2021), pp. 1–40. ISSN: 2564-1379.

[48] M. Krogsgaard. *Vattenfall internal contact, expert view*. Personal communication. 2023.

[49] Lhyfe. *Lhyfe and Chantiers de l Atlantique sign a MoU to develop offshore renewable green hydrogen production*. https://www.lhyfe.com/press/lhyfe-and-chantiers-de-latlantique-sign-a-mou-to-develop-offshore-renewable-green-hydrogen-production/. Accessed on 2nd July 2023. Accessed 2023.

[50] Yorick Ligen, Heron Vrubel, and Hubert Girault. “Energy efficient hydrogen drying and purification for fuel cell vehicles”. In: *International Journal of Hydrogen Energy* 45.18 (2020), pp. 10639–10647. ISSN: 0360-3199. DOI: https://doi.org/10.1016/j.ijhydene.2020.02.035. URL: https://www.sciencedirect.com/science/article/pii/S0360319920305176.

[51] Mihir Mehta, Michiel Zaaijer, and Dominic von Terzi. “Optimum Turbine Design for Hydrogen Production from Offshore Wind”. In: *Journal of Physics: Conference Series* 2265.4 (May 2022), p. 042061. DOI: 10.1088/1742-6596/2265/4/042061. URL: https://dx.doi.org/10.1088/1742-6596/2265/4/042061.

[52] E. Shashi Menon. *Pipeline Planning and Construction Field Manual*. 26 jun. Gulf Professional Publishing, 1978, p. 576. ISBN: 978-0872010621.

[53] National Renewable Energy Laboratory. *NREL Offshore Balance-of-System Model*. Technical Report NREL/TP-6A20-66874. 2017. URL: https://www.nrel.gov/mwg-internal/2535425/progress?id=9yDTylMskCPbjrVyQc4y9__cCNme5xErjig1zVKAZLQ.

[54] Offshore Renewable Energy Catapult. *Guide to an offshore wind farm*. Tech. rep. 2019. URL: https://ore.catapult.org.uk/app/uploads/2019/04/BVGA-5238-Guide-r2.pdf.

[55] Pierre Olivier, Cyril Bourasseau, and Pr. Belkacem Bouamama. “Low-temperature electrolysis system modelling: A review”. In: *Renewable and Sustainable Energy Reviews* 78 (2017), pp. 280–300. ISSN: 1364-0321. DOI: https://doi.org/10.1016/j.rser.2017.03.099. URL: https://www.sciencedirect.com/science/article/pii/S136403211730432X.

[56] Georgios Papakonstantinou et al. “Degradation study of a proton exchange membrane water electrolyzer under dynamic operation conditions”. In: *Applied Energy* 280 (2020), p. 115911. ISSN: 0306-2619. DOI: https://doi.org/10.1016/j.apenergy.2020.115911. URL: https://www.sciencedirect.com/science/article/pii/S0306261920313751.

[57] O. Partenie. *Mail contact, expert view*. Personal communication. 2022.

[58] Ramboll. *The rise of offshore hydrogen production at scale*. https://www.ramboll.com/net-zero-explorers/offshore-hydrogen-at-scale. Accessed 2023.

[59] Rijksdienst voor Ondernemend Nederland (RVO). *Offshore Wind Energy Plans 2030-2050*. Website URL: https://english.rvo.nl/information/offshore-wind-energy/offshore-wind-energy-plans-2030-2050. Year of Access (e.g., 2023).

[60] Etienne Rivard, Michel Trudeau, and Karim Zaghib. “Hydrogen Storage for Mobility: A Review”. In: *Materials (Basel, Switzerland)* (2019). DOI: 10.3390/ma12121973.

[61] M. J. Rosenfeld and J. F. Kiefner. “Basics of Metal Fatigue in Natural Gas Pipeline Systems, A Primer for Gas Pipeline Operators”. In: PR-302-03152 (June 2006). Prepared for the Materials Technical Committee of Pipeline Research Council International, Inc.

[62] O. Schmidt et al. “Future cost and performance of water electrolysis: An expert elicitation study”. In: *International Journal of Hydrogen Energy* 42.52 (2017), pp. 30470–30492. ISSN: 0360-3199. DOI: https://doi.org/10.1016/j.ijhydene.2017.10.045. URL: https://www.sciencedirect.com/science/article/pii/S0360319917339435.

[63] G. Sdanghi et al. “Review of the current technologies and performances of hydrogen compression for stationary and automotive applications”. In: *Renewable and Sustainable Energy Reviews* 102 (2019), pp. 150–170. ISSN: 1364-0321. DOI: https://doi.org/10.1016/j.rser.2018.11.028. URL: https://www.sciencedirect.com/science/article/pii/S1364032118307822.

[64] Michael A. Semeraro. “Renewable energy transport via hydrogen pipelines and HVDC transmission lines”. In: *Energy Strategy Reviews* 35 (2021), p. 100658. ISSN: 2211-467X. DOI: https://doi.org/10.1016/j.esr.2021.100658. URL: https://www.sciencedirect.com/science/article/pii/S2211467X21000444.

[65] S.K. Sharma and S. Maheshwari. “A Review on Welding of High Strength Oil and Gas Pipeline Steels”. In: *J Nat Gas Sci Eng* 38 (2017), pp. 203–217. DOI: 10.1016/j.jngse.2016.12.039.

[66] Siemens. *Silyzer 300*. https://assets.new.siemens.com/siemens/assets/public.1524040818.abae9c1e48d6d239c06d88e565a25040ed2078dc.ct-ree-18-047-db-silyzer-300-db-de-en-rz.pdf. 2018.

[67] Siemens Energy. *Efficiency - Electrolysis*. White paper. 2021. URL: https://www.siemens-energy.com/electrolyze.

[68] Siemens-Gamesa. *Unlocking the green hydrogen revolution*. Tech. rep. 2021, pp. 1–25. URL: https://www.siemensgamesa.com/en-int/products-and-services/hybrid-and-storage/green-hydrogen/unlocking-the-green-hydrogen-revolution.

[69] Sofia G. Simoes et al. “Water availability and water usage solutions for electrolysis in hydrogen production”. In: *Journal of Cleaner Production* 315 (2021), p. 128124. ISSN: 0959-6526. DOI: https://doi.org/10.1016/j.jclepro.2021.128124. URL: https://www.sciencedirect.com/science/article/pii/S0959652621023428.

[70] Shelly Singla et al. “Hydrogen production technologies - Membrane based separation, storage and challenges”. In: *Journal of Environmental Management* 302 (2022), p. 113963. ISSN: 0301-4797. DOI: https://doi.org/10.1016/j.jenvman.2021.113963. URL: https://www.sciencedirect.com/science/article/pii/S0301479721020259.

[71] Alessandro Singlitico, Jacob Østergaard, and Spyros Chatzivasileiadis. “Onshore, offshore or in-turbine electrolysis? Techno-economic overview of alternative integration designs for green hydrogen production into Offshore Wind Power Hubs”. In: *Renewable and Sustainable Energy Transition* 1 (2021), p. 100005. ISSN: 2667-095X. DOI: https://doi.org/10.1016/j.rset.2021.100005. URL: https://www.sciencedirect.com/science/article/pii/S2667095X21000052.

[72] K. Skaug. *Vattenfall internal contact, expert view*. Personal communication. 2023.

[73] P. Spies. *Vattenfall internal contact, expert view*. Personal communication. 2023.

[74] Strohm. *TCP: The Best Solution for Offshore Hydrogen Infrastructure*. Online article. 2023. URL: https://strohm.eu/articles/tcp-sustainability-3-tcp-the-best-solution-for-offshore-hydrogen-infrastructure.

[75] Francesco Superchi et al. “Techno-economic analysis of wind-powered green hydrogen production to facilitate the decarbonization of hard-to-abate sectors: A case study on steelmaking”. In: *Applied Energy* 342 (2023), p. 121198. ISSN: 0306-2619. DOI: https://doi.org/10.1016/j.apenergy.2023.121198. URL: https://www.sciencedirect.com/science/article/pii/S0306261923005627.

[76] Arcandra Tahar et al. “Float Over Installation Method—Comprehensive Comparison Between Numerical and Model Test Results”. In: *Journal of Offshore Mechanics and Arctic Engineering* 128 (Aug. 2006), p. 256. DOI: 10.1115/1.2199556.

[77] Emanuele Taibi et al. *Green Hydrogen Cost Reduction. Scaling up electrolyzers to meet the 1.5° C climate goal*. Tech. rep. International Renewable Energy Agency, 2020, p. 96. URL: www.irena.org/publications.

[78] C. Tang et al. “Effects of inertia on dynamic performance of wind turbines”. In: Jan. 2009, pp. 1–6.

[79] Engineering Toolbox. *Pumps - Power Cost and Efficiency*. Website. Accessed 2023. URL: https://www.engineeringtoolbox.com/pumps-power-d_505.html.

[80] E. Tractebel and H. Engie. *Study on early business cases for H2 in energy storage and more broadly power to H2 applications*. EU Comm. 2017. URL: https://www.fch.europa.eu/sites/default/files/P2H_Full_Study_FCHJU.pdf.

[81] E. Tractebel and H. Engie. *Study on early business cases for h2 in energy storage and more broadly power to h2 applications*. Tech. rep. EU Commission, 2017, p. 228. URL: https://www.fch.europa.eu/sites/default/files/P2H_Full_Study_FCHJU.pdf.

[82] C. Tsiklios, M. Hermesmann, and T.E. Müller. “Hydrogen transport in large-scale transmission pipeline networks: Thermodynamic and environmental assessment of repurposed and new pipeline configurations”. In: *Applied Energy* 327 (2022), p. 120097. ISSN: 0306-2619. DOI: https://doi.org/10.1016/j.apenergy.2022.120097. URL: https://www.sciencedirect.com/science/article/pii/S030626192201354X.

[83] C. Tsiklios, M. Hermesmann, and T.E. Müller. “Hydrogen transport in large-scale transmission pipeline networks: Thermodynamic and environmental assessment of repurposed and new pipeline configurations”. In: *Applied Energy* 327 (2022), p. 120097. ISSN: 0306-2619. DOI: https://doi.org/10.1016/j.apenergy.2022.120097. URL: https://www.sciencedirect.com/science/article/pii/S030626192201354X.

[84] Vattenfall. *Fossil-free Hydrogen*. https://group.vattenfall.com/what-we-do/roadmap-to-fossil-freedom/industry-decarbonisation/fossil-free-hydrogen. Accessed: July 6, 2023.

[85] Vattenfall. *Wind Power*. https://group.vattenfall.com/what-we-do/our-energy-sources/wind-power. Accessed: July 6, 2023.

[86] David Warsinger et al. “Reversing membrane wetting in membrane distillation: Comparing dryout to backwashing with pressurized air”. In: *Environ. Sci.: Water Res. Technol.* 3 (July 2017). DOI: 10.1039/C7EW00085E.

[87] Alexandra C. Weber and Lazaros G. Papageorgiou. “Design of hydrogen transmission pipeline networks with hydraulics”. In: *Chemical Engineering Research and Design* 131 (2018). Energy Systems Engineering, pp. 266–278. ISSN: 0263-8762. DOI: https://doi.org/10.1016/j.cherd.2018.01.022. URL: https://www.sciencedirect.com/science/article/pii/S0263876218300248.

[88] Ton van Wingerden et al. *Specification of a European Offshore Hydrogen Backbone*. Tech. rep. DNV, Feb. 2023.

[89] Tomasz Wlodek et al. “Thermodynamic and Technical Issues of Hydrogen and Methane-Hydrogen Mixtures Pipeline Transmission”. In: *Energies* 12 (Feb. 2019), p. 569. DOI: 10.3390/en12030569.

[90] Yamin Yan et al. “Roadmap to hybrid offshore system with hydrogen and power co-generation”. In: *Energy Conversion and Management* 247 (2021), p. 114690. ISSN: 0196-8904. DOI: https://doi.org/10.1016/j.enconman.2021.114690. URL: https://www.sciencedirect.com/science/article/pii/S0196890421008669.

[91] Andreas Zauner et al. *Innovative large-scale energy storage technologies and Power-to-Gas concepts after optimization*. Tech. rep. EIL, Feb. 2019.

A
Appendix Case study

A.1. Preliminary optimisation

Figure A.1 and A.2. illustrates the relationship between LCOH and compressor input pressure, along with the associated largest hydrogen pipeline diameter for the semi-centralised configurations separately.

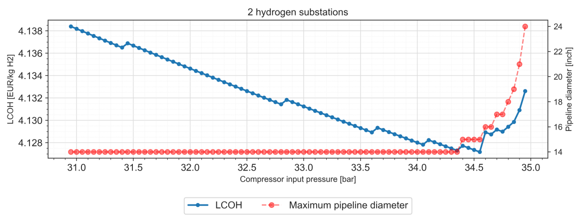

(a) 2 Substations

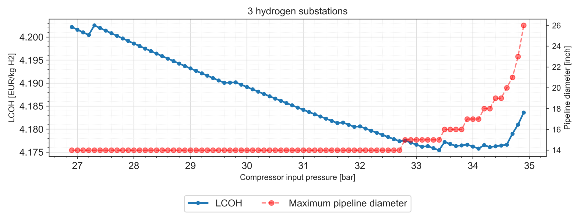

(b) 3 Substations

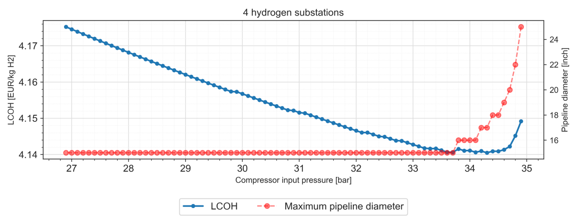

(c) 4 Substations

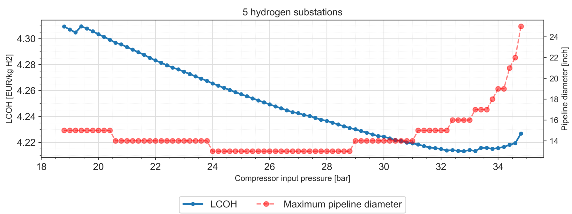

(d) 5 Substations

Figure A.1: LCOH and maximum pipeline diameter versus compressor input pressures for 2-5 hydrogen substation semi-centralised offshore wind-to-hydrogen configurations.

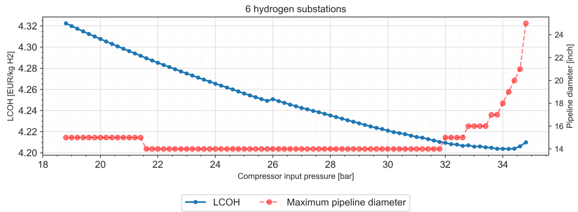

(a) 6 Substations

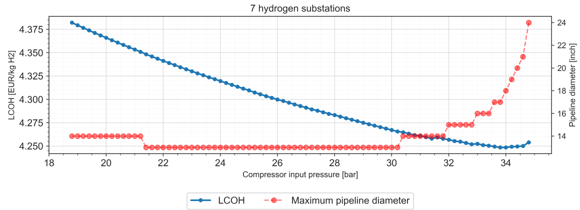

(b) 7 Substations

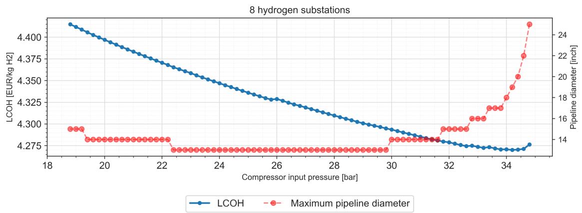

(c) 8 Substations

Figure A.2: LCOH and maximum pipeline diameter versus compressor input pressures for 6-8 hydrogen substation semi-centralised offshore wind-to-hydrogen configurations.

Figure A.3 represents the preliminary optimisation of the compressor output pressure, number of stack replacements and HPU sizing factor for the semi-centralised configurations.

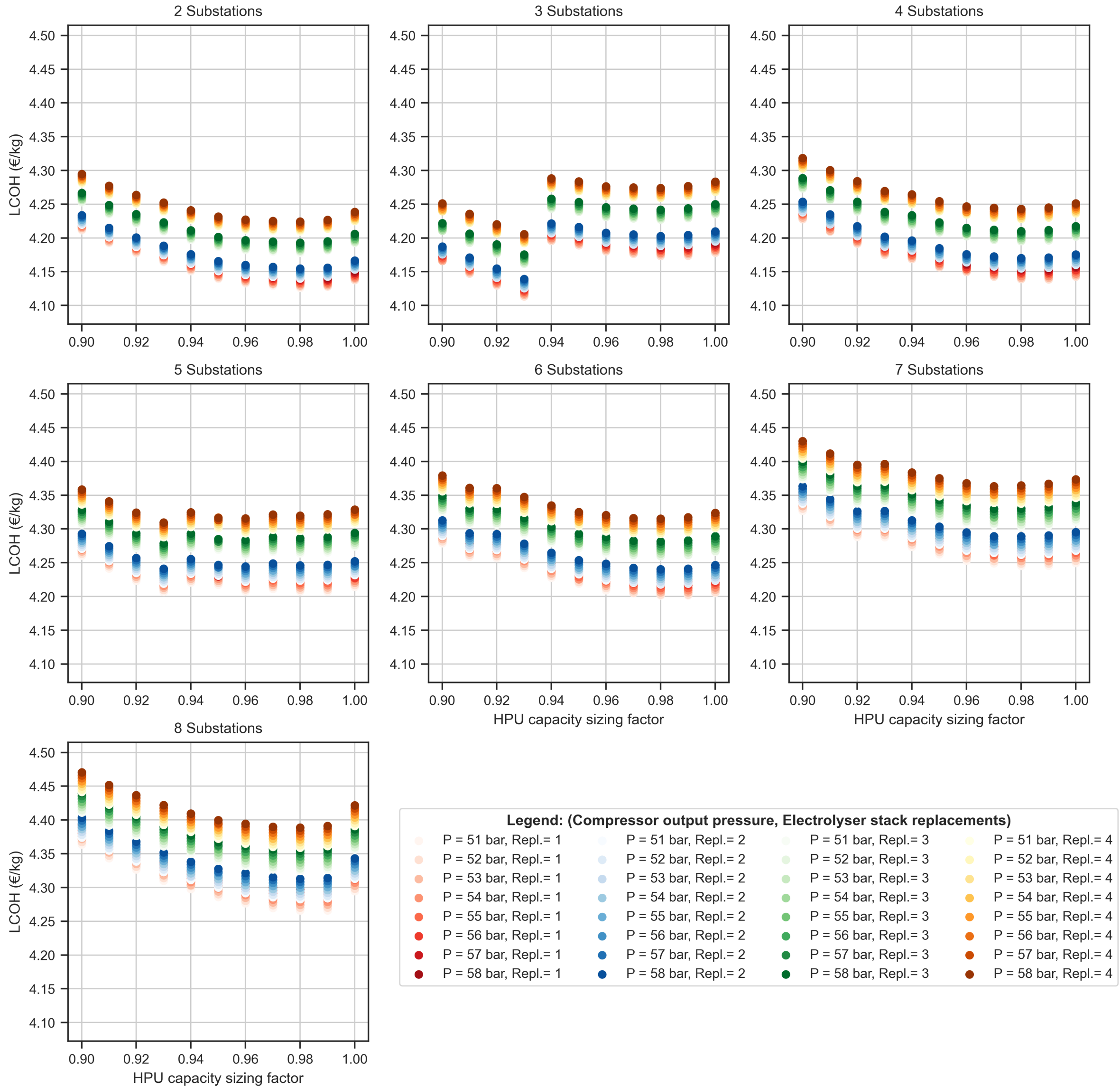

Figure A.3: Semi-centralised HPU sizing factors.

A.2. Semi-centralised wind-to-hydrogen layouts

The wind-to-hydrogen farm layouts for the semi-centralised configurations consisting of 2-8 hydrogen substations, are shown in Figure A.4 and A.5.

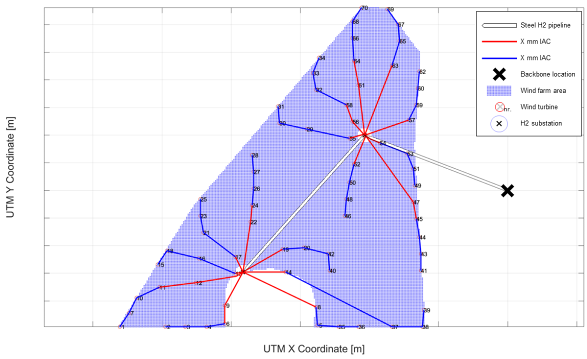

(a) H_2 substations: 2

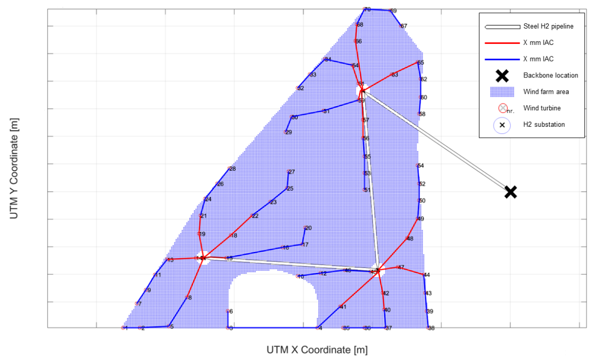

(b) H_2 substations: 3

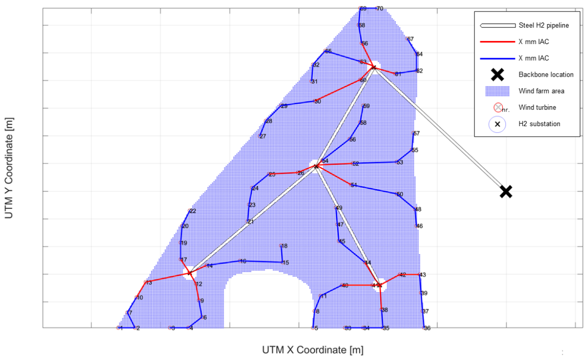

(c) H_2 substations: 4

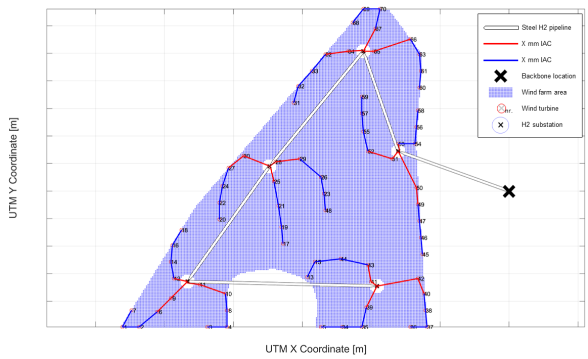

(d) H_2 substations: 5

Figure A.4: Semi-centralised offshore wind-to-hydrogen farm layouts including 2-5 offshore hydrogen substations.

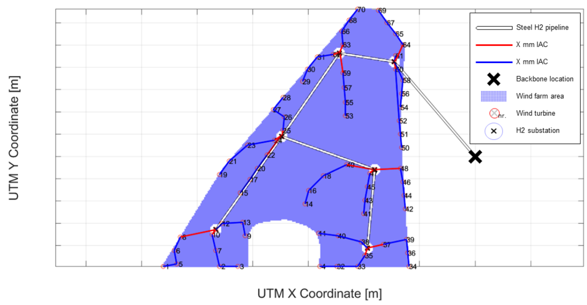

(a) H_2 substations: 6

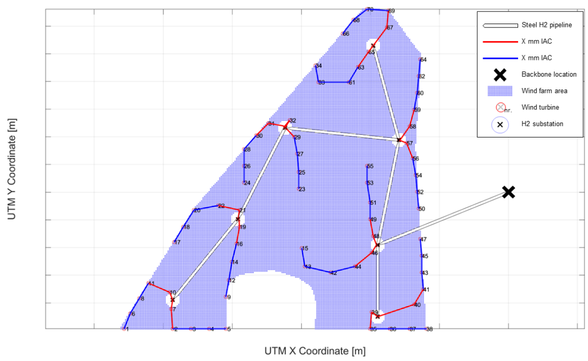

(b) H_2 substations: 7

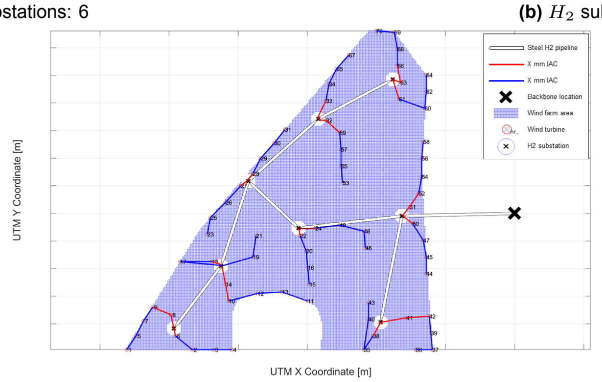

(c) H_2 substations: 8

Figure A.5: Semi-centralised offshore wind-to-hydrogen farm layouts including 6-8 offshore hydrogen substations.